PhD Thesis

Submitted by

Biu Torkiowei Victor

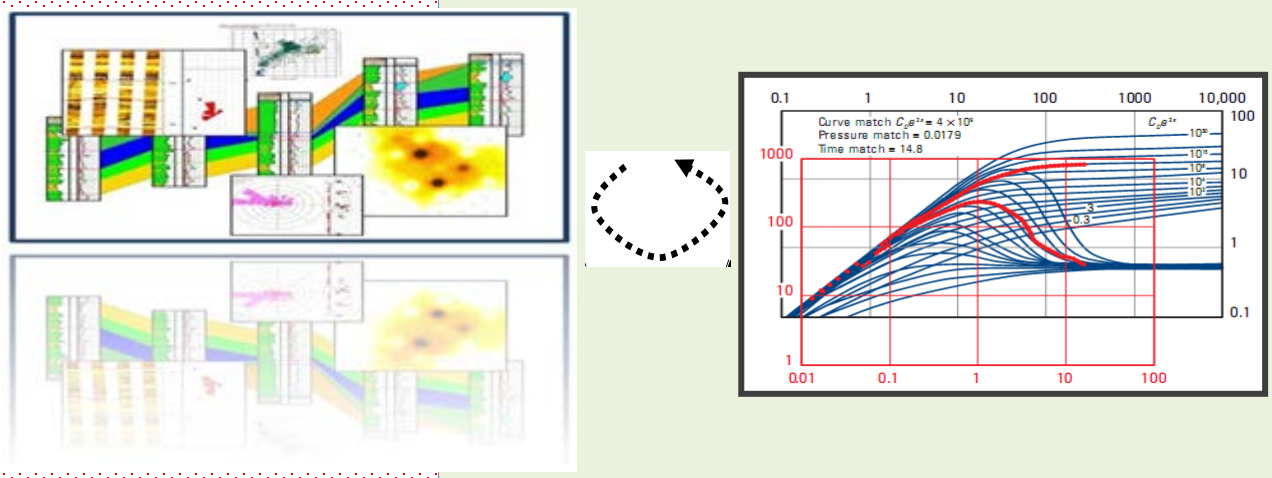

LSBU Student ID: 3224416
PhD Student
Department of Chemical Engineering
Faculty of Engineering, Science and Built Environment
London South Bank University LSBU

Supervisor Prof Shi-Yi Zheng
Chair Professor of Petroleum Engineering

October 2016

STATISTICAL & NUMERICAL DENSITY DERIVATIVES APPLICATION IN OIL AND GAS WELL TEST INTERPRETATION

Biu Torkiowei Victor

B.Eng. in PTE, University of Port Harcourt, Nigeria, 2005

M.Sc. in REM, Heriot Watt University, Edinburgh UK, 2008

M.Eng in PTE, University of Port Harcourt, Nigeria, 2012

Executive Master, International Oil and Gas Leadership IOG, The Graduate Institute Geneva, Switzerland, 2015

A thesis submitted in partial fulfillment of the requirements of London South Bank University for the degree of

Doctor of Philosophy

October 2016

CERTIFICATION

LONDON SOUTHBANK UNIVERSITY

SCHOOL OF ENGINEERING

Statistical & Numerical Density Derivatives Application in Oil and Gas Well Test Interpretation

By

BIU TORKIOWEI VICTOR

LSBU Student ID: 3224416

Supervisors: *Professor S Zheng and Dr D Zhao*
London South Bank University

Declaration

The School of Graduate Studies declares as follows:

That this thesis is the original work of the candidate and that it is accepted in partial fulfilment of the requirement for the award of the degree of **Doctor of Philosophy, Petroleum Engineering**

LONDON SOUTH BANK UNIVERSITY

SCHOOL OF ENGINEERING

This dissertation was presented

By

Biu Torkiowei Victor

It was defended on

October 17, 2016

and approved by

Zheng Shi-Yi, Ph.D., Professor, Department of Petroleum Engineering

Donglin Zhao, Ph.D., Associate Professor, Department of Petroleum Engineering

Fenghour Abdelhamid, Ph.D., Associate Professor, Department of Chemical Engineering

Mehran Sohrabi, Ph.D., External Examiner, Professor, Director, Centre for Enhanced Oil Recovery and CO_2 Solutions, Heriot Watt University Edinburgh

Dissertation Director: Shi-Yi Zheng Ph.D, Professor, Department of Petroleum Engineering

Declaration

I declare that this thesis

Statistical & Numerical Density Derivatives Application in Oil and Gas Well Test Interpretation

Is entirely my own research under the supervision of Prof. Shi-Yi Zheng and Dr. Donglin Zhao. The research was carried out in the Department of Chemical Engineering at London South Bank University. All published and unpublished material used in this thesis has been given full acknowledgement. None of this work has been previously submitted to this or any other academic institution for a degree or diploma, or any other qualification.

Biu Torkiowei Victor

PhD student

Department of Chemical Engineering

London South Bank University

Dedication

I dedicate this work to ALMIGHTY GOD, For His Wisdom and Knowledge freely given to me

Acknowledgment

I wish to express my sincere gratitude to my supervisor Professor Shi-Yi Zheng for providing me with excellent academic, professional, constructive and personal guidance during my 4 years on this research work. The completion of this thesis is the fruit of his renowned knowledge and in-depth experience of the subject. He has always broadened my perspective with better insight from anew point of view after each fruitful discussions. The past 4 years has been challenging and fun for me. I would like to thank Dr Donglin Zhao for all the help he accorded me to successfully complete this research work.

The methods presented in this thesis revolve around the new approach to improve interpretation of pressure transient data (statistical & density derivatives application in oil and gas reservoirs model

Appreciation to staffs, friends and colleagues at London South Bank University, Total S.A and EAGE Conference for providing the opportunities for many interesting discussions that have contributed to this work. Thanks to Oscar Fraute, for sharing your ideas on the subject. Also to Amara and Marvellous for proofreading and editing the published papers and thesis.

I wish to acknowledge Total S.A for paying my salary throughout this research work which helps to support my work financially. To my father and mother (Ebenadou and Cecilia Biu), my father and mother in laws (Michael and Felicia Adhekoyibo), my brothers Charles, Emmanuel and Andrew, families; Prisci, Mariam, Victor Edet etc and friends, Stanley, Obinna, Paul who were source of constant encouragement. I am indebted to my wife Edeosiwi, children Caleb and Valerie for denying them valuable time all these years. This is as much their accomplishment as mine and I look forward to making up.

London, October 2016
Biu Victor Torkiowei

List of publications

Biu..V T. and Zheng, S-Y,(2016) "Numerical Density Diffusivity Equation and Numerical Derivatives - A Generalised Approach for Well Test Analysis", *Int. J. Petroleum Engineering,* Vol. 2, No. 2, pp.91–124

Biu, V.T. and Zheng, S-Y. (2016) "A new approach in pressure transient analysis part I: improved diagnosis of flow regimes in oil and gas wells", *Int. J. Petroleum Engineering*, Vol. 2, No. 1, pp.38–59

Biu .V.T. and Zheng S.:"A New Approach in Pressure Transient Analysis: Using Numerical Density Derivatives to Improve Diagnosis of Flow Regimes and Estimation of Reservoir Properties for Multiple Phase Flow." *Journal of Petroleum Engineering Volume* 2015 (2015), Article ID 214084, 16 pages

Victor BT, Shi-Yi Z (2015) A New Approach in Pressure Transient Analysis Part I: Improved Diagnosis of Flow Regimes in Oil and Gas Wells. *J Pet Environ Biotechnol 6*: 244. doi:10.4172/2157-7463.1000244

Victor BT, Shi-Yi Z (2015) Distinctive Flow Regions in Crossform Fracture Model in Shale Gas Reservoir Using Numerical Density Derivative Part 3. *J Pet Environ Biotechnol* 6: 245. doi:10.4172/2157-7463.1000245

Biu..V T. and Zheng, S.Y,: *"A New Approach In Pressure Transient Analysis Part I: Improved Diagnosis Of Flow Regimes In Oil And Gas Wells"* Proceedings of Third EAGE/AAPG Workshop on Tight Reservoirs in the Middle East Abu Dhabi, October 4-6, 2015

Biu..V T. and Zheng, S.Y,: *"A New Approach in Pressure Transient Analysis: Using Numerical Density Derivatives to Improve Diagnosis of Flow Regimes and Estimation of Reservoir Properties for Multiple Phase Flow"* Proceedings of First Thermal and Fluids Engineering Summer Conference organized by ASTFE, New York, USA, 9-12 August, 2015.

Biu..V T. and Zheng, S.Y,: *"Distinctive Flow Regions in Crossform Fracture Model in Shale Gas Reservoir Using Numerical Density Derivative Part 3*" Proceedings of 77th EAGE Conference and exhibition, Madrid, Spain, 1-4 June, 2015.

Biu..V T. and Zheng, S.Y,: *"Distinctive Flow Regions in Crossform Fracture Model in Shale Gas Reservoir Using Numerical Density Derivative Part*" Proceedings of First Thermal and Fluids Engineering Summer Conference organized by ASTFE, New York, USA, 9-12 August, 2015.

Table of Contents

List of table

List of Figure

Other Figures in Appendix

Nomenclature

P = Pressure psi

T = Temperature ^{o}F

rw = Wellbore radius , ft

k = formation Permeability md

Ø = Porosity fraction

μ = Viscosity cp

t = Time hrs

q = Production rate bbl/day

B = Formation volume factor rb/Stb

qg = Gas rate, Mscf/day

Q = Cumulative production, STB

Ct = Total compressibility psi-1

rw = Wellbore radius ft

Δp = Change in pressure psia

h = Reservoir thickness ft

A = Drainage Area acres

C_A = Area compressibility psi-1

S = Skin dimensionless

Cs = Wellbore storage constant

Pwf = Bottom hole flowing pressure psi

Pi = Initial Pressure psi

m(p) = Pseudopressure (gas), psi2/cp

Pf = Fracture pressure psia

tp = Cumulative production time

Cs = Wellbore storage constant

k_f = fracture permeability of dual porosity models, md

km = Matrix permeability, md

kx =Permeability in the X-direction, md

ky =Permeability in the Y-direction, md

kz =Permeability in the Z-direction, md

w_f = fracture width ft

x_f = fracture half-length ft

wf = fracture width ft

A_{mf} = Fracture cross-sectional area to flow ft2

Bgi = Formation volume factor at initial reservoir pressure, rcf/scf

D = Diameter, fracture spacing, ft

l = Half of fracture spacing, ft

Dimensionless parameters

PflD = Dimensionless pressure in the fracture

Pm = Matrix pressure psia

PmlD = Dimensionless pressure in the matrix

qlwD = Dimensionless well rate based on matrix-fracture

tDXf = Dimensionless time coordinate

tDA=Dimensionless time based on fracture matrix geometry

yD = Dimensionless reservoir length (rectangular geometry)

xD = Dimensionless reservoir length (rectangular geometry)

LfD =Dimensionless fracture length

zD = Dimensionless coordinate, z-direction

Statistical parameter and other variables

xw =X-Cartesian coordinates of the production point

yw =Y-Cartesian coordinates of the production point

zw =Z-Cartesian coordinates of the production point

f(s)= Relation used in Laplace space to distinguish matrix geometry types

Z = Difference between two point/ time series

i = Subscript of an observed variable

c = Subscript of a calculated variable

Cov = Covariance of data point

δ = Standard deviation

STEYX = SSE of data point

n = Number of data point

δ = Standard deviation

Z = Difference between two point/ time series

$\bar{x}$ = Mean of data point

dz = Well position in reservoir, dimensionless

l−1 = Inverse Laplace space operator

L = General fracture spacing, ft

r = Radial geometry coordinate

s = Laplace space variable

S = Skin dimensionless

x = Observed or sample values of a variable

y = Observed or sample values of a variable

Subscript

i =initial

D=dimensionless

f =fracture system

g = gas

m =matrix

mf =total system (fracture+matrix)

P = Pressure

n = Number of data point

flD= Subscript of dimensionless fracture variable

mlD= Subscript of dimensionless matrix variable

i = Subscript of an observed variable

c = Subscript of a calculated variable

z = Coordinate, z-direction (matrix)

x = Observed or sample values of a variable

y = Observed or sample values of a variable

Abbreviation

PENA; Pressure Equivalent of Density Weighted Average

LBPR Local Grid Bottomhole Pressure

LDENO Local Grid Oil Density

LDENW Local Grid Water Density

LDENG Local Grid Gas Density

WBHP Well Bottomhole Pressure

BPR = Well Bottomhole Pressure

PDENOIL = Pressure Equivalent of LDENO

PDENGAS = Pressure Equivalent of LDENG

PDENWAT = Pressure Equivalent of LDENW

PDENDWA =Pressure Equivalent of Density Weighted Average (LDENO LDENG & LDENW)

Statdiff; Statistical difference

Statdev; Statistical deviation

Statdev (SQR); Square-root of Statistical deviation

StatSSE; Statistical sum of square error

Statdiv; Statistical divisible

Stdev; Standard deviation in Excel sheet

VEMST; Victor, Emmanuel, Mike Statistical techniques

SSE; Sum of Square Error

MSE; Mean Square Error

Δp = Pressure difference between point two time interval

PPD = Primary pressure derivative function

WBHP= Well bottomhole pressure

LGR= Local grid refinement

Abstract

Traditional transient well test analysis has been largely based on draw down solution, which works for the reservoir engineering problems of isothermal, uniform and single phase flow in porous media. After so many years of efforts on multi-phase flow approach, methods such as pseudo-pressure approach has been limited. Numerical well testing approach for multi-phase flow problems is the only method currently under further investigation.

Presented in this study are three analytical approaches. (1) Statistical pressure derivative which utilises the 2nd differencing of pressure and time series since pressure change and subsurface flow rate are non stationary series, then integrates the residual of its 1st differences using simple statistical functions such as sum of square error SSE, standard deviation, moving average MA and covariance of these series to formulate the model. (2) Pressure-density equivalent algorithm for each fluid phase, which is derived from the fundamental pressure-density relationship and its derivatives used for diagnosing flow regimes and calculating permeability. (3) Density transient analytical DTA solution derived with the same assumptions as (2) above, but the density derivatives for each fluid phase are used along with the semi-log density versus time plot to derive permeability for each fluid phase. (2) and (3) are solutions for multi-phase flow problems when the fluid density is treated as a function of pressure with slight change in density.

The first method demonstrated that for high water production well, a good radial stabilization can be identified for good permeability estimation without smoothing the data. Also it showed that in cases investigated, the drawdown fingerprint can be replicated in the build-up pressure response, hence a good match of the data and a better radial flow diagnosis.

The second and third methods can, not only derived each individual phase permeability, the derivative response from each phase is visualised to give much clearer picture of the true reservoir response, which in return ensures that the derived permeability originates from the

formation radial flow. These approaches were tested with synthetic and field data. The synthetic studies demonstrated that the calculated numerical density derivatives on the diagnostic plot yield much clearer reservoir radial flow regime and give more confident formation permeability estimation. The study also discovered that in the cases investigated, the heavier the fluid such as water, the better permeability estimation from the weighted average pressure-density equivalent derivatives.

In order to support further field application of this approach, field data sets were identified and analysed using the developed methods. In this case, the conventional pressure derivative diagnostic method failed to identify the radial flow, hence unable to estimate the reservoir permeability. In contrast, the three methods: statistical pressure, fluid phase numerical density and pressure-density equivalent derivatives gave very clear radial flow stabilizations on the diagnostic plot, from which the reservoir permeability was derived, which matched the up scaled core permeability from the same formation. The presented approaches provide an estimation of the individual fluid phase and formation effective permeabilities, reflecting the contribution of each phase to flow at a given point.

Thesis Organization

Chapter 1 contains introduction to PTA, research statement of problem, objective and methodology.

Chapter 2 reviews the evolution of the derivative method in PTA, its applications and limitations in conventional oil and gas reservoirs.

Chapter 3 introduces the statistical derivative approach, its mathematical formulation, assumptions and summary of the statistical derivative models. This chapter also presents the comparison of the statistical derivative approach with the conventional derivative using synthetic and design data. Examples of several reservoir architectures with log-log derivative curves and estimated k's are generated and presented.

Chapter 4 introduces the numerical density derivative approach, its mathematical formulation, assumptions and numerical simulation results of its application in six investigated cases. This chapter also presents the density transient analysis DTA (radial flow) equation derivation for each fluid phase for practical application of the method using numerical synthetic data.

Chapter 5 reviews the evolution of derivative and type curves method in unconventional reservoirs with fracture systems, identifying the possible number of flow regions. It presents the numerical density derivative approach in low k reservoirs and introduction of crossform fracture. The density derivative approach is tested with synthetic numerical data simulated with constant pressure and constant rate solutions.

Chapter 6 test the statistical and numerical density derivative application with field data.

Chapter 7 contains conclusion and recommendations for the future work.

Chapter one

1.1 Introduction

Flow in a reservoir is often characterized as either transient or boundary-dominated. Transient flow occurs when the reservoir boundaries have not been felt, in which the reservoir is said to be infinite-acting during the early life of a well. In reality, the size of the reservoir has no effect on the well productivity and performance, and from analysis of pressure or production data, nothing can be deduced about the reservoir size. Transient flow forms the basis of a domain of reservoir engineering called Pressure Transient Analysis (PTA), also known as well test interpretation, which is used for volumetric estimation, well deliverability, reservoir characterization and efficient field management. However, its accuracy depends on precise analysis and integrated reservoir studies. For over four decades, well testing has been transformed from a level mainly interested in determining a well's productivity to a sophisticated discipline capable of characterising the reservoir geometry, boundary and heterogeneity [83] [59][32][44[41][47][89].

Pressure transient analysis depends strongly on complex equations of fluid flow for a well flowing at a constant rate. At the initial conditions, the flow regime is transient, but when all the reservoir boundaries have been felt, the well flows at steady state (if a constant pressure boundary exists) or at pseudo-steady state (if all the boundaries are no-flow boundaries). It is well-known that during pseudo-steady state, the pressure throughout the reservoir declines at the same rate, and the reservoir is assumed to be acting like a tank. The theory of pseudo-steady state is applicable to a situation where the well is flowing at a constant flow state; however for an infinite- acting reservoir system, if there is a single well which is producing, the pressure distribution of this well as time changes is constant. Invariably, a well depicts infinite-acting reservoir condition if the boundary response has not been felt but immediately the pressure perturbation hits the boundary, the well is no longer infinite-acting in nature but in pseudo steady state flowing condition. Similarly, for an enclosed reservoir system with a

single producing well, the pressure distribution of this well can be described as boundary dominated which is pseudo-steady in nature when the pressure hits the boundary. Modelling the processes that governed these flowing conditions entails complex mathematical equations that have been simplified over the years by researchers, thereby introducing the pressure derivative which has remained a diagnostic tool for pressure transient analysis.

1.2 Statement of Problem

Pressure transient analysis techniques have advanced significantly over the past four decades with different methods currently available. However, for practice, each current method of transient data analysis has its own strengths and limitations with no single pressure and production data analysis method capable of handling all types of data and reservoir types with reliable result [42].

The analytical solution for PTA is limited to single phase flow which is unobtainable in field cases. In reality, production conditions with multiple phases are prompt to noisy data and difficult to interpret. Presently, there are few literatures or researches on multiphase PTA; therefore it is difficult to filter rate effect, fluid phase segregation or real reservoir fingerprint etc., in this condition. It has been noted that the current rate transient analysis (RTA) and pressure transient analysis (PTA) methods are inadequate for transient pressure data. A quality check (QC) approach is required so that the long-term noise and multiphase phase effects in most transient pressure data can be resolved to support the traditional analysis methods. It is this demand that motivated our research.

1.3 Objective

The main objective of this thesis is to develop an algorithm for analysing pressure transient data for different wells and reservoir conditions with noise and multiphase effect using

statistical formulation and numerical density approach. Therefore additional reservoir diagnostics and distant reservoir features, such as reservoir boundaries can be obtained. The result will serve as a reference tool for transient data analysis in complex reservoir architectures.

1.4 Significance of Study

This work addressed a wide spectrum of PTA while achieving the following significances;

- Promote an improved understanding of the limitation of the derivatives approach in near-wellbore effects in oil and gas reservoirs from well testing, with various well and reservoir characteristics and to use this understanding to develop new methods to better the interpretation of such complex conditions.
- Develop a new method (Statistical and Numerical density derivative) for analysing and diagnosing flow regimes and boundary response. Then estimate wellbore and reservoir parameters such as mobility, phased permeability in comparison with the existing reservoir diagnostic reference tools (derivative and type-curve).
- Test the approach with well test data from different oil and gas reservoirs (conventional and non conventional) obtained from synthetic, design and field cases.

1.5 Benefit

- The new algorithm developed from this study will help to provide a better understanding of overdependence and limitation of pressure derivatives and type curve approach which has remained the focus for over four decades in PTA. It will serve as a support tool to the derivatives approach, thus improve interpretation in complex reservoir systems with wide range of models solution (bounded aquifers, double porosity, horizontal fracture, vertical fracture, unconfined aquifer, etc.).

- Results from this work will provide new approach for estimating possible fluid phase permeabilities and the % of each phase contribution to flow at a given point, hence at several dp' stabilisation point, the relative k can be obtained. This will provoke further research on determining relative permeability data from field dynamic data (well test acquisition) instead of the lab.
- Substantial amount of knowledge acquired through this research will serve as reference tools to academia, industry partners and corporate body for reservoir modelling, characterization and management.

Chapter Two

Review of derivative and type curve methods in PTA

2.1 Introduction

Muskat [57] and Theis [74] introduced the fluid flow diffusivity model using only a small fraction of data to mimic fluid flow from producing water well assuming constant fluid compressibility and deformation of the aquifer behaviour. The model advanced into a complex diffusivity fluid flow equation used in PTA. PTA depends strongly on this complex fluid flow equation which is used to modelled the behaviour of a well flowing at a constant rate.

In 1949, Van Everdingen and Hurst [80] simplified the complex diffusivity model using Laplace transformation in flow problem and published solutions of the diffusivity equation which is the basis of PTA. Since then, more work has been done by renowned researchers such as MDH [55] who introduced the specialised pressure-time curve used for reservoir characterization. Horner [39] modified the method using the cumulative production time concept for wells with production history before shut-in for pressure build-up. This accounted for the superposition time effect resulting from the flowing period even after the well has been shut in. In 1954, MBH [52] worked on the specialised pressure time curve, thereby introducing the average reservoir pressure P* determination method. Poor gauge resolution, abrupt well operation interference and wellbore fluid compressibility issues resulting to a noisy Δp on the specialised pressure time plot, and difficulty in determining the radial flowing period, necessitated an improved reservoir model description for easier and faster identification of flow regimes. This prompted Agarwal [2] to introduce the dimensionless type curve using pressure function which helps to reduce the degree of uncertainties in the estimation and interpretation of the pressure-time result.

In 1979, Gringarten [33] and Ramey [70] proposed various dimensionless type curve for different well and reservoir conditions. Gringarten [33][35] improved on the type curve

developed by Agarwal [2] to produce a unique solution by plotting log P_D vs $\log(t_D / C_D)$ for several large range of wellbore / skin values C_De^{25}.

Gringarten and Ramey [34] also developed dimensionless type curve using pressure functions which is used for estimation and interpretation of the pressure-time curve results. Figure 2.1 is an example of a developed type curve by Bourdet [14].

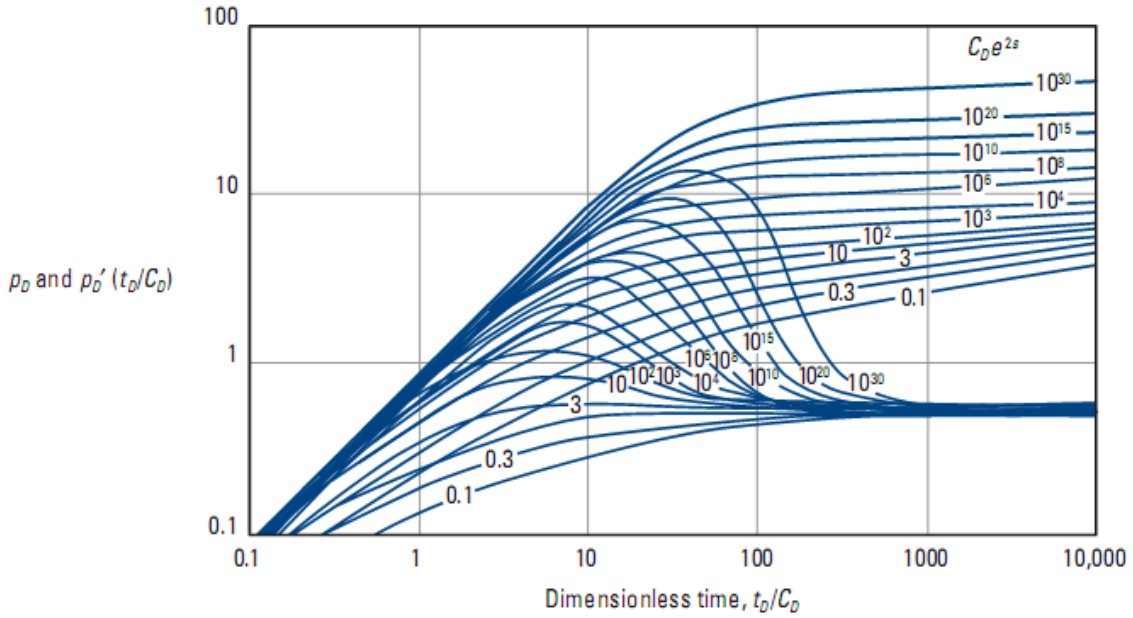

Figure 2.1: Type curves for a well with wellbore storage and skin effects [14]

The term Δp which is the initial pressure minus the measured pressure data point is plotted against Δt which is the time from the start of the test. Both delta pressure and delta time are plotted on a log-log scale. The well test analyst obtains a match between the type-curve and actual data by horizontal and vertical shifts of the data. Once a match is obtained, reservoir parameters such as permeability, skin, and storage coefficients are determined. Several type curves with different reservoir and boundary conditions were presented by researchers to improve the interpretation of PTA.

In well test interpretation, several flow regimes as seen in Figure 2.2 that exhibit characteristic flow patterns such as radial, spherical, linear and bilinear [27] are often present in a given test, however, identification of radial flow is paramount to compute values for

permeability (k) and skin factor (S). Different researchers attempted to improve the type curve matching approach toward capturing radial flow regions, nevertheless their solutions were non-unique.

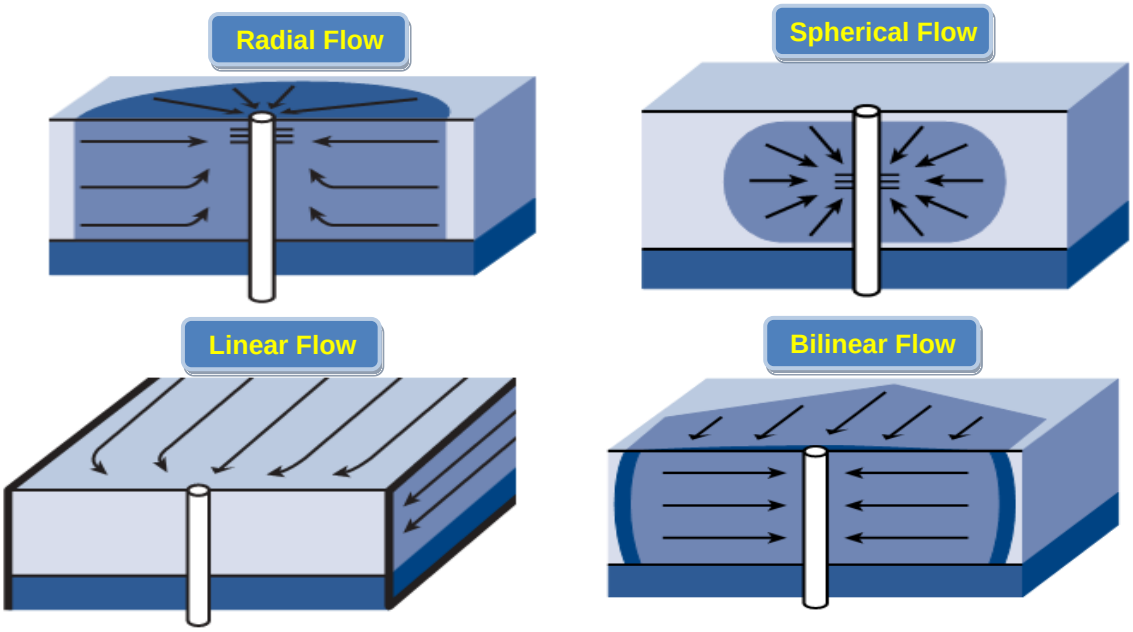

Figure 2.2: Distinct flow patterns in pressure transient tests design by Ehlig-Economides [27]

Identification of radial flow in PTA was still a difficult task for well test specialist, reservoir engineers and petroleum engineering researchers before the early eighties until the emergence of the derivative approach. The derivative method which is the greatest breakthrough in well test analysis was pioneered by Tiab [75] and advanced by French Mathematician Dominique Bourdet [14] in 1983. It has remained the reference solution for identifying flow regime, observing boundary response and diagnosing complex reservoir features till-date. This approach has helped to reduce the uncertainties surrounding the interpretation of well test data because key regions of radial flow and boundary features have been adequately diagnosed. However, due to the non-unique solution of the mathematical fluid flow equation mostly in heterogeneous reservoir, most engineers in the industry are compelled to use analytical model and type curve solution to match complex model which is

often times unrealistics. Assumptions made are ignored while pursuing a perfect match and results obtained from this approach are often misleading [92].

This marked the beginning of numerical well testing in the industry by Zheng [91]. This approach started from the early 1990s [38] [9][51][25][93][91]. Further advancement were made by Zheng [92] in 2006, providing more solutions to the non-unique solution problems in heterogeneous reservoir through numerical well testing, thereby promoting its application. More papers have been published by researchers on the subject reflecting the advancement of numerical well testing and its application in solving various reservoirs engineering practical problem.

Also in 2009, Biu et al [13] introduced the VEMST approach in diagnosing different flow regimes. This method involved estimating statistical pressure derivatives from pressure values using differencing approach. The technique was tested with different wellbore and reservoir conditions and the result showed similar log-log diagnostic response for all cases studied which included, channel sand, dual porosity, infinite conductivity fracture system, infinite acting system and stimulated well.

Summarily, one limitation of the derivatives is diagnosing flow regimes in multiphase flow condition around the wellbore; the derivative data are often noisy and difficult to interpret, resulting to the application of deconvolution and various smoothing techniques to obtain a perceived representative model, which often may alters the characteristics of the data. Therefore the application of the existing single phase analytical solution of PTA equation in multiphase condition is unreliable. Also, it is often difficult to clearly identify radial flow from PTA data in complex reservoir structures such as complex faulted systems, high permeability streak with interbedded shales, deepwater turbidite systems, channel-levee and lobe deposits etc.

In this study, the statistical pressure and numerical density derivative will be tested in both conventional hydrocarbon and shale gas reservoirs.

2.2 Derivation for single well pressure diffusion

Pressure transient analysis is based on the radial diffusivity equation which relates pressure to time and drainage radius. The simplest solution to this equation is valid for a single well in an infinite reservoir. The radial diffusivity equation is given by:

$$\frac{d^2P}{dr^2}+\frac{1}{r}\frac{dP}{dr}=\frac{1}{0.0002637}\frac{\phi\mu c_t}{k}\frac{dP}{dt} \tag{2.1}$$

Where the units of viscosity μ are in cp, permeability k is measured in mD, pressure P in psi, radius r in ft, compressibility ct as psi^{-1}, and time t in hours while porosity ϕ is dimensionless. The solution to the radial diffusivity equation 2.1 enabled reservoir engineers, fluid flow specialist and the academia to perform a conventional analysis for various bottom-hole pressure tests. Unfortunately, the assumptions made within the diffusivity solutions are not always applicable to all bottom-hole pressure tests.

For a closed reservoir system with single phase fluid and single producing well, the two possible flow regimes expected to be encountered includes: 1st flow state (radial flow) and 2nd flow state (pseudo-steady). The pressure distribution function and its derivation in the transient and pseudo-steady condition are outlined below:

2.3 Transient Flow:

The pressure distribution in the infinite reservoir is a function of the time and the distance to the producing well (space) which is expressed by the Exponential Integral function:

$$\Delta p(t,r)=-0.5\frac{141.2qB\mu}{kh}\left[-Ei\left(\frac{-\phi\mu c_t r^2}{0.001056kt}\right)\right] \tag{2.2}$$

For small x value $Ei(-x) = -\ln(\gamma x)$, the Exponential Integral can be approximated by a log function (with $\gamma = 1.78$, Euler's constant). Therefore:

$$\Delta p(t,r) = \frac{162.6qB\mu}{kh}\left[\log\left(\frac{-0.000254kt}{\phi\mu c_t r^2{}_w}\right)\right] \tag{2.3}$$

Where q is rate bopd, β is formation volume factor rb/stb

Hence the primary pressure derivative function here can be written as:

$$PPD' = d\Delta p = t\frac{dt}{cons\tan t} \tag{2.4}$$

And also the logarithmic derivative function can be expressed as:

$$\frac{d\Delta p}{d\ln t} = t\frac{d\Delta p}{dt} \tag{2.5}$$

2.4 Pseudo Steady State Flow (closed reservoir)

For closed reservoir systems, when all boundaries have been reached, the flow regime changes to pseudo steady state. The shape of the pressure profile becomes linear with time, and it simply declines as the reservoir is being depleted. During the pseudo steady state flow regime, the bottom-hole flowing pressure is a linear function of the elapsed time; hence the change in pressure is given as:

$$\Delta p = 0.234\frac{qB}{\phi c_t hA}t + 162.6\frac{qB\mu}{kh}\left[\log\frac{A}{r^2{}_w} - \log(C_A) + 0.351 + 0.87s\right] \tag{2.6}$$

While the primary pressure derivatives are given as:

$$\frac{d\Delta p}{dt} = \Delta p = \frac{d(p_i - p_{wf})}{dt} = 0.234\frac{qB}{\phi c_t hA} \tag{2.7}$$

And the Logarithm derivatives as:

$$\frac{d\Delta p}{d\ln t} = t\Delta p = \frac{td\Delta p}{dt} = 0.234\frac{qB}{\phi c_t hA}t \tag{2.8}$$

So the primary derivative of the pressure response versus time on log-log plot will be a zero slope line, while the corresponding logarithmic derivative on log-log scale is a constant value as seen in Figure 2.3 [94].

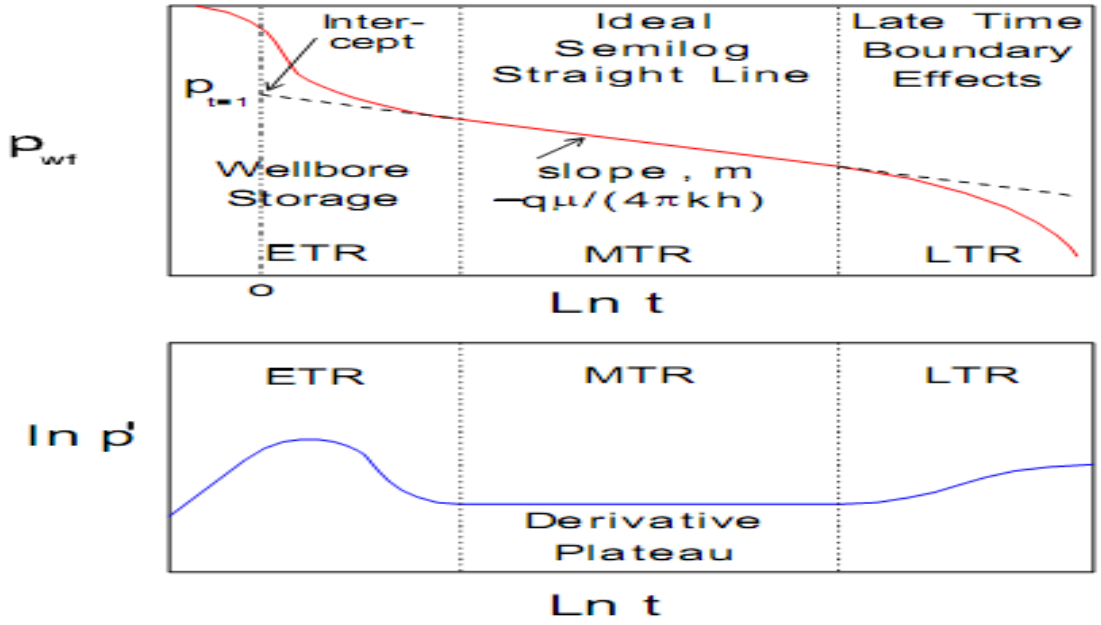

Figure 2.3: Schematics of a well test diagnostic plot after Zheng [94]

The diagnosis of flow regimes which appear as distinctive patterns in the pressure-derivative curve, is a vital point in well test interpretations since each flow regime reflects the geometry of the flow streamlines in the tested formation. Hence for each flow regime identified, a set of well and/or reservoir parameters can be estimated using the region of the transient data that exhibits the characteristic pattern behaviour [13]. These flow regimes exhibit characteristic flow patterns such as radial, spherical, linear and bilinear [27]; and are recognized as a horizontal line, negative half slope, half slope and quarter slope on the pressure-derivative curve.

The mathematical formulation for the pressure derivative by Horne [37] is given as:

$$\left(\frac{\partial p}{\partial \ln t}\right) = t\left(\frac{\partial p}{\partial p}\right)_i - A \tag{2.9}$$

where

$$A = \frac{\ln\left(t_i / t_{i-k}\right)\Delta p_{i+j}}{\ln\left(t_{i+j}/t_i\right)\ln\left(t_{i+j}/t_{i-k}\right)} + \frac{\ln\left(t_{i+j}t_{i-k}/t_i^{\,2}\right)\Delta p_i}{\ln\left(t_{i+j}/t_i\right)\ln\left(t_i/t_{i-k}\right)} - \frac{\ln\left(t_{i+j}/t_i\right)\Delta p_{i+k}}{\ln\left(t_i/t_{i-k}\right)\ln\left(t_{i+j}/t_{i-k}\right)}$$

[22]

Several sets well and reservoir models have been generated using the derivative model. Likewise, several type curves which accounts for different combinations of wellbore, reservoir characteristics, boundary effects associated flow regimes, and also for computation of well and reservoir parameters. This demonstrates that the log-log plot of the pressure-derivative is a powerful tool for model identification in pressure transient analysis.

However, in practice, each current method of transient data analysis has its own strengths and limitations with no single pressure and production data analysis method capable of handling all types of data and reservoir types with reliable result [42]. The log derivative and derivative type-curve which have remained reference flow regimes diagnostic tools for over four decades are the only unified approach for well-test interpretation and are applicable in a wide range of situations.

For situations where the production rates are varying, recovery data with changing sampling frequency have to be interpreted or there is time shift errors effect, the derivative diagnostic plot is conditionally used provided the data are pre-processed by a deconvolution technique. This shows that the derivative diagnostic plots have some limitations; hence a checkbox is needed to support its interpretation on various reservoir and well models with complex and varying frequency data.

Chapter Three

Statistical Pressure Time Curve and Derivative

3.1 Introduction

Pressure change in the formation caused by production or shut-in (drawdown, or build-up) can be modelled by a second order partial differential equation from the hydraulic diffusivity equation. For radial flow systems, the corresponding equation is:

$$\frac{d^2P}{dr^2}+\frac{1}{r}\frac{dP}{dr}=\frac{1}{0.0002637}\frac{\phi\mu c_t}{k}\frac{dP}{dt} \tag{3.1}$$

Simplifying the above equation considering the assumptions for modelling radial flow in pressure transient analysis, a unique solution for steady and pseudo-steady state condition is obtained. Therefore the primary pressure derivative function is given as:

$$PPD' = d\Delta p = t\frac{dt}{cons\tan t} \tag{3.2}$$

And also the logarithmic derivative function can be expressed as:

$$\frac{d\Delta p}{d\ln t}=t\frac{d\Delta p}{dt} \tag{3.3}$$

In closed reservoirs systems, when all boundaries have been reached, the flow regime changes to pseudo steady state. The shape of the pressure profile becomes linear with time, and it simply declines as the reservoir is being depleted. During the pseudo steady state flow regime, the bottom-hole flowing pressure is a linear function of the elapsed time; hence the change in pressure is given as:

$$\Delta p = 0.234\frac{qB}{\phi c_t hA}t+162.6\frac{qB\mu}{kh}\left[\log\frac{A}{r^2{}_w}-\log(C_A)+0.351+0.87s\right] \tag{3.4}$$

While the primary pressure derivatives are given as:

$$\frac{d\Delta p}{dt}=\Delta p=\frac{d\left(p_i-p_{wf}\right)}{dt}=0.234\frac{qB}{\phi c_t hA} \tag{3.5}$$

And the Logarithm derivatives

$$\frac{d\Delta p}{d\ln t} = t\Delta p = \frac{td\Delta p}{dt} = 0.234\frac{qB}{\phi c_t hA}t \tag{3.6}$$

The new methods tend to derive the pressure derivative functions $\frac{d\Delta p}{dt} = \frac{d(p_i - p_{wf})}{dt}$, $\frac{d\Delta p}{d\ln t} = t\Delta p = \frac{td\Delta p}{dt}$ using 1st and 2nd pressure and time series differencing with the series differences residuals modeled with statistical parameters. The statistical models are derived from differencing method in time series analysis which is common in advanced statistical forecasting where it is often used to transform a non-stationary time series into a stationary time series.

3.2 Stationary and non stationary model

Time series forecasting, takes an existing series of data $x_{t-n},\ldots,x_{t-2},x_{t-1},x_t$ and forecasts the $x_{t+1},x_{t+2},\ldots$ data values. Most often, the goal in time series analysis is to observe or model the existing data series to mimic the past and predict the future unknown/missing data accurately. Examples of data series include financial data series (stocks, indices, rates, etc.), physically observed data series (sunspots, weather, etc.), and mathematical data series (Fibonacci sequence, integrals of differential equations, etc.). The phrase "time series" generically refers to any data series, whether the data are dependent or independent on a certain time increment [28]. It also accounts for data points taken over time that may have an internal structure (such as autocorrelation, trend or seasonal variation).

A common assumption in many time series techniques is that the data are stationary. A stationary process has the property that the mean, variance and autocorrelation structure do not change over time [64]. Intuitively, a time series is stationary if the statistical properties such as mean and variance of the time series are essentially constant through time. If the time

series is not stationary, it can be transformed to stationarity with one of the following techniques.

- Take the difference of the data. That is, given the series X_t, the new series will be:

$$z_t = x_t - x_{t-1} \tag{3.7}$$

- The differenced data will contain one less point than the original data. Although more than one difference can be taken. Nevertheless one difference is usually sufficient.
- If the data contain a trend, some type curve is fitted to the data then models the residuals from that fit. Since the purpose of the fit is to simply remove long term trend, a simple fit, such as a straight line, is typically used.
- For non-constant variance, taking the logarithm or square root of the series may stabilize the variance. For negative data, suitable constant to make all the data positive is added before applying the transformation. This constant can then be subtracted from the model to obtain predicted (i.e., the fitted) values and forecasts for future points.

The above steps are intended to generate series with constant mean and variance. The following plots are from oil and gas synthetic pressure data during a shut-in condition.

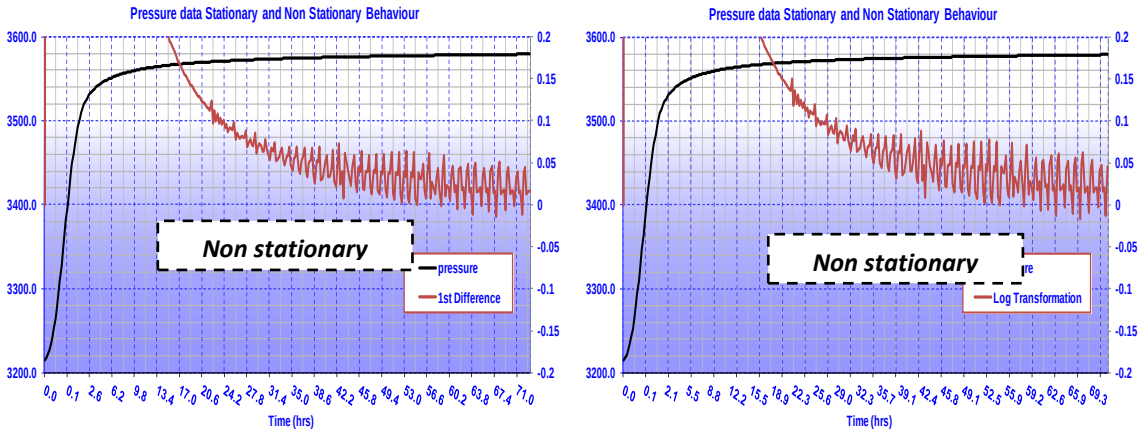

Figure 3.1:1st difference and log transformation series for pressure-time data showing non stationarity in early part of the data

The pressure data in Figure 3.1 indicates a pressure build-up and stabilisation after 25 hrs. A visual inspection of this plot indicates a constant mean and variance after 20 hrs. However the 1st difference of pressure series and log transformation of pressure depicts a non stationary behaviour up to 45 hrs of the data which is within the range of radial flow period, therefore depicting that the 1st difference is insufficient to analyse the data.

Figures 3.2 a and b show the 2nd differences of pressure series and log transformation of pressure which infers that the data have a constant location and variance after 2-4 hrs, although the early part depart from the model in a systematic way. In this case, the data have been transformed to stationary series and suitable for integrating the residual of the 1st pressure differences using statistical parameters. This is the foundation of the statistical derivatives.

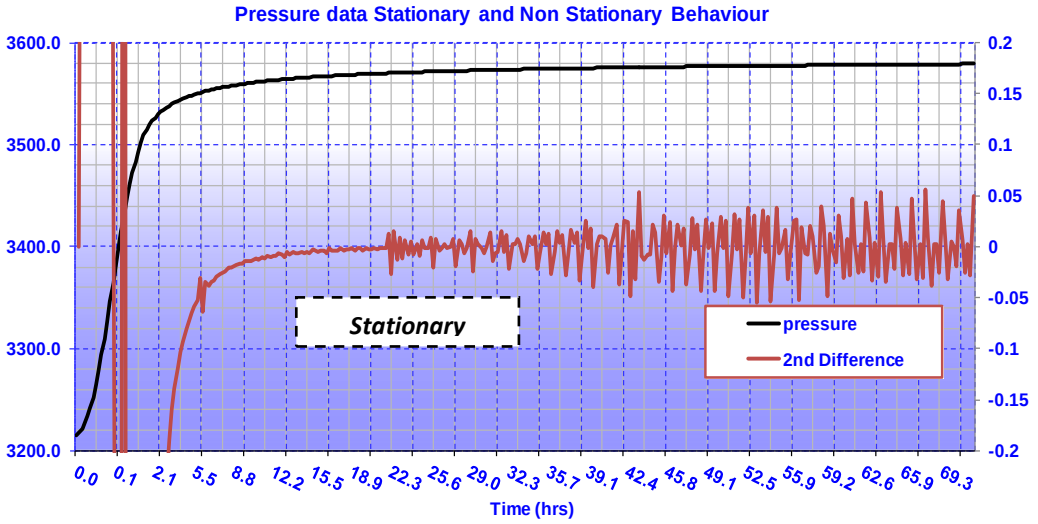

Figure 3.2a:2nd difference for pressure time showing data transformation to stationary series

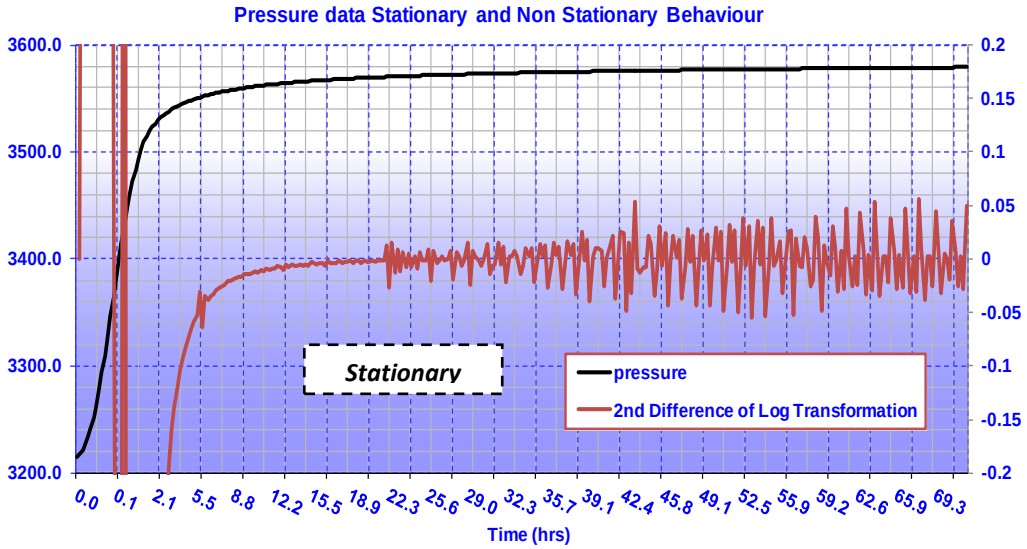

Figure 3.2b:2nd difference log transformation showing data transformation to stationary series

The new statistical models tend to integrate the residual of the 1st pressure and time difference series into the 2nd pressure differences of pressure and time using statistical functions such as sum of square error SSE and standard deviation; then, divide second difference of pressure series in reference to the initial point. The physics of the approach is that for any event, there is a likelihood that the pressure series will behave in a stationary way i.e., constant mean and variance of the data during each event, hence the stationarity of the pressure - time series are integrated in the statistical model with the application of STDEV and STEYX functions on the residual of 1st difference pressure series.

If n values of P_1, P_2,……. P_n of a given pressure-time series are observed, a plot of these values against time can be used to determine whether or not the time series is stationary. If the n values seem to fluctuate with constant variation around a constant mean, then it is reasonable to assume that the time series is stationary. However, if the n values are stable around a constant mean or with constant variation, then it is reasonable to assume that the time series is non-stationary.

The first difference of the pressure series values P_1, P_2,…… P_n are;

$$z_t = p_t - p_{t-1} \quad (3.8)$$

Where t = 2...n

To illustrate, the original values and the difference values of a pressure series are listed where subscript of z denotes the stage of the difference i.e., first, second or third etc.

Original values	First Difference	Second Difference
P_1		
P_2	$z_2 = P_2 - P_1$	
P_3	$z_3 = P_3 - P_2$	$z_3 = P_3 - P_2 - P_1$
P_{n-1}		
P_n	$z_n = P_n - P_{n-1}$	$z_n = P_n - P_{n-1} - P_{n-2}$

Although in statistical data analysis for time series and forecasting, the first difference may not accurately transform the non-stationary time series into stationary time series, hence the second difference approach serve as an alternative to such condition as we have seen in Figures 3.1 and 3.2.

3.3 Statistical Function Definition

In formulating the statistical model for this study, the residuals of the stationary function is needed, hence the following statistical parameters are used:

I. **Unexplained Variation;** Given n observation pairs $\{(x_1, y_1), \ldots, (x_n, y_n)\}$, the sum of squares error (SSE) is a measure of the variation of Y that is not explained by the regression equations. SSE is the sum of the squared differences between the observed values of Y and the calculated value of Y. This is the random variation of the observations around the regression line. The SSE is given as:

$$SSE = \sum (Y_i - Y_c)^2 \qquad [84] \tag{3.9}$$

Also the following formula can be used to hasten SSE calculation,

$$SSE = \sum Y^2 - A\sum Y - B\sum XY \quad [84] \tag{3.10}$$

II. **Standard Error of the Estimate:** The standard error of the estimate (SEE) is a measure of the accuracy of the estimating (regression) equation. The SEE indicates the variability of the observed (actual) points around the regression line (predicted points), i.e., it measures the extent to which the observed values (Y_i) differ from their calculated values (Y_c). Given the first two assumptions required for use of the regression model (for each value of X there is an array of possible Y values which is normally distributed about the regression line and the mean of this distribution (Yc) is on the regression line), the SEE is interpreted in a way similar to the way in which the standard deviation is interpreted. So, given a value for X, we would generally expect the following intervals (based on the Empirical Rule), the equation for the standard error of the predicted y is;

$$STEYX = \sqrt{\frac{1}{(n-2)}\left[\sum (y-\bar{y})^2 - \frac{\left[\sum (x-\bar{x})(y-\bar{y})\right]^2}{\sum (x-\bar{x})^2}\right]} \quad [96][84] \tag{3.11}$$

Where x and y are the sample means AVERAGE (known_x's) and AVERAGE (known_y's), and n is the sample size.

The SEE is equal to the square root of the MSE.

$$SSE = \sqrt{MSE} \tag{3.12}$$

Where

$$SSE = \frac{SSE}{n-2} \tag{3.13}$$

III. **Covariance:** Covariance is a measure of the association between two variables. Occasionally, this measure is less insightful by itself, but important in understanding the other measure of association, correlation [73].

The equation for Covariance is shown below.

$$Cov(X,Y) = \frac{\sum (x-\bar{x})(y-\bar{y})}{n} \quad [96] \qquad (3.14)$$

Where x and y are the sample means AVERAGE (array1) and AVERAGE (array2), and n is the sample size. Also the Standard deviation of a random variable is used for the model formulation.

The standard deviation of a random variable X is defined as:

$$\sigma = \sqrt{\sum \left(\left(X - \sum (X) \right)^2 \right)} = \sqrt{\sum \left(X^2 \right) - \left(\sum (X) \right)^2} \quad [96] \qquad (3.15)$$

Where E(X) is the expected value of X.

Not all random variables have a standard deviation, since these expected values need not exist. For example, the standard deviation of a random variable which follows a Cauchy distribution is undefined.

If the random variable X takes on the value x1.....xn (which are real numbers) with equal probability, then its standard deviation can be computed as follows. First, the mean of X, $\bar{x}$, is defined as a summation:

$$\bar{x} = \frac{1}{N} \sum_{I=1}^{N} x_i = \frac{x_1 + x_2 + ... + x_N}{N} \quad [84] \qquad (3.16)$$

Where N is the number of samples taken. Next, the standard deviation simplifies to

$$\sigma = \sqrt{\frac{1}{N} \sum_{i=1}^{N} (x_i - \bar{x})^2} \qquad (3.17)$$

In other words, the standard deviation of a discrete uniform random variable X, the above expression can also be replaced with

$$\sigma = \sqrt{\frac{1}{N} \sum_{i=1}^{N} x^2{}_i - \bar{x}^2} \quad [96] \qquad (3.18)$$

The goal of using these statistical parameters is to provide both positive and negative relationships of pressure and time (high correlation) in order to mimics the pressure

derivatives generated from differentiating the linear solution of the fluid flow diffusivity equation for radial systems.

3.4 Statistical Method

This section introduces the new statistical method for diagnosing flow regime for both flowing and shut-in conditions. The method utilize the 2nd differencing of pressure and time series since pressure change and subsurface flow rate are non stationary series and then integrate the residual of its 1st differences using simple statistical functions such as sum of square error SSE, standard deviation, moving average MA and covariance of data to formulate the model.

The statistical approach utilized simple statistical function such as the product and exponential of 1st and 2nd difference of a well bottom-hole flowing or shut-in pressure tied to the standard deviation; and sum of square difference of 1st difference residual series to generate the statistical diagnostic models such as StatDiv, StatSSE, StatDev, StatExp, StatTdev and StatDdev. These models help to identify key flow regimes for reservoir description and serve as checkbox to the derivative approach for better interpretation of complex features.

If n values P_1, P_2,……. P_n of a time series are observed, the first difference of the time series values P_1, P_2,…… P_n are;

$$\Delta P_t = P_0 - P_i \tag{3.19}$$

Where i = 1, 2, 3,……., t_n

$$StatDiv(i) = \frac{\Delta P_i}{P_i} \tag{3.20}$$

And

$$StatSSE(i) = \left[\frac{\Delta P_i}{P_2}\right]^{\frac{\delta dev}{SEE}} \tag{3.21}$$

Where $\frac{\delta dev}{SEE} = \left[\frac{STDEVP(StatDiv(\Delta P))}{STEYX(StatDiv(\Delta P), \Delta^2 P(i))}\right]$ and

$$\Delta^2 P(i) = \Delta P(i+1) - \Delta P(1)$$

Equations 3.20 and 3.21 are known as model A and B. These are similar to semi log pressure-time curve developed by MDH [55] and Horner [39] but differ completely in terms of sharp contrast between each flowing regimes which is clearly seen; thus better approach for wellbore and reservoir parameters estimation to support interpretation from conventional, type-curve and derivatives methods. These semi log models are simple to generate and good for easy identification of different flow regimes to obtain reliable reservoir properties.

For better reservoir characterization, six statistical models mimicking the log-log pressure derivative approach are derived using the steps below;

First the 1st pressure and time differencing are obtained:

$$\Delta P_t = P_0 - P_i \tag{3.22}$$

$$\Delta t_t = t_{i+1} - t_i \tag{3.23}$$

Then the divided 1st differencing for pressure and time is derived:

$$\Delta dev(i) = \frac{\Delta P(i+1)}{\Delta P(2)} \tag{3.24}$$

$$\Delta tt_t = \Delta t_i / \Delta t_{i+1} \tag{3.25}$$

The residual for the pressure and time differencing are generated using the statistical functions such as standard deviation between data point:

$$\delta\Delta pt(i) = STDEV\left(\Delta tt(i+1),(i+2),\Delta^2 P(i+1),(i+2)\right) \tag{3.26}$$

To reduce the noise effect arising from the differencing, the square root of the standard deviation of the 1st differencing and the divided 1st differencing for pressure is obtained:

$$pdd(i) = SQRT\left(\delta\Delta pt(i) x STDEV\left(\Delta dev(\ ),\Delta^2 P(\ )\right)\right) \tag{3.27}$$

Finally, the six statistical models for flow regime diagnosis are given as:

Model 1:

$$StatDev1(i) = SQRT\left(pdd(i) x\Delta dev(i) x\Delta^2 P(i)\right) \tag{3.28}$$

Model 2: The Exponential function

$$StatExp(i) = SQRT\left(EXP\left(SQRT\left(\Delta^2 P\right)\right)\right) x pdd(i) x\Delta^2 P(i) \tag{3.29}$$

Model 3:

$$StatdDev(i) = SQRT\left(pdd(i) x\Delta dev(i) x\Delta^2 P(i) x\Delta^2 P(i)\right) \tag{3.30}$$

Model 4: The Time function

$$StattDev(i) = STDEV\left(\Delta tt(i),\Delta tt(i+1),StatDev(i),StatDev(i+1)\right) \tag{3.31}$$

Model 5:

$$StatDev2(i)^{0.4} = (\Delta p(i+1) - \Delta p(i)) * pdd(i) * \frac{\Delta dev(i)}{\Delta p(i)} * Exp\left(\frac{\Delta tt(i)}{\Delta tt(i+1)}\right) + \sqrt{\left(t_{i+1}^{\ 2} + t_i^{\ 2}\right) - \left(t_i^{\ 2} - t_{i-1}^{\ 2}\right)} * \frac{\delta\Delta pt(i)}{\Delta p(i)} \tag{3.32}$$

Model 6:

$$StatDev3(i)^2 = \left(\frac{\Delta p(i+1)}{\Delta p(0)}\right) * \sqrt{\Delta p(i)} + Exp\left(\frac{\Delta tt(i)}{\Delta tt(i+1)}\right) * \delta\Delta pt(i) * pdd(i) \tag{3.33}$$

Equations 3.28 to 3.33 are regarded as statistical pressure diagnostic models for interpreting pressure transient data. These are similar to the log log derivative method developed by Tiab [75] and Bourdet [14], and are reliable diagnostic tools for flow regimes identification and reservoir characterisation. They are also used for estimating wellbore and reservoir parameters in order to support the interpretation from the derivative method or type-curve

after the analysis. The workflows for generating these models are shown in Figures 3.3 and 3.4. The statistical models are tested with synthetic well test data with constant pressure and rate conditions as well as in well with high water production. In all three conditions investigated, equations 3.32 and 3.33 are used for the analyses which will be discussed in the next section.

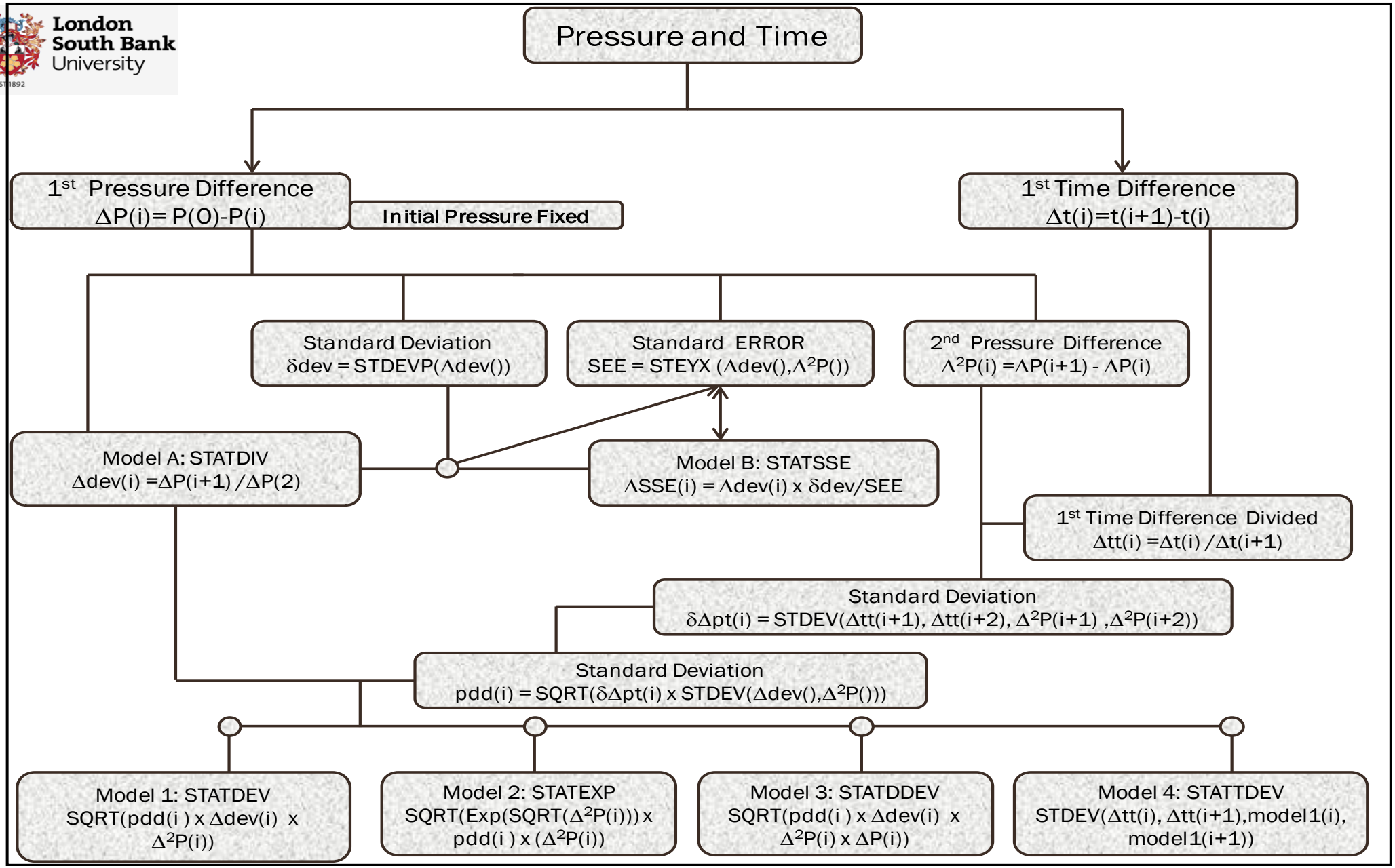

Figure 3.3: Workflow for Statistical Models Formulation Using Pressure Data

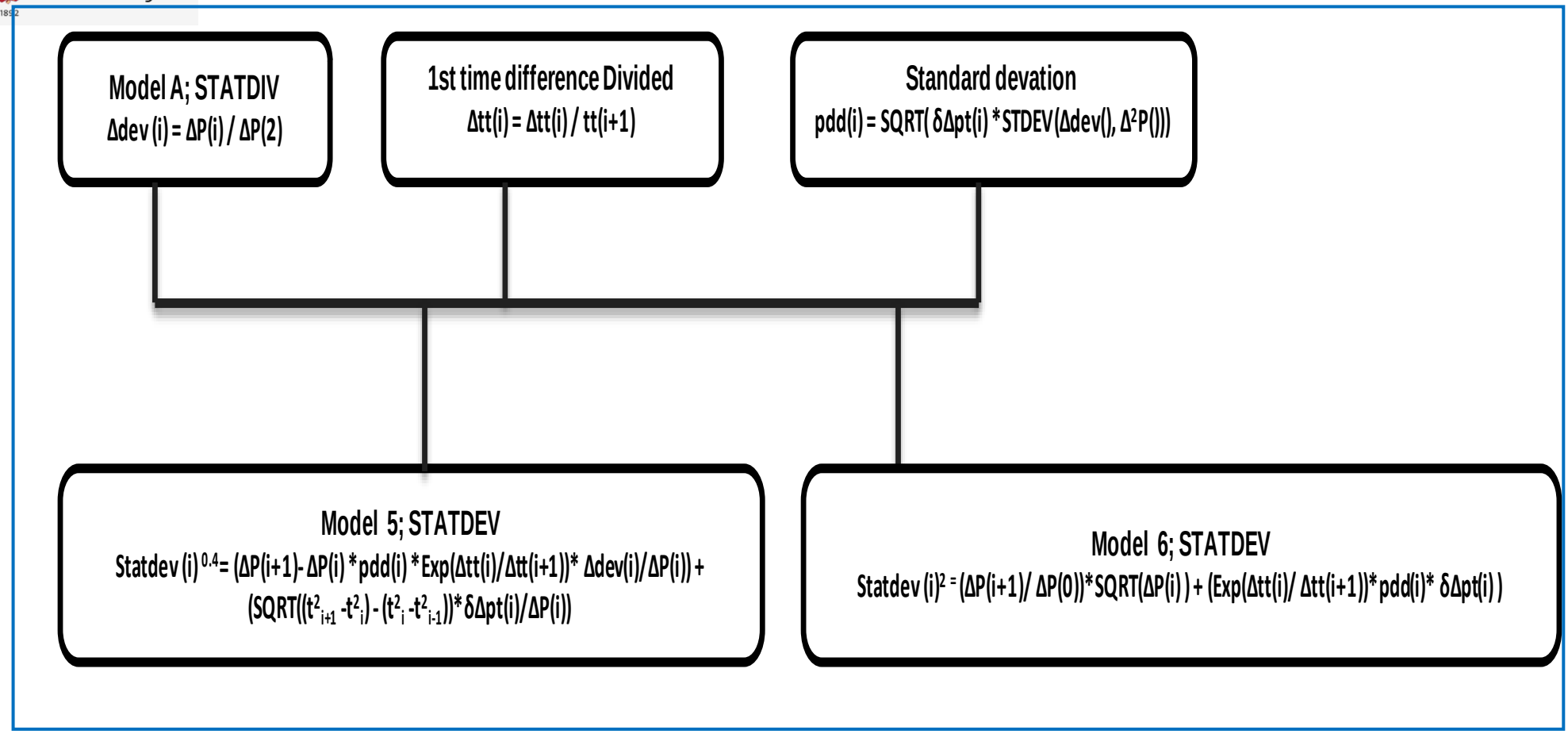

Figure 3.4: Statistical models for flow regime identification

Figure 3.3 shows the stepwise workflow that generated statistical models StatDiv, StatSSE, StatDev1, StatExp, StatdDev and StattDev used for analysing well test bottom hole pressure data. Figure 3.4 displays StatDev2 and StatDev3 which are improvement on StatDev1 and is used to analyse examples 1.0 and 2.0 which will be discussed in the next section. Figure 3.5 shows the different statistical models generated from equations 3.28 to 3.33.

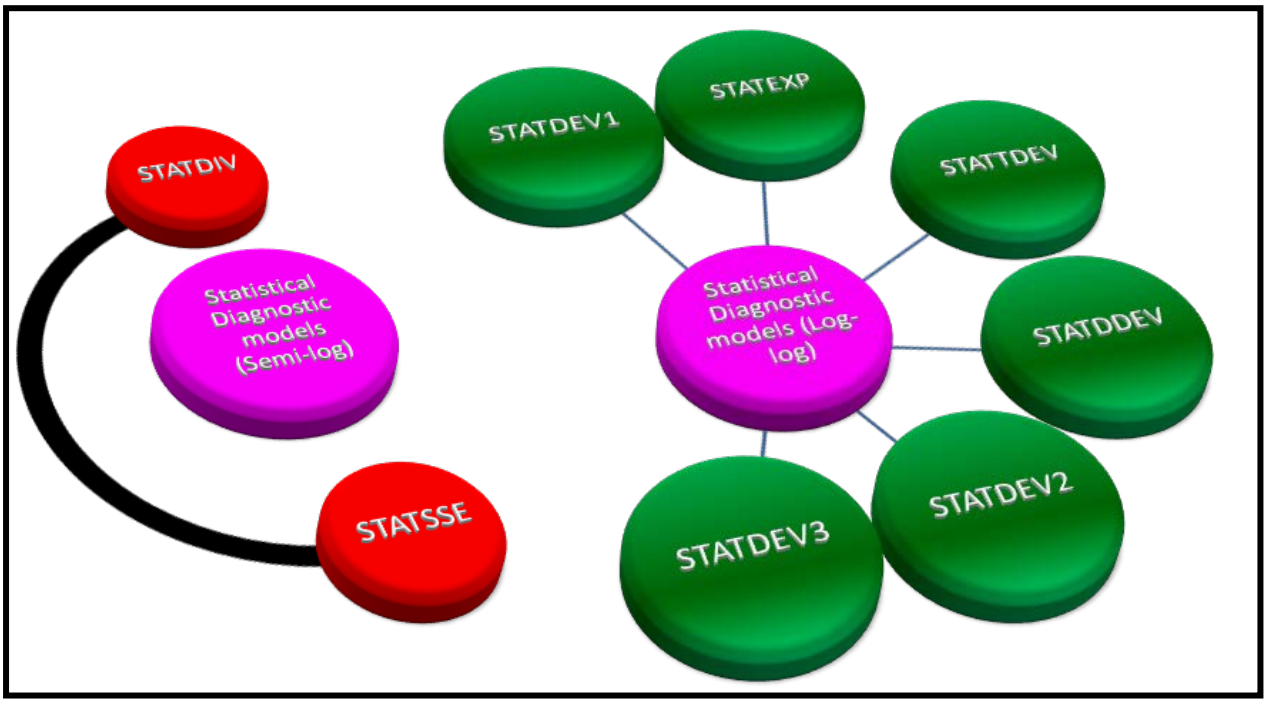

Figure 3.5: Summary of Statistical models for flow regime identification

3.5 Statistical Derivative: Applications

3.5.1 Example 1.0 → Synthetic data with good k reservoir

Table 3.1 presents a summary of the well and reservoir synthetic data used for the build-up and drawdown simulated scenario with additional information given below. It is required to generate the pressure statistical derivatives using equations 3.32 and 3.33; compare the drawdown and build-up diagnostic signatures of the conventional and statistical derivative method; then draw possible inferences.

Table 3.1: Reservoir and fluid data for example 1.0 constant pressure scenario

Parameters	Design Value
Eclipse model	Black Oil
Model dimension	10 X 5 X 5
Length by Width ft by ft	400 X 400
Thickness ft	250
Permeability kx by ky mD	50.0 by 50.0
Porosity %	20
Well diameter ft	0.65
Initial water saturation Swi %	22
Permeability, k, md	50
Gas Oil contact GOC ft	8820
Oil water contact OWC ft	9000.0
Initial Pressure, Pi, psia	3600.0
Formation Temperature, T,°F	200.0

Assumption:

- Oil reservoir + Gas Cap, completed with one well.
- LGR was imposed around the well and far across to account for pressure changes. Well bottom hole pressure WBHP around the local grid refinement LGR (wellbore) is output with Eclipse keywords. The schematics for the basic fluid flow concept and the simulated eclipse model with LGR are shown in Figures 3.6 and 3.7.

In this example, three scenarios with reservoir production conditions are investigated. These include;

a. Constant pressure solution

b. Constant rate solution

c. High water production imposed on well

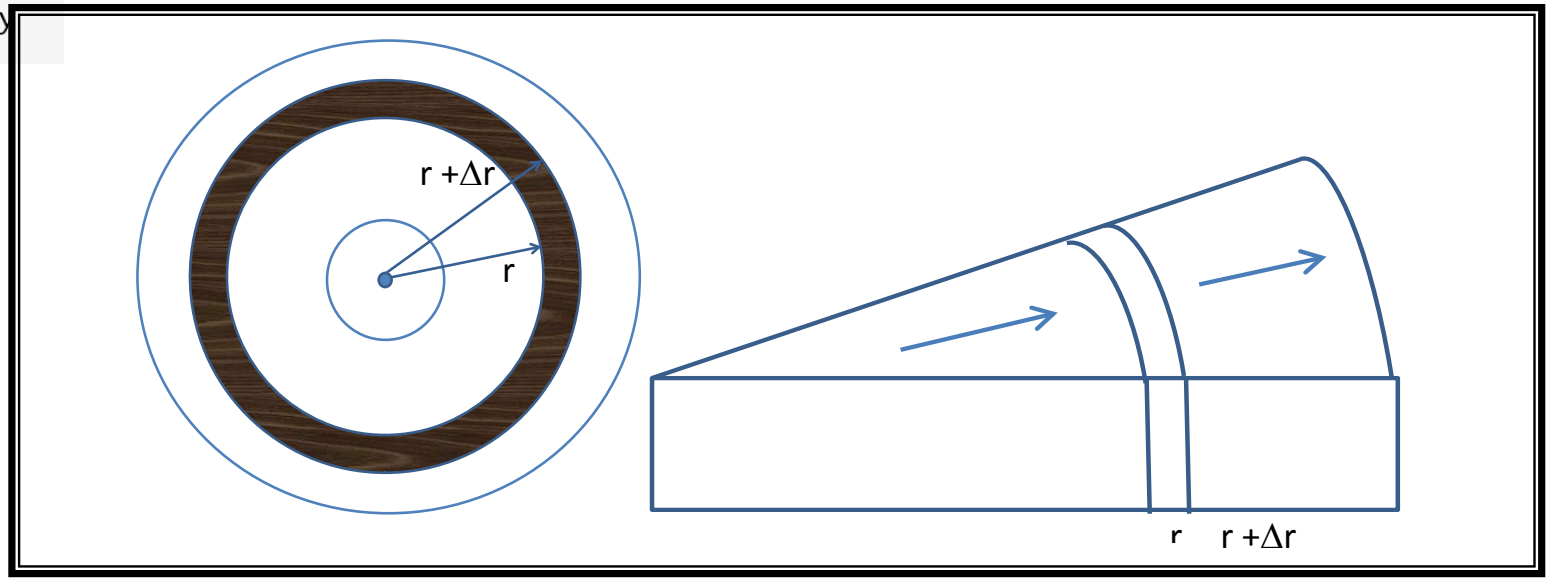

Figure 3.6: Schematics of basic fluid flows concept

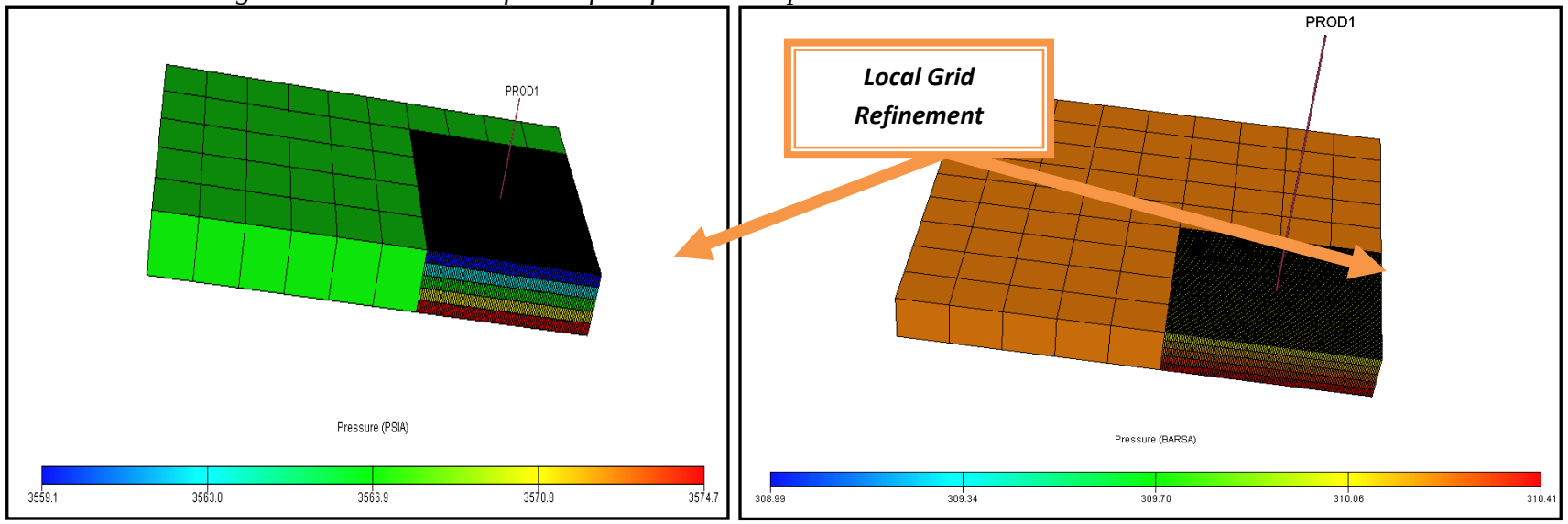

Figure 3.7: Eclipse model for Gas cap + oil + water reservoir and Gas condensate+ water showing local grid refinement around the well

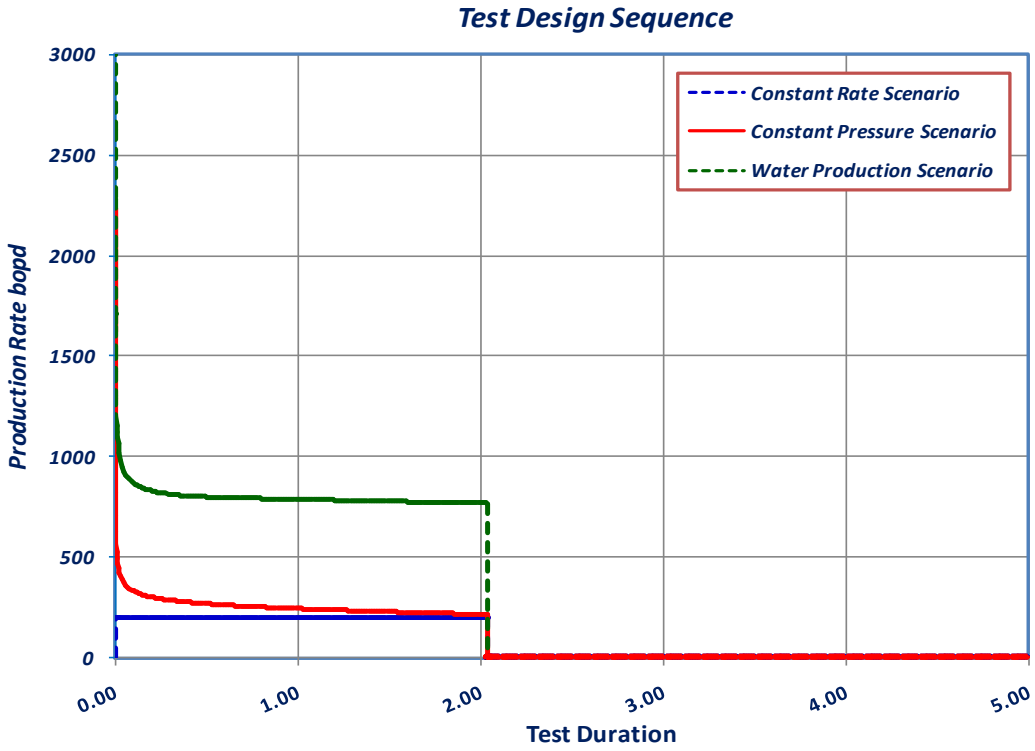

Figure 3.8: Production and shut-in test sequence for three scenarios (Drawdown and Build-up).

In scenario a, the bottom hole flowing pressure is fixed at 3500 psia and the well is allowed to produce as much as possible. The WBHP is measured from the LGR keyword in order to monitor the sharp changes in pressure around the wellbore. The ideal drawdown and build-up data were analyse using the conventional and statistical methods.

The statistical derivative plot in Figure 3.9 shows a good radial stabilization after 1.0hrs for both (drawdown and build-up analysis) but with different dp' flat point. In addition, the late time effect is seen in the drawdown clearly indicating a change in mobility effect.

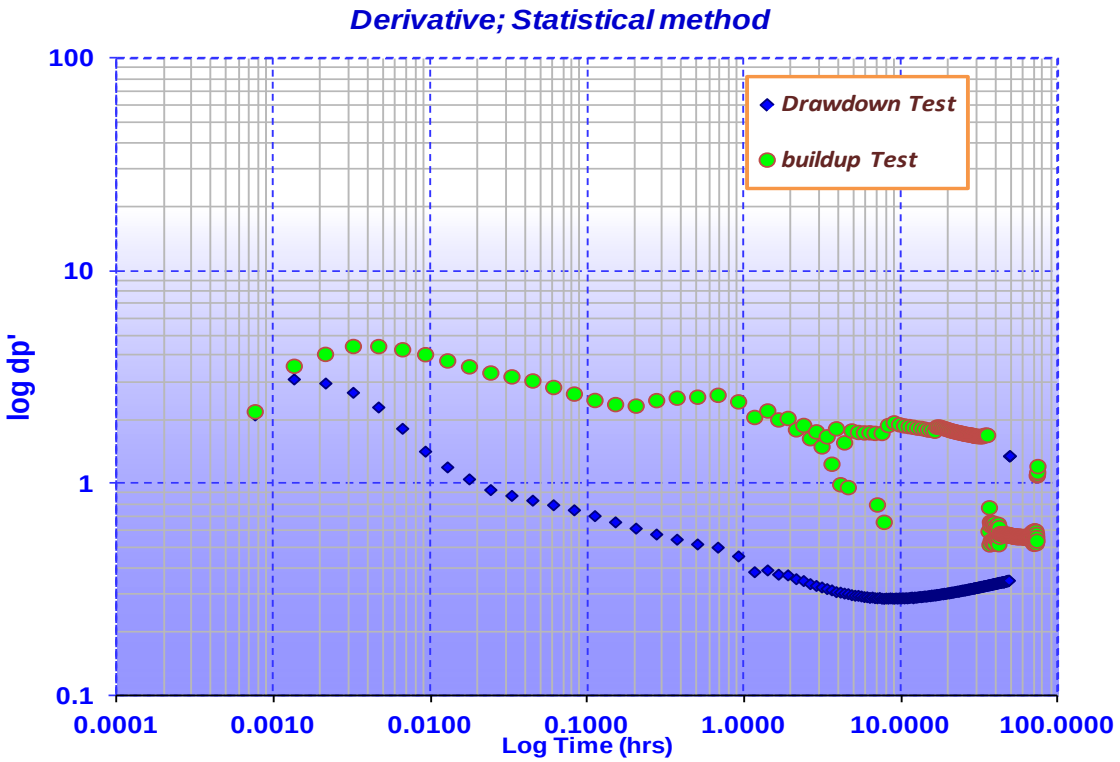

Figure 3.9: Statistical derivative for constant pressure scenario (build-up and drawdown).

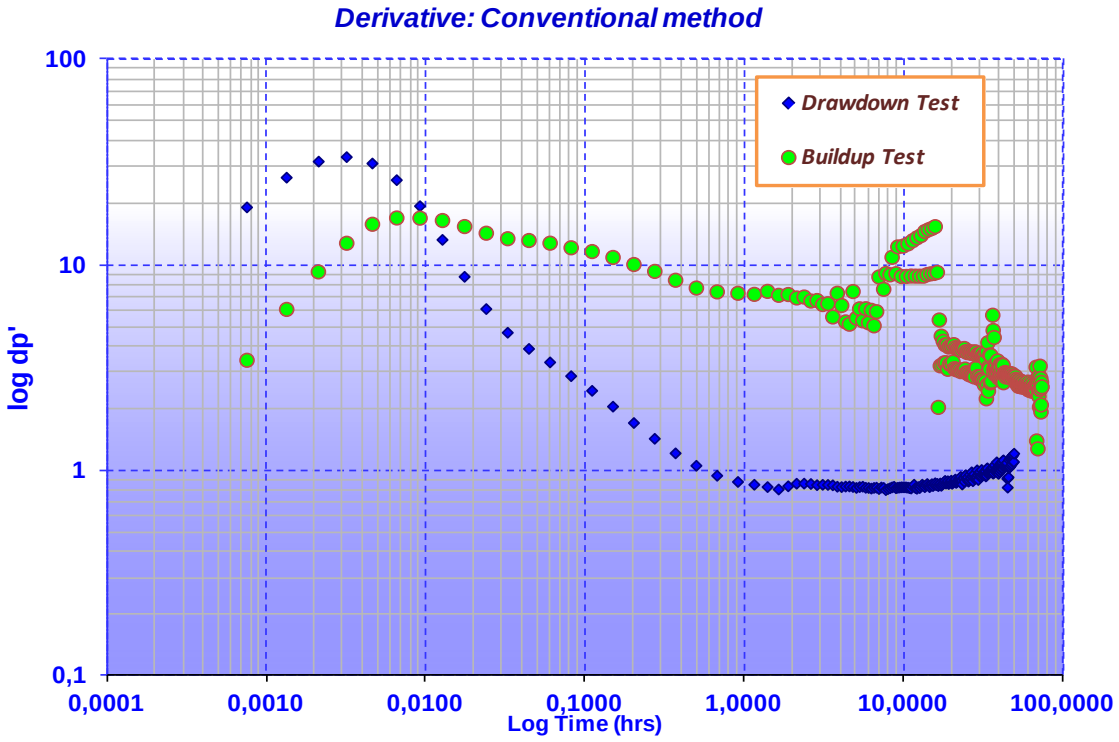

Figure 3.10: Conventional derivative for constant pressure scenario (build-up and drawdown).

For the convention derivative method, the log-log build-up plot depict similar radial stabilization fingerprint in the drawdown but noisy and continuous drop in the build-up derivative indicating external support seen in Figure 3.10. This feature differs with the drawdown scenario in the conventional and the statistical methods. It is pertinent to note that, in both approaches, no smoothing is considered in order to capture the real data behaviour.

To test this approach with constant production rate solution, a fixed rate of 200 bopd is imposed on the well while the bottom hole pressure is monitored and analysed without smoothing. In this scenario b, the statistical derivative log-log plot shown in Figure 3.11 exhibit good radial stabilization after 1.0hrs in both build-up and drawdown as depicted in scenario a. This confirms that the radial flow effect starts at 1.0hrs, however, this feature is absent in the conventional method but slightly seen in the build-up derivative curve shown in Figure 3.12.

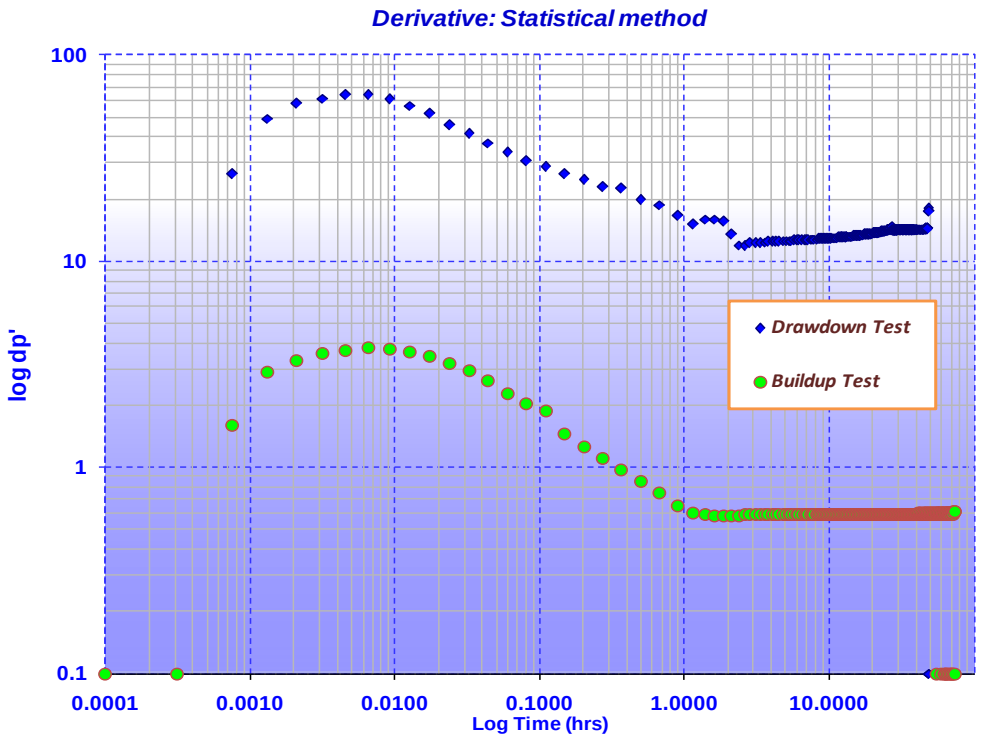

Figure 3.11: Statistical derivative for constant rate scenario (buildup and drawdown).

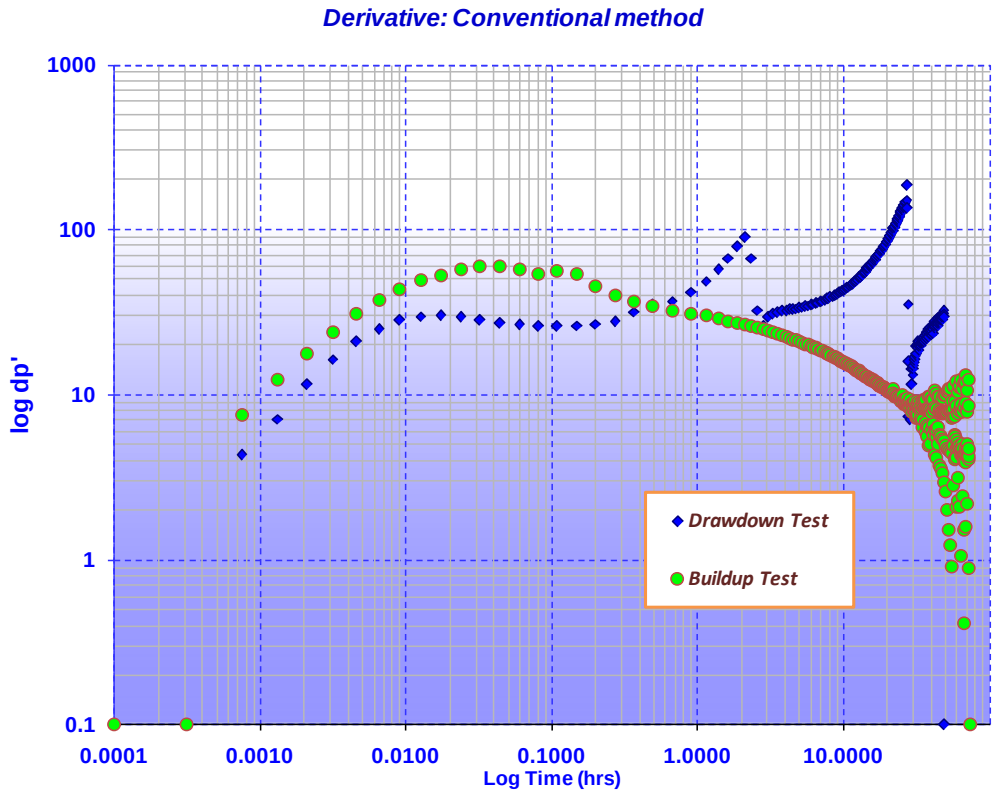

Figure 3.12: Conventional derivative for constant rate scenario (build-up and drawdown)..

One important limitation of the derivatives is diagnosing flow regimes in two phase fluid flow conditions due to the fact that drawdown are prompt to noisy data. To view the effect of two phase flow on the statistical derivative, a fixed bottom hole pressure of 1000 psia is imposed on the well and allow the BSW starting from 20% to increase to almost 70% during the drawdown test.

In this scenario, the radial stabilization is deferred to 3hrs during the drawdown and 6hrs for the build-up for the statistical derivative. The first 1.0 hrs witness a flat line and change of mobility probably due to two phase fluid flow at the wellbore (gravity effect). A final radial flow for both build-up and drawdown is seen in Figure 3.13 after 10hrs, nevertheless, the result is consistent with scenario a and b. However for the conventional method, a sharp drop in build-up derivative is seen after 1hrs with no radial stabilization as shown in Figure 3.14. The derivative could not identify the radial flow for both drawdown and build-up but drops at late time which differs with scenario a and b interpretation.

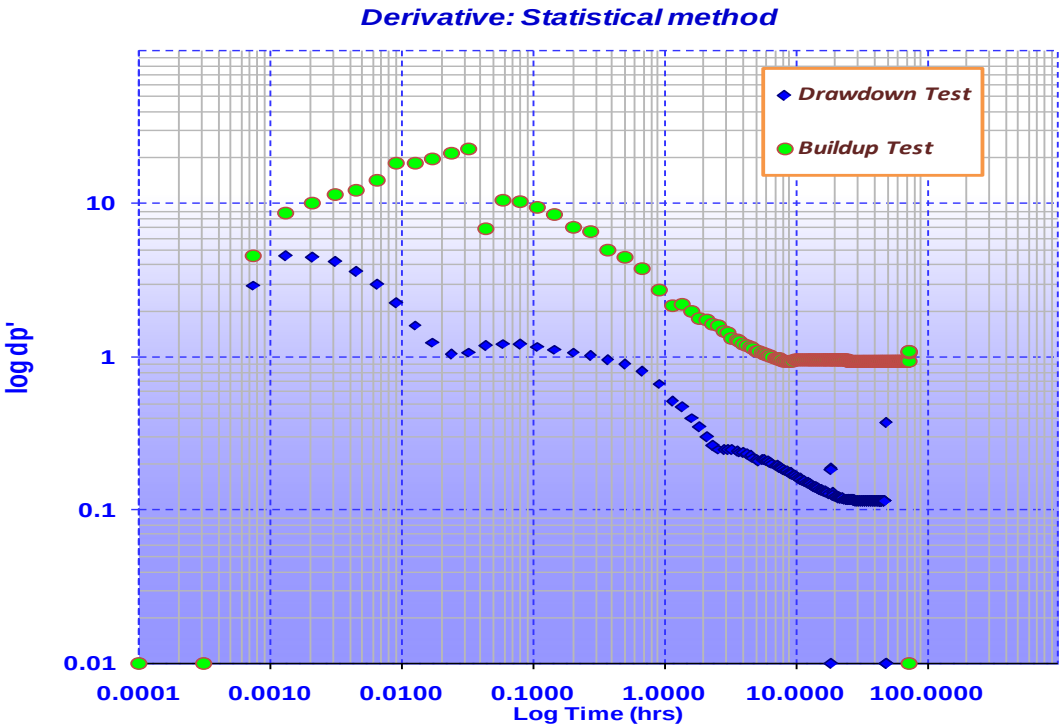

Figure 3.13: Statistical derivative for high water production scenario (build-up and drawdown).

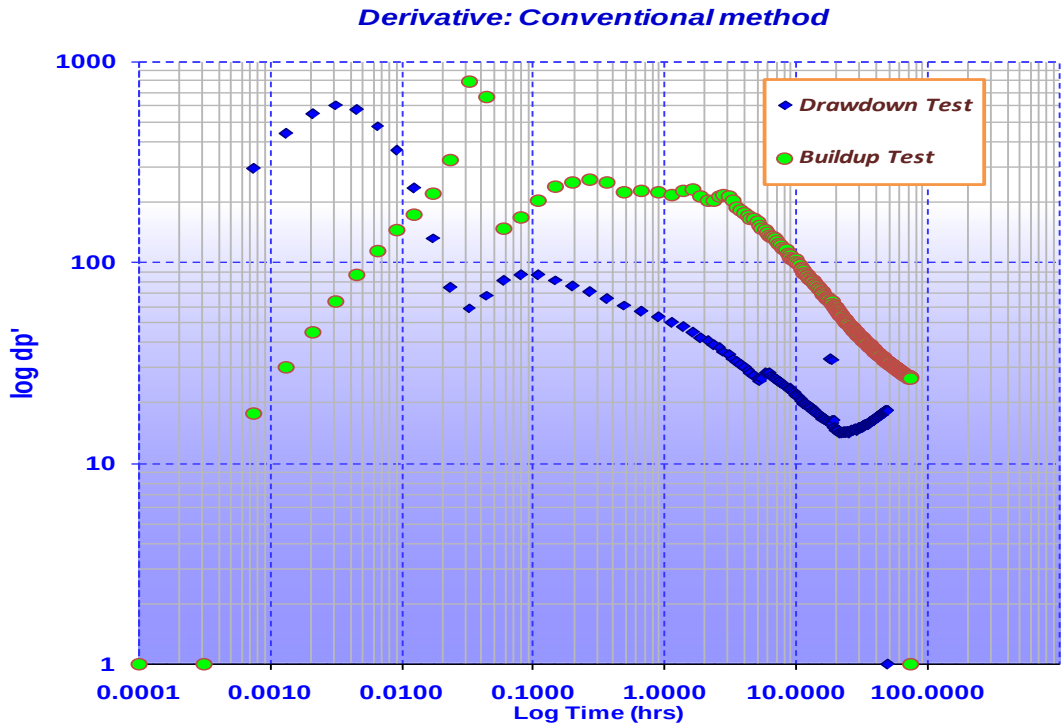

Figure 3.14: Conventional derivative for high water production scenario (build-up and drawdown).

In summary, the statistical derivative has demonstrated that for high water production well, a good radial stabilization can be identified for good permeability estimation without smoothing the data. It has also shown that shown in all three scenarios, the drawdown fingerprint can be replicated in the build-up pressure responses, hence a good match of the data i.e. consistency between build-up and drawdown analysis.

3.5.2 Summary of Result

The following inference was drawn from the three scenarios reviewed;

- For constant pressure, constant rate conditions, and in well with high water production, the statistical derivatives display distinctive radial flow fingerprint with further unseen features revealed with high degree of accuracy compared to the conventional bottom hole pressure method.
- It also demonstrated that for high water production well, a good radial stabilization can be identified for good permeability estimation without smoothing the data.
- In all three scenarios, it has shown that, the drawdown fingerprint can be replicated in the build-up pressure responses, hence a good match of the data.
- The model aided the identification of possible unseen features used to diagnose key reservoir flow regimes for reservoir description and acts as a support tool to the pressure derivative approach to interpret and confirm reservoir features.

3.6 Estimation of Permeability k (mD) after Statistical Derivative Diagnostic Approach

3.6.1 Example 2.0 → High k reservoir in using design data

a. Analysis of Ideal BHP Data with Statistics Derivative (STATDEV)

The ideal BHP data is obtained by simulating the drawdown test using parameters in Table 3.2. The reservoir permeability ranges between 800mD and above, with light oil PVT

properties. The well capacity is above 1000 bbl/days with reservoir pressure close to 5000psi. The ideal drawdown data is analysed using the conventional and type-curve methods. Results obtained are used in generating simulated profiles.

Table 3.2: Parameters for Test Design [62]

Parameters	**Design Value**
Wellbore radius, rw, ft	0.50
Total Compressibility, ct, psi-1	20 x 10-6
Formation Thickness, h, ft	50
Porosity, Ø	0.25
Oil formation volume factor, Bo, rb/stb	1.13
Oil viscosity, μ, cp	0.6
Production rate,q, STB/D	1000.0
Production time before shut-in, tp, hr	1000.0
Permeability, k, mD	1000.0
Total skin, s	25.0
Wellbore Storage Constant, Cs	9.0 x 10-3
Initial Pressure, Pi, psia	5000.0
Formation Temperature, T, oF	200.0

The derivative plot from Figure 3.15 (b) indicates high permeability sand with a linear flow at the late time; however the StatDev in Figure 3.15(a) diagnostic plot exhibit same reservoir response but indicates a double permeability features at the late time period, possibly a layer reservoir system that is in communication. The interpretation of the late time response differs from the derivative. To improve on the interpretation of this unseen feature in the derivative, the semilog StatSSE and StatDiv are plotted in Figure 3.19 which also indicates three flow regimes (radial—linear--radial). Another confirmation of the late time feature was done using the three other statistical tools such as StatdDev, StatExp and StattDev as shown in Figures 3.16 to Figure 3.18. All three models depict same responses at the late time identifying possible unseen features. It is pertinent to note that, the results from the statistical derivatives could serve as a checkbox to improve the interpretation of this unseen feature which could not be identified by the conventional method. Therefore in situations where the pressure

derivative may not be able to capture flow event due to smaller Δp (sampling frequency), the statistical derivative may help.

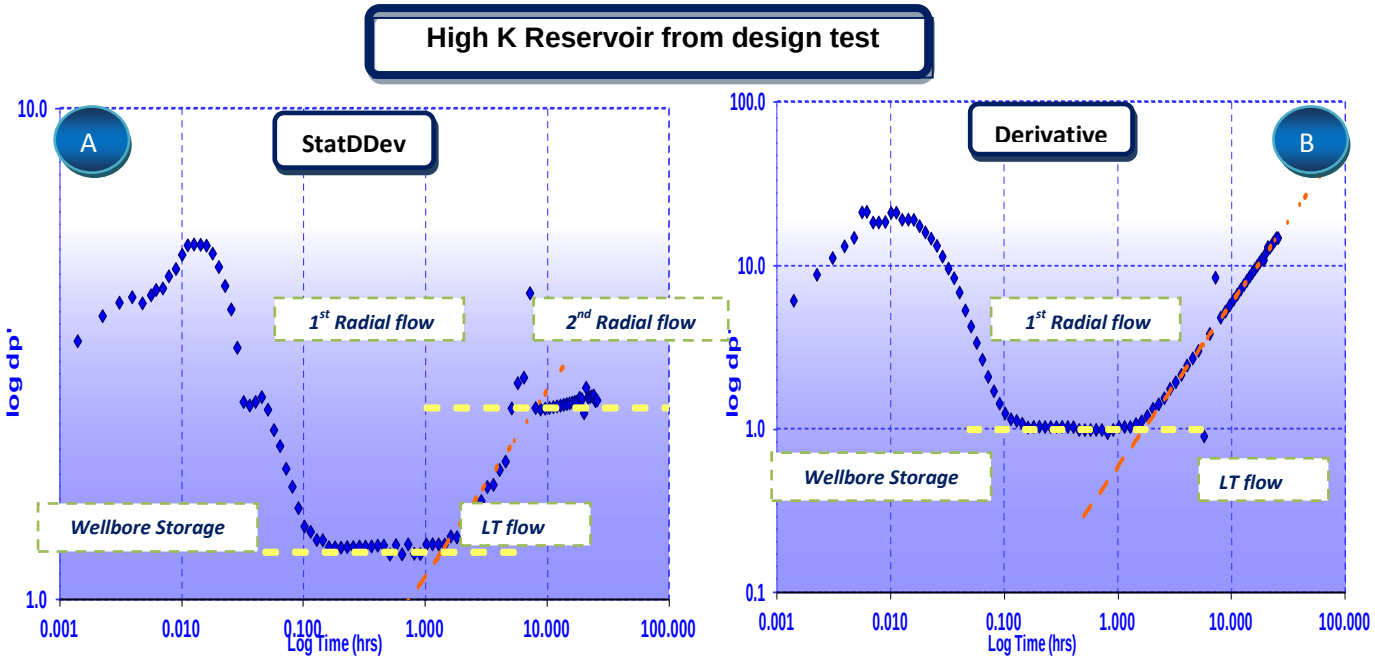

Figure 3.15: Comparisons of Derivative and StatDev Diagnostics Approach

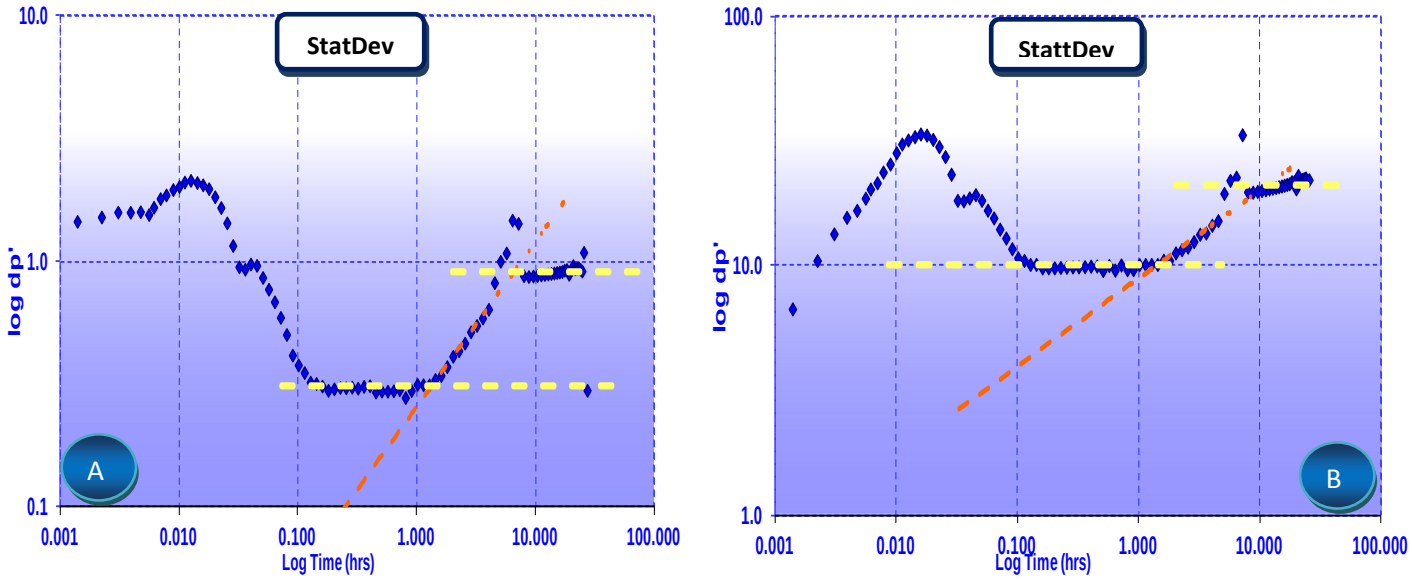

Figure 3.16: Comparisons of StatDDev and StattDev Diagnostics Approach

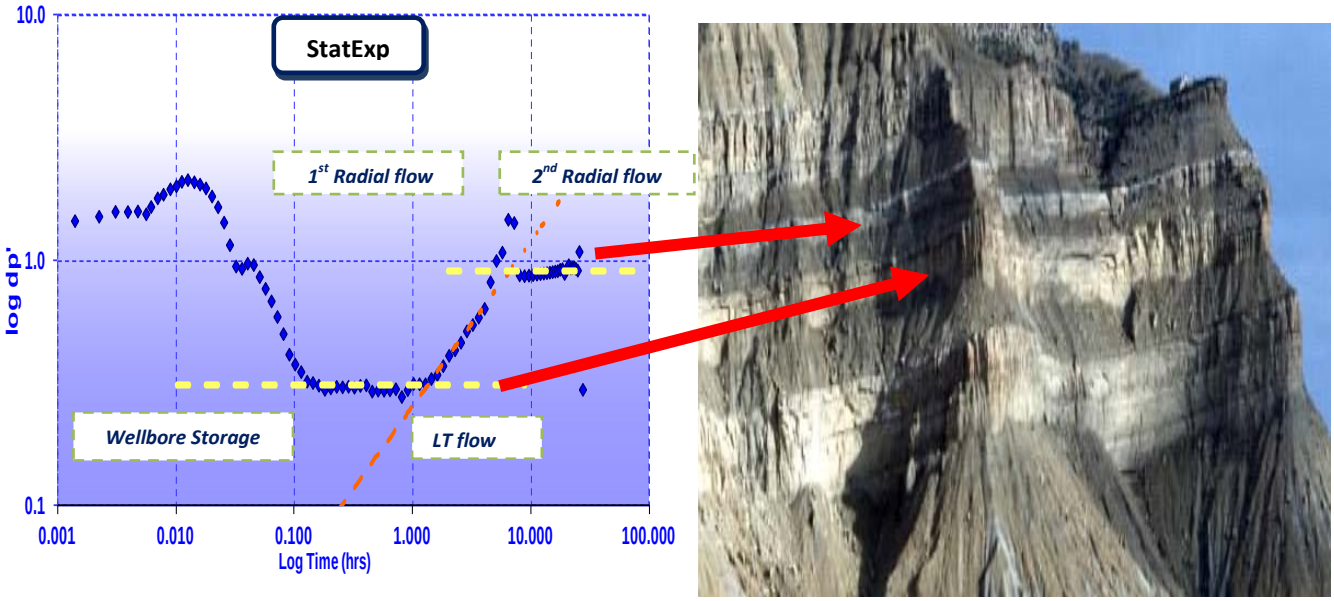

Figure 3.17: StatExp for high K with undefined boundary response.

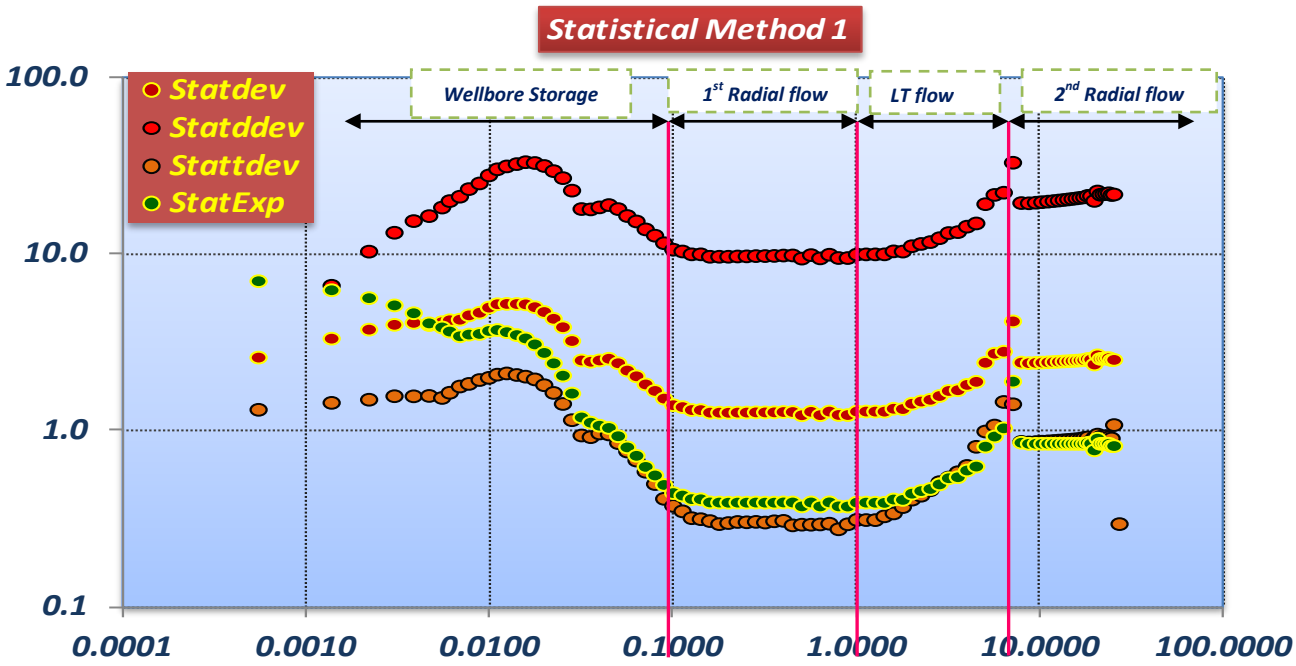

Figure 3.18: All Statistical models for reservoir model diagnosis

In summary, the StatExp displayed in Figure 3.17 supports the result exhibiting same reservoir response. Plotting all four statistical models as shown in Figure 3.18 clearly depicts radial flow regime at transient period and pseudo-steady flow at the late time. This is similar to the derivative approach but differ after the late time response which depicts the presence of another radial flow which could be interpreted as double

permeability feature. Table 3.3 is a summary of calculated results from the conventional, type curve and statistical approach.

Table 3.3 Build-up Analysis Results [62]

Parameters	Calculated Results		Statistical
	Conventional	TypeCurve	
Permeability k, mD	1000	1000.29	930
Skin S	25.01	25.01	37
Cs rb/psi	1.03×10^{-2}	0.8996×10^{-2}	1.0×10^{-2}
P* psia	3251	3251	3251
DPs (additional pressure drop due to skin) psi	48	48	76

b. Reservoir Characterization

Estimated permeability and skin are 930 mD and 37 using the statistical approach. In comparison with the derivative, K and S differ by 7% and 48% respectively. Difference in result is related to the slope of the pressure time semi-log specialised plot which depends on the extent of the transient period as identified from the statistical diagnostics models and conventional derivative log-log plot. Figures 3.19 and 3.20 show the statistical delta- pressure and pressure time semi-log plot from model A and B used for reservoir properties estimation.

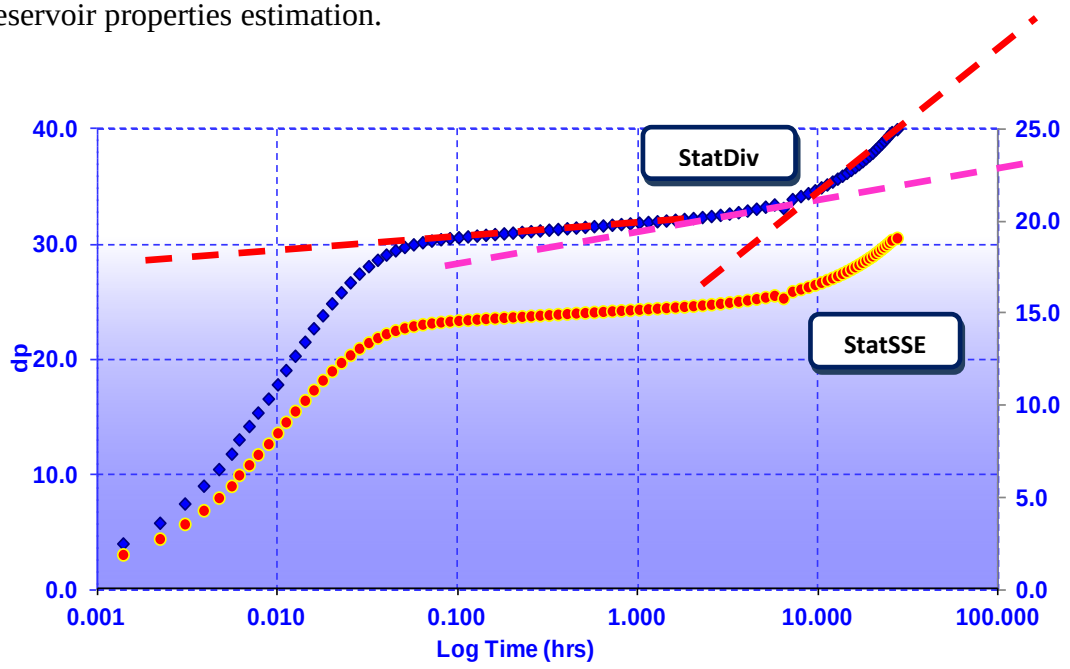

Figure 3.19: StatSSE and StatDiv semi-log for high K reservoir [62]

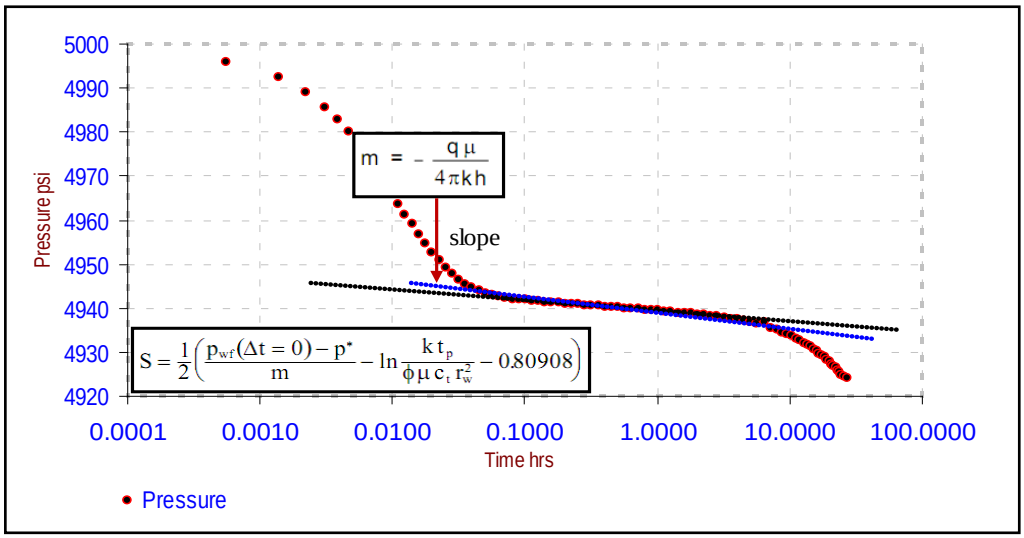

Figure 3.20: MDH semi-log for high K reservoir [62]

3.6.2 Example 3.0 → Low k reservoir with closed boundary (design data)

a. Analysis of Ideal BHP Data with Statistics Derivative (STATDEV)

The ideal BHP data are designed well test data obtained from the examples of Application Well test Software, Demo copy Automate Windows[tm] [86] simulating the drawdown test using parameters in Table 3.4.The reservoir permeability range is ≥ 70 md, with light oil PVT properties. The well capacity is above 2500 bbl/days with initial reservoir pressure close to 6000 psi.

Table 3.4: Parameters for Test Design [86]

Parameters	Design Value
Wellbore radius, rw, ft	0.40
Total Compressibility, ct, psi-1	7 x 10-6
Formation Thickness, h, ft	23
Porosity, Ø	0.21
Oil formation volume factor, Bo, rb/stb	1.21
Oil viscosity, μ, cp	0.9
Production rate,q, STB/D	2500.0
Production time before shut-in, tp, hr	-
Permeability, k, mD	81.7
Total skin, s	6.8
Wellbore Storage Constant, Cs	8.7
Initial Pressure, Pi, psia	6000.0
Formation Temperature, T, oF	200.0

This drawdown test shows the effect of a closed boundary response at late time period. In Figure 3.21 (a), the StatDev depicts a radial flow regime with a unit slope straight line at late time indicating a close boundary response. The derivative also exhibits same radial and boundary response as shown in Figure 3.21 (b). The StatDiv and StatSSE plots as shown in Figures 3.22 (a) and (b) also indicate two flow regimes (radial-pseudosteady) supporting the reservoir and boundary response diagnose by the StatDev. Nevertheless noisy data is noticed within the radial region of both StatDev and the derivative. Another validation of the radial-pseudo-steady response is clearly seen by plotting three other statistical models such as StatdDev, StatExp and StattDev as shown in Figure 3.22 to 3.24. All three models depict same reservoir response both at middle and late time period. This also serves as checkbox to improve interpretation of reservoir features diagnosed with the log-log pressure derivative.

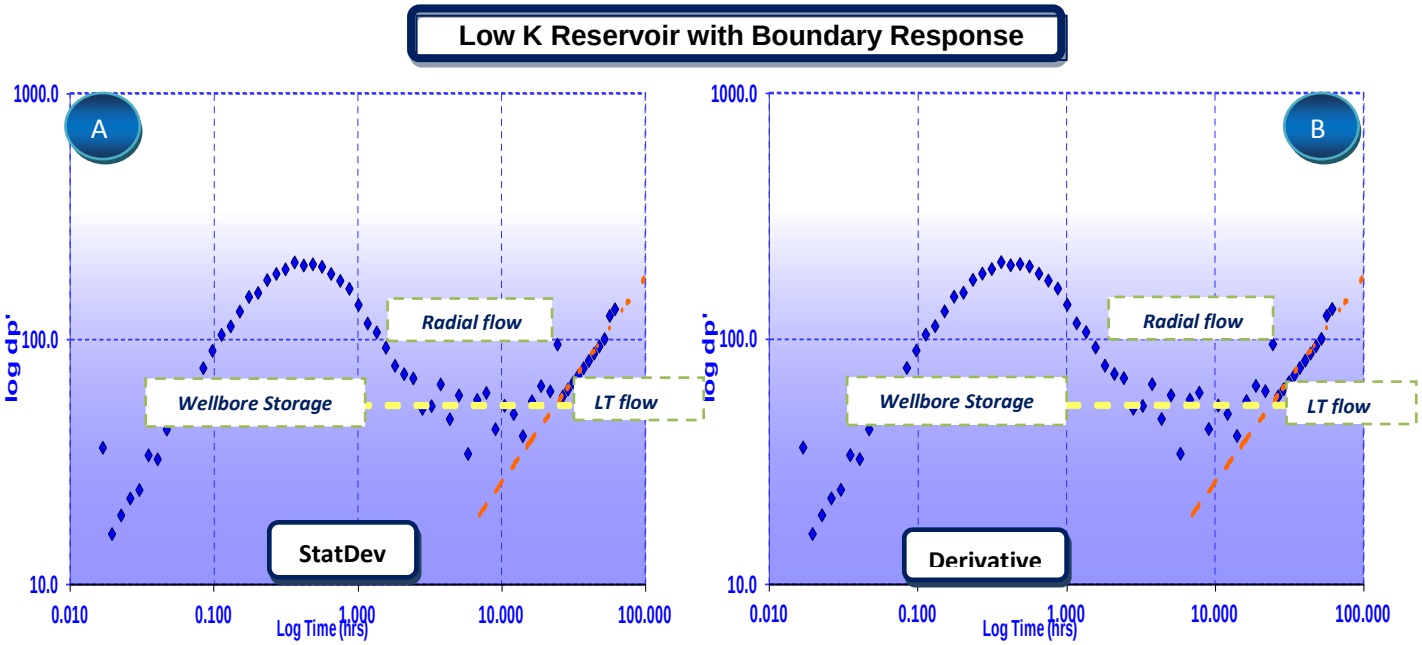

Figure 3.21: Comparisons of Derivative and StatDev plot for reservoir model diagnosis

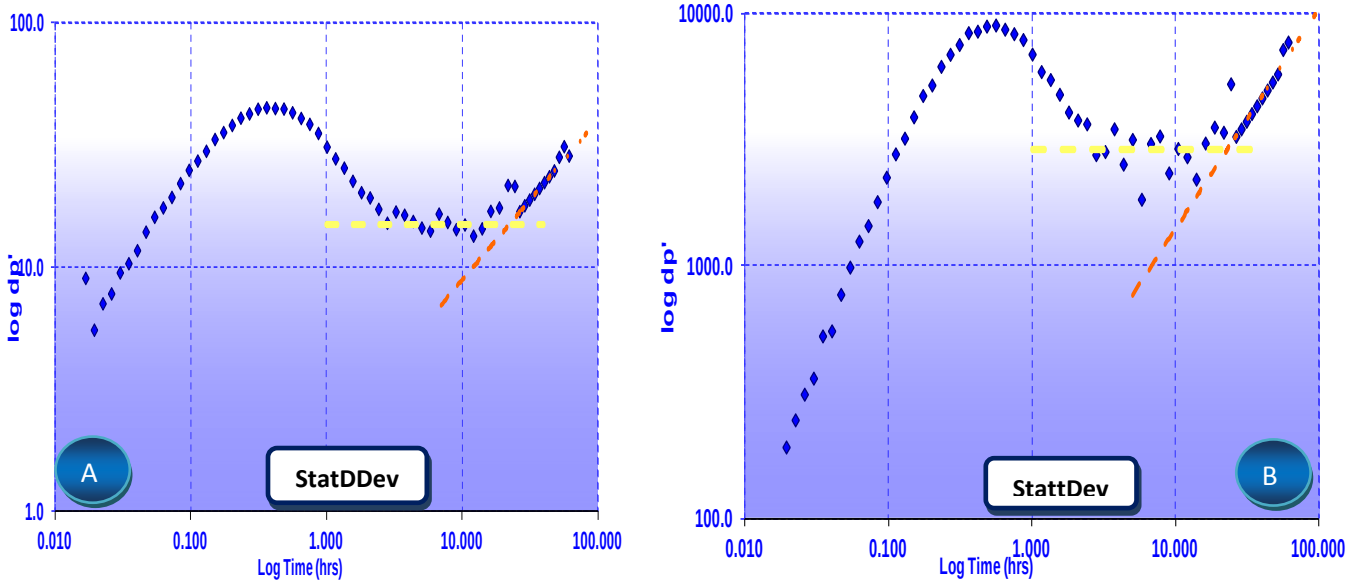

Figure 3.22: Comparisons of StatDDev and StattDev Diagnostics Approach

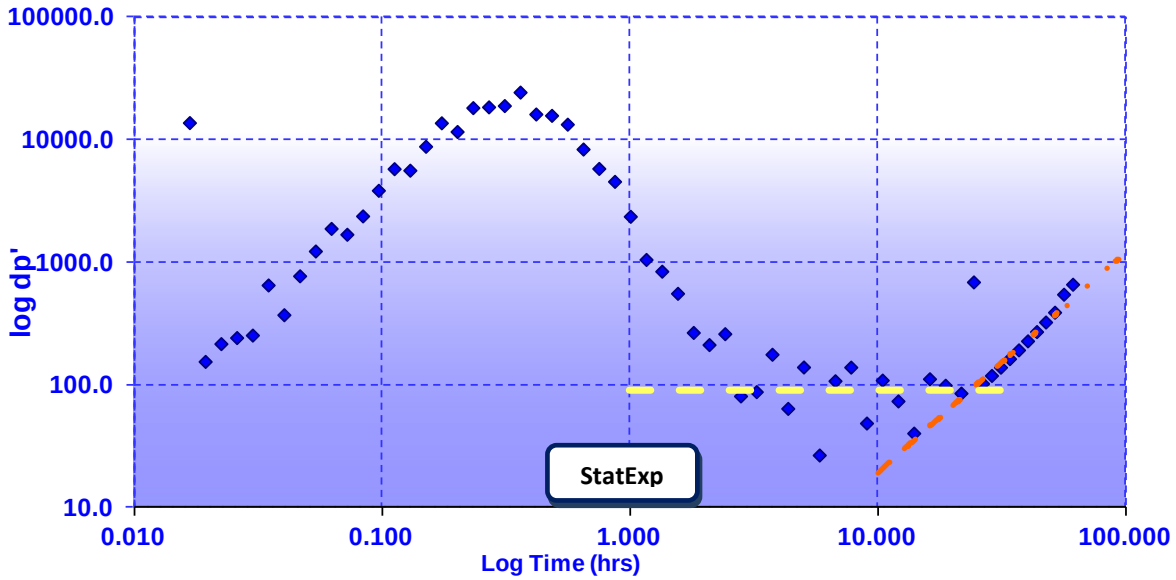

Figure 3.23: StatExp for low K in a closed boundary response.

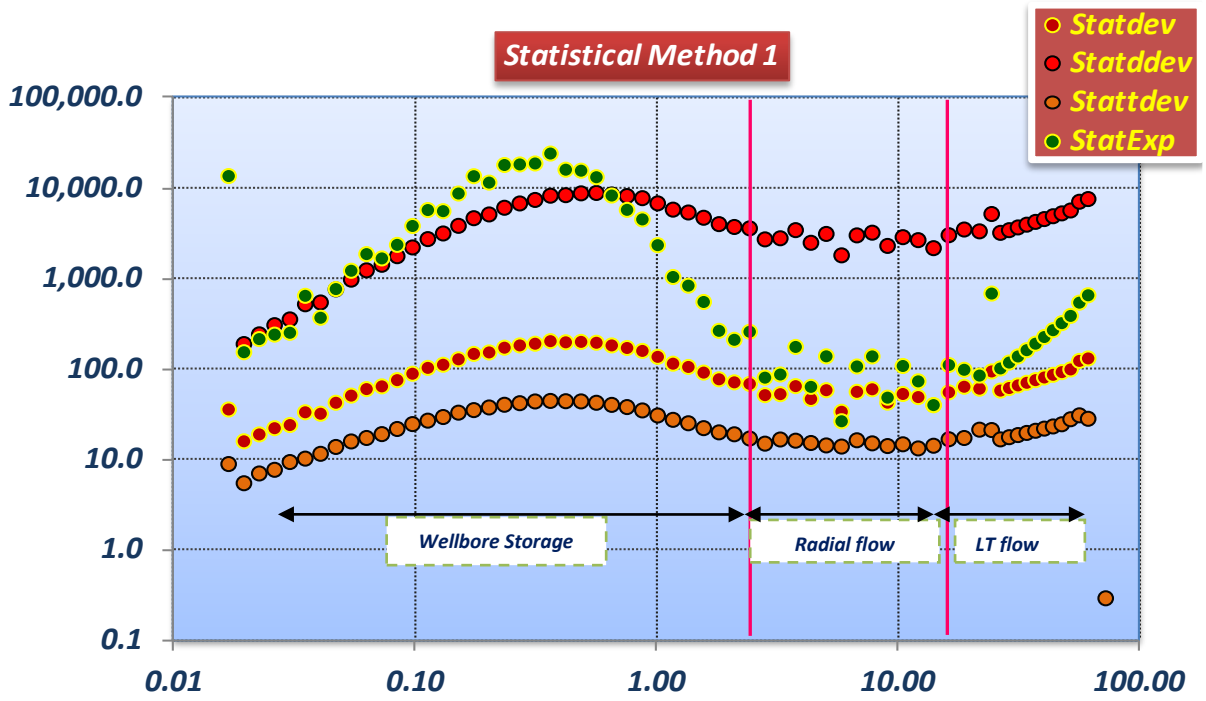

Figure 3.24: All Statistical models for reservoir model diagnosis

b. ***Reservoir Characterization:***

Estimated permeability and skin are 71.3 mD and 12.1 respectively using the statistical derivative approach. In comparison with the pressure derivative method, k and S differ by 13% and 77% respectively. Difference in result is related to the slope of the pressure time semi-log specialised plot which depends on the extent of the transient period as identified from the statistical models and conventional derivative log-log plot. Figure 3.25 shows the pressure time semi-log plot for reservoir properties estimation. Table 3.5 is a summary of calculated results from the conventional, type-curve and statistical approach.

Table 3.5: Build-up Analysis Results [86]

Parameters	Calculated Results		Statistical
	Conventional	Type Curve	
Permeability k, mD	81.7	81.7	71.3
Skin S	6.83	6.83	12.1
Cs rb/psi	8.72	8.9	8.5
P* psia	-	-	-
DPs (additional pressure drop due to skin) psi	1427	1427	2907

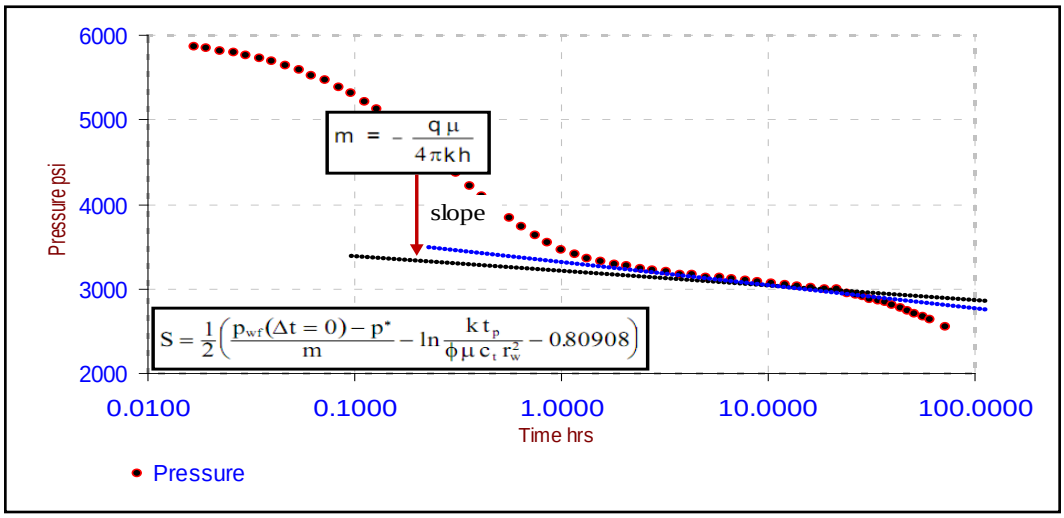

Figure 3.25: MDH semi-log for low K boundary response [86]

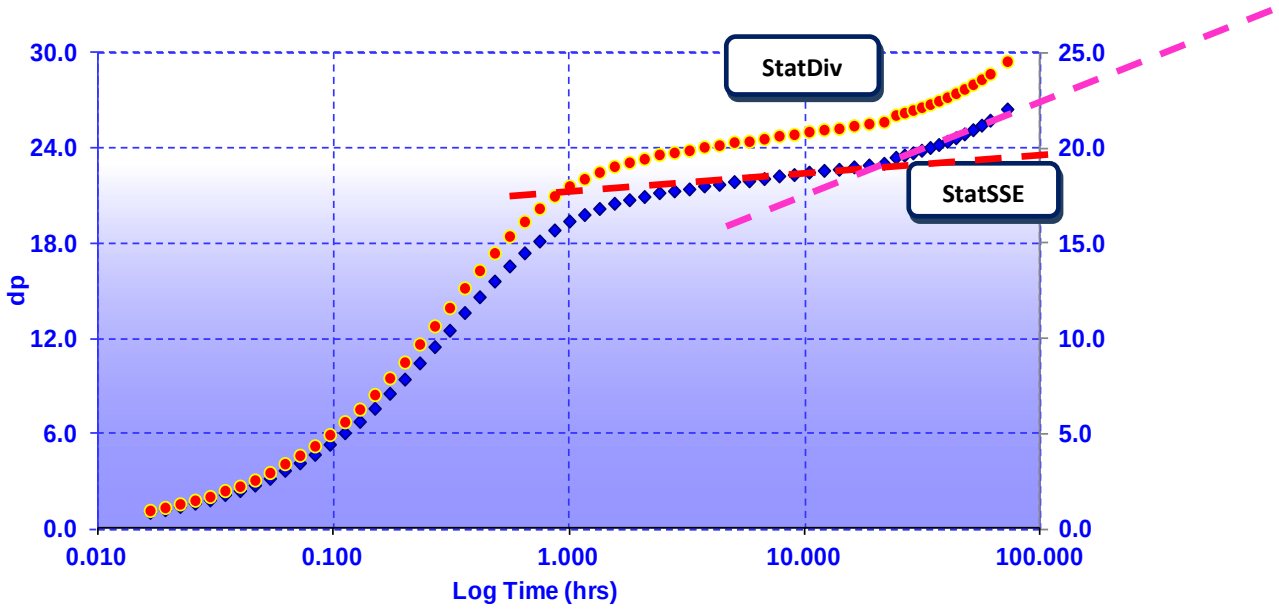

Figure 3.26: StatSSE and StatDiv semi-log for low K boundary response

A summary of the statistical versus conventional pressure derivatives log-log are shown in Figure 3.27 to 3.37 for different well and reservoir conditions using design data from Automate Windows[tm] [86]. The following cases were analysed and presented:

- Dual Porosity Reservoir model
- Channel Sand Reservoir
- Infinite Conductivity Fracture Reservoir Response
- Short Test Response: Data from Bourdet [14]
- Homogeneous Reservoir Response: Data from Meunier [54]

Dual Porosity Reservoir Response:→ Figure 3.27 to 3.29

In Figure 3.29, all statistical models identified the dual porosity feature including radial flow within the primary and secondary porosity. The dip between the radial flows along the porosity model which is the key dual porosity signature is also depicted with StatDDev as seen in Figure 3.28 but in the reverse direction. The conventional derivative in Figure 3.27b exhibits the same reservoir response confirming the presence of double radial flow (primary and secondary porosity response) which is consistent for all statistical models

Channel Sand Reservoir Response:→ Figure 3.30 to 3.32

In Figure 3.30a, the StatDev late time response shows a long period of linear flow, which is characteristic of flow along channels. This channel-like feature is also depicted in the conventional derivative as shown in Figure 3.30b at the late time response. Other statistical models display similar response as seen in Figure 3.31 and 3.32 supporting the hypothesis of radial-linear flow response which is consistent with the reservoir and boundary response diagnose by the derivative.

Infinite Conductivity Fracture Reservoir Response:→Figure 3.33 to 3.35

For an infinite conductivity fracture reservoir as shown in Figure 3.33 a and b, both StatDev and the derivative exhibits the similar response depicting a long period of linear flow, characteristic of flow in infinite conductivity fractures. Also other statistical models as seen in Figure 3.34 and 3.35 depict a clear feature of infinite conductivity fracture with a long linear flow regime supporting the reservoir response identified by the StatDev.

Data from Bourdet [7]: Short Test Response:→ Figure 3.36

This is a build-up test to show the superposition time effect on reservoir response. In this case, the well producing time of 21.6 hrs is short relative to the shut-in time, so the effect of superposition time is seen on the derivative in Figure 3.36 a. It is difficult to identify the radial stabilisation with the derivative as the derivative continues to drop at middle time

period. However, the statistical models exhibit similar reservoir response but with possible radial stabilisation at middle time period sufficient for k estimation.

Data from Meunier [33]: Homogenous Reservoir Response:→ Figure 3.37

This case is similar to the short test response scenario where it was difficult to identify the radial stabilisation with the derivative due to continue drop of the derivative curve. However as seen in Figure 3.37, the statistical models give better wellbore and reservoir response compare to the derivative with good radial stabilisation for k estimation

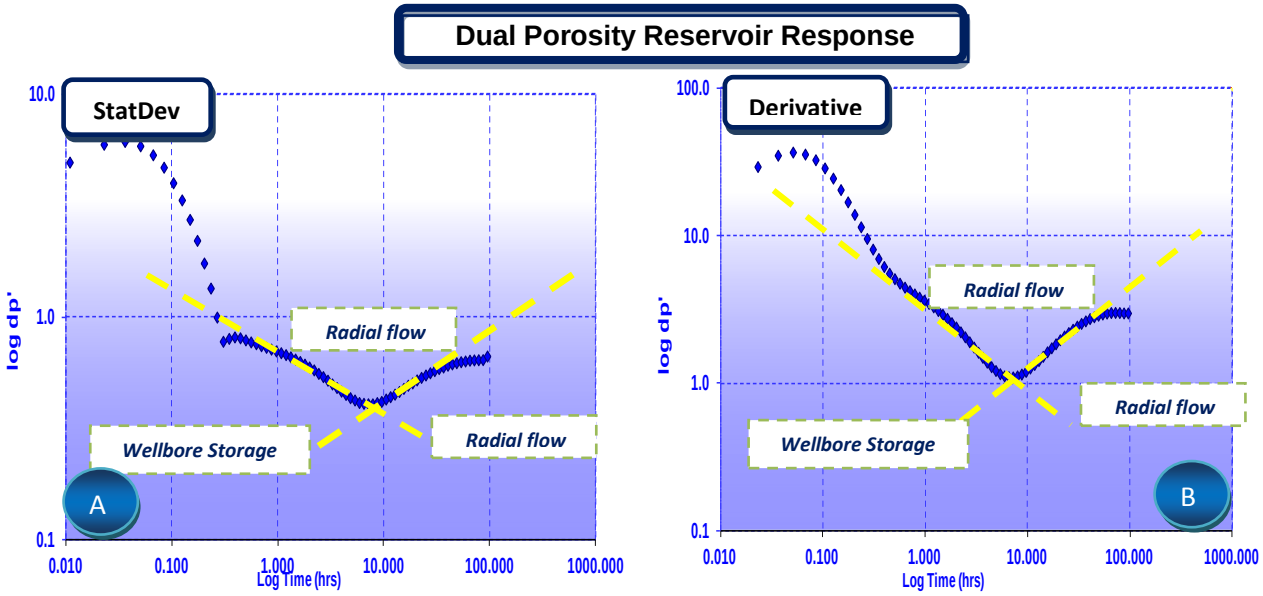

Figure 3.27: Comparisons of Derivative and StatDev Diagnostics Approach

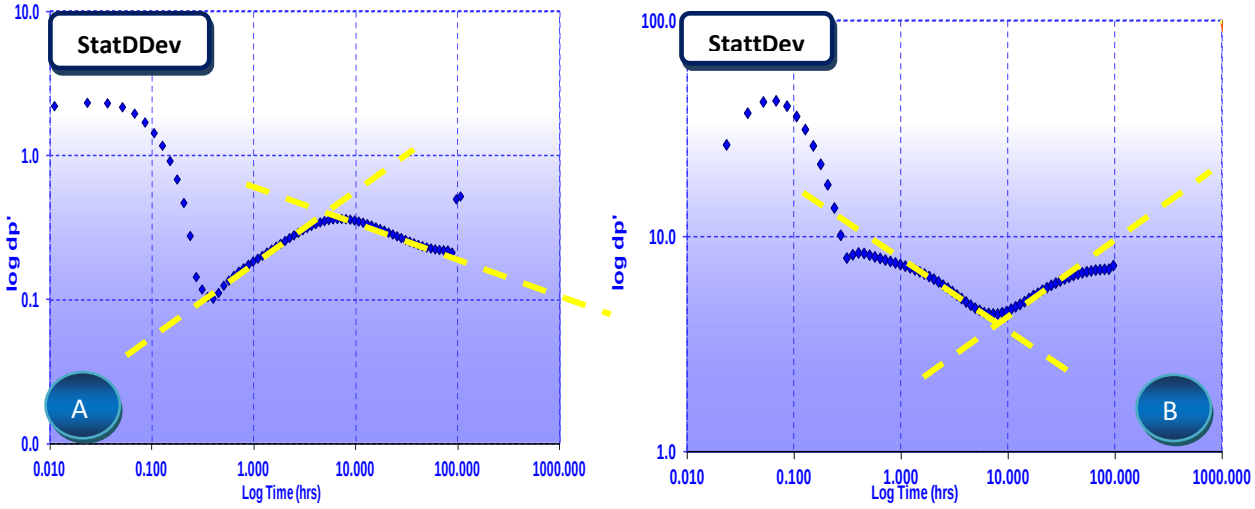

Figure 3.28: Comparisons of StatDDev and StattDev Diagnostics Approach

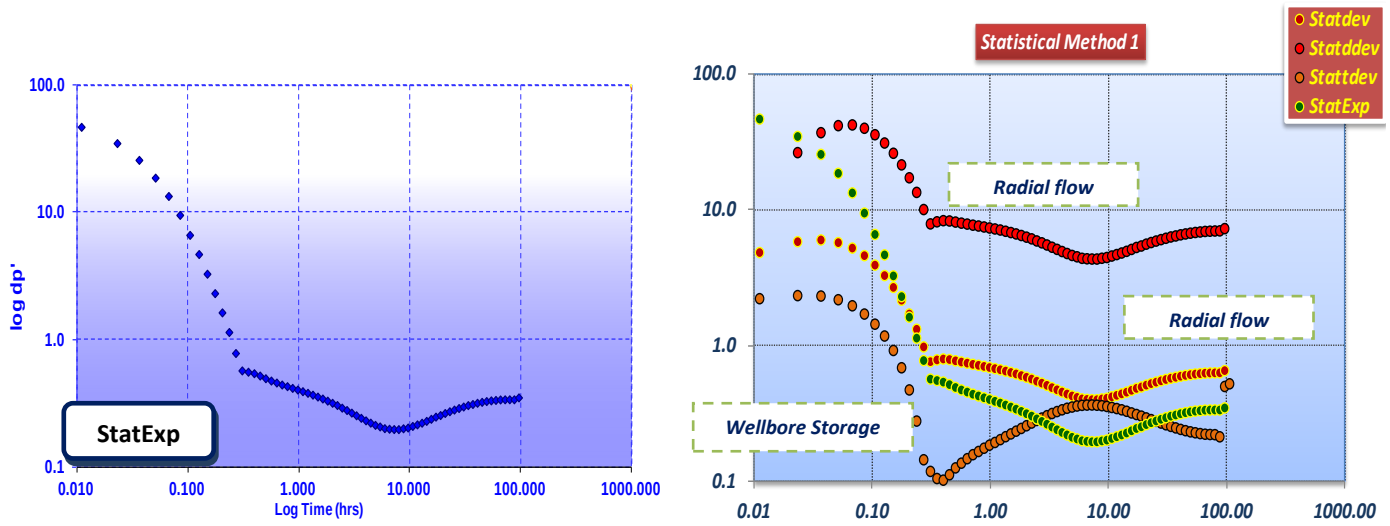

Figure 3.29: StatExp for dual porosity reservoir model.

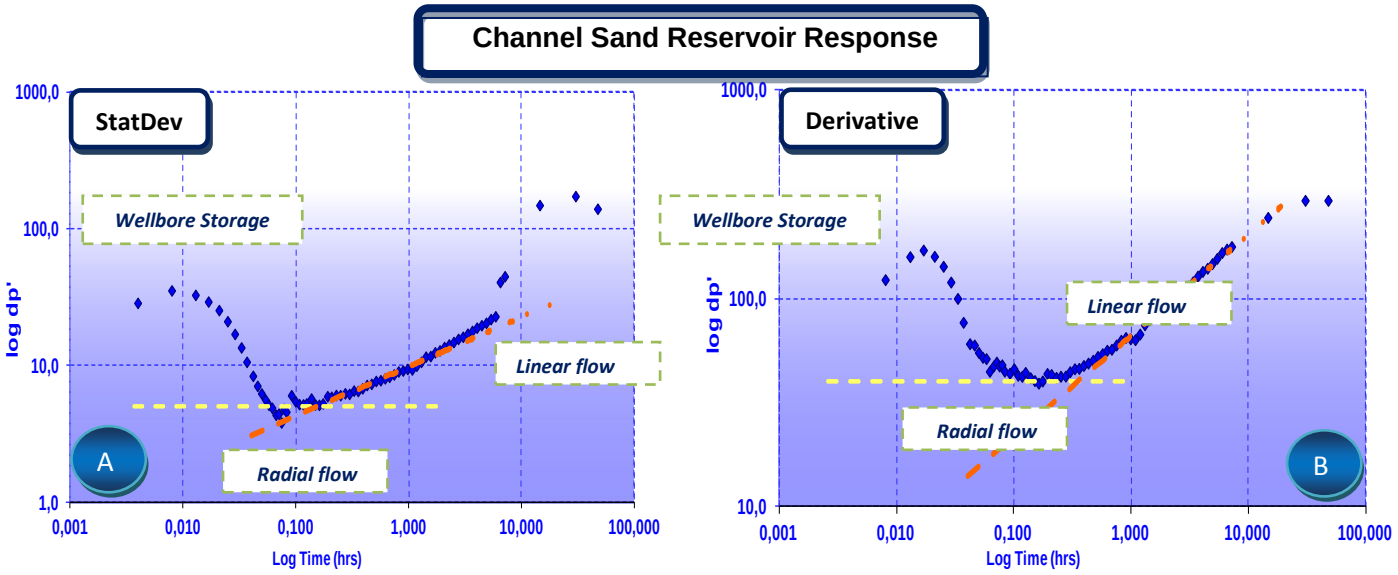

Figure 3.30: Comparisons of Derivative and StatDev Diagnostics Approach

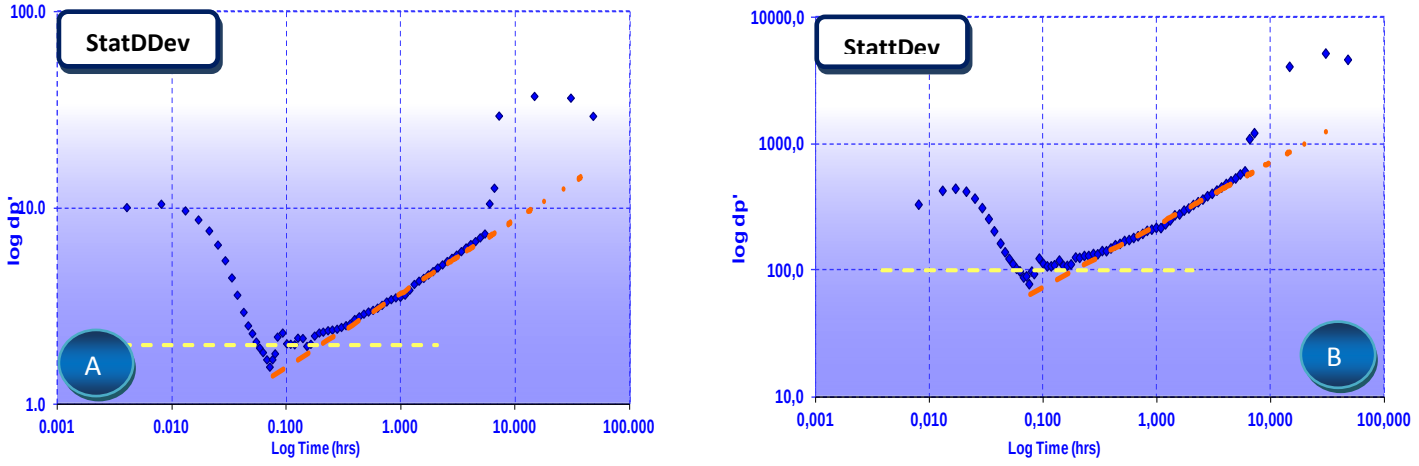

Figure 3.31: Comparisons of StatDDev and StattDev Diagnostics Approach

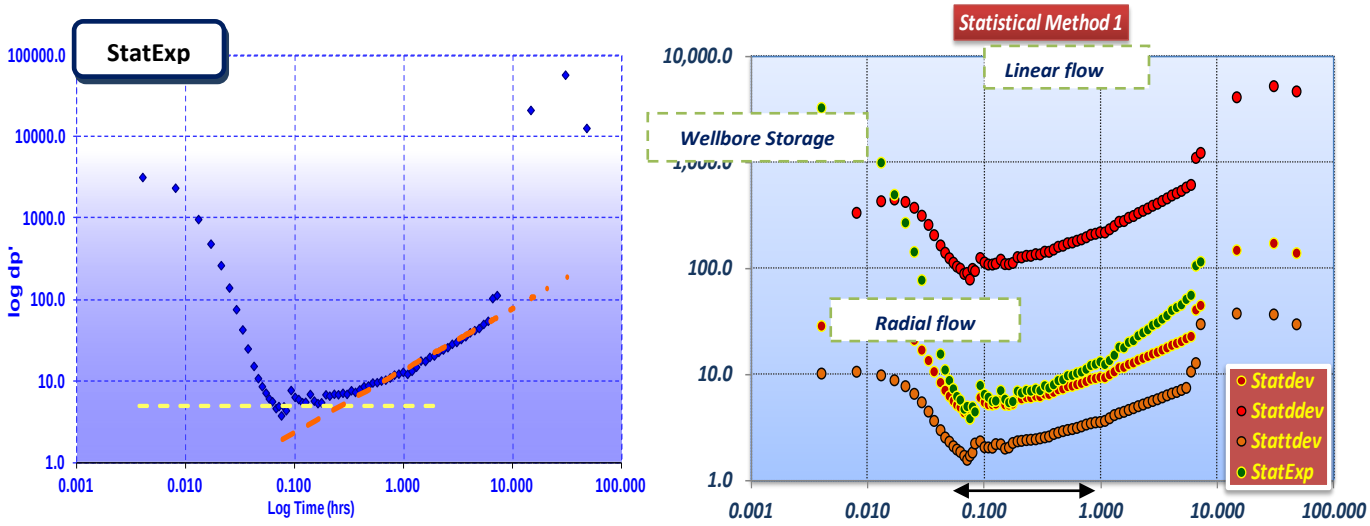

Figure 3.32: StatExp for channel reservoir model.

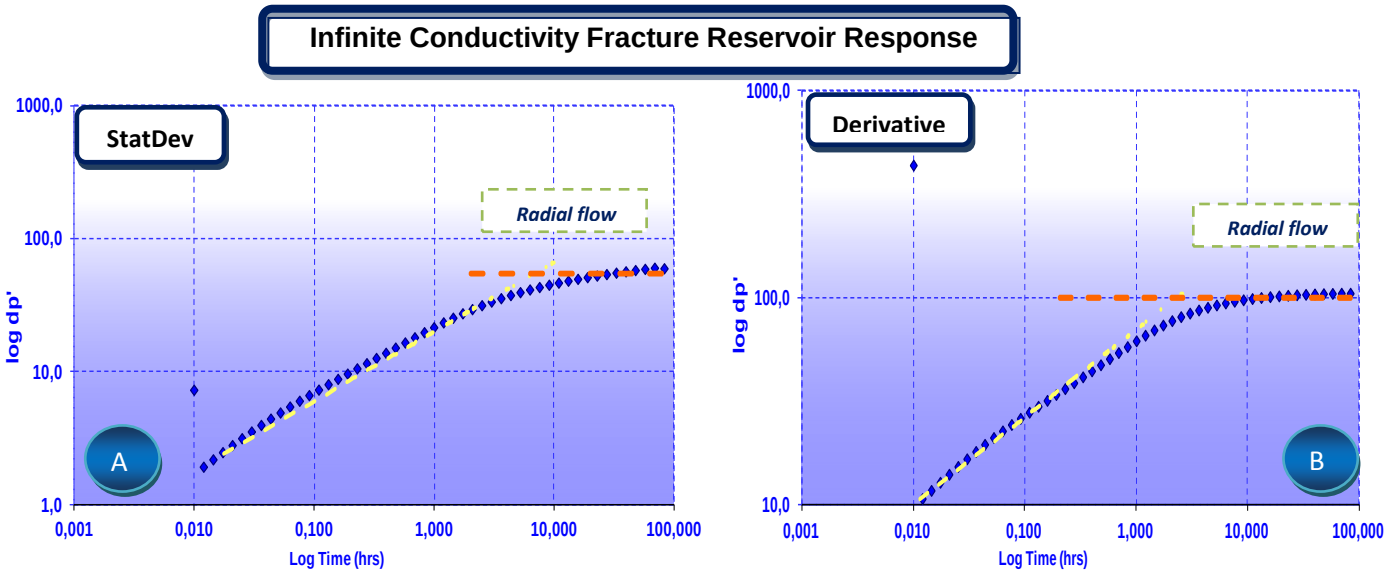

Figure 3.33: Comparisons of Derivative and StatDev Diagnostics Approach

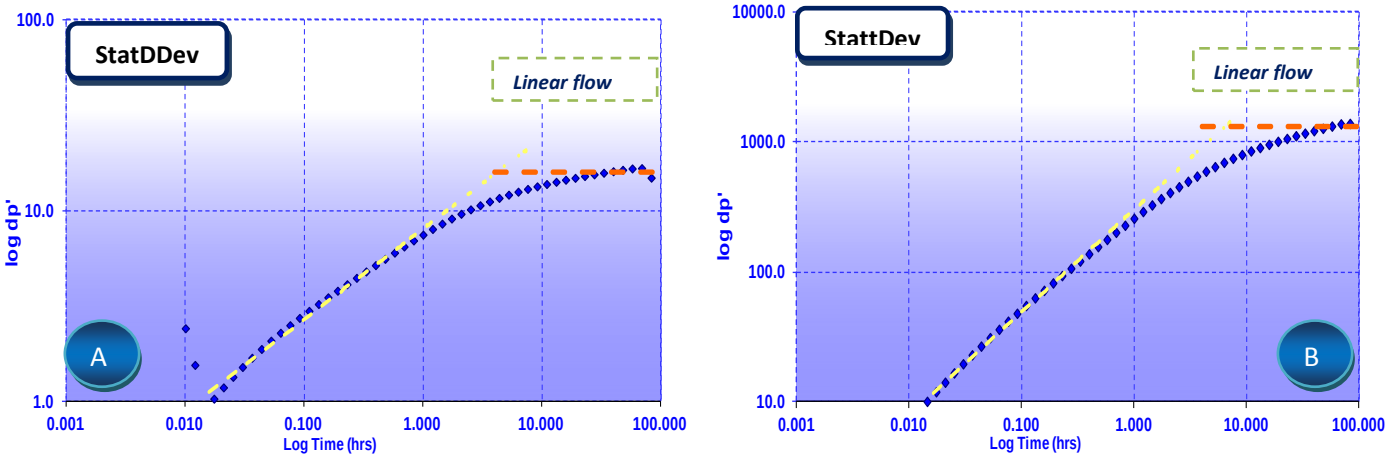

Figure 3.34: Comparisons of StatDDev and StattDev Diagnostics Approach

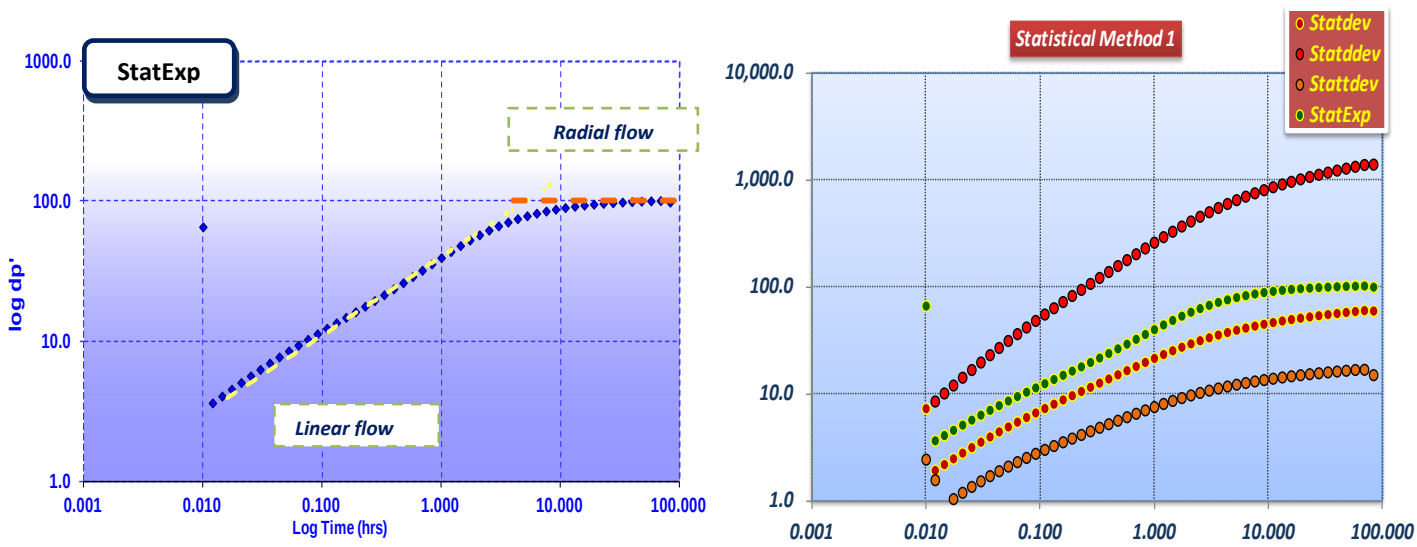

Figure 3.35: StatExp for infinite conductivity fracture response.

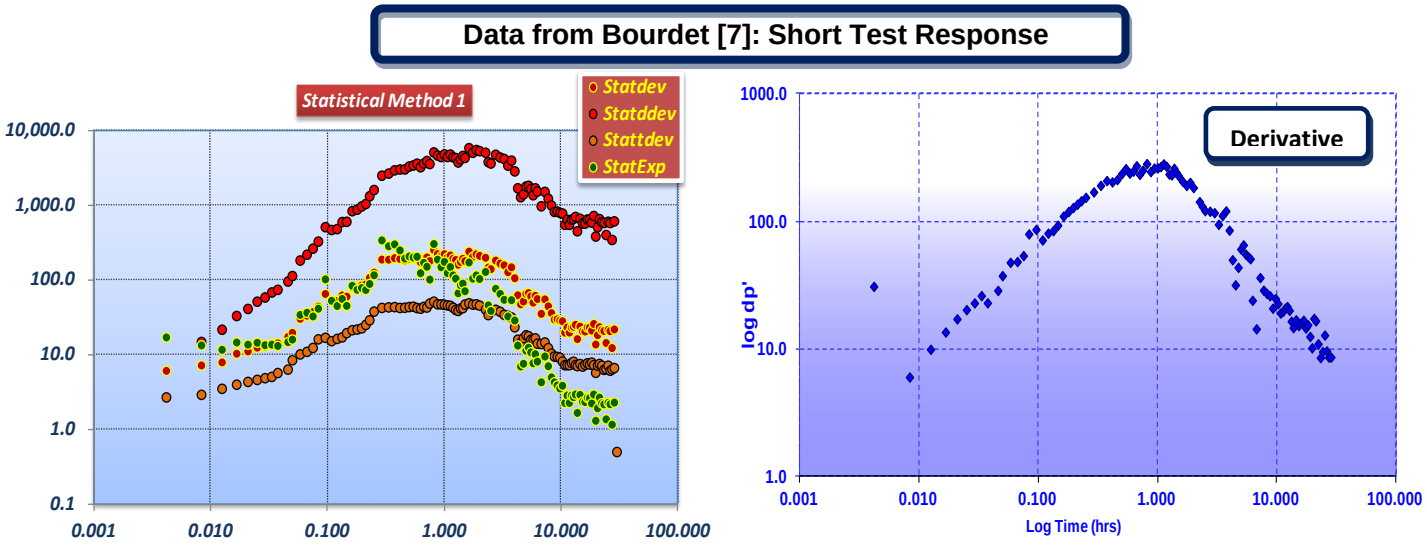

Figure 3.36: All Statistical models for reservoir model diagnosis and StatExp for a short test response

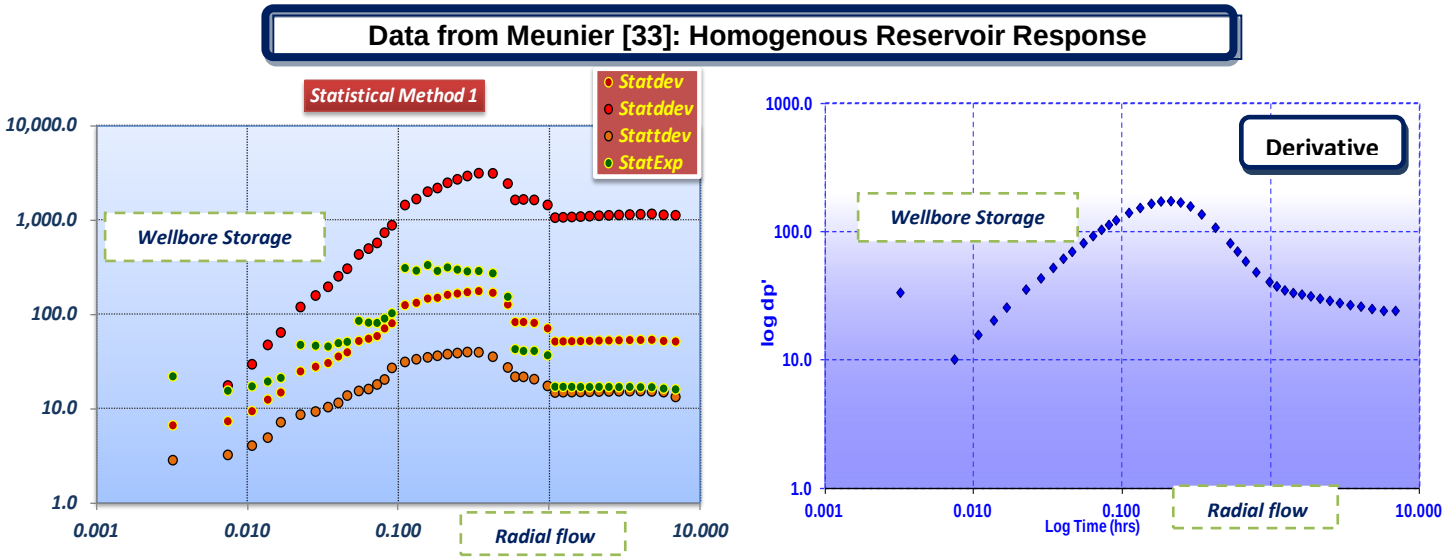

Figure 3.37: All Statistical models for reservoir model diagnosis and StatExp for homogeneous response

Chapter four

Numerical Density Derivative

4.1 Introduction

One of the main limitations of the pressure derivative is that in situation of multiphase flow around the wellbore, the derivative data are often noisy and difficult to interpret, resulting to the application of deconvolution and various smoothing techniques to obtain a perceived representative model which often might not be. Also, the analytical solution for transient pressure analysis is limited to single phase flow which in real case is never the situation, hence production condition with multiple phase are difficult to interpret. Presently, there are few literatures on multiphase transient pressure analysis.

Chapter 4 introduces the numerical density derivative approach (another phase of numerical well testing) in which each fluid densities around the wellbore are measured and used to generate pressure equivalent for each phase using simplified pressure-density correlation or directly used for transient analysis. Then the new statistical 'pressure' derivative method is used to determine the individual fluid phase permeabilities, and then the average effective permeability for the system is estimated from a newly introduced empirical model. Incipiently, we chronicled some of the interesting research work performed so far on multiphase conditions in PTA.

4.2 Multiphase Theory:

The single phase flow equation which has remained the basis for dynamic behavior of subsurface fluid is derived from Darcy's law [20], conservation of mass and PVT relationship.

$$\nabla \bullet \left[\frac{\rho k}{\mu} \left(\nabla P - \gamma \nabla z \right) \right] = \frac{\partial}{\partial t} \left(\phi \rho \right) \qquad 4.1$$

This equation assumed continuous flow of a single phase at a given time limiting its application to complex multiphase phase fluid behavior. However, the equation can be modified considering the different fluid phases (gas, oil, water) to accommodate the simultaneous flow of more than one phase in the reservoir. The effective mobility of the reservoir differs for each phase and is often less than that when the reservoir is fully saturated with a single phase. The single phase permeability is denoted by the absolute permeability, k, while specific phase permeabilities are represented as effective phase permeabilities, $k_{p,}$ where subscript p is oil, water or gas. The relationship between the absolute permeability and effective phase permeabilities is the relative permeabilities $k_{r.}$ Therefore for multiphase condition, applying the Darcy's and conservation of mass, the flow equation would be written as:

$$v_p = \frac{kk_{rp}}{\mu_p} \bullet \left[\frac{\rho k}{\mu} \left(\nabla P - \gamma \nabla z \right) \right] \qquad 4.2$$

Where the subscript p denotes each phase.

The phase p relative permeability, k_{rp}, is a rock property concept used to represents the dynamic multiphase fluid flow behavior at pore scale. Rapoport and Leas [71], demonstrated the reliability of relative permeability with the following assumptions:

1. The fluid phases are continuous with laminar flowing condition.
2. A flow direction that is strongly a function of saturation.

In general, multiphase flow condition is best described by the combination of Darcy's law, thermodynamic equilibrium and fluid PVT properties which encompass the mass transfer across fluid interphase. Therefore for multiphase condition, with negligible gravity and capillary pressure effects, assuming that there is equilibrium between three phases (no mass transfer or evaporation effect), the general equation for such multiphase condition is given as:

For oil

$$\nabla \bullet \left[\frac{kk_{ro}}{\mu_o B_o} \nabla p \right] = \frac{\partial}{\partial t} \bullet \left[\frac{\phi S_o}{B_o} \right] \quad 4.3$$

For gas

$$\nabla \bullet \left[k \left[\frac{k_{rg}}{\mu_g B_g} + \frac{R_s k_{ro}}{\mu_o B_o} \right] \right] \nabla p = \frac{\partial}{\partial t} \bullet \left[\phi \left[\frac{S_g}{B_g} + \frac{R_s S_o}{B_o} \right] \right] \quad 4.4$$

For water

$$\nabla \bullet \left[\frac{kk_{rw}}{\mu_o B_w} \nabla p \right] = \frac{\partial}{\partial t} \bullet \left[\frac{\phi S_w}{B_w} \right] \quad 4.5$$

Where

B = Formation volume factor,

Rs = Solution gas-oil ratio,

s = Saturation

Subscript p =phase

Subscript o, g, w = oil, gas, water

4.3 Multiphase well testing

Well test has remained the most important tool for characterizing the dynamic fluid flow behavior of oil and gas reservoirs. Researches, publications, books, monographs on PTA and its application in different reservoir and testing conditions have been presented and published in the last six decades by engineers, well test specialist, academia, renowned researchers on the subjects including Matthews et al, Russell, Earlougher, Lee; [53] [26] [48] but with limited research work done on multiphase flow concept. Nygard [60] worked on the possibility of generating relative permeability curves from PTA but his results on pseudo pressure m(p) as a function of relative permeability were sensitive.

Till date, the two most reported researches done on multiphase flow condition in PTA with acceptable application in the industry and academia are the pressure approach by Perrine [63] and the pseudo pressure approach by Raghavan [65]. These approaches have gained prominent in well test interpretation of multiphase condition and has remained the reference and background for all new development.

4.3.1 Perrine's Approach

Perrine [63] modified the existing single phase flow equation by integrating an empirical observation to take into account the multi-phase flow effects. He considered two key parameters such as phase mobility and compressibility; assumed by replacing the total mobility and compressibility by their individual phases, the multiphase condition effect can be incorporated. This is shown below:

1. Total mobility k / p modification

$$\lambda_t = \left(\frac{k}{\mu}\right)_o + \left(\frac{k}{\mu}\right)_g + \left(\frac{k}{\mu}\right)_w \qquad 4.6$$

2. Total-system compressibility modification

$$c_t = S_o\left[-\frac{1}{B_o}\frac{\partial B_o}{\partial p} + \frac{B_g}{B_o}\frac{\partial R_s}{\partial p}\right] + S_g\left[-\frac{1}{B_g}\frac{\partial B_g}{\partial p}\right] + S_w\left[-\frac{1}{B_w}\frac{\partial B_w}{\partial p} + \frac{B_g}{B_w}\frac{\partial R_{sw}}{\partial p}\right] + c_f \qquad 4.7$$

Considering the wellbore skin and total system compressibility, Earlougher [26] summarizes the Perrine's individual phase mobilities as:

$$k_p = \frac{162.6 q_p \mu_p B_p}{m^* h} \qquad 4.8$$

And m* = slope of specialist plot (semi log of pressure time curve as developed by MBH, MDH, Horner; [39] [52[55])

Fetkovich & Vienot [31] and Raghavan [66] developed the solution for total system mobility as:

$$\lambda_t = \left(k/\mu\right)_t \frac{162.6 q_t}{m * h} \quad 4.9$$

Where

$$q_t = q_o B_o + \left[q_g - q_o R_s - q_w R_{sw}\right] B_g + q_w B_w \quad 4.10$$

Perrine's summarized the wellbore skin as:

$$s = 1.151\left[\frac{p_{1hr} - p_i}{m*}\right] - \log\left(\frac{\lambda_l}{\phi c_t r_w^{\,2}}\right) + 3.23 \quad 4.11$$

Martin [50] developed a pressure equation to support Perrine's analytical solution without taking into account pressure and saturation gradients. He concluded that Perrine solution was based on:

$$\nabla^2 p = \frac{\phi c_t}{\lambda_t}\frac{\partial p}{dt} \quad 4.12$$

He linearised the equation above assuming constant total compressibility-mobility ratio, but applied the inner boundary condition below assuming constant oil rate:

$$\lim_{r \to r_w}\left[r \frac{k_{rl}}{\mu_l B_l}\frac{\partial p}{\partial r}\right] = \frac{q_l}{2\pi k h} \quad 4.13$$

Other researchers such as Weller [85] and Kazemi [45] tried to advance the Perrine's solution using depletion reservoir and near wellbore simulator with several transient tests. They concluded that Perrine's approach is less reliable when gas saturation increases around the well; but can still be used to calculate the skin and the average reservoir pressure. In this case, the liquid compressibility will be used instead of the total compressibility.

Likewise, Chu et al. [16], Ayan and Lee [8] worked on the Perrine's approach for cases with and without saturation gradient on several oil and gas reservoirs (saturated and under saturated). While Chu et al. concluded that total mobility can be determined; estimating the individual phase mobility is unrealistic unless saturation distribution is uniform. In the case of Ayan and Lee [8], they concluded that for the Perrine's method, the estimated skin is a

function of the saturation distribution around the wellbore, therefore estimating relative permeability curve and absolute permeability could be unreliable.

4.3.2 Raghavan's Approach and Other Researchers

Raghavan [65] worked on multiphase PTA using pseudo pressure obtained from solution gas-drive reservoirs to analyze and interpret well test data, then determine reservoir permeability and well bore skin. Below is the pseudo pressure developed by Raghavan's [65] :

$$m(p) = \int_{p_{ref}}^{p_e} \frac{k_{ro}}{\mu_o B_o} \partial p \qquad 4.14$$

After investigating several buildup and drawdown tests, he demonstrated that m(p) is dependent on pressure and GOR to perform a good analysis but the process of generating m(p) is tedious and frustrating. Therefore he concluded that the principle of superposition used in traditional well test interpretation is not applicable for multiphase test in solution gas-drive reservoirs [81].

BΦe et. al [15] advanced Raghavan's [65] multiphase pseudo pressure equation above by using producing gas-oil ratio to resolve the m(p) integral and then apply Boltzmann transformation. They concluded that for infinite reservoir, the reservoir saturation is strongly dependent on pressure. With constant compressibility-mobility term, they developed the approximate line source solution defined below:

$$m(p_w) = m(p_i) - \frac{141.2 q_o}{kh}\left[0.5\left(\ln t_D + 0.80907 + 2s\right)\right] \qquad 4.15$$

Where

$$t_D = \frac{0.000264kt}{\phi r_w^{\,2}\left(\frac{c}{\lambda}\right)^{*/}} \qquad 4.16$$

Aanonsen [1] worked on Raghavan's approach but discovered that m(p) is strongly dependent on the relative permeability curves which are often generated from laboratory. Therefore, he concluded that Ragbavan's [65] approach could be susceptible to error unless the laboratory conditions in which the curves are generated were identical to the reservoir. Aanonsen's study also demonstrated that the non-linear two phase solutions are unsuitable for superposition application.

Raghavan [66] reviewed the analytical solution developed by Perrine and concluded as follows:

- For solution gas drive reservoirs:
    - The instantaneous total rate is used to normalise the drawdown rate as recommended by Winestock and Colpitts [87]
    - The total rate at shut-in (q, at $\Delta t = 0$) is used to normalise the buildup rate as recommended by Uraiet and Raghavan [79]
    - The pressure change during drawdown and buildup are identical, $p_i - p_{wf} = p_{ws} - p_{wf}$

Evinger and Muskat [29] worked on well productivity in a multiphase condition considering steady state radial flow condition and developed the equation below:

$$q_o = \frac{kh_l}{141.2 \bullet \ln \frac{r_e}{r}} \int_{p}^{p_e} \frac{k_{ro}}{\mu_o B_o} \partial p \qquad 4.17$$

Where r_e = external radius, h = thickness and k_{ro} is dependent on oil saturation. They developed a general procedure for applying the equation $GOR = R_s + \frac{k_{rg}}{k_{ro}} \frac{\mu_o B_o}{\mu_g B_g}$ and oil rate integral solution in PTA as follows:

1. P_{wf} and GOR are monitored during the test.

2. The relative permeability term in the GOR equation are determined for each GOR value and tabulated against each P_{wf}.
3. Pressure-saturation values are generated with the replacement of k_{rg} / k_{ro} with saturation from the k_{rg} / k_{ro} - saturation curve.
4. Replacing the saturations with each k_{ro} values from the k_{ro} - saturation curve, a new table of k_{ro} versus pressure is generated.
5. The table is then used to resolve the integral of oil flow rate.

To advance on the method of Evinger and Muskat [29], Levine and Prats [49] investigated transient test in solution gas-drive reservoirs with numerical models and concluded that the maximum variation of GOR from the outer to the inner boundary was only 10.9% for the cases investigated; however, the impact of gas-oil ratio with time was unexplored.

Fetkovich [30] developed an empirical model for isochronal testing of gas wells in solution gas-drive reservoirs. Comparing oil and gas well behavior, he introduced the equation that is similar to back pressure equation for gas wells:

$$q_o = j_o'\left(\bar{p}^2 - p_{wf}{}^2\right)^n \qquad 4.18$$

Where:

J_o = back-pressure curve coefficient,

P = average reservoir pressure,

P_{wf} = wellbore flowing pressure, and

n = exponent.

Additionally, he introduced the pseudo pressure concept m(p) and developed a solution for two phase gas-oil model for interpreting transient and pseudo steady state with the equation:

$$m(p) = \int_{p_{ref}}^{p_e} \frac{k_{ro}}{\mu_o B_o} \partial p$$

Where P_{ref} is a base pressure.

For the transient period, the oil flow rate is defined as follows:

$$q_o = \frac{kh_l}{141.2\left(0.5\ln t_D + 0.4045 + s\right)}\left[m\left(p_i\right) - m\left(p_{wf}\right)\right] \quad 4.19$$

While for the pseudo steady state period, oil flow rate is defined as follows:

$$q_o = \frac{kh_l}{141.2\left[\ln\frac{0.472r_e}{r_w} + s\right]}\left[m\left(p_i\right) - m\left(p_{wf}\right)\right] \quad 4.20$$

Where:

q_o = oil rate,

p_i = initial pressure,

p= average pressure,

s = skin

t_D= dimensionless time defined as:

$$t_D = \frac{0.000264kt}{\phi\left(\mu c_t\right)_i r_w{}^2}$$

Other researchers including Nygard, Whitson, Evinger-Muskat's, Al-Khalifah, Jones and Raghavan; [60][88][29][4][43] have attempted to estimate absolute permeability from buildup and drawdown test using pseudo pressure m(p) – relative permeability curve to resolve the m(p) integral for steady and pseudo steady state. These methods were further work on the existing Perrine and Raghavan's approach on multiphase testing. Although, they were able to estimate permeability and wellbore skin which agree with Fetkovich's, Al-Khalifah, Al-Khalifah et al, Raghavan results;[30][5][6][66], the results were susceptible to error because of the relative permeability curves used in generation m(p).

Generally PTA is limited to single phase test, but where multiphase well test analysis is required, only two methods: "Perrine [63] and Raghavan [65] "approaches are references for such interpretation. While the Perrine method has helped to estimate the total mobility,

Ragbavan's method is reported to underestimate the phase permeabilities. Several studies have shown that Raghavan's method is very sensitive to relative permeability curves, and requires iterative computation thereby making it complex in practical application and non-user friendly. Conclusively, applying both methods in current well testing techniques depend on the reliability of the relative permeability curve used in determining the absolute and phase permeability.

This study introduces the density derivative method which uses the densities of each fluid phase to generate pressure-density equivalent derivatives or directly density derivatives, hence a better approach for estimating phase permeabilities and average absolute permeability. This approach also provides the % of each phase contribution to flow at a given point and with further work can be used to generate relative k at several dp' stabilisation points. Therefore, it is pertinent to say that a combination of the statistical 'pressure' derivative by Biu and Zheng [12] and density derivative approach would serve as support transient analysis tool for interpreting well test data.

In this chapter, the pressure derivative formulation from Horne [37] and the new statistical 'pressure' derivative demonstrated in chapter 3 would be used throughout this analysis. Also, the derivation of the density radial flow equation for each fluid phase and the non-unique analytical solution obtained from Laplace transformation considering inner and outer boundary assumptions is presented.

4.4 Theoretical Concept of the Density Derivatives

The basic concept involved in the derivation of fluid flow equation includes:

I. Conservation of mass equation,

II. Transport rate equation (e.g Darcy's Law),

III. Equation of State,

Consider a flow in a cylindrical coordinates with flow in angular and z-directions neglected, the equations are given as follow:

Mass rate in – Mass rate out =Mass rate storage (4.21)

The above equation 4.21 represents the conservation of mass. Since the fluid is moving, the equation below is applied.

$$q = -\frac{k}{\mu} A \frac{\partial p}{\partial r} \tag{4.22}$$

By conserving mass in an elemental control volume shown in Figure 3.6 and applying transport rate equation, the following equation is obtained:

$$-\left[\frac{2\pi rhk}{\mu}\rho\frac{\partial p}{\partial r}\right]_r = -\left[\frac{2\pi rkh}{\mu}\rho\frac{\partial p}{\partial r}\right]_{r+\Delta r} + 2\pi r\Delta rh\frac{\partial}{\partial t}(\rho\phi) \tag{4.23}$$

Expanding the equation using Taylor Series

$$\frac{1}{r}\frac{\partial}{\partial r}\left[\frac{rk\rho}{\mu}\frac{\partial p}{\partial r}\right] = \frac{\partial}{\partial t}[\rho\phi] \tag{4.24}$$

Equation 4.21 to 4.24 applies to both liquid and gas. Equation 4.24 is known as the general diffusivity equation, and for each fluid, the density or pressure term in equation 4.24 can be replaced by the correct expression in terms of density or pressure.

For slight or compressibility liquid,

$$\rho = \rho_o e^{c[p-p_o]} \tag{4.25}$$

Substituting for pressure in the equation, the diffusivity equation in terms of density is given as:

$$\frac{\partial^2\rho}{\partial r^2} + \frac{1}{r}\frac{\partial\rho}{\partial r} = \frac{\phi\mu[c+cr]}{k}\frac{\partial\rho}{\partial t} \tag{4.26}$$

$$\frac{\partial^2\rho}{\partial r^2} + \frac{1}{r}\frac{\partial\rho}{\partial r} = \frac{\phi\mu c_t}{k}\frac{\partial\rho}{\partial t} \tag{4.27}$$

Equation 4.27 is known as the density diffusivity equation which can also be rewritten in form of pressure. Over the decades, the transient test analysis has applied the general diffusivity equation in pressure term to generate several non-unique solutions using several pressure- rate data.

Invariably as in pressure term, the density term is also implored

$$\frac{\partial^2 \rho}{\partial r} + \frac{1}{r}\frac{\partial \rho}{\partial r} = \frac{1}{r}\frac{\partial}{\partial r}\left(r\frac{\partial \rho}{\partial r}\right) = 0 \tag{4.28}$$

For inner boundary condition

$$\left[r\frac{\partial \rho}{\partial r}\right]_{rw} = \frac{q\mu}{2\pi kh} = \text{Constant} \tag{4.29}$$

Outer boundary condition

$$\rho = \rho_e \quad \text{at} \quad r = r_e \tag{4.30}$$

Presently, industry design tools for measuring fluid densities at well bottom hole during flowing and shut-in testing conditions are unavailable. For simplification and application of the density derivative in existing well test software, the density-pressure equivalent equation is formulated.

To comprehensively investigate the application of this approach, five synthetic case studies for both oil and gas condensate reservoirs were considered using numerical model built with eclipse simulator.

The eclipse keywords LBPR, LDENO, LDENW, LDENG AND WBHP were output to obtain the density and pressure change around the well and as far as the perturbation could extend.

4.5 Software Suitability (Pressure Equivalent)

To apply the numerical density approach in existing software, the pressure equivalent of the fluid density change at the wellbore is generated from the relationship below:

Using the isothermal compressibility coefficient c, in terms of density,

$$c = \frac{1}{\rho}\frac{\partial \rho}{\partial p} \tag{4.31}$$

For slightly compressibility fluid such as oil and water, re-arranging the parameters w.r.t ∂p and $\partial \rho$

$$-c\int_{p_i}^{p} dp = \int_{\rho_i}^{\rho} \frac{\partial \rho}{\rho} \tag{4.32}$$

Integrating

$$e^{c[p_i - p]} = \frac{\rho}{\rho_i} \tag{4.33}$$

$$c[p_i - p] = \ln\left[\frac{\rho}{\rho_i}\right]$$

$$p = p_i - \frac{\ln\left[\frac{\rho}{\rho_i}\right]}{c} \tag{4.34}$$

Or

Applying the e^x expansion series,

$$e^x = 1 + x + \frac{x^2}{2!} + \frac{x^3}{3!} + ... + \frac{x^n}{n!} \tag{4.35}$$

Because the term $c(p_i - p)$ is very small, the e^x term can be approximated as:

$$e^x = 1 + x$$

Therefore equation 4.34 can be rewritten as

$$\rho = \rho_i[1 - c(p_i - p)]$$

$$\frac{\rho}{\rho_i} = 1 - c[p_i - p]$$

$$p = p_i - \left[\frac{\frac{\rho}{\rho_i} + 1}{c}\right] \tag{4.36}$$

Equations 4.34 and 4.36 are the density equivalent pressure algorithm for slightly compressible fluid such as oil and water

$$p = p_{oi} - \frac{\ln\left[\frac{\rho}{\rho_{oi}}\right]}{c} \quad \text{or} \quad p = p_{oi} - \left[\frac{\frac{\rho}{\rho_{oi}} + 1}{c}\right]$$

Either equation 4.34 or 4.36 can be used to generate the pressure equivalent from each phase densities for slightly compressibility fluid such as oil and water. Pressure is then analysed in any of the well test software.

For compressible fluid, considering isothermal conditions

$$c_g = -\frac{1}{v}\left[\frac{\partial v}{\partial p}\right]_T \tag{4.37}$$

For real gas equation of state

$$v = \frac{nRTz}{P}$$

Differentiating the above equation with respect to pressure at constant temperature

$$\left(\frac{\partial v}{\partial p}\right)_T = nRT\left[\frac{1}{p}\left(\frac{\partial z}{\partial p}\right) - \frac{z}{p^2}\right] \tag{4.38}$$

Substituting equation 4.38 into 4.37 gives

$$c_g = \frac{1}{p} - \frac{1}{z}\left[\frac{dz}{dp}\right]$$

In terms of density

$$c_g = \frac{1}{p} - \frac{1}{\rho}\left[\frac{\partial \rho}{\partial p}\right] \tag{4.39}$$

This equation is applicable for real gas condition.

Rearranging the parameters w.r.t ∂p and $\partial \rho$

$$\frac{1}{\rho}\left[\frac{\partial \rho}{\partial p}\right] = \frac{1}{p} - c_g$$

$$\int_{\rho_i}^{\rho} \frac{\partial \rho}{\rho} = \int_{p_i}^{p}\left[\frac{\partial p}{p} - \partial p c_g\right]$$

$$\ln\left[\frac{\rho}{\rho_i}\right] = \ln\left[\frac{p}{p_i}\right] - [p - p_i]c_g \tag{4.40}$$

Applying the power series for $\ln p$

$$\ln[\rho] = [\rho - 1] - \frac{[\rho - 1]^2}{2} + \ldots\ldots\ldots + \frac{[-1]^n[\rho - 1]^n}{n} + \ldots\ldots\ldots 0 < \rho \le 2 \tag{4.41}$$

Limit $\ln x$ to only the 1st term only

$$\left[\frac{\rho}{\rho_i}\right] - 1 = \left[\frac{p}{p_i}\right] - 1 - [p - p_i]c_g \tag{4.42}$$

$$\left[\frac{\rho}{\rho_i}\right] = \left[\frac{p}{p_i}\right] - [p - p_i]c_g$$

$$\left[\frac{\rho}{\rho_i}\right] = \frac{p - pp_i c_g - p_i^{\,2} c_g}{p_i} \tag{4.43}$$

$$\frac{p_i \rho}{\rho_i} - p_i^{\,2} c_g = p\left[1 - p_i c_g\right]$$

$$p = \frac{\frac{p_i \rho}{\rho_i} - p_i^{\,2} c_g}{1 - p_i c_g} \tag{4.44}$$

Equation 4.44 is used to generate the pressure equivalent from the fluid density for compressible fluid such as gas, which is then analysed in well test interpretation software. Besides the software, pressure equivalent or individual phase densities can be directly analysed with the Horne [37] mathematical model or statistical 'pressure' derivative approach presented in chapter 3. To test this method, a synthetic numerical model as shown in Figure 3.7 was considered.

4.6 Density Weighted Average DWA

While equations 4.34, 4.36 or 4.44 give the pressure equivalent for independent fluid phases such as gas, oil and water; the weighted average method is used to obtain the density equivalent for two or three phase combination. This equivalent pressure derived from the densities of all three fluid components such as gas, oil and water is defined as:

$$P_i = \frac{\rho_g p_i + \rho_o p_o + \rho_w p_w}{\rho_g + \rho_o + \rho_w} \tag{4.45}$$

Equation 4.45 comprises of all the fluid phases in the system and as such will be comparable to the conventional bottom hole pressure measurement interpretation during the derivative analysis.

4.7 Geometrical correlation between fluid phases k

Warren and Price [99] reviewed permeability estimate from a number of core samples, assuming the sample represent a heterogeneous reservoir and illustrated experimentally that the most probable behaviour of a heterogeneous formation approaches that of a uniform system having a permeability that is equal to the geometric average. The geometric average is defined mathematically by the following relationship:

$$k_{ave} = \exp\left[\frac{\sum_{j=1}^{n}\left(h_j \ln\left(k_j\right)\right)}{\sum_{j=1}^{n} h_j}\right]$$ [99]. If the thicknesses (h_j) of all core samples are the same

$$k_{ave} = \left(k_1 k_2 k_3 \ldots\ldots\ldots\ldots\ldots k_n\right)^{\frac{1}{n}}$$

Therefore, for a given set of bottom hole fluid density data, integrating the three fluid phases' permeabilities for a multiphase system with the phases more heterogeneous, the average reservoir permeability can be estimated using the geometric correlation with fluid phases modelled as heterogeneous parameters. The geometric average is given as:

$$k_{ave} = \sqrt[4]{k_o k_w k^2{}_g} \ . \qquad (4.46)$$

Where

k_o = oil phase permeability

k_g = gas phase permeability

k_w = water phase permeability

With the phases' permeabilities, it is possible to estimate each phase percentage contribution to flow at given point; so generating relative permeability curve is feasible in future work

To illustrate the applicability of this approach, five examples in conventional oil and gas condensate reservoir as shown in Figures 4.1 and 4.2 are considered using numerical model. The eclipse keywords - Local refinement bottom hole pressure: (LBPR), Local refinement oil density: (LDENO), Local refinement water density: (LDENW), Local refinement gas density: (LDENG) and well bottom hole pressure: (WBHP), were output to obtain the density and pressure change around the well.

4.8 Flow Regime Identification and Estimation of Permeability k (mD) after Pressure-Density Equivalent PDE Diagnostic Approach

4.8.1 Example 1.0 → Low k, oil and gas reservoir using Synthetic data

To test the density derivative method, numerical well test model with the following assumptions are considered:

i. Simulation model with size 10, 5, 5 was built
ii. Oil reservoir + Gas Cap, completed with one well.
iii. Oil thickness = 180 ft, Gas column = 20 ft and water column = 50 ft
iv. Dx ,Dy and DZ assumed to be 500 ft, 400 ft and 50 ft
v. Uniform permeability of 50 mD assign to kx, ky and kz, while average porosity of 20% was imputed in the model. Also, multiply kz by 0.02 was applied.
vi. A conditional Sw and relative permeability was used.
vii. LGR was imposed around the well and far across to account for pressure and density changes. Gas, Oil, Water densities around the local grid refinement (wellbore) and WBHP were output using Eclipse keywords

Four scenarios of different well flowing conditions are investigated. These include:

Production test:

a→: Flowing + Build-up Sequence: Well perforated hp = 30 ft between oil and water layer. Net sand thickness h = 250 ft

b→: Flowing + Build-up Sequence: Well perforated hp = 30 ft inside the oil layer. Net sand thickness h = 250 ft

c→: Flowing + Build-up Sequence. Well perforated hp = 30 ft between gas and oil layer. Net sand thickness h = 250 ft

Falloff Test:

d→: Flowing + Build-up Sequence. Well perforated hp = 30 ft between oil and water layer. Net sand thickness h = 250 ft

Table 4.1: Reservoir and fluid data for example 1.0

Parameters	Design Value
Eclipse model	Black Oil
Model dimension	10 X 5 X 5
Length by Width ft by ft	500 X 400
Thickness ft	250
Permeability kx by ky mD	50.0 by 50.0
Porosity %	20
Well diameter ft	0.60
Initial water saturation Swi %	22
Permeability, k, mD	50
Gas Oil contact GOC ft	8820
Oil water contact OWC ft	9000.0
Initial Pressure, Pi, psia	5000.0
Formation Temperature, T, ^{o}F	200.0

Table 4.1 presents a summary of the well and reservoir synthetic data used for build-up and drawdown simulated scenario with additional information given below. It is required to generate the pressure equivalent, obtain the derivative for each phase, compare their diagnostic signatures and determine the phase permeabilities as well as average reservoir permeability.Figure 4.3 shows the production, shut-in and injection sequence for four scenarios in example 1.0

Example 1.0

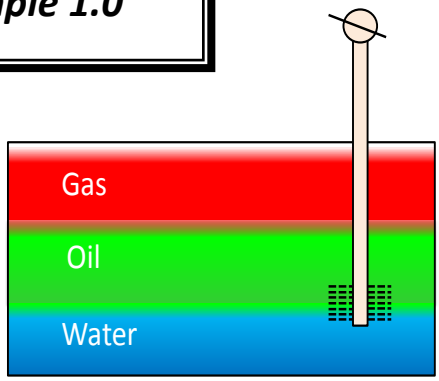

Case 1: Production Test
Flowing + Buildup Sequence
Well perforated hp = 30ft between oil and water layer. Net sand thickness h = 250ft

a

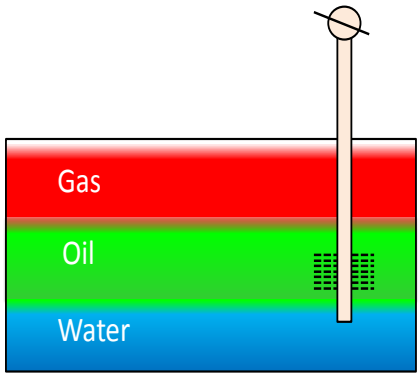

Case 2: Production Test
Flowing + Buildup Sequence
Well perforated hp = 30ft inside the oil layer. Net sand thickness h = 250ft

b

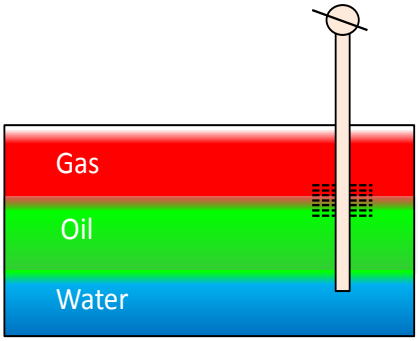

Case 3: Production Test
Flowing + Buildup Sequence
Well perforated hp = 30ft between gas and oil layer. Net sand thickness h = 250ft

c

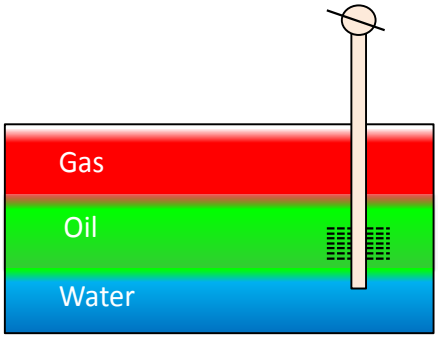

Case 4: Falloff Test
Flowing + Buildup Sequence
Well perforated hp = 30ft between oil and water layer. Net sand thickness h = 250ft

d

Figure 4.1: Schematics of well perforation interval and sand thickness for oil + gas cap + water reservoir

Example 2.0

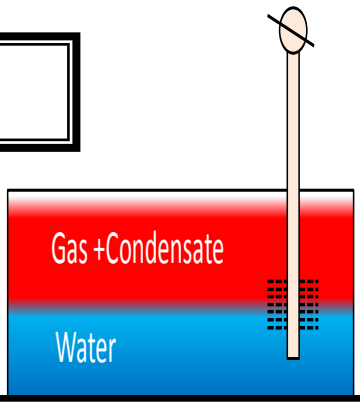

Case 1: Production Test
Flowing + Buildup Sequence
Well perforated hp = 30ft between gas condensate and water layer.
Net sand thickness h = 148ft

a

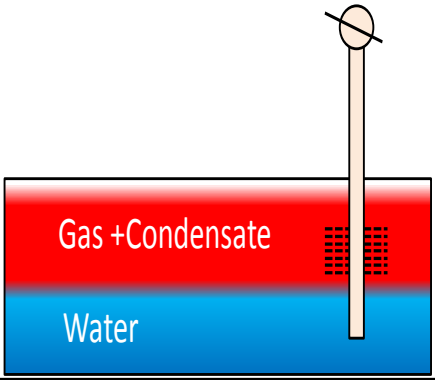

Case 2: Production Test
Flowing + Buildup Sequence
Well perforated hp = 30ft inside gas condensate layer.
Net sand thickness h = 148ft

b

Figure 4.2: Schematics of well perforation interval and sand thickness for gas condensate+ water reservoir

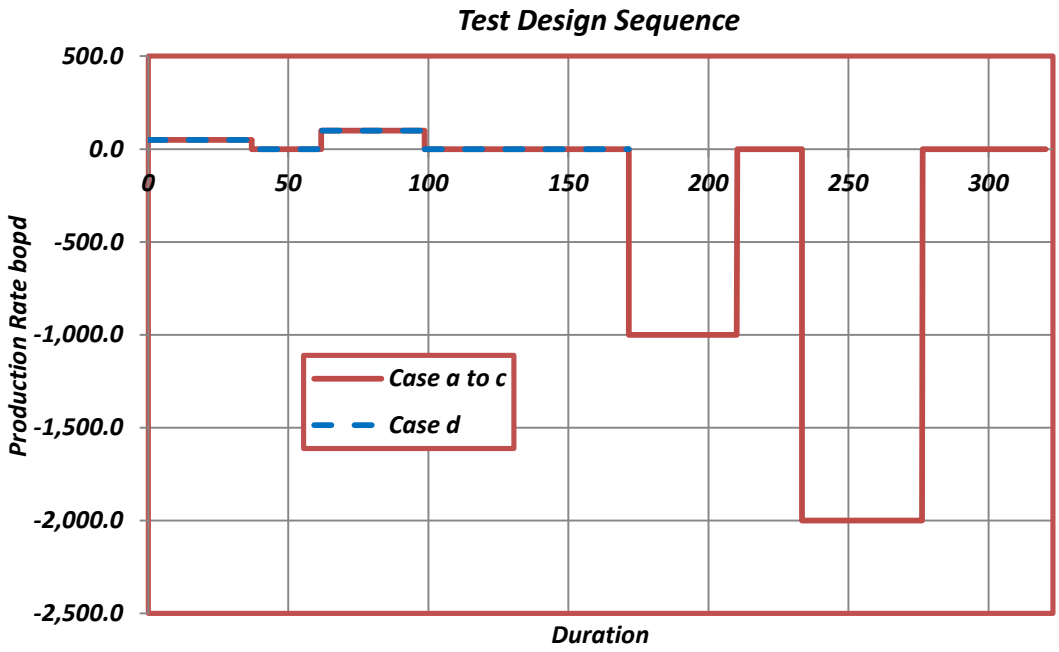

Figure 4.3: Simulation model for Gas cap + oil + water reservoir and Gas condensate+ water showing

a→ In scenario a, the well is completed between the oil and water layer to mimic multiphase conditions at the wellbore and some distance away from the well. Also this scenario enables the observation of the effect on pressure distribution, fluid densities changes around the wellbore as well as estimate fluid phase permeabilities k using the specialised plot and k_{ave} from the geometrical equation for three phase conditions.

The derivative in Figure 4.4 shows a good radial flow but drops at late time due to numerical artefact and constant pressure support. A continuous drop is seen from 10 hrs in all fluid phases derivative signatures confirming the strong presence of this feature. The derivatives for all fluid phases depict same well and reservoir fingerprint three flow regimes, early to late time response) but with different dp' stabilisation. PDENA derivative displays a better and longer stabilisation period than the BPR.

The well bottom hole pressure (BPR→BHP) response shows good overlay with Pressure Equivalent of Density Weighted Average (PDENDWA→PDENA) and Pressure Equivalent of Water Density (PDENWAT→PDENW) while Pressure Equivalent of Gas Density (PDENGAS→PDENG) and Pressure Equivalent of Oil Density (PDENOIL→PDENO) differ completely. The PDENDWA gives a better fingerprint that is less noisy compared to the BPR.

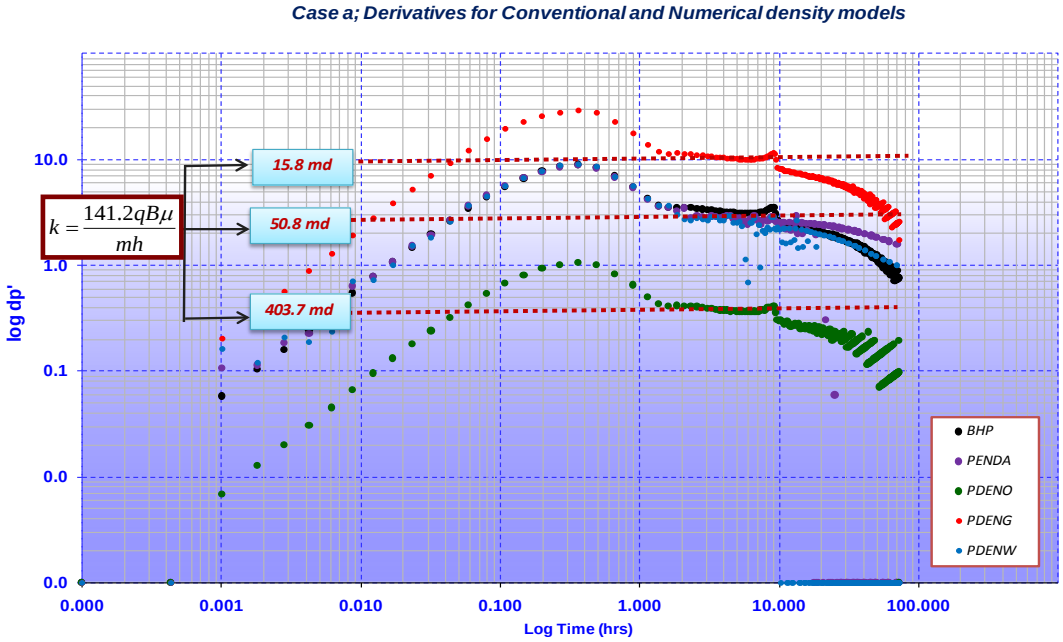

Figure 4.4 Derivative and K estimation for scenario a

A permeability value of 50.8 mD is estimated from the bottom hole pressure BPR where $k = \frac{162.7qB\mu}{mh}$ and m obtained from the specialised plot. This is an approximate of the input value in the simulation model. PDENG and PDENO give 15.8 mD and 403.7 mD respectively while PDENA = PDENW = 50.8 mD. At h=50 ft, the best k estimate is obtained depicting h= 50 ft as the optimise thickness contributing to flow. At h> 50 ft, k drop below

the k imputed in the model. Using the geometrical equation 4.46, the k_{ave} = 47.6 mD is obtained which is approximately close to that of BPR, hence a good estimate of the individual phase permeabilities. A summary of the result is shown in Table 4.2 and 4.7.

Table 4.2; k estimates for new approach versus Conventional approach for scenario a

Parameters	Numerical Density k (mD)	Equivalent h (ft)
BHP	50.8	50
PDENA	50.8	"
PDENG	15.8	"
PDENO	403.7	"
PDENW	50.8	"

b→ In scenario b, the well is completed within the oil section to capture the pressure and fluid densities changes around the well. The derivative in Figure 4.5 shows a good radial flow but with noisy numerical artefact. It is likely the boundary response is masked by numerical artefact. Also a continuous drop is seen after 10hrs in the derivative which is consistent with example 1.0.

BPR gives a permeability value of 50.0 mD, similar for PDENDWA and PDENWAT but differ for PDENGAS and PDENOIL with k = 12.1 and 484.4 mD respectively. At h ➔50 ft (20% of net thickness), 83% of contributing phase to flow comes from the oil phase, using the estimated fluid phase permeabilities, the k_{ave} from geometrical equation 4.46 is around 43.2 mD as shown in Table 4.7.

Table 4.3; k estimates for new approach versus Conventional approach for scenario b

Parameters	Numerical Density k (mD)	Equivalent h (ft)
BHP	50.0	50
PDENA	50.0	"
PDENG	12.1	"
PDENO	484.2	"
PDENW	50.0	"

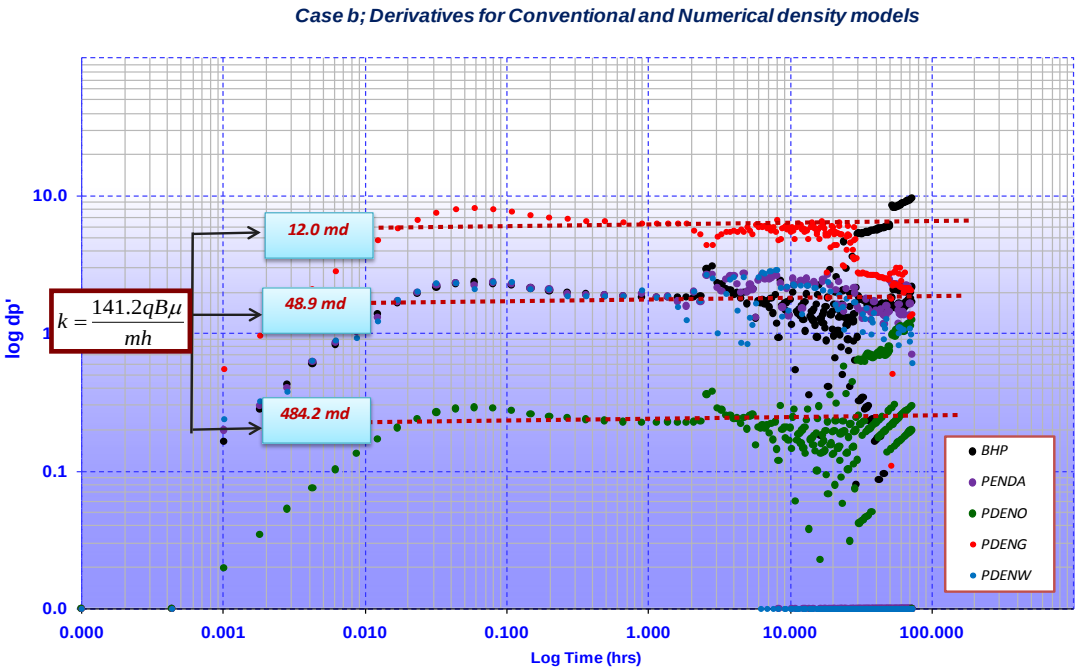

Figure 4.5: Derivative and K estimation for scenario b

To test this approach in the gas column, the well was completed in between the gas and oil layer, which is considered as scenario c. For scenario d, the well is completed within the oil layer but with water injection after flowing and shut-in sequence. In both scenarios, the multiphase fluid distribution is triggered at the wellbore in order to capture the density changes for each phase and calculate fluid phase permeabilities. First, the well fluid densities equivalent pressures and pressures at bottom hole for flowing and build-up test are generated.

c and d → The derivatives for both scenarios show good radial flow but decline at late time due to fluid redistribution but noisy (numerical artefact) as shown in Figure 4.6 and 4.7. A continuous drop is seen from 3-5 hrs in all fluid phases derivative signatures as in example 1.0 a and b confirming the strong presence of this feature. The derivatives for all fluid phase depict the same well and reservoir fingerprint (3 flow regimes, early to late time response) but with different dp' stabilisation. Likewise, as obtained in scenario a and

b, k_{ave} values of 57 and 52 mD from equation 5.46 is obtained for scenario c and d respectively. This is slightly higher than k = 50 mD imputed in the simulation model. Breakdown of the result is presented in Table 4.4. For scenario c, at h =150 ft (60% of sand thickness, the estimated k_{ave} is about 41.2 mD which implies that 83% of oil thickness is contributing to flow.

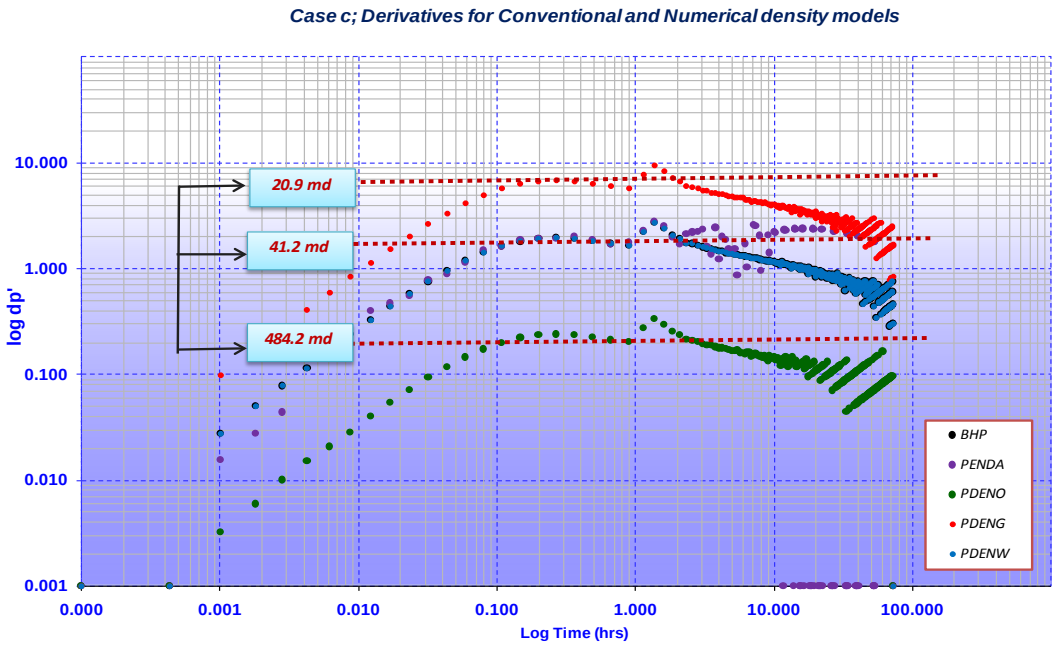

Figure 4.6: Derivative and K estimation for scenario c

However for scenario d, permeability value of 50.0 mD (BPR = PDENDWA = PDENWAT) can only be achieved if h =100 ft (40% of sand thickness). Likewise PDENGAS and PDENOIL will yield 35.0 mD at h = 50ft and 196.0 mD at h=250 ft respectively. This depicts the impact of water injection on densities and pressures changes around the well and consequently its impact on sand thickness contributing to flow. The derivative fingerprint at late time seen in Figure 4.7 shows the strong impact of injected water with precise and clarity.

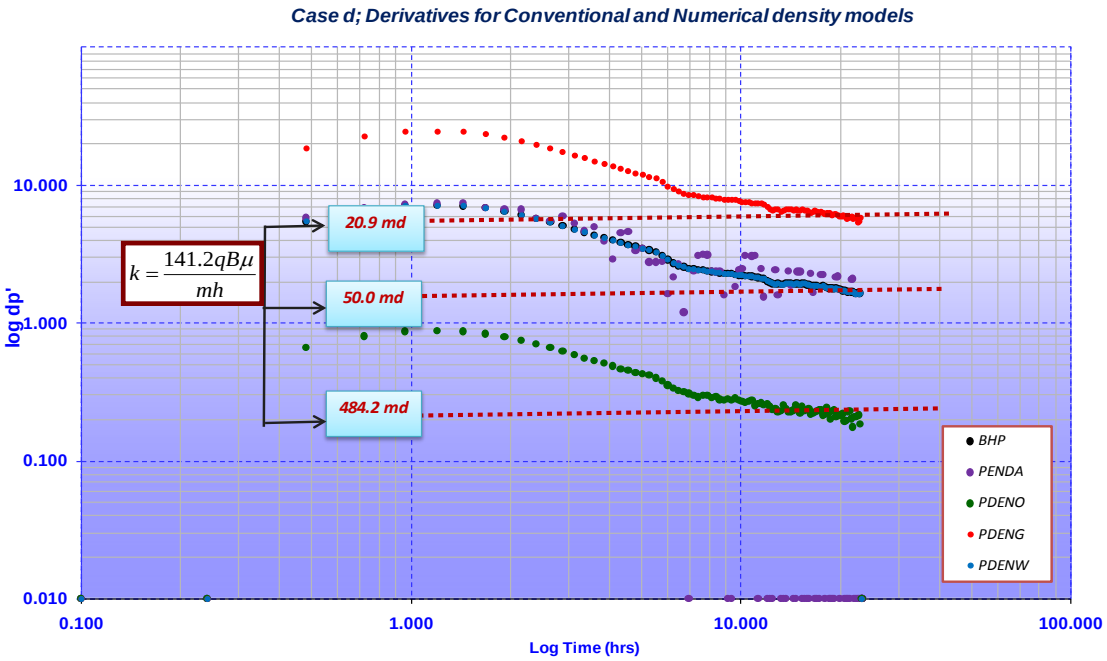

Figure 4.7: Derivative and K estimation for scenario d

Summarily from the 4 cases investigated (scenario a to d), k value of 50.0 mD is achieved if the thickness contributing to flow ranges from 50 to 150 ft. The 4 cases investigated demonstrated that the heavier the fluid such as water, the better permeability estimation from the weighted average pressure-density equivalent derivatives and also the k values for BPR is the same as those estimated from PDENDWA and PDENWAT. Result from Table 4.7 shows that k_{ave} values from geometrical equation 4.26 ranges 47 to 57 mD, which is within that used in the simulation model; therefore the approach provides an estimate of the possible fluid phase permeabilities and the % of each phase contribution to flow as shown in Table 4.7.

Table 4.4; K Estimates for new approach versus Conventional approach for scenario c and d

	Parameters	Numerical Density k (mD)	Equivalent h (ft)
Scenario c	BHP	50.0	50
	PDENA	50.0	"
	PDENG	20.9	"
	PDENO	484.2	"
	PDENW	50.0	"
Scenario d	BHP	50.0	100
	PDENA	50.0	"
	PDENG	17.5	50
	PDENO	490	250
	PDENW	50.0	100

4.9 Flow Regime Identification and Estimation of Permeability k (mD) after Pressure-Density Equivalent PDE Diagnostic Approach

4.9.1 Example 2.0 → Good k, gas and condensate reservoir using Synthetic data

To capture the influence of highly compressible fluid on estimated fluid phase permeabilities, an example on gas condensate reservoir (volatile system) is tested. Table 4.5 presents a summary of the well and reservoir synthetic data used for the build-up and drawdown simulated scenarios with additional information given below. It is required to generate the pressure equivalent and derivative for each fluid phase, compare their diagnostic signatures, determine the phases permeabilities and average reservoir permeability.

To test the density derivative method in a gas reservoir, numerical well test model with the following assumption is considered;

I. Simulation model with size 9, 3, 3 was built

II. Retrograde condensate reservoir completed with one well.

III. Gas thickness = 98 ft and water column = 50 ft

IV. Dx ,Dy and DZ were assumed to be 1312 ft, 984 ft and 49 ft

V. Uniform permeability of 400 mD and 300 mD assign to kx and ky respectively while average porosity of 30% was imputed in the model. Also kz = 0.01

VI. A conditional Sw and rel perm was used. .

VII. LGR was imposed around the well and far across to account for pressure and density changes

VIII. Gas, Oil, Water densities around the local grid refinement (wellbore) and WBHP were output using Eclipse keywords.

Table 4.5: Summary of reservoir simulations data

Parameters	***Design Value***
Eclipse model	Black Oil
Model dimension	9 X 3 X 3
Length by Width ft by ft	1312 X 984
Thickness ft	150
Permeability kx by ky mD	400.0 by 300.0
Porosity %	30
Well diameter ft	1.15
Initial water saturation Swi %	60
Permeability, k, mD	400
Gas Oil contact GOC ft	6890
Oil water contact OWC ft	6890
Initial Pressure, Pi, psi	4495
Formation Temperature, T, ^{o}F	248

Two scenarios of different well flowing conditions were investigated. This includes:

Production test:

a→: Flowing + Build-up Sequence. Well perforated hp = 30 ft between gas condensate and water layer.

b→: Flowing + Build-up Sequence. Well perforated hp = 30 ft inside gas condensate layer.

Figure 4.8 shows the production and shut-in sequence for 2 scenarios in example 2.0

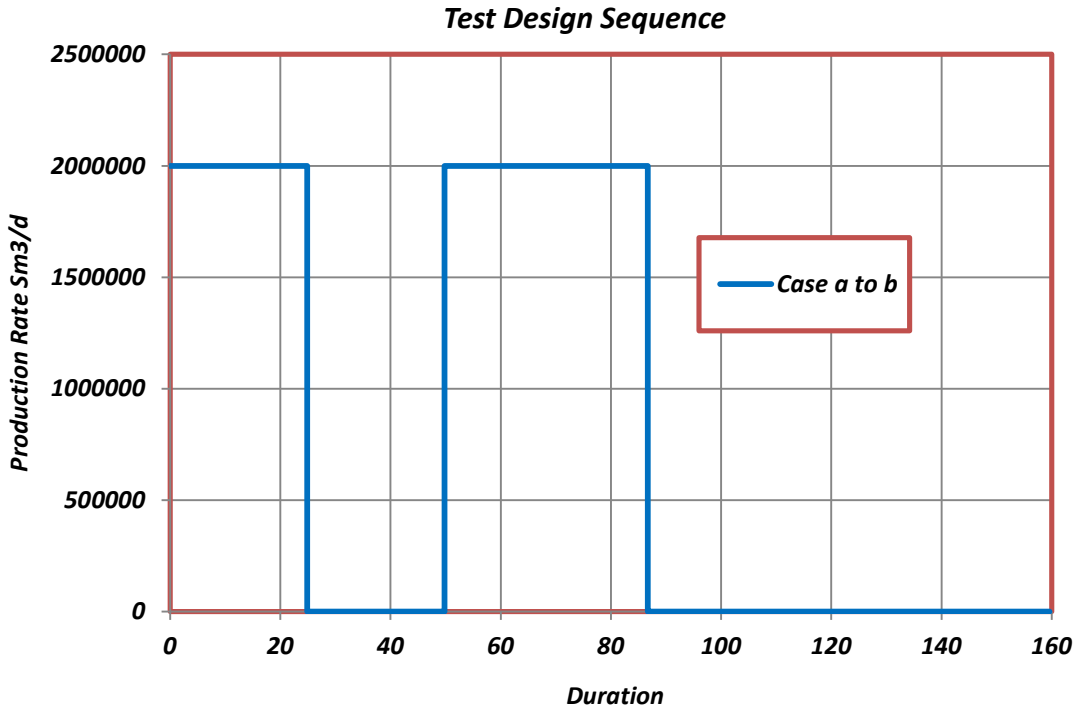

Figure 4.8: Simulation model for Gas cap + oil + water reservoir and Gas condensate+ water showing

a and b → As in example 1.0, the derivative in scenario a of example 2.0 also shows good radial flow from 4.0hrs in the model which is more of infinite as seen in Figure 4.9. Both BPR and pressure-density equivalent derivatives display similar well and reservoir signature (2 flow periods, early to middle time response) but with different dp' stabilisation. From the conventional method BPR, k value of 370.7 mD which is the same for PDENDWA and PDENWAT, but differ for PDENGAS and PDENOIL that yield 35.0 mD and 3574.7 mD respectively if h = 150 ft. This aligns with the uniform k (k_x = 400 mD and k_y = 300 mD) imputed in the simulation model

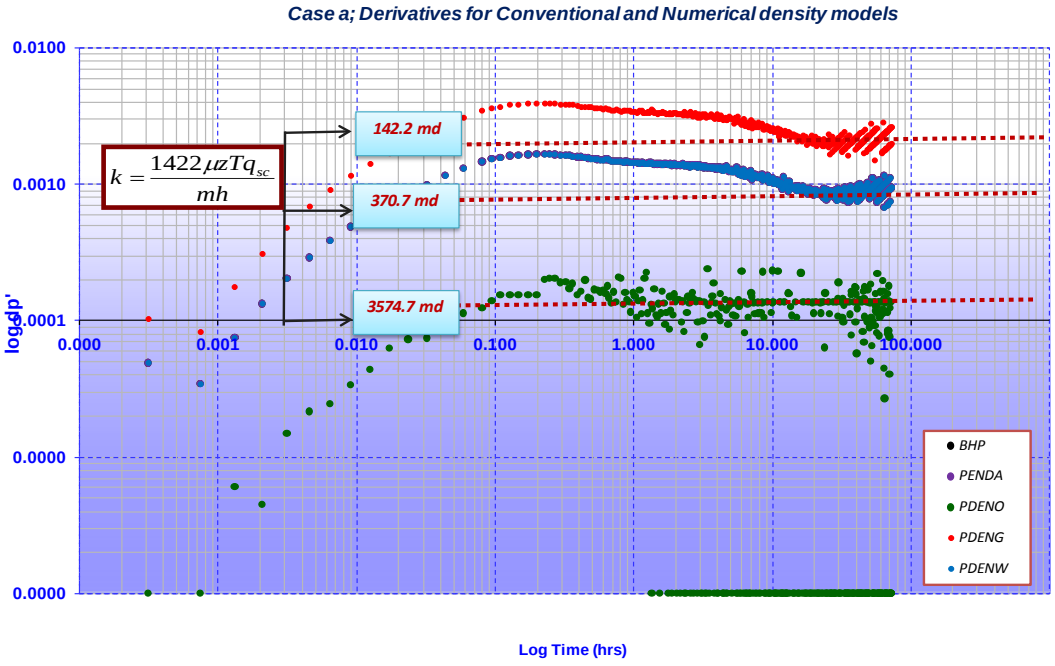

Figure 4.9: Derivative and K estimation for scenario a

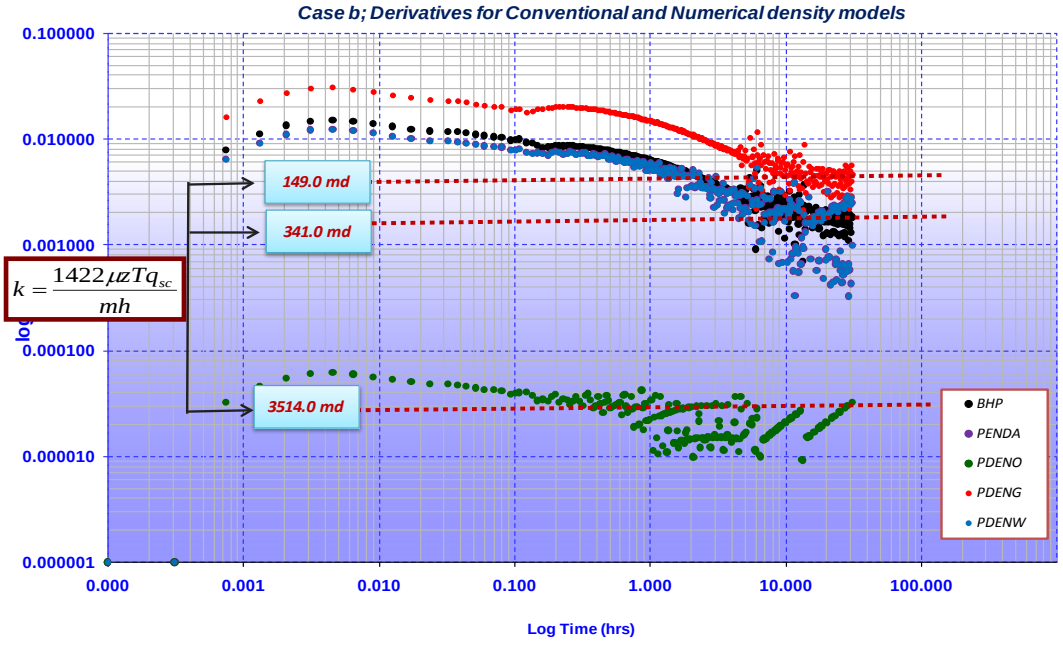

Figure 4.10: Derivative and K estimation for scenario b

The results in scenario b are similar to a as seen in Figure 4.10 with good radial flow and some noisy data (numerical artefact) in all the fluid phase derivatives but still good enough

to identify dp' stabilisation. For each fluid phase permeabilities, k value of 340.9 mD at h=148ft is obtained for BPR, PDENDWA and PDENWAT while PDENGAS and PDENOIL yield 149.0 and 3514.1mD respectively. Breakdown of the results are presented in Table 4.6.

Table 4.6; Summary of reservoir modelling properties imputed in eclipse model for case study 2.0

	Parameters	Numerical Density k (mD)	Equivalent h (ft)
Scenario a	BHP	371	148
	PDENA	371	"
	PDENG	142	"
	PDENO	3575	"
	PDENW	371	"
Scenario b	BHP	341	
	PDENA	341	"
	PDENG	149	"
	PDENO	3514	"
	PDENW	341	"

For scenario a and b, k_{ave} values of 405.0 and 403.0 mD are obtained respectively using geometrical equation 4.26. This is similar to the permeability imputed in the simulation model. As in example 1.0, it demonstrates that in the 2 cases investigated, the heavier fluid such as water and the weighted average pressure-density equivalent yield exact effective k as BPR. A summary of the result is shown in Table 4.8.

4.9.2 Geometrical model correlation between fluid phases K

The geometrical equation 4.46 integrating all the fluid phase permeability to determine the average reservoir permeability k_{ave} is given:

$$k_{ave} = \sqrt[4]{k_o k_w k^2_g}$$

Where

k_o= oil related permeability

k_g= gas related permeability

k_w = water related permeability

This approach estimates the possible phase permeabilities and % phase contribution to flow. Below is the breakdown of the calculation for example 1.0 and 2.0 using the geometrical equation.

Example 1.0

The average estimated permeability for scenario is calculated by:

$$k_{ave} = \sqrt[4]{50x403.7x15.8^2}$$

$$k_{ave} = 47.5mD$$

The average estimated permeability for scenario b is calculated by:

$$k_{ave} = \sqrt[4]{50x484.2x12.1^2}$$

$$k_{ave} = 43.4mD$$

The average estimated permeability for scenario c is calculated by:

$$k_{ave} = \sqrt[4]{50x484.2x20.9^2}$$

$$k_{ave} = 57.0mD$$

The average estimated permeability for scenario d is calculated by:

$$k_{ave} = \sqrt[4]{50x490x17.5^2}$$

$$k_{ave} = 52.3mD$$

Example 2.0

The average estimated permeability for scenario a is calculated by:

$$k_{ave} = \sqrt[4]{371x3575x142^2}$$

$$k_{ave} = 404.4mD$$

The average estimated permeability for scenario b is calculated by:

$$k_{ave} = \sqrt[4]{341x3514x149^2}$$

$$k_{ave} = 403.9mD$$

Table 4.7 and 4.8 show the comparison of simulated and calculated BPR k_{ave} as well as one point relative k estimated for each phase to see the contribution to flow by each phase. Significantly, this approach estimates the fluid phase permeabilities and the % phase contribution to flow at a given point.

4.9.3 Summary of Result

The derivatives of pressure-density equivalent depict distinctive wellbore and reservoir fingerprint with good stabilisation and k_{ave} estimates, making it suitable for interpretation of pressure transient analysis. Results from 6 scenarios investigated yield k_{ave} that is within acceptable range compared to the conventional approach and as input in the simulation model. It is discovered that in all cases reviewed, the heavier fluid such as water and PDENDWA gives exact effective k as BPR.

Table 4.7; Comparison of k estimates between conventional and numerical density parameters

Scenario	Numerical Density method		Calculated K (mD)	Conventional k(mD)	Simulation model K(mD)	Relative K	% Phase contribute to flow
	Phases	K (mD)					
a	*Gas*	*15.8*				*0.03*	*3.0*
	Oil	*403.7*				*0.86*	*86.0*
	Water	*50.8*				*0.11*	*11.0*
			47.6	***50.8***	***50.0***		
b	*Gas*	*12*				*0.03*	*2.0*
	Oil	*484.4*				*1.13*	*89.0*
	Water	*50*				*0.12*	*9.0*
			43.3	***50.0***	***50.0***		
c	*Gas*	*20.9*				*0.04*	*4.0*
	Oil	*484.2*				*0.86*	*87*
	Water	*50*				*0.09*	*9.0*
			57.0	***50.0***	***50.0***		
d	*Gas*	*17.5*				*0.03*	*3.0*
	Oil	*490*				*0.95*	*88.0*
	Water	*50*				*0.10*	*9.0*
			52.3	***50.0***	***50.0***		

Scenario	Numerical Density method		Calculated K (mD)	Conventional k(mD)	Simulation model K(mD)	Relative K	% Phase contribute to flow
	Phases	K (mD)					
a	*Gas*	*142.2*				*0.04*	*3.0*
	Oil	*3574.7*				*0.89*	*87.0*
	Water	*370.7*				*0.09*	*9.0*
			404.6	***370.7***	***400***		
b	*Gas*	*149*				*0.04*	*4.0*
	Oil	*3514.1*				*0.89*	*88.0*
	Water	*340.9*				*0.08*	*9.0*
			403.8	***340.9***	***400***		

Table 4.8; Comparison of k estimates between conventional and numerical density parameters

4.10 Density Radial Flow Equation Derivation for Each Fluid Phase

To derivate the density transient analytical equation for slightly and small compressibility fluid phase, the following assumption is applicable:

- There is small change in fluid densities at the wellbore
- The fluid phase flow independently
- Rock density is constant

Radial diffusivity equation is given as

$$\frac{1}{r}\frac{\partial \rho}{\partial r}\left[r\frac{\partial \rho}{\partial r}\right]=\frac{\phi\mu c}{k}\frac{\partial \rho}{\partial t} \tag{4.47}$$

For oil

$$\frac{1}{r}\frac{\partial \rho}{\partial r}\left[r\frac{\partial \rho_o}{\partial r}\right]=\frac{\phi\mu_o c}{k_o}\frac{\partial \rho_o}{\partial t} \tag{4.48}$$

For water phase

$$\frac{1}{r}\frac{\partial \rho}{\partial r}\left[r\frac{\partial \rho_w}{\partial r}\right]=\frac{\phi\mu_w c}{k_w}\frac{\partial \rho_w}{\partial t} \tag{4.49}$$

For gas phase

$$\frac{1}{r}\frac{\partial \rho}{\partial r}\left[r\frac{\partial \rho_g}{\partial r}\right]=\frac{\phi\mu_g c}{k_g}\frac{\partial \rho_g}{\partial t} \tag{4.50}$$

For slightly and small compressibility fluid such as water and oil, the pressure-density relationship from equation 4.36 is given as:

$$p = p_{oi} - \left[\frac{\frac{\rho}{\rho_{oi}}+1}{c}\right]$$

Differentiating with respect to ρ

$$\frac{\partial p}{\partial \rho} = -\frac{1}{c_{oi}\rho_{oi}} \text{ And } \partial p = -\frac{\partial \rho}{c_{oi}\rho_{oi}} \tag{4.51}$$

From Darcy's flow equation

$$q = -\frac{2\pi kh}{\mu} r \frac{\partial p}{\partial r} \tag{4.52}$$

Substitute for ∂p

$$q = -\frac{2\pi kh}{\mu} r \Big/ c_{oi}\rho_{oi} \frac{\partial \rho}{\partial r} \tag{4.53}$$

To derivate the analytical density transient equation for oil and water phases, the following assumption is applicable;

For oil phase, the radial diffusivity equation (equation 4.48) is given as;

$$\frac{1}{r}\frac{\partial \rho}{\partial r}\left[r \frac{\partial \rho}{\partial r} \right] = \frac{\phi \mu c}{k} \frac{\partial \rho}{\partial t}$$

Initial condition

$$\rho(r, t=0) = \rho_i \tag{4.54}$$

BC at the wellbore (inner)

$$\lim_{r \to 0} \frac{2\pi kh}{\mu} r \Big/ c_{oi}\rho_{oi} \frac{\partial \rho}{\partial r} = Q \tag{4.55}$$

BC at infirmity

$$\lim_{r \to \infty} \rho(r, t) = \rho_i \tag{4.56}$$

Using the Boltzmann transformation

Assuming $\eta = \frac{\phi \mu c r^2}{kt}$

$$\frac{\partial \rho}{\partial r} = \frac{\partial \rho}{\partial \eta}\frac{\partial \eta}{\partial r} = \frac{2\phi \mu c r}{kt}\frac{\partial \rho}{\partial \eta} = \frac{\phi \mu c r^2}{kt}\frac{2}{r}\frac{\partial \rho}{\partial \eta} = \frac{2\eta}{r}\frac{\partial \rho}{\partial \eta} \tag{4.57}$$

Therefore,

$$\frac{1}{r}\frac{\partial}{\partial r}\left[r\frac{\partial \rho}{\partial r}\right]=\frac{2\eta}{r^2}\frac{\partial}{\partial \eta}\left[2\eta\frac{\partial \rho}{\partial \eta}\right]=\frac{4\eta}{r^2}\frac{\partial}{\partial \eta}\left[\eta\frac{\partial \rho}{\partial \eta}\right] \tag{4.58}$$

Differentiating with respect to r is equal to differentiating with respect to η, multiply by $2\eta/r$

From equation 4.48, the L.H.S is resolves as follows

$$\frac{\partial \rho}{\partial t}=\frac{\partial \rho}{\partial \eta}\frac{\partial \eta}{\partial t}=\frac{\phi\mu c r}{kt^2}\frac{\partial \rho}{\partial \eta}=-\frac{\eta}{t}\frac{\partial \rho}{\partial \eta} \tag{4.59}$$

$$\frac{\phi\mu c}{k}\frac{\partial \rho}{\partial t}=\frac{-\phi\mu c}{k}\frac{\eta}{t}\frac{\partial \rho}{\partial t}=\frac{-\phi\mu c r^2}{kt}\frac{\eta}{r^2}\frac{\partial \rho}{\partial \eta}=\frac{-\eta^2}{r^2}\frac{\partial \rho}{\partial \eta} \tag{4.60}$$

Equating equation 4.57 and 4.60, we have

$$\frac{\partial}{\partial \eta}\left[\eta\frac{\partial \rho}{\partial \eta}\right]=\frac{-\eta}{4}\frac{\partial \rho}{\partial \eta} \tag{4.61}$$

This is the simplified ordinary differential equation of ρ as a function of η

Applying boundary conditions

Initial condition

$$\lim_{r\to\infty}\rho(\eta)=\rho_i \tag{4.62}$$

Substituting equation 4.58 into 4.53

$$\lim_{r\to 0}\frac{2\pi kh}{\mu}\,r/c_{oi}\rho_{oi}\,\frac{\partial \rho}{\partial r}=Q \tag{4.63}$$

$$\lim_{r\to 0}\left[\eta\frac{\partial \rho}{\partial \eta}\right]=\frac{\phi\mu c_{oi}\rho_{oi}}{4\pi kh}$$

Assuming $m=\eta\left(\frac{\partial \rho}{\partial \eta}\right)$

From equation 4.61

$$\frac{\partial m}{\partial \eta} = \frac{-m}{4} \tag{4.64}$$

Integrating from $\eta = 0$ to η

$$\Rightarrow \int_{m(0)}^{m(\eta)} \frac{\partial m}{\partial \eta} = -\int_{0}^{\eta} \frac{\partial \eta}{4}$$

$$\Rightarrow \ln\left[\frac{m(\eta)}{m(0)}\right] = \frac{-\eta}{4}$$

$$\Rightarrow m(\eta) = m(0)e^{-\eta/4} \tag{4.65}$$

Recall inner boundary condition

$$\lim_{r\to 0}\left[\eta \frac{\partial \rho}{\partial \eta}\right] = \frac{Q\mu c_{oi}\rho_{oi}}{4\pi kh}$$

$$m(0) = \frac{Q\mu c_{oi}\rho_{oi}}{4\pi kh} \text{ And } m(\eta) = \frac{Q\mu c_{oi}\rho_{oi}}{4\pi kh} e^{-\eta/4}$$

Recall that $m = \eta\left(\frac{\partial \rho}{\partial \eta}\right)$

Therefore ,

$$\frac{\partial \rho(\eta)}{\partial \eta} = \frac{\mu Q c_{oi}\rho_{oi}}{4\pi kh} \frac{e^{-\eta/4}}{\eta} \tag{4.66}$$

Integrating from $\eta = \infty$ where $\rho = \rho_i$

$$\int_{\rho_i}^{\rho(\eta)} \partial\rho = -\int_{\infty}^{\eta} \frac{\mu Q c_{oi}\rho_{oi}}{4\pi kh} \frac{e^{-\eta/4}}{\eta} \partial\eta$$

$$\rho(\eta) = \rho_i - \frac{\mu Q c_{oi}\rho_{oi}}{4\pi kh} - \int_{\eta}^{\infty} \frac{e^{-\eta/4}}{\eta} \partial\eta \tag{4.67}$$

Where,

$$\eta = \frac{\phi\mu c r^2}{kt}$$

Assuming $u = \eta/4$, then $\partial\eta/\eta = \partial u/u$

and $u = \frac{\phi\mu c r^2}{4kt}$

Hence,

$$\rho = \rho_i - \frac{\mu Q c_{oi}\rho_{oi}}{4\pi kh} - \int_{\frac{\phi\mu c r^2}{4kt}}^{\infty} \frac{e^{-\eta/4}}{\eta}\partial\eta \tag{4.68}$$

Where

$$-Ei(-x) = \int_x^{\infty} \frac{e^{-u}}{u}\partial u \tag{4.69}$$

known as the exponential integral function defined by Matthews and Russell [53].

$$\rho(r,t) = \rho_i + \frac{\mu Q c_{oi}\rho_{oi}}{4\pi kh} Ei(-x) \tag{4.70}$$

Where $x = \frac{\phi\mu c r^2}{4kt}$ and

$$-Ei(-x) = \int_x^{\infty} \frac{e^{-u}}{u}\partial u$$

At large times, x will be small applying Taylor's series and integrating

$$-Ei(-x) = \ln(\gamma)$$

$$\ln(\gamma) = \ln(1.781) = 0.5772 \tag{4.71}$$

Where γ is known as Euler's number

For $\frac{1}{4x} > 25$

Then,

$$\rho(r,t) = \rho_i + \frac{\mu Q c_{oi} \rho_{oi}}{4\pi kh}\left[\ln x + \ln \gamma\right] \tag{4.72}$$

$$\rho(r,t) = \rho_i + \frac{\mu Q c_{oi} \rho_{oi}}{4\pi kh} \ln\left[\frac{\phi \mu c r^2 \gamma}{4kt}\right]$$

$$\rho(r,t) = \rho_i - \frac{\mu Q c_{oi} \rho_{oi}}{4\pi kh} \ln\left[\frac{2.246kt}{\phi \mu c r^2}\right]$$

$$\rho(r,t) = \rho_i - \frac{\mu Q c_{oi} \rho_{oi}}{4\pi kh}\left[\ln\left[\frac{2.246kt}{\phi \mu c r^2}\right] + 0.80907\right] \tag{4.73}$$

Plotting $\rho_{wb}(t)$ versus $\ln(t)$will yield a straight line at longer time and the slope of the line is given as:

$$\frac{\partial \rho_{wb}}{\partial \ln t} = m_{oil} = \frac{\mu Q c_{oi} \rho_{oi}}{4\pi kh} \tag{4.74}$$

Therefore,

$$kh = \frac{\mu Q c_o \rho_o}{4\pi m_{oil}} \tag{4.75}$$

For water phase, the radial density equation is given as:

$$\rho(r,t) = \rho_i - \frac{\mu Q c_{wi} \rho_{wi}}{4\pi kh}\left[\ln\left[\frac{2.246kt}{\phi \mu c r^2}\right] + 0.80907\right] \tag{4.76}$$

Plotting $\rho_{wb}(t)$ versus $\ln(t)$will yield a straight line at longer time and the slope of the line is given as:

$$\frac{\partial \rho_{wb}}{\partial \ln t} = m_{woter} = \frac{\mu Q c_{wi} \rho_{wi}}{4\pi kh} \tag{4.77}$$

Where

$$kh = \frac{\mu Q c_{wi} \rho_{wi}}{4\pi m_{water}} \tag{4.78}$$

Equation 4.73 and 4.76 are the density transient analytical DTA solutions for slightly compressible fluid such as oil and water used for generating density derivatives including specialised density time plot for further interpretation.

For Gas Phase:

For compressible fluid such as gas, pressure-density relationship from equation 4.44 is given as;

$$p = \frac{p_{gi}\rho - p_{gi}^{\,2}\rho_{gi}c_g}{\rho_{gi}\left(1 - p_{gi}c_g\right)}$$

And

$$\frac{\partial p}{\partial \rho} = \frac{p_{gi}}{\rho_{gi}\left(1 - p_{gi}c_g\right)}$$

$$\partial p = \frac{p_{gi}}{\rho_{gi}\left(1 - p_{gi}c_g\right)}\partial \rho \tag{4.79}$$

From the PVT relationship fundamental

$$n = \frac{PV}{zRT} \tag{4.80}$$

At standard condition

$$\frac{PV}{zT} = \frac{P_{sc}V_{sc}}{T_{sc}}$$

$$\frac{P\left(5.615q\right)}{zT} = \frac{P_{sc}Q_{sc}}{T_{sc}}$$

$$q = \frac{P_{sc}}{T_{sc}}\left(\frac{zT}{P}\right)\frac{Q_{sc}}{5.615} \tag{4.81}$$

And

$$q = \frac{P_{sc}}{T_{sc}} \frac{Q_{sc}}{5.615} \left(\frac{zT}{P} \right) = \frac{2\pi kh}{\mu} r \frac{\partial p}{\partial r}$$

$$q = \frac{P_{sc}}{T_{sc}} \frac{Q_{sc}}{5.615} (zT) = \frac{2\pi kh}{\mu} r \frac{P\partial p}{\partial r} \tag{4.82}$$

Where

$$\partial p = \frac{p_{gi}}{\rho_{gi}(1 - p_{gi} c_g)} \partial \rho \text{ and } \alpha = \frac{p_{gi}}{\rho_{gi}(1 - p_{gi} c_g)}$$

$\partial p = \alpha \partial \rho$ and $p = \rho RzT$

Substitute into the equation

Where

$$m(\rho_i) - m(\rho_{wf}) = \frac{2}{\mu} \int_{\rho_{wf}}^{\rho_i} \rho \partial \rho \tag{4.83}$$

$$m(\rho_i) - m(\rho_{wf}) = \frac{{\rho_i}^2 - {\rho_{wf}}^2}{\mu} \tag{4.84}$$

and $\bar{\rho} = \sqrt{\frac{{\rho_i}^2 + {\rho_{wf}}^2}{2}}$ (4.85)

From the diffusivity equation for gas

$$\frac{1}{r} \frac{\partial \rho}{\partial r} \left[r \frac{\partial \rho_g}{\partial r} \right] = \frac{\phi \mu_g c}{k_g} \frac{\partial \rho_g}{\partial t}$$

Initial condition

$$\rho(r, t = 0) = \rho_i \tag{4.86}$$

BC at the wellbore (inner)

$$\lim_{r \to 0} \frac{4\pi kh\alpha R}{\mu} \left(\frac{5.615 T_{sc}}{P_{sc}} \right) r\rho \frac{\partial \rho}{\partial r} = Q \tag{4.87}$$

BC at infirmity

$$\lim_{r\to\infty}\rho(r,t)=\rho_i \tag{4.88}$$

Where R, P_{sc} and T_{sc} are gas constant, pressure and temperature respectively at standard condition.

Therefore, Integrating from $\eta=\infty$ where $\rho=\rho_i$

$$\int_{\rho_i}^{\rho(\eta)}\rho\partial\rho=-\int_{\infty}^{\eta}\frac{\mu Q}{4\pi kh\alpha R}\left(\frac{P_{sc}}{5.615T_{sc}}\right)\frac{e^{-\eta/4}}{\eta}\partial\eta$$

$$\rho^2(\eta)=\rho_i{}^2-\frac{\mu Q}{4\pi kh\alpha R}\left(\frac{P_{sc}}{5.615T_{sc}}\right)-\int_{\eta}^{\infty}\frac{e^{-\eta/4}}{\eta}\partial\eta \tag{4.89}$$

Where

$$\eta=\frac{\phi\mu cr^2}{kt}$$

Assuming $u=\eta/4$ $\partial\eta/\eta=\partial u/u$ and $u=\frac{\phi\mu cr^2}{4kt}$

Hence

$$\rho^2=\rho_i{}^2-\frac{\mu Q}{4\pi kh\alpha R}\left(\frac{P_{sc}}{5.615T_{sc}}\right)-\int_{\frac{\phi\mu cr^2}{4kt}}^{\infty}\frac{e^{-\eta/4}}{\eta} \tag{4.90}$$

Where $-Ei(-x)=\int_{x}^{\infty}\frac{e^{-u}}{u}\partial u$

known as the exponential integral function defined by Matthews, C.S. and Russell [53].

$$\rho^2=\rho_i{}^2-\frac{\mu Q}{4\pi kh\alpha R}\left(\frac{P_{sc}}{5.615T_{sc}}\right)-Ei(-x) \tag{4.91}$$

Where $x=\frac{\phi\mu cr^2}{4kt}$ and $-Ei(-x)=\int_{x}^{\infty}\frac{e^{-u}}{u}\partial u$

At large times, x will be small applying Taylor's series and integrating

$$-Ei(-x)=\ln(\gamma)$$

$$\ln(\gamma)=\ln(1.781)=0.5772$$

Where γ is known as Euler's number

For $\frac{1}{4x}>25$

Then

$$\rho^2(r,t)=\rho_i{}^2+\frac{\mu Q}{4\pi kh\alpha R}\left(\frac{P_{sc}}{5.615T_{sc}}\right)[\ln x+\ln\gamma] \tag{4.92}$$

$$\rho^2(r,t)=\rho_i{}^2+\frac{\mu Q}{4\pi kh\alpha R}\left(\frac{P_{sc}}{5.615T_{sc}}\right)\ln\left[\frac{\phi\mu cr^2\gamma}{4kt}\right]$$

$$\rho^2(r,t)=\rho_i{}^2-\frac{\mu Q}{4\pi kh\alpha R}\left(\frac{P_{sc}}{5.615T_{sc}}\right)\ln\left[\frac{2.246kt}{\phi\mu cr^2}\right] \tag{4.93}$$

$$m(\rho_i)-m(\rho_{wf})=\frac{2}{\mu}\int_{\rho_{wf}}^{\rho_i}\rho\partial\rho$$

$$m(\rho_{wf})=m(\rho_i)-\frac{\mu Q}{4\pi kh\alpha R}\left(\frac{P_{sc}}{5.615T_{sc}}\right)\left[\ln\left[\frac{2.246kt}{\phi\mu cr^2}\right]+0.80907\right] \tag{4.94}$$

Equation 4.94 is the density transient analytical DTA solution for compressible fluid such as gas used for generating density derivatives and specialised density time plot for further interpretation.

Plotting $\rho_{wb}{}^2(t)$ or $m(\rho_{wb})$ versus $\ln(t)$ will yield a straight line at longer time and the slope of the line is given as:

$$\frac{\partial m(\rho_{wb})}{\partial\ln t}=m_{gas}=\frac{\mu Q}{4\pi kh\alpha R}\left(\frac{p_{sc}}{5.615T_{sc}}\right) \tag{4.95}$$

Where

$$kh = \frac{\mu Q}{4\pi kh\alpha R}\left(\frac{P_{sc}}{5.615T_{sc}}\right)\frac{1}{m_{gas}} \tag{4.96}$$

Figure 4.11 shows example of the specialised semi log plot of fluid densities (oil, water and gas) versus time (Horner/Agawal time) for permeability estimation. Figure 4.12 represents the expected density derivatives for each fluid phase generated from Horne [37] and statistical 'density' derivative [12].

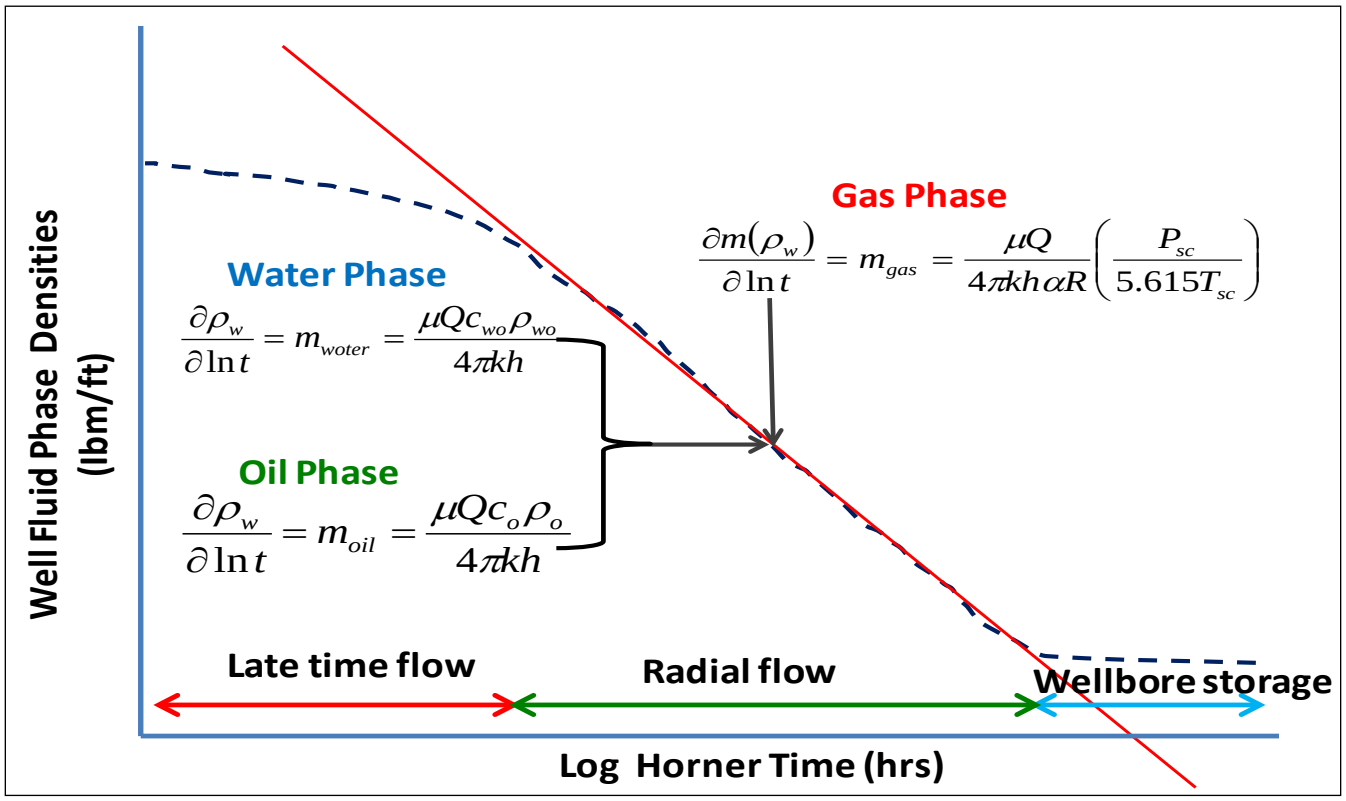

Figure 4.11: Specialised diagnostic semi-log plot of fluid densities (gas, oil and water phase) versus Horner time

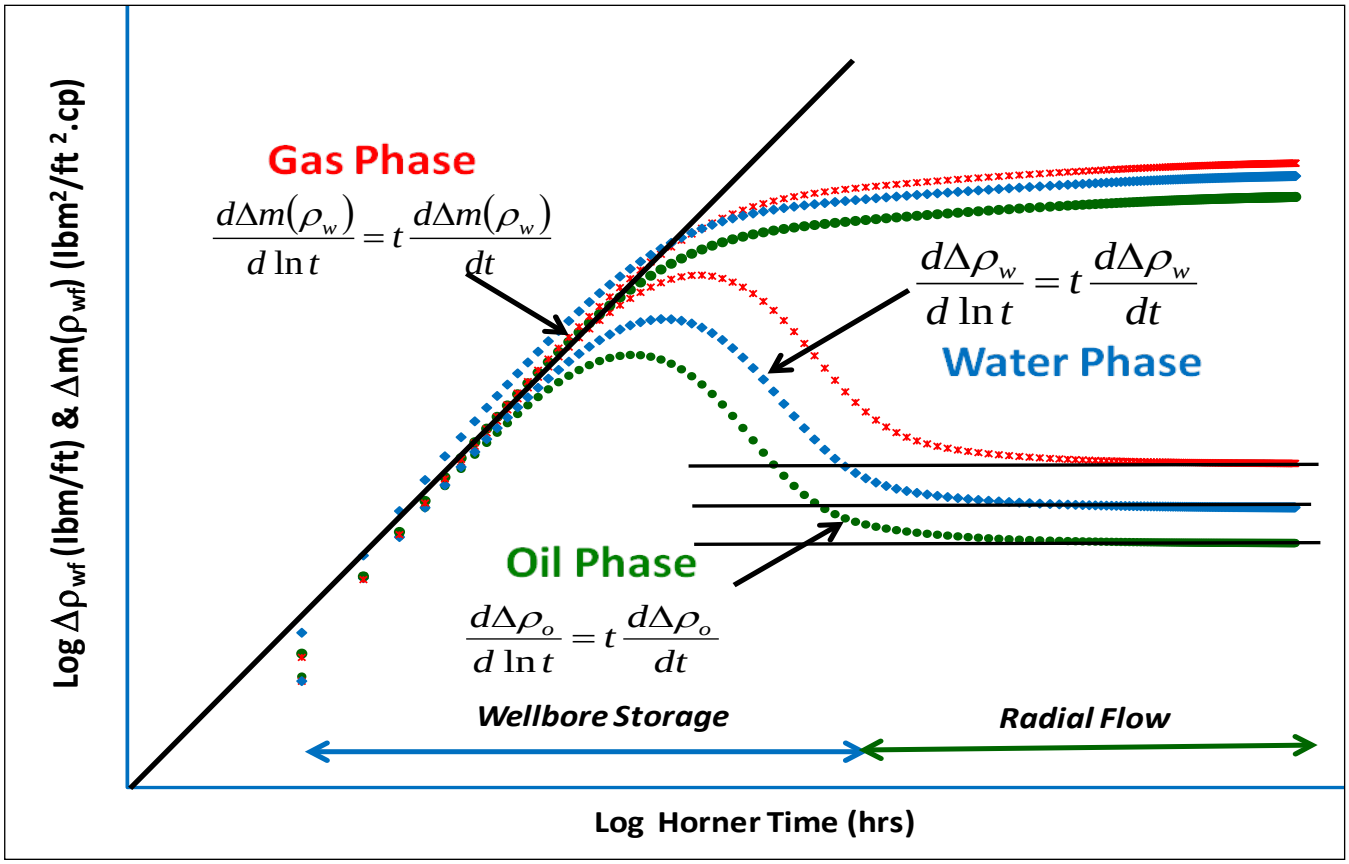

Figure 4.12: Diagnostic log-log plot of fluid densities (gas, oil and water) derivatives versus time

4.10.1 Estimation of Permeability k (mD) After Numerical Density Transient Analysis

DTA Approach

4.10.1.1 Example 3.0a → Low k, oil and gas reservoir using Synthetic data

Data from example 1.0a is used with phase permeabilities and k_{ave} calculated from specialised semi-log of phase densities versus time. Log of Horner or Agarwal time can also be used in place of ordinary log time.

*** Q used for k calculation is the average rate for all flowing periods.*

Direct Numerical density derivatives

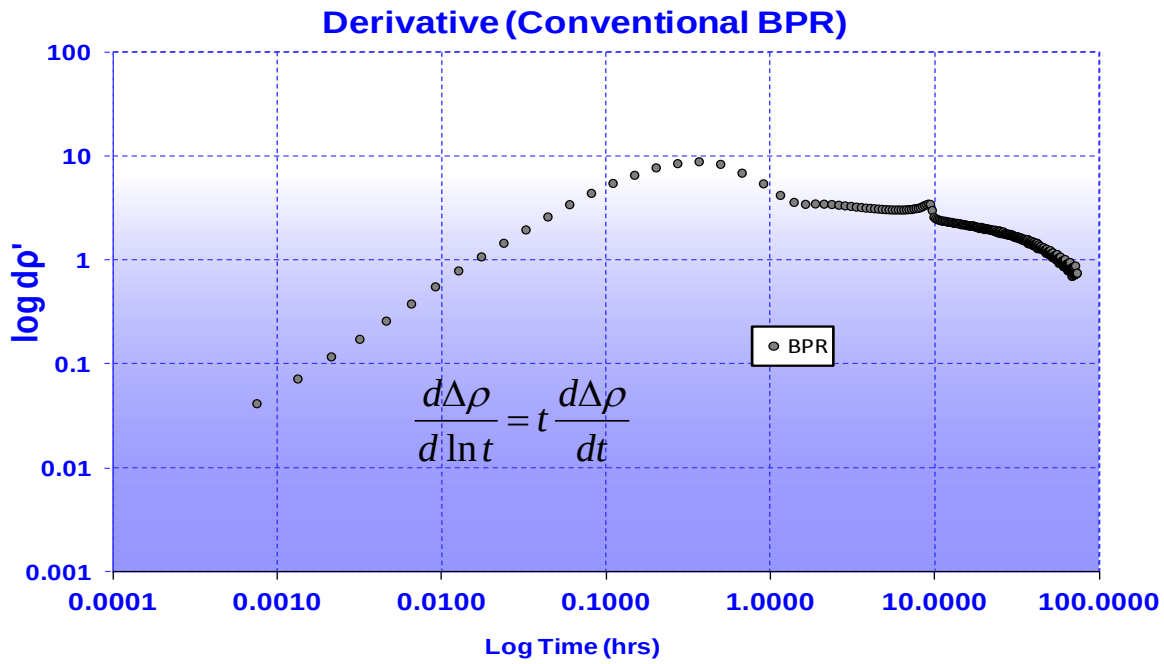

Figure 4.13; Conventional BPR derivative versus time showing good stabilisation with numerical artefact effect

Result from each phase density derivatives from the DTA solution depicts good reservoir fingerprint which is continuous and without noise for gas and water phase density as shown in Figure 4.14 and 4.15. This is in support of PDENA interpretation with better stabilisation discussed in example 1.0 scenario a (section 4.81). However, the oil phase derivative shows similar fingerprint as the pressure-density equivalent and BPR derivatives response seen in Figure 4.4 and 4.13.

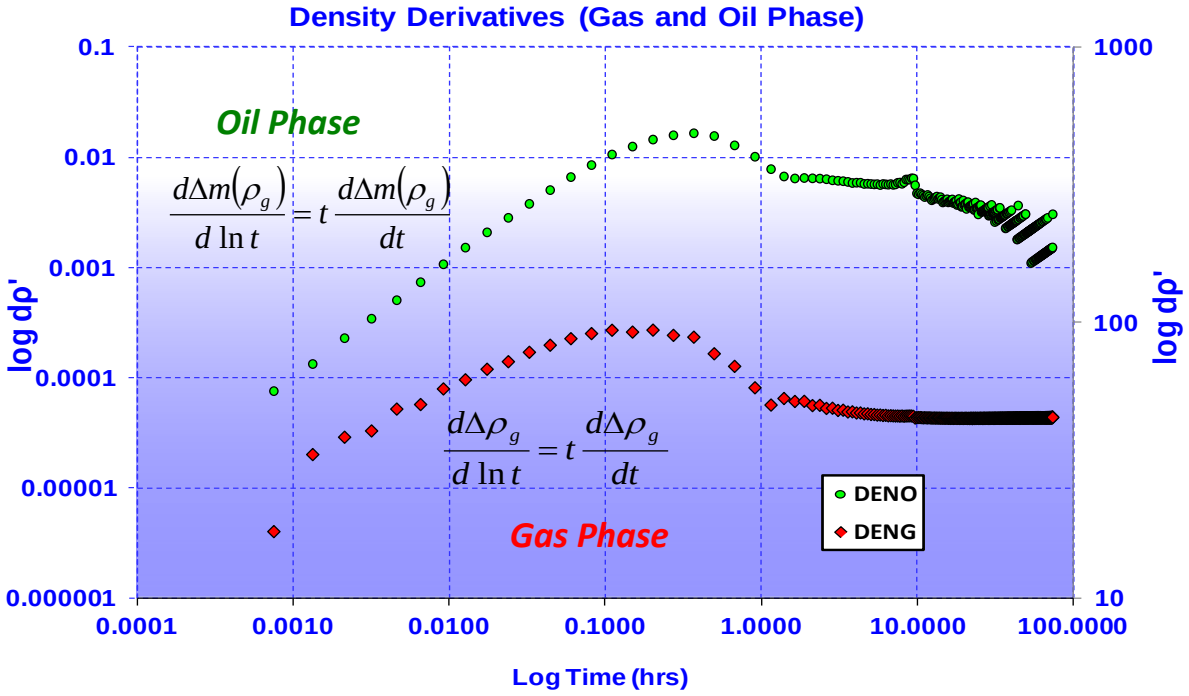

Figure 4.14; Oil and Gas densities derivative versus time showing good stabilisation without numerical artefact in the gas density derivative

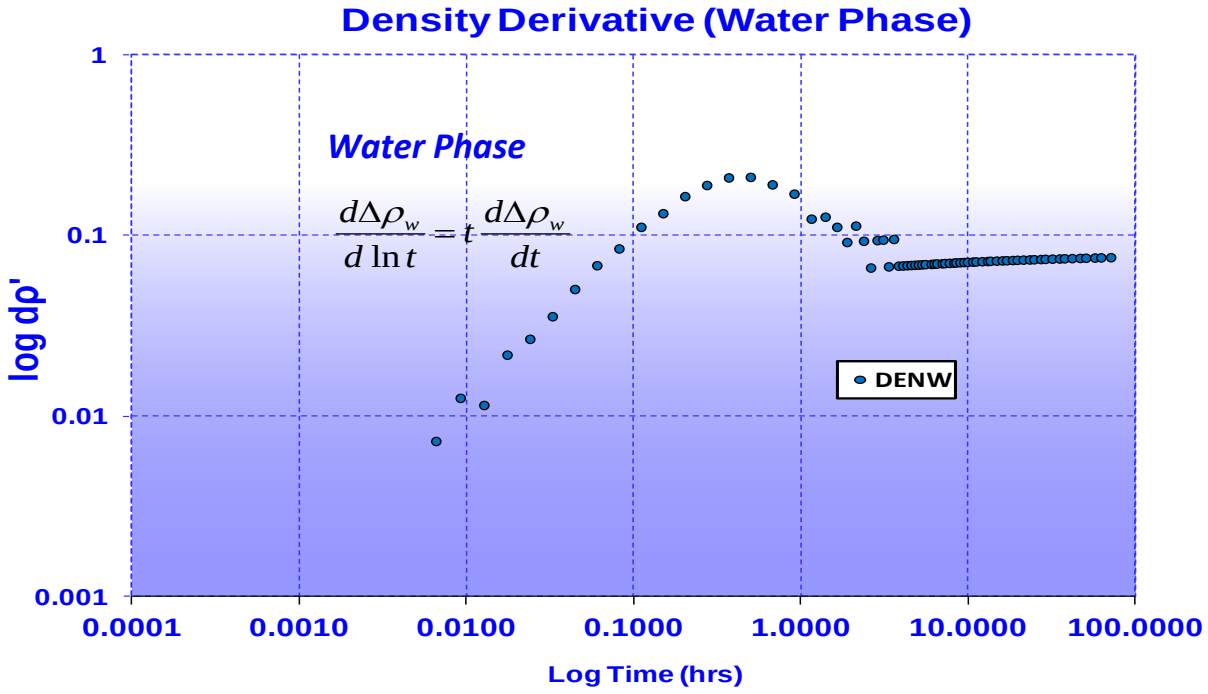

Figure 4.15; Fluid Phase (water) Density Derivative versus time showing good stabilisation without numerical artefact in the water density derivative

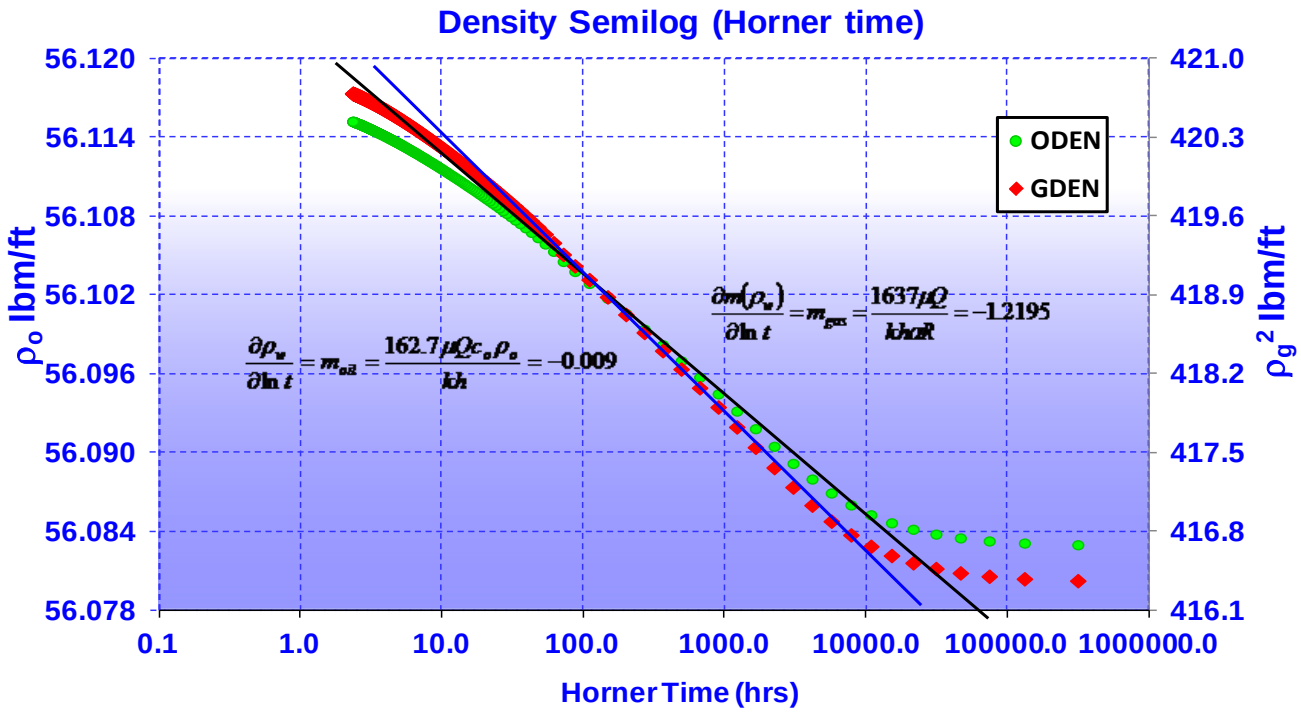

Figure 4.16: Specialised semi log oil and gas phase densities versus Horner time

Applying the DTA solutions derived in equation 4.53, 4.56 and 4.74, well bottom hole flowing and shut-in densities from example 1.0a are analysed with the semi-log plot of wellbore flowing density for each phase (oil, water and gas) versus Horner time as shown in Figure 4.16 and 4.17.

For oil and water phase, the calculated semi-log slope for radial flow period is given as:

$$\frac{\partial \rho_w}{\partial \ln t} = m_{oil} = \frac{162.7\mu Q c_o \rho_o}{kh} = -0.009 \text{ And}$$

$$\frac{\partial \rho_w}{\partial \ln t} = m_{water} = \frac{162.7\mu Q c_o \rho_o}{kh} = -0.0003$$

The estimated phase permeabilities are:

$$k_{oil} = \frac{162.7\mu Q c_o \rho_o}{h m_{oil}} = 445mD \text{ And}$$

$$k_{water} = \frac{162.7\mu Q c_o \rho_o}{h m_{water}} = 50mD$$

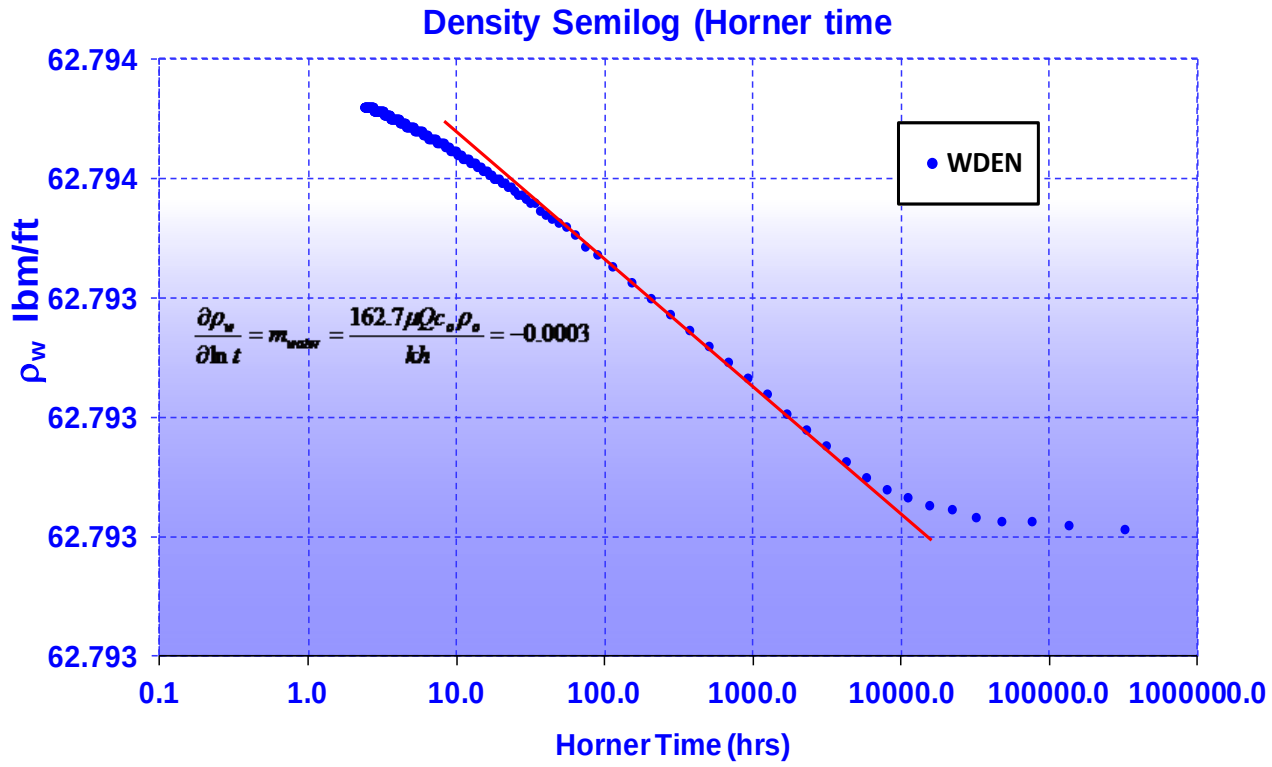

Figure 4.17: Specialised semi log water phase density versus Horner time

Also for the gas phase, the calculated semi-log slope for radial flow period is given as:

$$\frac{\partial m(\rho_w)}{\partial \ln t} = m_{gas} = \frac{1637\mu Q}{kh\alpha R} = -1.2195$$

And estimated gas permeability is given as:

$$k_{gas} = \frac{1637\mu Q_o}{h\alpha R m_{gas}} = 17.0mD$$

Using the geometrical equation 4.46 for all three phase, the average estimated permeability

$$k_{ave} = \sqrt[4]{50x445x17.0^2}$$

$$k_{ave} = 50mD$$

4.10.1.1 Example 3.0b → Low k, oil and gas reservoir using Synthetic data

Data from Example 1.0c is used with phase permeabilities and k_{ave} calculated from specialised semi-log of phase densities (oil, water and gas) plotted against time. Log of Horner or Agarwal time can also be used in place of ordinary log time.

*** Q used for k calculation is the average rate for all flowing periods.*

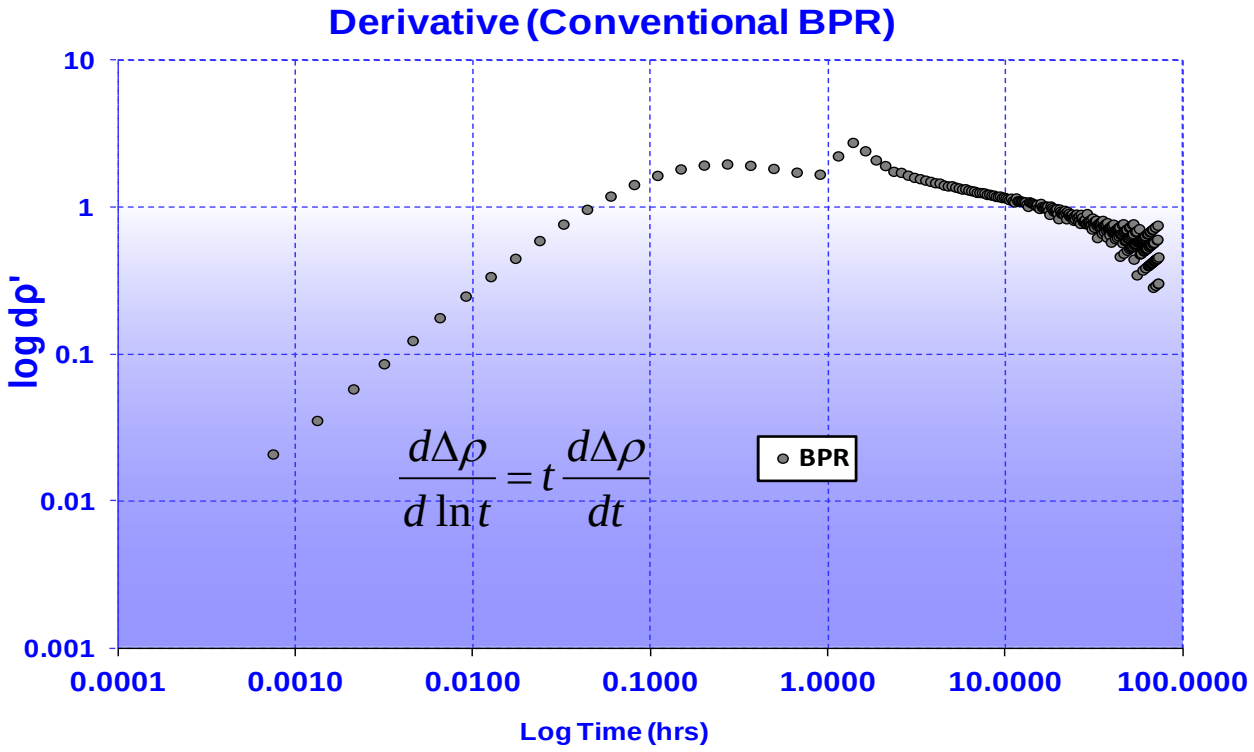

Figure 4.18; Conventional BPR derivative versus time showing good stabilisation with numerical artefact effect

Results in Figure 4.19 and 4.20 show each phase density derivatives with good reservoir response similar to signature seen in Example 3.0a which is continuous and without noise for the gas and water phase density. Also this is in support of PDENA interpretation discussed in example 1.0 scenario c (section 4.81) with oil phase derivative displaying similar fingerprint as the pressure-density equivalent and BPR derivatives response seen in Figure 4.6 and 4.18.

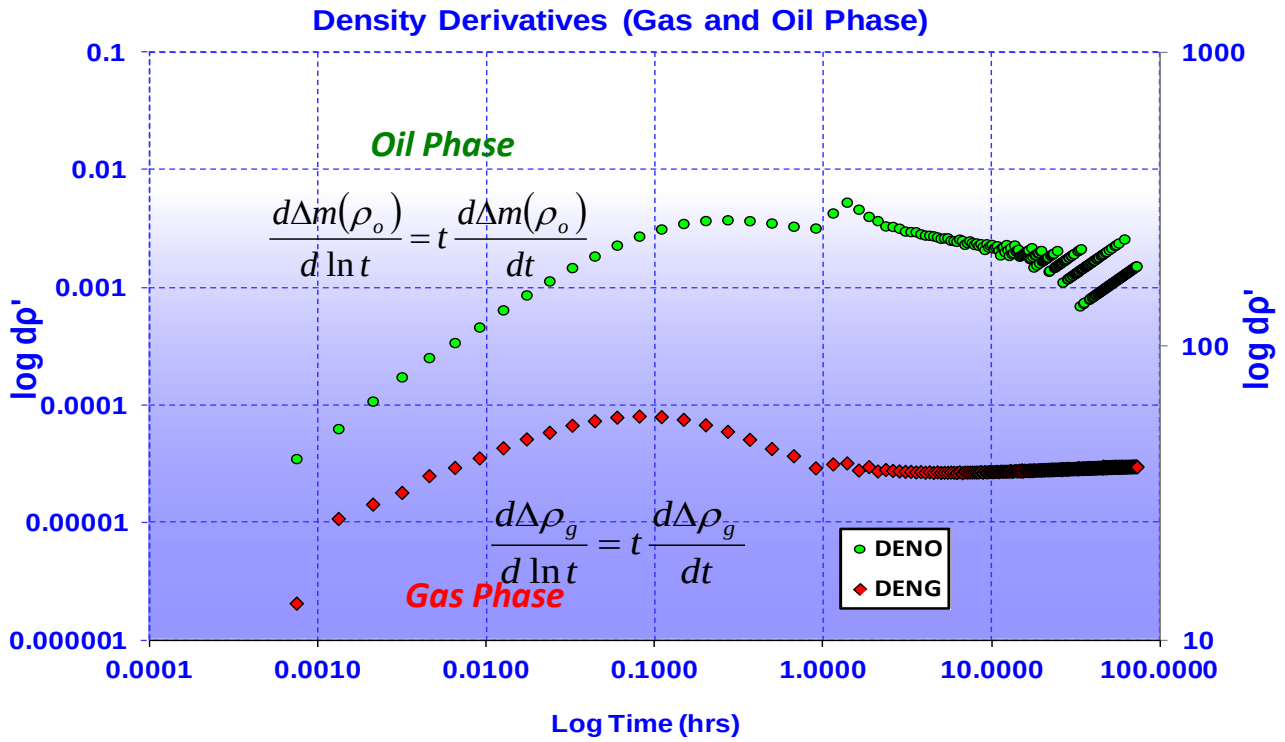

Figure 4.19; Oil and Gas densities derivative versus time showing good stabilisation without numerical artefact in the gas density derivative

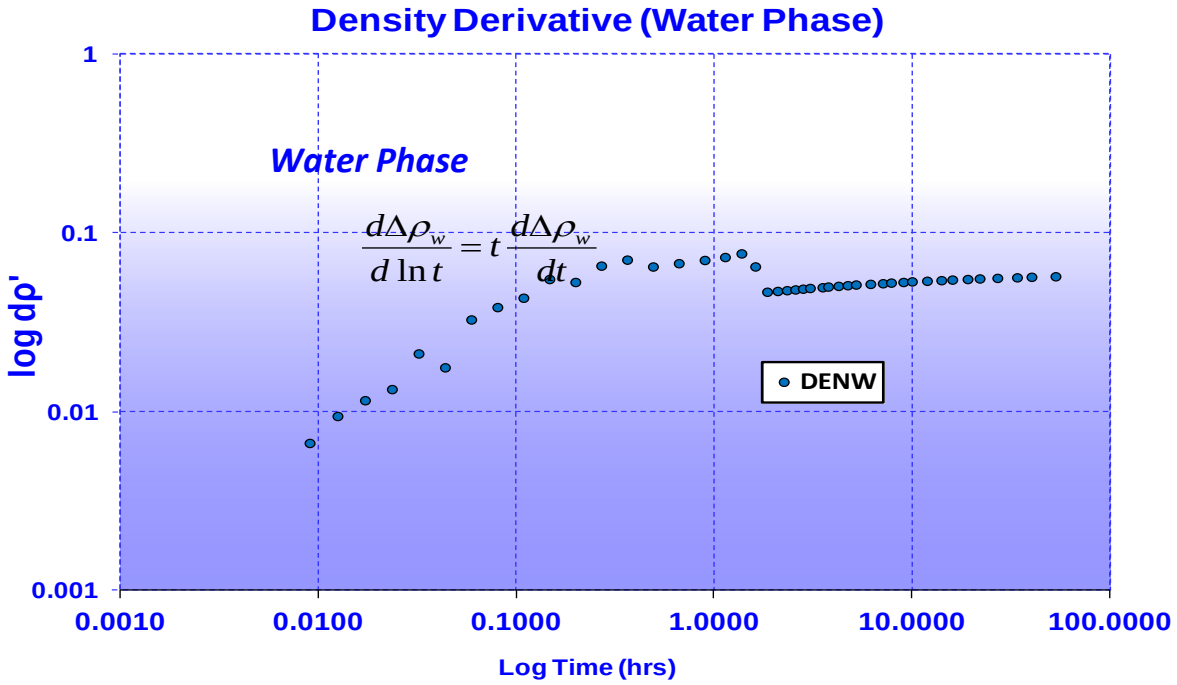

Figure 4.20; Fluid Phase (water) Density Derivative versus time

Applying the DTA solutions derived in equation 4.53, 4.56 and 4.74, well bottom hole flowing and shut-in densities from Example 1.0c are analysed with the semi-log plot of wellbore flowing density for each phase (oil, water and gas) plotted against Horner time as shown in Figure 4.21 and 4.22.

For oil and water phase, the calculated semi-log slope for radial flow period is given as:

$$\frac{\partial \rho_w}{\partial \ln t} = m_{oil} = \frac{162.7\mu Q c_o \rho_o}{kh} = -0.009 \text{ And}$$

$$\frac{\partial \rho_w}{\partial \ln t} = m_{water} = \frac{162.7\mu Q c_o \rho_o}{kh} = -0.0003$$

The estimated phase permeabilities are:

$$k_{oil} = \frac{162.7\mu Q c_o \rho_o}{hm_{oil}} = 435.2mD \text{ and } k_{water} = \frac{162.7\mu Q c_o \rho_o}{hm_{water}} = 49mD$$

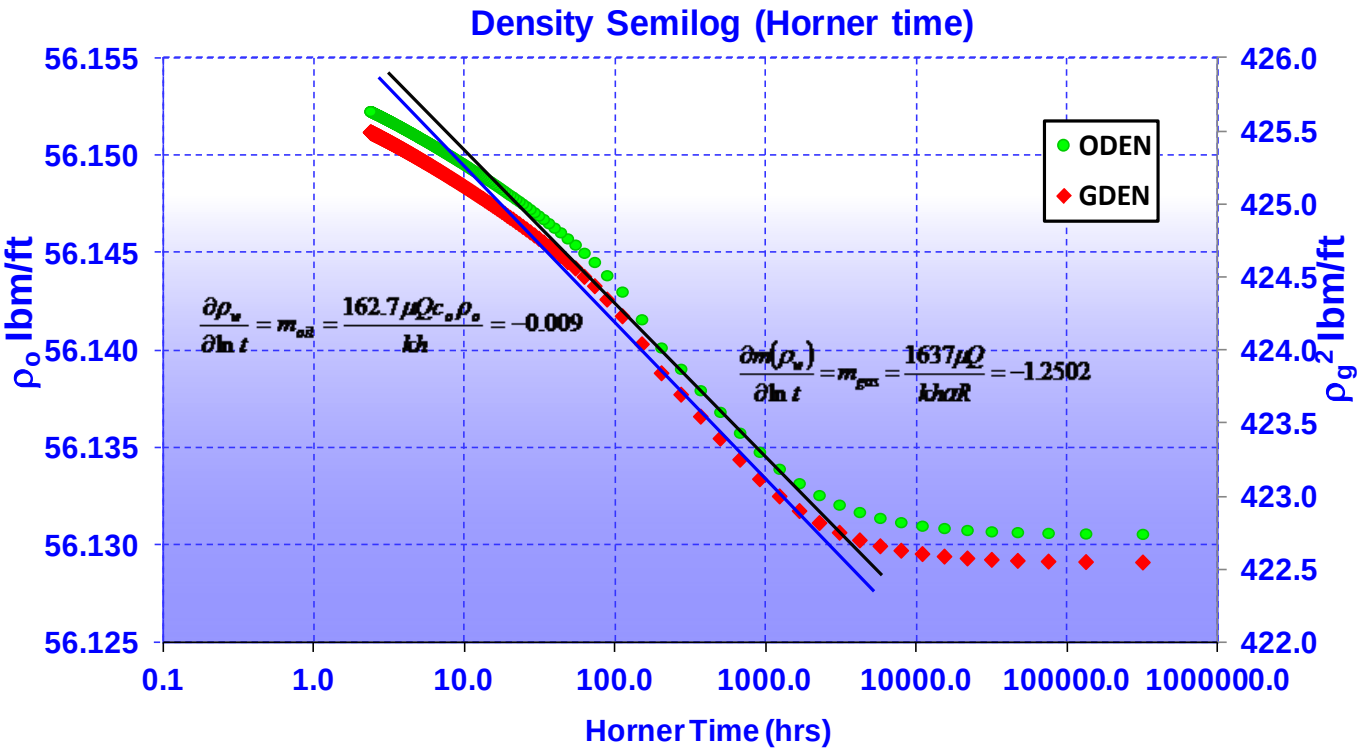

Figure 4.21: Specialised semi log oil and gas phase densities versus Horner time

Also for the gas phase, calculated semi-log slope for radial flow period is given as:

$$\frac{\partial m(\rho_w)}{\partial \ln t} = m_{gas} = \frac{1637\mu Q}{kh\alpha R} = -1.2502$$

And estimated gas permeability is:

$$k_{gas} = \frac{1637\mu Q_o}{h\alpha R m_{gas}} = 17.9mD$$

Using the geometrical equation 4.46 for all three phase, the average estimated permeability

$$k_{ave} = \sqrt[4]{49x435.2x17.9^2}$$

$$k_{ave} = 51mD$$

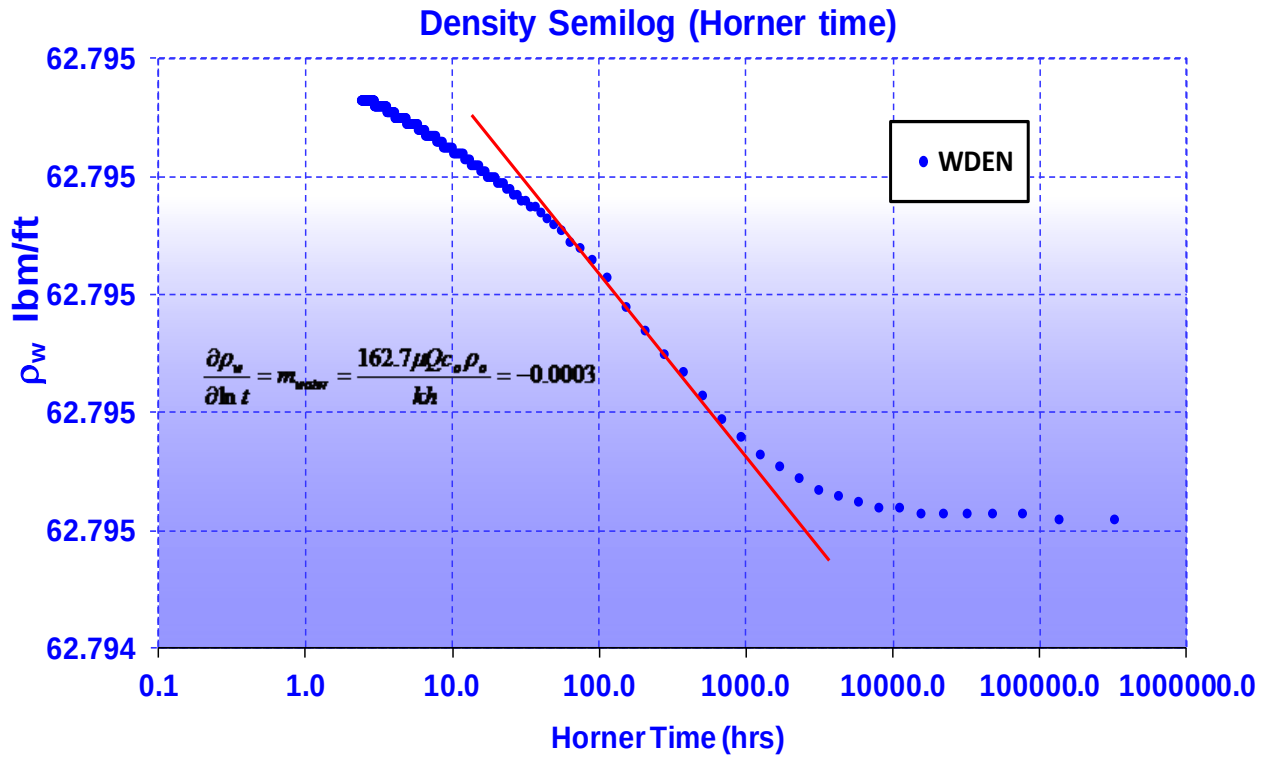

Figure 4.22: Specialised semi log water phase density versus Horner

4.10.2 Summary of Result

Pressure–density equivalent and numerical density derivative methods can derive phase permeabilities along with good visualisation of phase derivatives response which amplify the

true picture of the reservoir response to ensure that the average reservoir permeability is right from the formation radial flow. Results from investigated cases indicate that numerical density derivatives yield a clearer reservoir radial flow regime which gives more confident formation permeability estimation. Also, result obtained demonstrates that heavier fluid such as water and the weighted average pressure-density equivalent derivatives yield a good permeability estimate as the traditional pressure derivative method.

Chapter Five

Numerical density application in unconventional gas reservoir

5.1 Introduction

Unconventional gas reservoirs are often defined as a gas bearing sandstone or carbonate matrix with in-situ permeability to gas less than 0.1 millidarcies, e.g. shale gas. They acts as both a source rock and reservoir with pores that are irregularly distributed through the reservoir and poorly connected by very narrow capillaries resulting in very low permeability. Gas is produced from shale reservoir via natural fractures for a long time, but with the introduction of hydraulic fracturing stimulation, improvement of its production can be achieved. Notably, the primary objective behind developing a shale formation is to maximize the surface area available to flow, hence creating hydraulic fractures or improving the connectivity of existing fractures is critical to achieving this.

Moridis [56] discovered four distinct fracture systems present in producing shale-gas reservoirs. Figure 5.1 shows an example of the four fracture systems, which are discussed below:

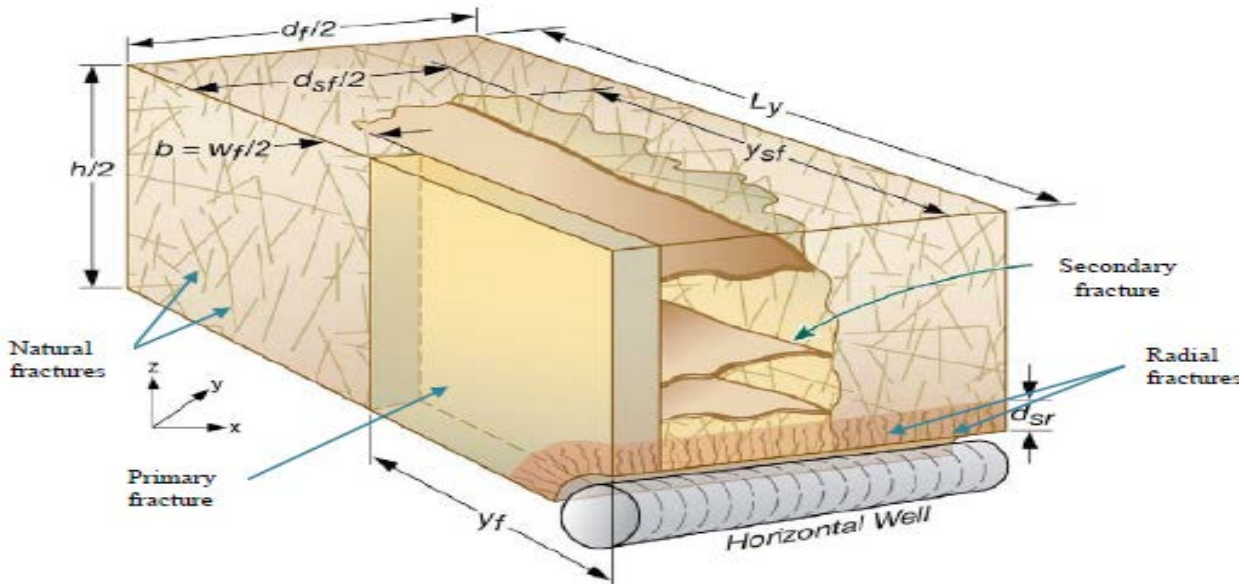

Figure 5.1: Identification of the four fractured systems [56]

- Primary or hydraulic fractures: “These are fractures created by injecting hydro-fracturing fluids (with or without proppants) into the formation. Proppants provide high-permeability flow paths that allow gas to flow more easily from the formation matrix into the well” [40].
- Secondary fractures: “These are fractures induced as a result of changes in the geomechanical status of a rock when the primary fractures are being created. Microseismic fracture mappings suggest that they generally intersect the primary fractures, either orthogonally or at an angle” [40].
- Natural fractures: “These fractures are native to the formation in the original state, prior to any well completion or fracturing process” [40].
- Radial fractures: “These are fractures that are created as a result of stress releases in the immediate neighbourhood of the horizontal well” [40].

In hydraulically fractured well, three types of fractures occur, namely; Uniform-flux fracture, Infinite-conductivity fracture and finite conductivity fracture. Uniform-flux fractures occur when fluid enters the fracture at a uniform flow rate per unit area of fracture face enabling pressure drop in the fracture. Infinite-conductivity fractures are fractures with infinite permeability in which conductivity have little or no pressure drop along its axis. They exist in highly propped tight-gas formations. Usually, fractures with dimensionless conductivity $F_{CD} > 500$ are treated as infinite-conductivity fractures. Finite-conductivity fractures are the fractures with significant pressure drop along its axis. This model is very common case, unless formation permeability is extremely low – in microdarcy range.

5.2 Shale Gas Fractured System Flow Behaviour

Four flow regimes occur in the reservoir with hydraulically fractured well as shown in Figure 5.2:

- Linear Flow
- Bilinear Flow
- Formation Linear Flow
- Pseudo-Radial Flow

Linear flow is often short and most of the fluid entering the well bore comes from fluid expansion in the fracture [95]. Sometimes it may be masked by well bore-storage effects. Bilinear flow evolves only in finite-conductivity fractures as fluid in the surrounding formation flows linearly into the fracture and before fracture-tip effects begin to influence well behaviour [95]. Most of the fluid entering the well bore during this flow period comes from the formation into the fracture. Formation linear flow often occurs depending on the length of the test and increases with higher fracture conductivities [95].

Pseudo-radial flow occurs with fractures of all conductivities and in most cases as late time features. After a sufficiently long flow period, the fracture appears to the reservoir as an expanded well bore. If the fracture length is large relative to the drainage area, then boundary effects change or mask the pseudo-radial flow regime [18][95].

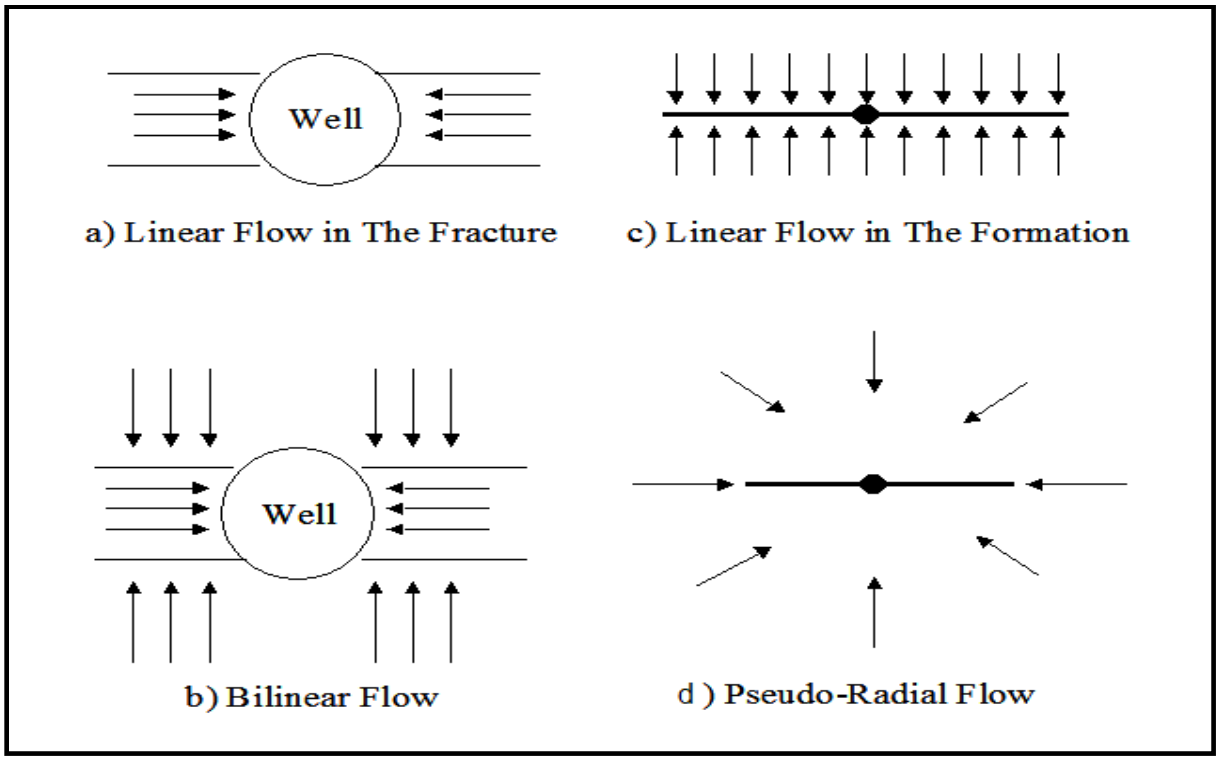

Figure 5.2: Fracture flow regimes [19]

5.3 Flow region identification with type curve and derivative method

For hydraulically fractured wells, several flowing regions may occur in or around due to the 3D nature of formations flow geometry for which the radial flow symmetry do not often exists. These flow regions are difficult to define by basis of pressure transient data because of near wellbore and formation factors, such as penetration ratio (the ratio of the fractures height to the formation height), inclination angle from the vertical direction, the spacing between fractures, heterogeneities - vertical or horizontal permeabilities, and anisotropy [78]. These parameters influence the well sand-face pressure and derivative response. Variation in irreducible and critical water saturation often influences how the derivative fingerprint or signature might look like near and far the wellbore. The nature of geometrical architectures of naturally induced fractures system determines the derivative signature for different flowing regions.

Since early seventies, PTA industry's experts and researchers have developed several models considering different well, reservoir and boundaries conditions to describe the pressure transient behaviour with or without hydraulic fractures in vertical or horizontal wells. These models were developed based on the source solution and Green's function to solve unsteady-state flow problem in the reservoir which was presented by Gringarten et al [35]. Newman product method and source function have been used for solving transient flow problem interpreting pressure behaviours.

Cinco-Ley et al [18] developed the concept of finite flow capacity and applied semi analytical approach to illustrate the importance of finite fracture when $F_{CD} < 300$ which is similar to long fractures and low capacity fractures. Their ideas facilitated the evaluation of massive hydraulic fracturing programs, although with limitation applicable to systems with small or constant compressibility. Also, their type curve is presently the reference for data analysis from a constant-rate flow or a pressure build-up test, depicting vertical hydraulic fracture model in an infinite-acting reservoir. They introduced a relationship between dimensionless time and pressure behaviour which depends on time, and dimensionless fracture conductivity F_{CD}

$$F_{CD} = \frac{K_f w_f}{K x_f}.$$

In this study, a mathematical model representing different flowing regions in a vertical well completed within a cross form fracture in a shale gas reservoir is developed and analysed with the numerical density derivative approach to visualise these flowing regions. To have a better understanding of fracture systems and their influence on derivative response for these flowing regions, several literatures on fracture model developed over the last four decades is chronicled below.

Agarwal [3] developed finite conductivity derivative type curves (F_{CD} ranging from 0.1 to 500) for constant pressure and constant rate production solution as shown in Figure 5.3, generated with numerical simulation assuming uniform fracture flow capacity, constant compressibility-viscosity product in the system, no wellbore storage effect and damage, neglected confining pressure or turbulence effects, and insignificant drainage boundary effects for the duration of the test. However, it can only be applied if producing time (t_p) prior to shut-in is significantly greater than the shut-in time (Δt) or else the lower the fracture flow capacity.

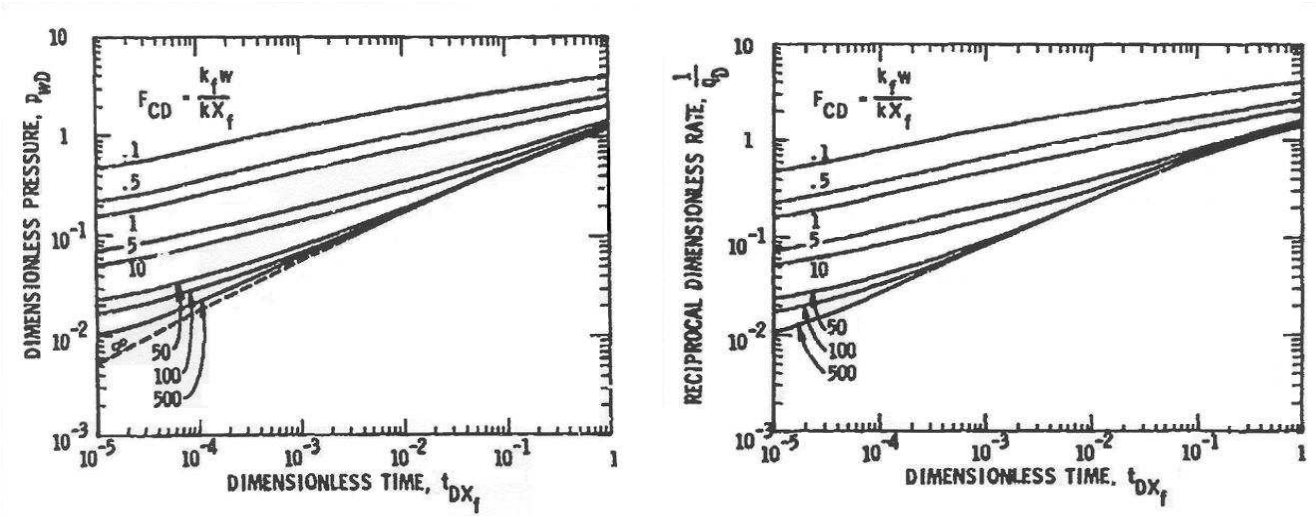

Figure 5.3; Agarwal [3] constant rate and constant pressure finite conductivity type curve

Cinco-Ley and Samaniego [19] defined bilinear flow regime as the result of two linear flow regimes and attribute its flow pattern to a well in a finite conductivity fractures system. They regarded the first flow as linear flow within the fracture, second as flow from the matrix into the fracture with a derivative signature characterized by ¼ and ½ slopes for linear and bilinear flow respectively. In their analytical conclusion, bilinear flow exists when fracture tip effects have not yet affected the well behaviour.

Bennett [10] established finite conductivity type-curves (F_{CD} ranging from 0.1 to 500) to distinguish the linear and bilinear flow region with a straight line for multi layered reservoirs

using analytical solution for cases of constant pressure and rate as shown in Figure 5.4. They concluded that this approach is applicable only if the productive interval is within the fracture and that the fracture conductivity is dependent on depth.

In 1986, an improvement of the work was done using numerical simulation model assuming the reservoir is uniform and homogeneous, fluid is slightly compressible with constant viscosity, gravitational effects are negligible, flow in the reservoir parallel to the fracture face is negligible and reservoir is infinite in the direction perpendicular to the fracture face.

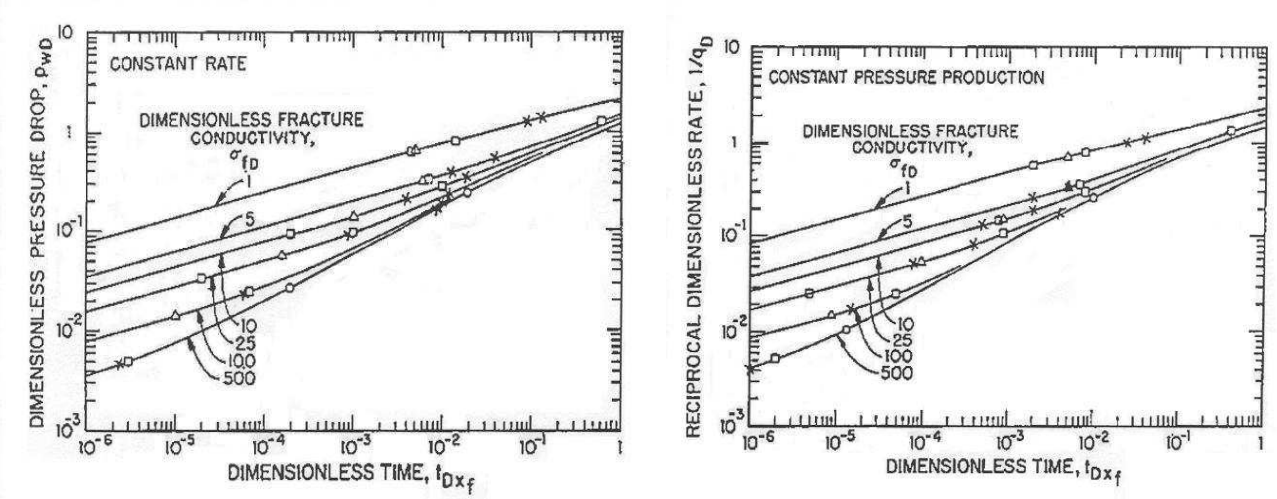

Figure 5.4: Bennett [10] constant rate and constant pressure finite conductivity type curve

Tiab [78] developed multiple curves of pressure and pressure derivatives versus time with several straight lines that represent bilinear, linear, infinite-acting radial flow and pseudo-steady state flow for different ratios of x_e/x_f for a vertically fractured well inside a finite conductivity closed system.

Raghavan et al.[68] formulated a mathematical model to understand the characteristic response of a network of fractured horizontal wells and discovered that three significant flow periods have been observed based on their model: the early time period in which the system behaved like the one with n-layers, the intermediate time period in which the system reflected the interference

between the fractures, and late time period in which the system mimicked a single horizontal well fracture signature.

Zerzar [90] integrated the boundary element method and Laplace transformation to publish a comprehensive solution for multiple vertical fractures in horizontal wells. In this study, seven flow regions were identified which include bilinear, first linear, elliptical, radial, pseudo-radial, second linear and pseudo-steady state.

Alpheus and Tiab [7] studied the effect of the partial penetrating infinite conductivity hydraulic fractures on the pressure behaviour of horizontal well extending in naturally fractured formation and concluded that the duration of early linear flow regime is dependent on the hydraulic fractures height.

Summarily, several studies on modelling flow patterns in hydraulically fractured wells have already been done by researchers over the last four decades with well documented results in various engineering and mathematical research journals. These are just few extracted from the pool of research work on the topic since this research is not focused on modelling fracture flow but using statistical "pressure" and numerical density derivatives to diagnose flow regimes in fractured systems. From the literatures review so far, four flow regions have been reliably identified to occur in the reservoir with hydraulically fractured well. These flow regions are highlighted below:

Firstly, linear flow: which is due to flow from fluid expansion along the fracture parallel to the wellbore. Occasionally, the wellbore storage effect could mask its response. Its occurrence depends on the length of the test and the fracture conductivities. This flow regime is recognized as a ½ slope in the log-log pressure derivative diagnostic plot and is used to determine fracture half-length, channel or reservoir width if vertical permeability is known [19][68]. Secondly,

bilinear flow: a combination of two simultaneous linear flows in perpendicular directions. This only occurs for finite-conductivity fracture where linear flow exists both in the fracture and to the fracture plane. This flow regime is recognized as a $^1/_4$ slope in the log-log pressure derivative diagnostic plot and is used to determine the fracture conductivity [19][73]. Thirdly, pseudo-radial flow with fractures of all conductivities and in most cases as late time features. It does occur after sufficient long flowing period.

Lastly, trilinear flow model has been developed over the last few years to account for flow from dual fracture features. Literatures on this topic are very limited but are attracting renewed attention with focus on modelling trilinear flow in finite conductivity fractures in tight gas formation. Further researches are been carried out to ascertain the flow source and sink.

This chapter introduces a mathematical model for interpreting pressures behaviour of a vertical well with crossform fracture in shale gas reservoir using numerical density approach. It focuses on developing mathematical model for different flow regions (Linear, Bilinear and Trilinear) existing in shale gas reservoir with vertical and cross form fractures. The imposed fractures can be longitudinal and transverse but symmetrical to a reference point (the wellbore). The major advantage is that it simplified the complex fracture-matrix flow equation by applying ordinary Laplace Transform Model OLTM to formulate Linear, Bilinear and Trilinear flow model. The model is tested with constant pressure and constant rate conditions with average fluid phase pressure-densities equivalent generated to visualise the distinctive fractures flow regions fingerprint on the numerical density derivative plot.

5.4 Mathematical Model for Vertical Well With CrossForm Fracture in Shale Gas Reservoir

The main goal of this study is to apply the numerical density derivative method in answering some questions regarding influence of the interference of the finite conductivity fractures on the pressure data for constant rate production and constant pressure production mode. The aim is to extend the current solution from finite conductivity vertical fractured wells to crossform fracture with vertical wells. It is necessary to develop type curves for constant rate and pressure production mode, with dimensionless fractures conductivities, and different length to distance ratios as parameters. Final goal is to provide sensitivity analysis of the achieved results – developed type curves for different reservoir and well performances.

The following steps were used to generate dimensionless density derivative curves

- Developed the mathematical equation for different flow regions for a vertical well completed within a crossform fracture in shale gas reservoir.
- Developed a reservoir model for numerical simulation using synthetic data (reservoir rock properties, reservoir geometry, and fluid properties).
- Converted simulation results– flow rates and pressure density equivalent of fluid phase to dimensionless rate derivative.
- Plotted and compared results of dimensionless rate derivative for conventional BHP and numerical density derivative (pressure-density equivalent).

5.4.1 Crossform fracture Model

Research on finite conductivity fracture model has been laden with vertical fracture networks connected in horizontal well. Extensive research and various mathematical models have been developed by Cinco-Ley [17], [19] and other researchers.

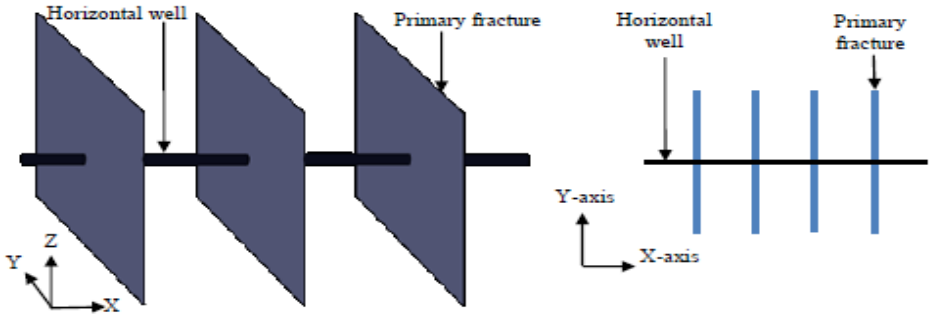

Figure 5.5: 3D and 2D plan views of planar orthogonal fractures [61]

However, this research designs the cross-form fractures model. The aim is to achieve a large surface area exposure of low permeability formation to allow more flow into the well bore by creating high conductive path close and some distance away from the well bore. This is depicted in Figures 5.6, 5.7 and 5.8 below. In summary, greater volume of fluid produced into the well bore per unit of time, results to an increased production rate without drilling another well.

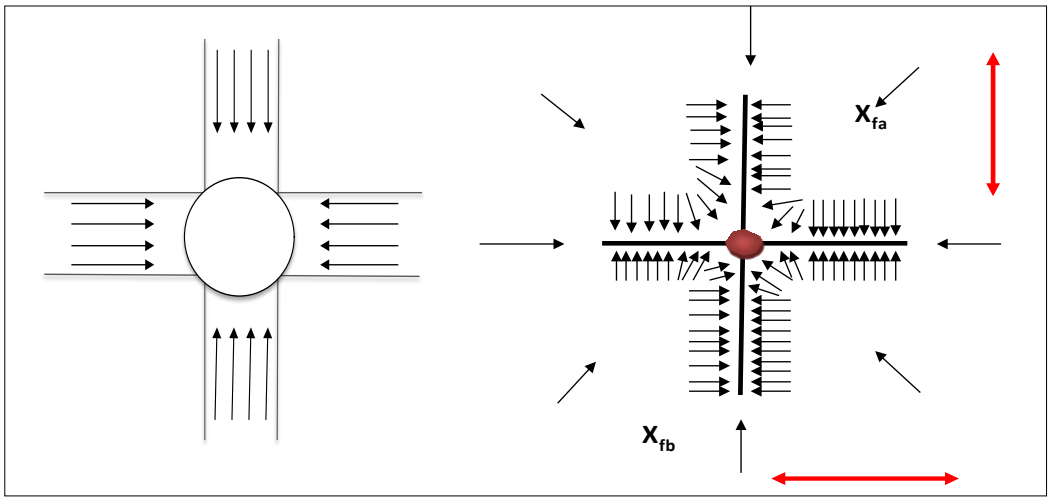

Figure 5.6: 2D view of a centred secondary fracture intersecting two primary fractures

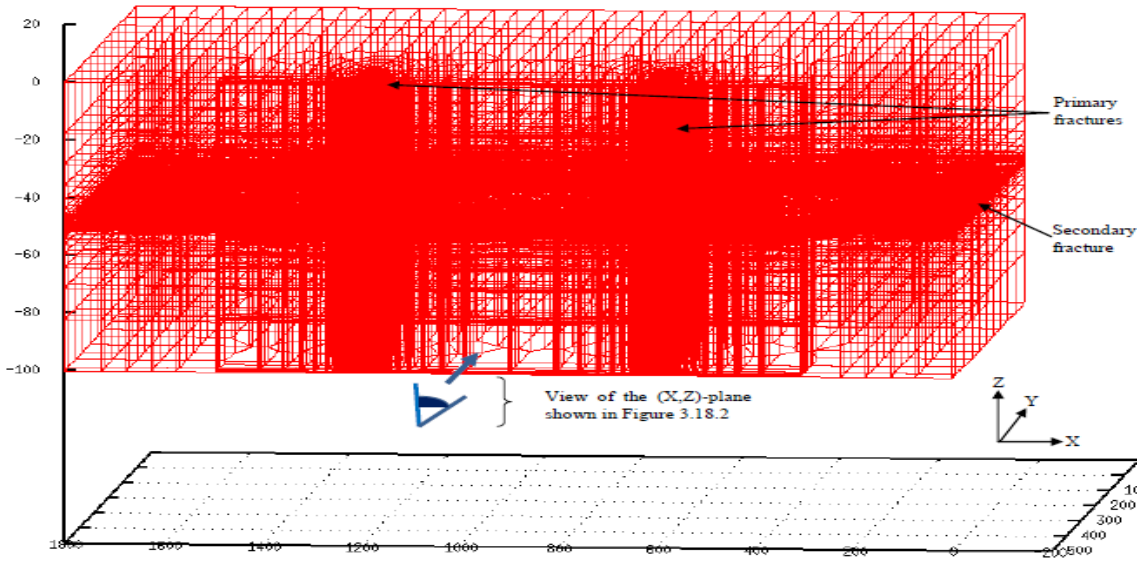

Figure 5.7: 3D view of a centred secondary fracture intersecting two primary fractures [61].

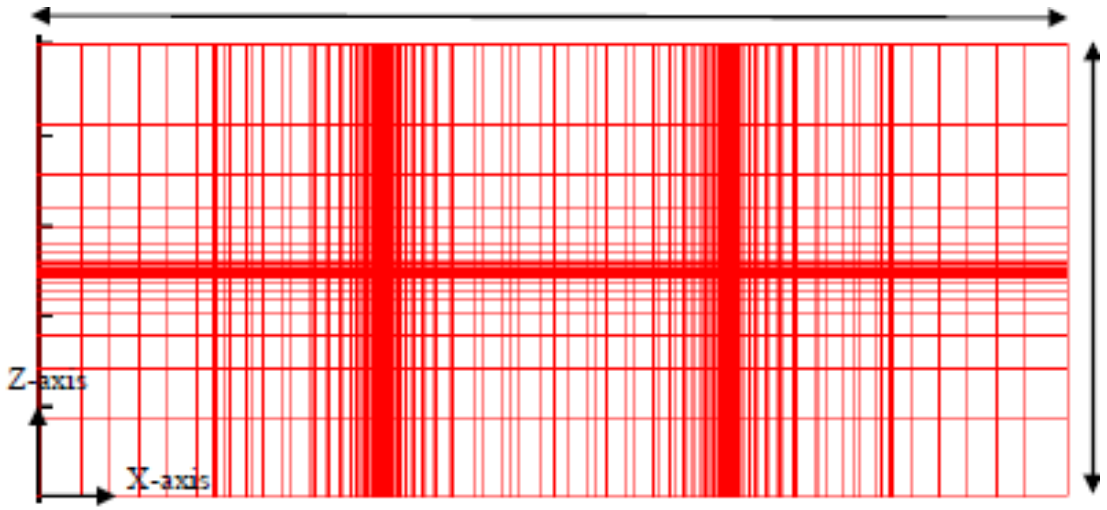

Figure 5.8: Side view (X-Z plane, at the middle of the Y-axis) of the mesh shown in Figure 6.7 showing the logarithmic spacing, with discretization becoming coarser away from the fracture [61].

5.4.2 Model assumptions

The mathematical analytical model for the pressure behaviour of a vertical well in a cross-form fracture system can be derived based on the solution for the diffusivity equation in the porous

media. The following assumptions are considered in the mathematical modelling of the flow regimes as in horizontal well in a multiple hydraulic fracture systems:

- Single phase fluid and constant compressibility, constant viscosity, and formation volume factor, flows from the reservoir to the wellbore.
- Reservoir pressure is initially constant.
- Constant porosity and permeability in each direction, but the formation is anisotropic.
- Fluid flows from the reservoir to the well through planar hydraulic fractures.
- Flow from the reservoir to the wellbore between fractures is negligible as compared with the flow from the reservoir to the fracture section.
- Fluid enters the fractures at a uniform rate per unit area of the fracture face i.e. the behaviour of the system is the uniform flux fracture.
- Reservoir is homogenous, having constant and uniform thickness
- Gravitational and frictional effects are negligible.
- Vertical well is extending in the midpoint of the formation height and reservoir (symmetrical).

5.4.3 Mathematical model and flow regime for crossform model.

The expected flow regime for crossform fracture model includes;

- Linear or dual linear flow into the well from the primary and secondary fractures depending on the flow capacity of the fractures
- Possible pseudo radial flow close to the well but could be masked by wellbore storage
- Bi-linear or trilinear flow from the matrix away from the well into the fractures
- Pseudo radial flow at the end of the fractures flow.

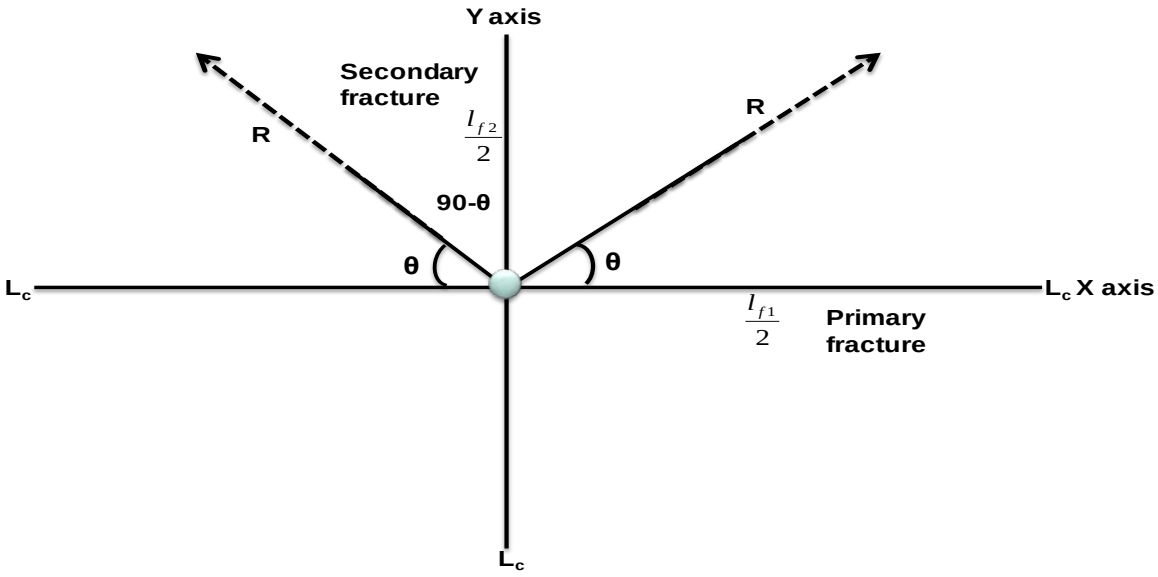

Figure 5.9: x and y axis orientation crossform fracture model symmetrical at the wellbore

For crossform fractures symmetrical to a reference point (the wellbore) at an arbitrary angle to the horizontal axis x as shown in Figure 5.9, the following assumptions are made to formulate the general solution:

- The reservoir system is dual porosity in nature
- The system is naturally fracture reservoir consisting of natural fractures.
- Flow are via the two fractures into the wellbore
- Pressure at the wellbore is the sum of combining pressure units along the fractures
- The matrix part act as a uniformly source of flow distribution into the fracture
- Viscosity is constant and slightly compressible fluid
- Reservoir is on a rectangular shape with producing well located at the centre.
- Transient interporosity flow model is adopted for the matrix and fracture transient flow.
- The fractures are modelled as homogeneous slab porous median with primary fracture = L_{f1} and secondary fracture = L_{f2}.
- The fractures have width w_f and fully penetrate the entire pay zone.
- Flows into the fractures are along the fractures and no flow via the fractures tips.

- The fractures centreline is resolved along x axis and y axis by virtue of the angle of inclination.

The benefit of the crossform fracture model is that it creates a high conductive path close and some distance away from the well bore which allows large surface area exposure of low permeability formation resulting to more flow into the wellbore, therefore it is good to visualise the numerical density derivative response in terms of flow regimes identification. Also in this case, large volume of fluid per unit of time is produced into the wellbore resulting in an increased production rate without drilling another well.

The following dimensionless parameters are defined for the formulation:

Dimensionless Pressure:

$$P_{fd} \Rightarrow P_d \Rightarrow \frac{2\pi kh\Delta p}{q_t \mu B} \tag{5.1}$$

Dimension Time:

$$t_{fd} \Rightarrow \frac{k_f t}{\left[\left[\phi c_t\right]_m + \left[\phi c_t\right]_t\right]\mu l_f^{\,2}} \tag{5.2}$$

Dimensionless Length Coordinate (L), assuming Isotropic Properties

$$x_D = \frac{x}{L_c}\sqrt{\frac{k}{k_x}} \tag{5.3}$$

$$y_D = \frac{y}{L_c}\sqrt{\frac{k}{k_y}} \tag{5.4}$$

$$z_D = \frac{z}{l_{f1}/2} = \frac{z}{l_{f2}/2} \tag{5.5}$$

Where l_{f1} and l_{f2} are lengths of primary and secondary fractures, L_c = distance along the fracture path.

For isotropic system:

$$L_{fD} \Rightarrow \frac{l_f}{L_c} \tag{5.6}$$

$$h_D \Rightarrow \frac{h}{L_c} \tag{5.7}$$

The dimensionless variable rescaling the anisotropy system to an equivalent isotropic system is given as;

$$L_{fD} \Rightarrow \frac{l_f}{L_c}\sqrt{\frac{k\cos^2\theta}{k_x}+\frac{k\sin^2\theta}{k_y}} \tag{5.8}$$

h = reservoir thickness, kx and ky are permeabilities along x and y axis If the fractures are of same length, then

$l_{f1} = l_{f2} = L_c$ =equivalent fracture length

The dimensionless fracture conductivity is defined as:

$$C_{fD} = \frac{k_f w_f}{k\lambda_{mf}} \tag{5.9}$$

Interporosity flow parameter:

$$\lambda_{mf} \Rightarrow \frac{12k_m}{{l_f}^2 k_f} A_{mf} \tag{5.10}$$

as defined by Warren and Root [82]

Dimensionless storativity:

$$\omega \Rightarrow \frac{[\phi c_t]_f}{[\phi c_t]_m + [\phi c_t]_f} \tag{5.11}$$

For fracture one (Primary fracture), the diffusivity equation is given as:

$$\frac{\partial^2 P_f}{\partial x^2} = \left[\frac{\varphi \mu c_t}{k}\right]_f \frac{\partial P_f}{\partial t} - \frac{k_m}{k_f \, l_{f1}/2} \frac{\partial P_m}{\partial z}\Big|_{z = l_{f1}/2}. \tag{5.12}$$

And for fracture two (Secondary fracture)

$$\frac{\partial^2 P_f}{\partial y^2} = \left[\frac{\varphi \mu c_t}{k}\right]_f \frac{\partial P_f}{\partial t} - \frac{k_m}{k_f \, l_{f2}/2} \frac{\partial P_m}{\partial z}\Big|_{z = l_{f2}/2} \tag{5.13}$$

If the fractures are of same length, then

$$l_{f1} = l_{f2} = l_f$$

First the diffusivity equation for the matrix is given as:

$$\frac{\partial P_m}{\partial z^2} = \left[\frac{\varphi \mu c_t}{k}\right]_m \frac{\partial P_m}{\partial t} \tag{5.14}$$

For the matrix and fracture interflowing period, the diffusivity equation is similar for both fractures; therefore the following boundary conditions BCs are applicable

Initial condition:

$$P_m(z,0) = P_i \tag{5.15}$$

Initial boundary:

$$\frac{\partial P_m}{\partial z}\Big|_{z=o} = O \tag{5.16}$$

Outer boundary

$$\left|P_m\right|_{z = l_f/2} = P_f \tag{5.17}$$

Resolving the matrix diffusivity, equation (5.14) into dimensionless form using equation (5.1), (5.3) and (5.7), we have:

$$\frac{\partial^2 P_{lmD}}{\partial z_D^{\,2}} \Rightarrow (1-\omega)\frac{l_f^{\,2}}{4}\frac{k_f}{k_m}\frac{1}{A_{mf}}\frac{\partial P_{lmD}}{\partial t_{AD}} \tag{5.18}$$

$$\frac{\partial^2 P_{lmD}}{\partial z_D^{\ 2}} \Rightarrow (1-\omega)\frac{l_f^{\ 2}}{4}\frac{k_f}{k_m}\frac{1}{A_{mf}}\frac{\partial P_{lmD}}{\partial t_{AD}} \tag{5.19}$$

Therefore

$$\frac{\partial^2 P_{lmD}}{\partial z_D^{\ 2}} \Rightarrow \frac{3}{\lambda_{mf}}[1-\omega]\frac{\partial P_{lmD}}{\partial t_{AD}} \tag{5.20}$$

Where interporosity flow parameter

$$\lambda_{mf} = \frac{12k_m}{l_f^{\ 2}k_f}A_{mf}$$ Warren and Root [82]

The fracture solution for the cross-form fracture model is formulated as follows:

The primary fracture

The diffusivity equation as stated in equation (5.12) is given as:

$$\frac{\partial^2 P_f}{\partial x^2} = \left[\frac{\varphi\mu c_t}{k}\right]_f \frac{\partial P_f}{\partial t} - \frac{k_m}{k_f}\frac{\partial P_m}{l_{f1}/2}\frac{\partial}{\partial z}\Big|_{Z=l_{f1}/2} \tag{5.21}$$

Resolving the equation in dimensionless form using equation (5.1), (5.2) and (5.5)

$$\frac{\partial^2 P_{lfD}}{\partial x_D^2} \Rightarrow R^2\cos^2\theta\frac{k}{k_x}\left[\frac{\varphi\mu c_t}{k}\right]_f - \frac{k_f}{[(\varphi c_t]_m + [\varphi c_t]_f]\mu l_{f1}^{\ 2}}\frac{\partial P_{lfD}}{\partial t_{AD}} - \frac{4k_m}{k_f}\frac{R^2\cos^2\theta}{l_{f1}^{\ 2}}\cdot\frac{\partial P_{lmD}}{\partial z_D} \tag{5.22}$$

Substitute for $l_{f1} = R^2\cos^2\theta$ along x axis, we have:

$$\frac{\partial^2 P_{lfD}}{\partial x_D^{\ 2}} \Rightarrow \frac{R^2\cos^2\theta}{l^2_{f1}}\frac{k}{k_x}\omega\frac{\partial P_{lfD}}{\partial t_{AD}} - \frac{4k_m}{k_f}\frac{\partial P_{lmD}}{\partial z_D} \tag{5.23}$$

For secondary fracture resolve in y axis from equation (5.13)

$$\frac{\partial^2 P_f}{\partial y^2} = \left[\frac{\varphi\mu c_t}{k}\right]_f \frac{\partial P_f}{\partial t} - \frac{k_m}{k_f}\frac{\partial P_m}{l_{f2}/2}\Big|_{z=L_{f2}/2} \tag{5.24}$$

Converting the equation dimensionless form using equation (5.1), (5.2) and (5.5)

$$\frac{\partial^2 P_{fD}}{\partial y_D^2} \Rightarrow R^2 \sin^2\theta \frac{k}{k_y}\left[\frac{\varphi\mu c_t}{k}\right]_f - \frac{k_f}{\left[[\varphi c_t]_m + [\varphi c_t]_f\right]\mu l_{f2}^{\ 2}} \frac{\partial P_{fD}}{\partial t_{AD}} - \frac{4k_m}{k_f}\frac{R^2\sin^2\theta}{l_{f2}^{\ 2}} \cdot \frac{\partial P_{mD}}{\partial z_D} \tag{5.25}$$

Substituting for $l_{f2} = R^2 \sin^2\theta$ along y axis

$$\frac{\partial^2 P_{lfD}}{\partial y_D^2} \Rightarrow \frac{R^2\sin^2\theta}{l_{f2}^2}\frac{k}{k_y}\omega\frac{\partial P_{lfD}}{\partial t_{AD}} - \frac{4k_m}{k_f}\frac{\partial P_{lmD}}{\partial z_D} \tag{5.26}$$

Assuming the flux is uniform along the fracture and the pressure at the wellbore is a summation of pressure along the fractures segment, hence P_{fD} x axis = P_{fD} y axis

Combining equation (5.23) and (5.26)

$$\frac{\partial^2 P_{lfD}}{\partial x_D^2} + \frac{\partial^2 P_{lfD}}{\partial y_D^2} \Rightarrow \left[\frac{k\cos^2\theta}{k_x l_{f1}^{\ 2}} + \frac{k\sin^2\theta}{k_y l_{f2}^{\ 2}}\right]\omega R^2 \frac{\partial P_{lfD}}{\partial t_{AD}} - \frac{8k_m}{k_f}\frac{\partial P_{lmD}}{\partial z_D} \tag{5.27}$$

Resolving in x axis

$$\frac{\partial^2 P_{lfD}}{\partial x_D^2} \Rightarrow \left[\frac{k\cos^2\theta}{k_x l_{f1}^{\ 2}} + \frac{k\sin^2\theta}{k_y l_{f2}^{\ 2}}\right]\frac{\omega R^2}{2}\frac{\partial P_{lfD}}{\partial t_{AD}} - \frac{8k_m}{k_f}\frac{\partial P_{lmD}}{\partial z_D} \tag{5.28}$$

See full detail at the Appendix B

The general solution combining the matrix and fractures differential equations with different BCs is given as:

$$P_{lfD} \Rightarrow A\cosh(\sqrt{ms}x_D) + B\sinh\left(\sqrt{ms}x_D\right) \tag{5.29}$$

Resolving the above equation by differentiating and applying BC, the final solution for crossform fractures model is given as:

$$q_{lwD} \Rightarrow \frac{1}{P_{lwD}} = \frac{-\pi s}{C_{fD}\sqrt{ms}}\coth\left(\sqrt{ms}x_D\right) \tag{5.30}$$

$$m = \omega + \frac{l_f}{\pi h}\left[\sqrt{\frac{\lambda_{mf}(1-\omega)}{3s}}\tanh\sqrt{\frac{3(1-\omega)s}{\lambda_{mf}}}\right] \tag{5.31}$$

This is general solution for the crossform fractures model connecting at the wellbore. This equation can be inverted to obtain time dependant solution using Laplace inversion such as Stehfest's inversion algorithm.

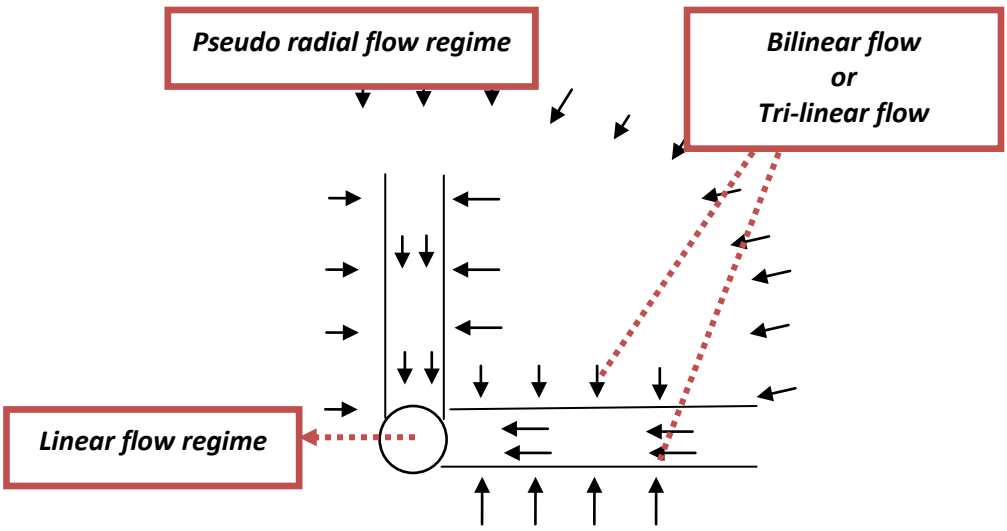

Figure 5.10: Pictorial view of expected Cros-form fracture flow region

Figure 5.10 shows the flowpath and expected flow regions for the cross-form fracture in a vertical well. The flow geometry phase system for crossform is summarise in Figure 5.11 below.

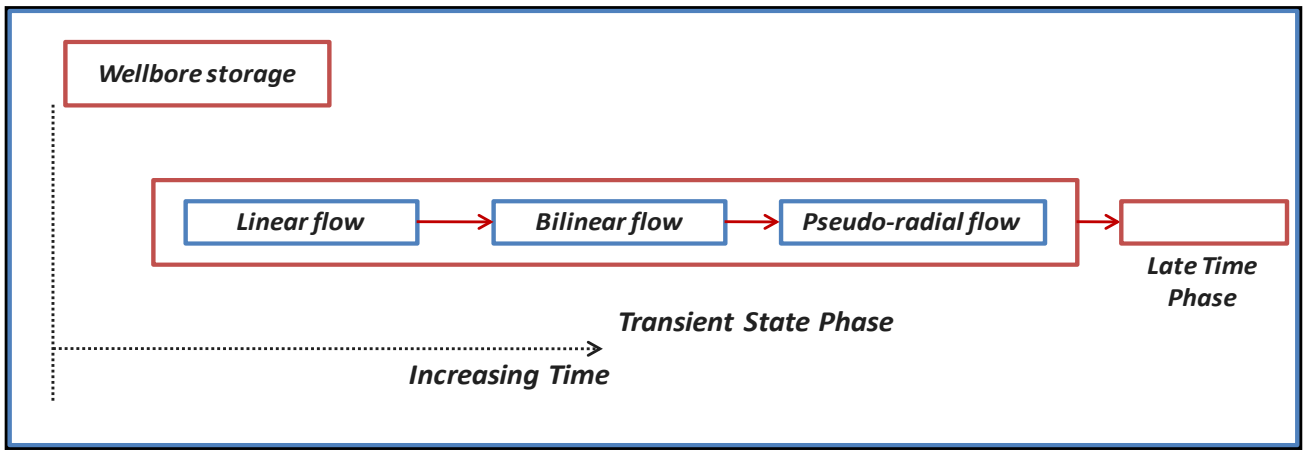

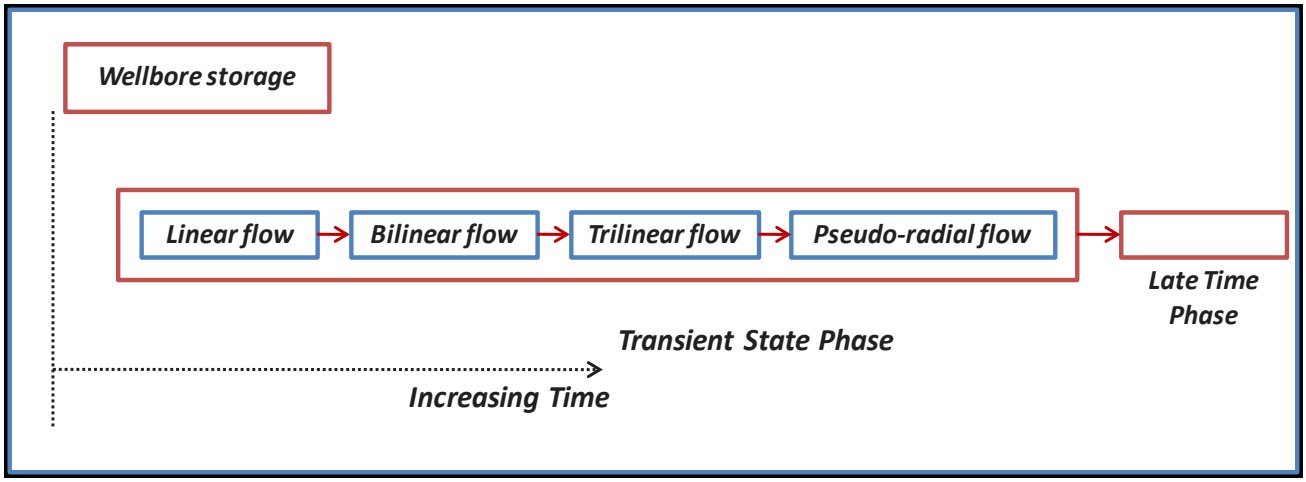

Figure 5.11: Flow geometry phases system for crossform fracture model

At $x > 4.5$ and $\coth(x) = 1$

Hence

$$\coth\left(\sqrt{ms}\,x_D\right) = 1 \quad \text{if} \quad \sqrt{ms}\,x_D > 4.5$$

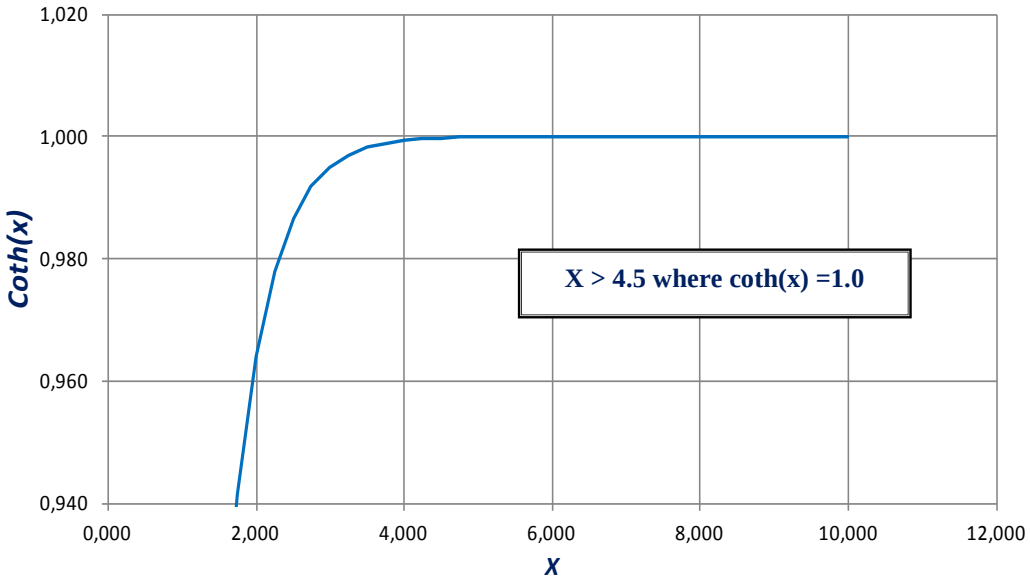

Figure 5.12: Coth(x) definition as x >4.5

Therefore

$$\frac{1}{q_{lwD}} \Rightarrow \frac{-\pi s}{C_{fD}\sqrt{ms}} \tag{5.32}$$

Where

$$m = \omega + \frac{l_f}{\pi h}\left[\sqrt{\frac{\lambda_{mf}(1-\omega)}{3s}}\tanh\sqrt{\frac{3(1-\omega)s}{\lambda_{mf}}}\right]$$

CASE (I) → Bilinear flow

If ω = 0 (5.33)

$$m = \frac{l_f}{\pi h}\sqrt{\frac{\lambda_{mf}}{3s}}\tan\sqrt{\frac{3s}{\lambda_{mf}}} \quad (5.34)$$

If

$$\tanh\left[\sqrt{\frac{3s}{\lambda_{mf}}}\right] = 1.0$$

Then

$$\sqrt{\frac{3s}{\lambda_{mf}}} \geq 4.5$$

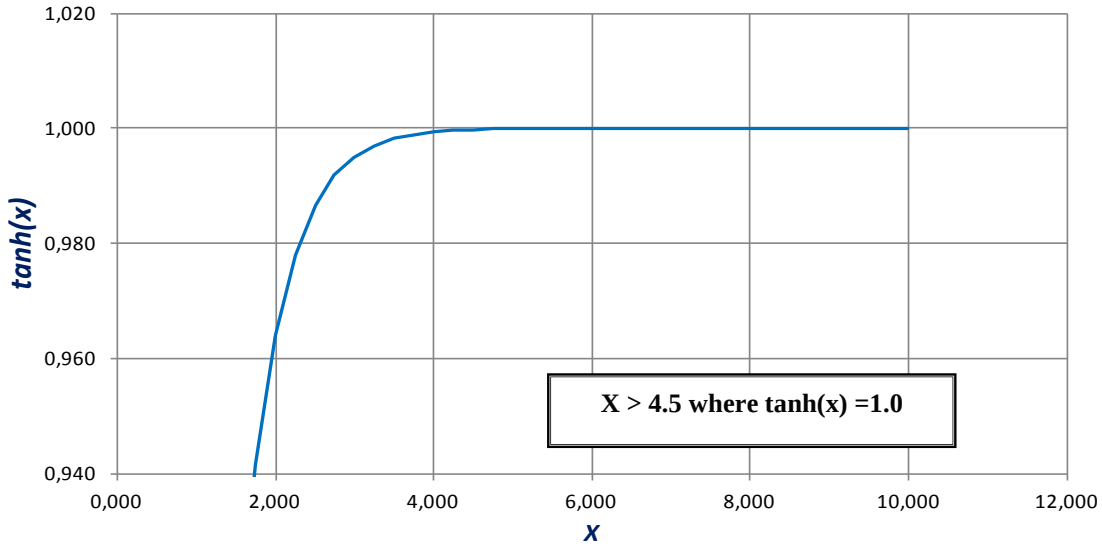

Figure 5.13: Tanh(x) definition as x >4.5

Therefore

$$\sqrt{ms}x_D > 4.5 \text{ If } \cosh\left(\sqrt{ms}x_D\right) = 1$$

$$\frac{1}{q_{lwD}} \Rightarrow \frac{-\pi s}{C_{fD}\sqrt{ms}}$$

The general solution is given as;

$$q_{lwD} \Rightarrow \frac{C_{fD}}{6.84 t_{AD}^{1/4}} \sqrt{\frac{l_f}{h_D}} \left[\lambda_{mf} / 3 \right]^{1/4} \tag{5.35}$$

This equation is due to bilinear flow period.

However considering the assumptions, the flow regime is limited by;

$$\sqrt{\frac{3s}{\lambda_{mf}}} \geq 4.5 \tag{5.35a}$$

Therefore equation (5.35) is limited to:

$$t_{AD} \leq \frac{3}{20.3\lambda_{mf}} \text{ and } t_{AD} \leq \frac{m x_D^{\,2}}{20.3\lambda_{mf}}$$

CASE (II) → Linear flow

$$\omega = 1 \tag{5.36}$$

$$m = \omega + \frac{l_f}{\pi h}\left[\sqrt{\frac{\lambda_{mf}(1-\omega)}{3s}} \tanh \sqrt{\frac{3(1-\omega)s}{\lambda_{mf}}} \right]$$

$$m \Rightarrow 1 + 0$$

$$m = 1$$

Therefore

$$\frac{1}{q_{lwD}} \Rightarrow -\frac{\lambda_{mf} s}{C_{fD}\sqrt{ms}} \coth\left[\sqrt{ms}\, x_D\right] \tag{5.37}$$

This is the general solution for;

$$q_{lwD} \Rightarrow \frac{C_{fD}}{5.57 t_{AD}^{1/2}} \tag{5.38}$$

This equation is due to the linear flow period with assumption limiting to t.

Equation (5.38) is limited to the region:

$$t_{AD} = \frac{m x_D^{\ 2}}{20.3} \tag{5.38a}$$

CASE (III) → Radial Homogeneous flow

For homogenous case, $f(s) \Rightarrow 1.0$

Recall that for matrix slab

$$f(s) = \omega + \sqrt{\frac{\lambda_{mf}(1-\omega)}{3s}} \tanh \sqrt{\frac{3(1-\omega)s}{\lambda_{mf}}} \tag{5.39}$$

$$\sqrt{\frac{\lambda_{mf}(1-\omega)}{3s}} \tanh \sqrt{\frac{3(1-\omega)s}{\lambda_{mf}}} \Rightarrow 1-\omega$$

Therefore

$$m = \omega + \frac{l_f}{\pi h} \sqrt{\frac{\lambda_{mf}(1-\omega)}{3s}} \tanh \sqrt{\frac{3(1-\omega)s}{\lambda_{mf}}}$$

$$m = \omega + \frac{l_f(1-\omega)}{\pi h} \tag{5.40}$$

Substitute into equation

$$\frac{1}{q_{lwD}} \Rightarrow -\frac{\pi s}{C_{fD}\sqrt{ms}} \coth\left[\sqrt{ms}\, x_D\right]$$

$$\Rightarrow -\frac{\pi s}{C_{fD}\sqrt{\left(w + \frac{l_f(1-w)}{\pi h}\right)s}} Coth\left[\sqrt{ms}\, x_D\right] \tag{5.41}$$

If

$$Coth\left[\sqrt{ms}x_D\right] \Rightarrow 1.0 \;,\quad \sqrt{ms}x_D \geq 4.5$$

$$\frac{1}{q_{lwD}} \Rightarrow -\frac{\pi s^{1/2}}{C_{fD}\sqrt{\omega + \frac{l_f(1-\omega)}{\pi h}}} \tag{5.42}$$

The general solution is given as;

$$q_{lwD} \Rightarrow -\frac{C_{fD}\sqrt{\omega + \frac{l_f(1-\omega)}{\pi h_D}}}{5.57 t_{AD}^{1/2}} \tag{5.43}$$

This equation represents the homogenous flow.

Also this equation is limited by

$$t_{AD} \leq \frac{m x_D^{\,2}}{20.3} \tag{5.43a}$$

CASE (IV) → Trilinear flow

If $f(s) \Rightarrow 0$ and

$$\omega = \left.\begin{matrix} \frac{1}{s^{3/4}} \\ \frac{1}{s^2} \\ \frac{1}{s^{3/2}} \end{matrix}\right\} \text{ Asymptons}$$

Recall that for matrix slab

$$f(s) = \omega + \sqrt{\frac{\lambda_{mf}(1-\omega)}{3s}} \tanh \sqrt{\frac{3(1-\omega)s}{\lambda_{mf}}}$$

$$\sqrt{\frac{\lambda_{mf}(1-\omega)}{3s}} \tanh \sqrt{\frac{3(1-\omega)s}{\lambda_{mf}}} \Rightarrow -\omega$$

If

$$\tanh\left[\sqrt{\frac{3s}{\lambda_{mf}}}\right] = 1.0$$

$$\sqrt{\frac{\lambda_{mf}(1-\omega)}{3s}} \Rightarrow -\omega$$

Therefore

$$1-\omega = \frac{-\omega^2 3s}{\lambda_{mf}} \tag{5.44}$$

Recall

$$m = \omega + \frac{l_f}{\pi h}\sqrt{\frac{\lambda_{mf}(1-\omega)}{3s}}\tanh\sqrt{\frac{3(1-\omega)s}{\lambda_{mf}}}$$

Substitute equation 8.44 and the asympton $\omega = \frac{1}{s^{3/4}}$ into above equation

$$m = \frac{1}{s^{3/4}} - \frac{l_f}{\pi h_D s^{3/2}} \tag{5.45}$$

Substitute into equation 5.30

$$\frac{1}{q_{lwD}} \Rightarrow -\frac{\pi s}{C_{fD}\sqrt{ms}}\coth\left[\sqrt{ms}x_D\right]$$

$$\Rightarrow -\frac{\pi s}{C_{fD}\sqrt{\left(s^{-3/4} - \frac{l_f}{\pi h_D s^{3/2}}\right)s}}Coth\left[\sqrt{ms}x_D\right] \tag{5.46}$$

If

$$Coth\left[\sqrt{ms}x_D\right] \Rightarrow 1.0\ ,\quad \sqrt{ms}x_D \geq 4.5$$

$$q_{lwD} \Rightarrow -\frac{C_{fD}}{\pi s^{7/8}} - \frac{C_{fD}l_f}{\pi^2 s^{5/4}h_D} \tag{5.47}$$

Converting to time dependent function using Laplace inverse

$$q_{lwD} \Rightarrow -\frac{C_{fD}t_{AD}^{-0.125}}{\pi\Gamma 0.875} - \frac{C_{fD}l_f t^{-0.25}}{\pi^2\Gamma 0.75 h_D} \tag{5.48}$$

Where Γ = Gamma Function

Γ 0.875 = 1.456

Γ 0.75 = 1.225

Therefore

$$q_{lwD} \Rightarrow -C_{fD}\left(\frac{0.22}{t_{AD}^{1/8}} - \frac{0.083 l_f}{t_{AD}^{1/4} h_D}\right) \tag{5.49}$$

This equation is due to trilinear flow period. Also this equation is limited by

$$t_{AD} \leq \frac{m x_D^{\,2}}{20.3} \tag{5.49a}$$

Summary of the matrix and fractures diffusivity PDEs and the generated equations for each flow regimes is shown in Figure 5.14.

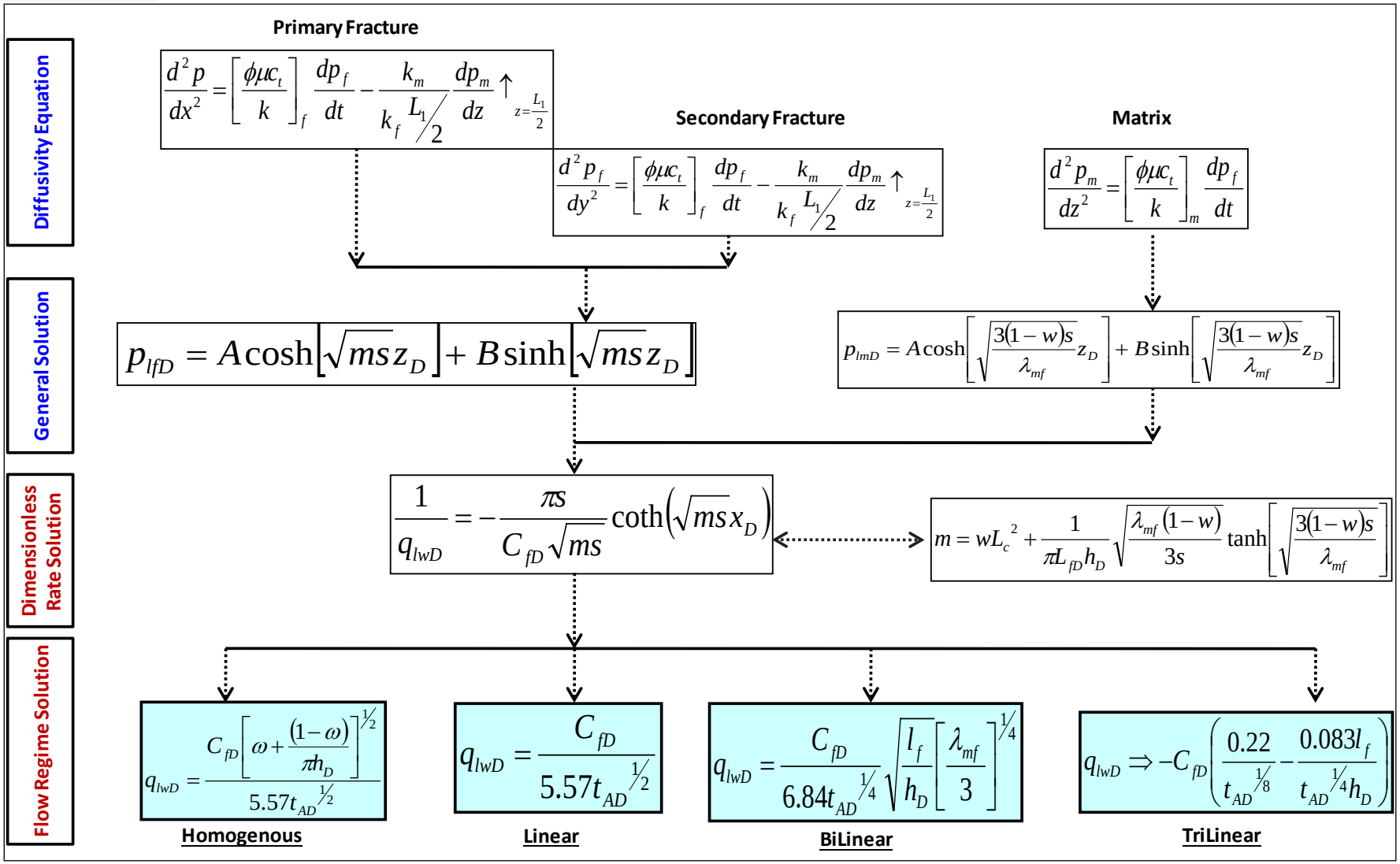

Figure 5.14: Derived mathematical for four flowing regions (Crossform fracture model)

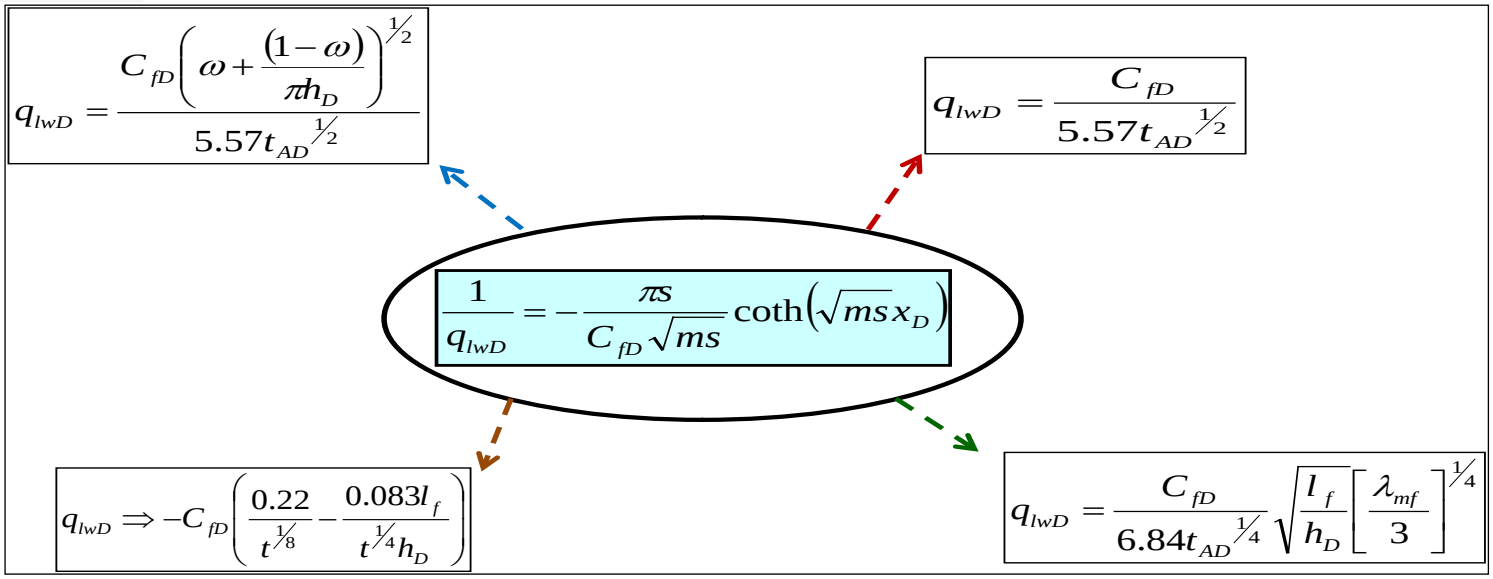

Figure 5.15: Derived mathematical for four flowing regions (Crossform fracture model)

5.5 Numerical density derivative Application in Shale Gas

5.5.1 Example 1.0: Numerical Simulation Model

The numerical simulation model was performed using a synthetic reservoir and fluid data. First the reservoir is discretized into blocks, and the Bennett [10] empirical guideline as show in Table 5.1 is used to design the x and y grids (block dimensions and fracture aperture) for the fracture pathway. Single layer reservoir is discretized into 10,000 blocks with distribution as x: y: z=100:100:1 with crossform fractures and a vertical well modelled in such a way that there are no boundary effects.

A single-well simulation model in 3D reservoir is set up with the Black Oil Simulator Eclipse-100 from Geoquest-Schlumberger. To develop the physical model, the following assumptions are considered:

- isothermal flow and no diffusion nor dispersion process presented
- no chemical reactions presented and thermodynamically equilibrium
- one phase system

The Peaceman's formula is used where necessary in an anisotropic reservoir:

$$r_0 = 0.28 \frac{\left(D_x^{\,2} \left(\frac{k_y}{k_x} \right)^{\frac{1}{2}} + D_y^{\,2} \left(\frac{k_x}{k} \right)^{\frac{1}{2}} \right)^{\frac{1}{2}}}{\left(\frac{k_y}{k_x} \right)^{\frac{1}{4}} + \left(\frac{k_x}{k_y} \right)^{\frac{1}{4}}} \mathrm{r_o} \qquad (5.50)$$

where:

Dx, Dy – the x- and y- dimensions of the grid block

Kx, Ky – x- and y- direction permeabilities

Table 5.1: The Bennett [10] empirical guidelines for design of x and y grids

A. For All Grid Blocks

$$\Delta x_{i+1}/2 \le \Delta x_i \le 2\Delta x_{i-1} \qquad i=2.... N_x - 1$$

$$\Delta y_{j+1}/2 \le \Delta y_j \le 2\Delta y_{j-1} \qquad j = 2.... N_x - 1$$

B. Near the Fracture $\Delta x/L_{xf} \le 1.5,\ \Delta y/L_{xf} \le 1$

$(\Delta x/L_{xf} \le 10^{-2}$ at the well for $C_{fD} \ge 100$

$\Delta x/L_{xf} \le 10^{-3}$ at the well for $C_{fD} \ge 100$

$\Delta x/L_{xf} \le 1.5x10^{-2}$ at the fracture tip

$\max\left(\Delta x/L_{xf}\right) \le 0.15$

$b/L_{xfj} \le 2\Delta y_i/L_{xf} \le 2x10^{-3}$

$\Delta y_1 = \Delta y_2 = \Delta y_3 = \Delta y_4$

$\max\left(\Delta y/L_{xf}\right) \le 0.20$

C. Away From the Fracture $\Delta x/L_{xf} \le 1.5,\ \Delta y/L_{xf} \le 1$

$\max\left(\Delta x/L_{xe}\right) \le 0.17$

$\max\left(\Delta y/L_{xe}\right) \le 0.17$

The fracture's blocks in x direction are model with different dimensions that are increasing to maximum value and decreasing to the minimal dimension for each well grid block. The minimal dimension is regarded as the tip of the fracture and at that point, the distance between the well and fracture tip is the half-fracture length in x direction. All next grid blocks have the same dimension and adjacent grid block dimensions are increased until the maximum. However, the minimal dimension of the grid has the block with well in y direction.

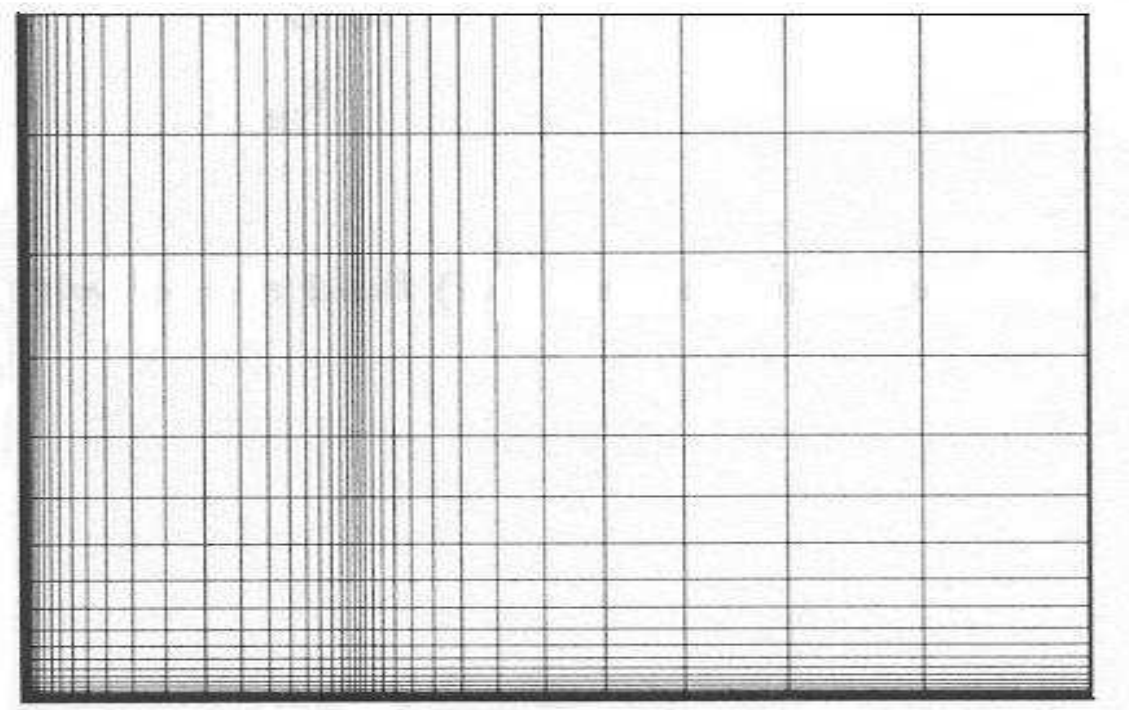

Figure 5.16: Quarter of the reservoir, grid block distribution [61]

From 5.16, the dimension of the adjacent grid blocks increases to the maximal value and then they have constant dimension. This indicates that there is uneven distribution of grid blocks in the reservoir. However, since the reservoir is symmetrically related to the fracture position and the well, a quarter of the reservoir has been observed. For the crossform fracture model, the fracture is reoriented in the x and y direction.

5.5.2 Data Input of Fluid and Reservoir Properties

Tables 5.2 and 5.3 present a summary of the well and reservoir synthetic data used for the build-up and drawdown simulated scenario with additional information given below. It is required to generate the pressure-density equivalent and its derivative for each phase, compare their diagnostic signatures and also identify the crossform fracture flowing regions. To test the density derivative method, a numerical well test model is considered with data in Table 5.2 and the following assumptions:

Table 5.2: Reservoir and fluid data for example

Parameters	Design Value
Eclipse model	Black Oil
Model dimension	100 X 100 X 1
Length by Width ft by ft	Bennett (1985) model
Thickness ft	100
Permeability kx by ky md	0.1 by 0.1
Porosity %	10
Well diameter ft	0.15
Initial water saturation Swi %	20
Permeability, k, mD	Bennett (1985) model
Gas Oil contact GOC ft	4100
Oil water contact OWC ft	4100
Initial Pressure, Pi, psia	4000
Formation Temperature, T, ^{o}F	200

Assumptions:

- Shale Gas reservoir, completed with one well.
- Model with Bennett [10] empirical guidelines on grid sizes close to the well to account for pressure and density changes.
- Only flowing condition is simulated.
- Uniform permeability of 0.1 md assign to kx, ky and kz while average porosity of 10% was imputed in the model.

- A conditional Sw and relative permeability is used.
- Model does not account for well bore storage, skin, frictional losses in the well bore and capillary pressures.
- Gas, Oil, Water densities around the local grid refinement (wellbore) and WBHP is output using Eclipse keywords.

Other Data Included in Numerical Model

The initial fracture width 0.5 in is very low, so unsuitable for the simulation because the well bore radius is 0.3 ft. The fracture width was increased to achieve better pressure response. The best value for modelling the fracture width is 2 ft, which is the dimension of the smallest grid block with well. The equivalent fracture porosity is calculated using the equation below since the fracture porosity of 35% corresponds to the fracture width of 0.5 ft.

$$\phi_e = \frac{w\phi_f}{w_e} \tag{5.51}$$

where:

w [ft] – fracture width

we [ft] – equivalent fracture width

ϕ_f – fracture porosity, fraction

ϕ_{fe} – equivalent fracture porosity, fraction

Fracture permeability is the function of the dimensionless fracture conductivity.

$$k_f = \frac{F_{Cd} k x_f}{w} \tag{5.52}$$

where: F_{CD} – dimensionless fracture conductivity

k [md] – formation permeability

x_f [ft] – fracture half-length

w [ft] – fracture width

Equivalent fracture permeability

$$k_{fe} = \frac{k_f w}{w_e} \tag{5.53}$$

Where w_{fe} [ft] – equivalent fracture width

Summary of all reservoir, fracture and fluid properties are listed in Table 5.3.

Table 5.3: Reservoir, fracture and fluid PVT properties for constant pressure case

Reservoir Properties	**Value**
Initial pressure psia	4000
Bottom hole flowing pressure psia	3500
Formation porosity fraction	0.1
Formation permeability	0.1
Reservoir thickness ft	100
Rock compressibility 1/psi	3.0E-06
Well perforated ft	50
Skin	
Well bore radius rw ft	0.0875
Fracture Properties	
Fracture half length ft	2043
Fracture width w ft	0.5
Fracture porosity fraction	0.35
Equivalent Fracture Properties Adjusted for Numerical Simulation	
Equivalent fracture width We ft	2
Equivalent fracture porosity Øe fraction	0.0875
Fluid Properties	
Compressibility cf 1/psi	3.0E-06
Viscosity µ cP	1.0

Production test:

The two approaches for analysing the transient flow behaviour include;

- Constant pressure solution
- Constant rate production solution

For the constant rate production, the gas rate is fixed at 500Mscf/day while for the constant pressure production, the BHFP is assumed to be 3500psi. The bottom hole flowing rate and pressure are determined from the result of the numerical simulation for constant pressure and constant rate production respectively.

The well is positioned in the centre block (50, 50, 1) with 2 ft dimension while the fractures are in the x and y directions. The middle of the fracture starts in block 50 and fractures continues to the adjacent 20 blocks in both directions of x and y axis to the total fracture half-length of 2,043 ft each for primary fracture in x direction and secondary fracture in y direction as shown in Figure 5.17

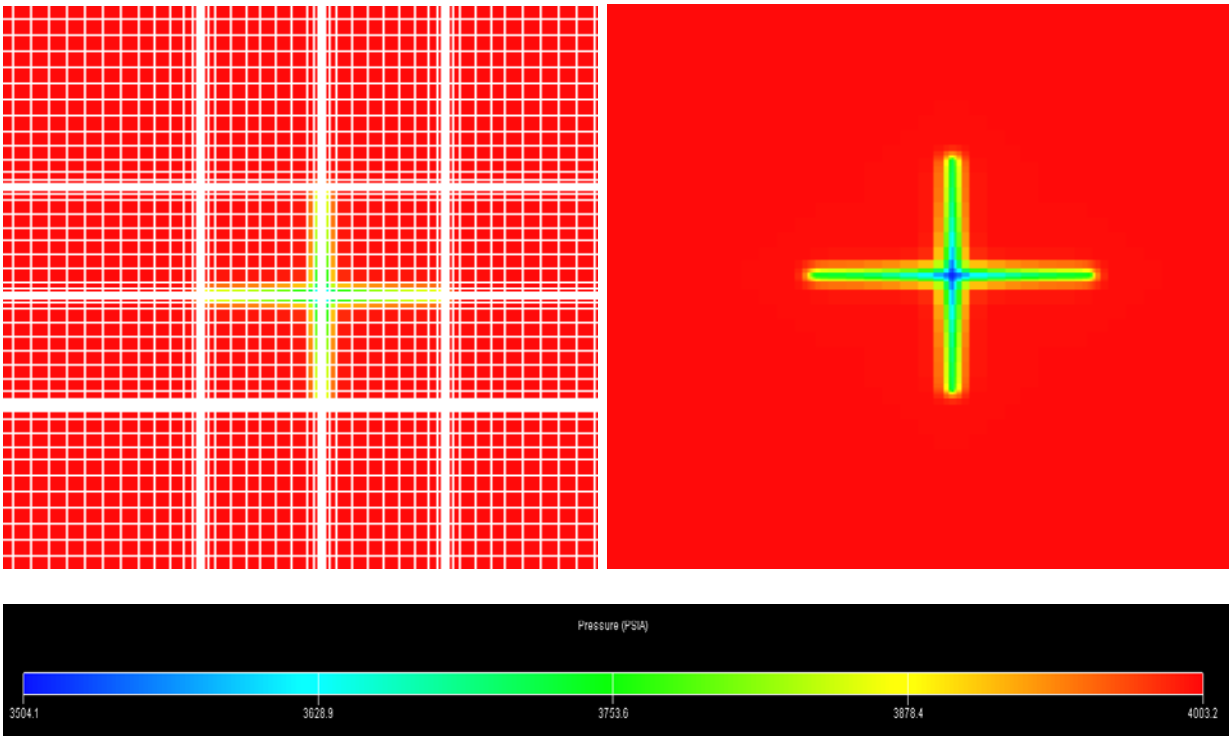

Figure 5.17: (a) Reservoir with 10000 grid blocks (b) Part of reservoir grid with crossform fracture and well. Both imported from Eclipse

Grid blocks are defined with red lines while white thick lines are the effect of fine gridding due to primary and secondary fractures pathway. Fractures are extending in x and y direction with fracture half-length x_f, defined by green-white line while black circle at the centre is the well. According to the scale below, initial reservoir pressure value is correspondent to red

colour and during numerical simulation, decrease in pressure is observed by colour change beginning from red to final blue.

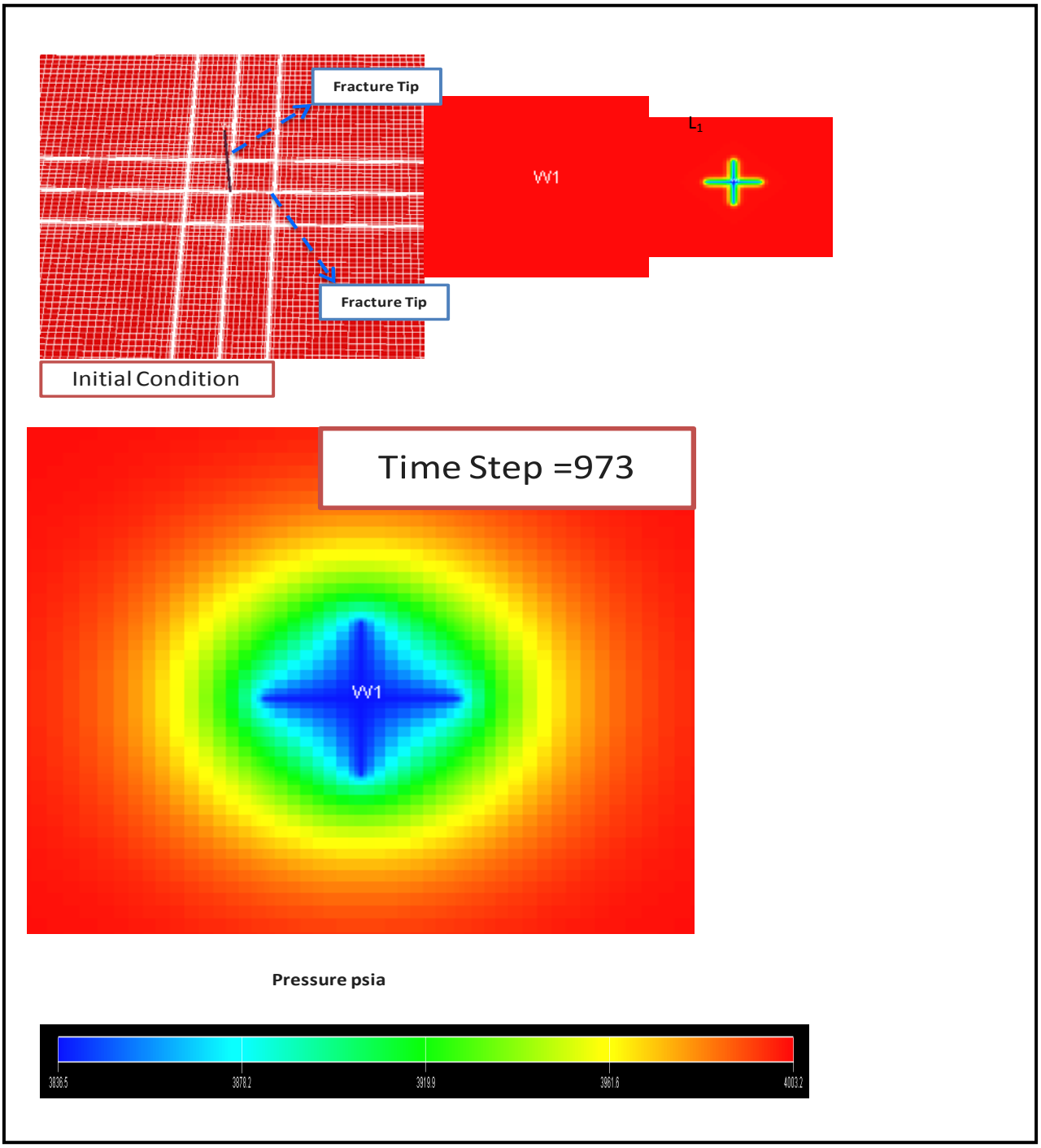

Figure 5.18: Pressure distribution at each time step (Crossform fracture model)

5.5.3 Result Analysis:

5.5.3.1 Constant Pressure solution

For constant bottom hole pressure solution, the bottom hole flowing pressure is fixed at 3500psia to trigger multiphase fluid distribution at the wellbore in order to capture the density changes for each fluid phase. The fluid density equivalent pressures are calculated from the phase densities at bottom hole flowing conditions. Then the derivative dimensionless rate $q_D^{\,i}$ is calculated from the inverse of dimensionless pressure equation (5.1) in (field unit) transformed into the derivative form using Statdev equations (3.32) and (3.33). Throughout this study, the Gas and Pressure Equivalent of Density Weighted Average (PDENG→PDENG, PDENDWA→PDENA) will be used.

5.5.3.1.1 Numerical density solution (Limit and without limit)

Figure 5.18 shows the regions with developed fracture flow equations (5.35), (5.38) and (5.43) with limitation using equations (5.35a), (5.38a) and (5.43a). Five flow regions: Linear-bilinear-Transition-Linear-Pseudoradials are identified with this model. Region 1 which is linear is due to transient flow only in the fractures. Region 2 is the response for a homogeneous reservoir which is dominated by transient matrix drainage and is the transient flow regime of interest. At this point, a small transition region dominated by a mix of linear and bilinear flow effect. Region 4 is bilinear flow and occurs when the matrix drainage begins simultaneously with the transient flow in the fractures.

Region 5 is trilinear flow which accounts for flow from dual fracture features. Its response is similar to the bilinear flow response but a slight deviation from the bilinear flow curve depicts its present. This Trilinear flow regime is believed to be caused by transient drainage of low permeability matrix blocks into adjoining fractures and parallel flow into the

fractures depending on the length of the fractures and permeability distribution. Finally is the flow boundary dominated transient response.

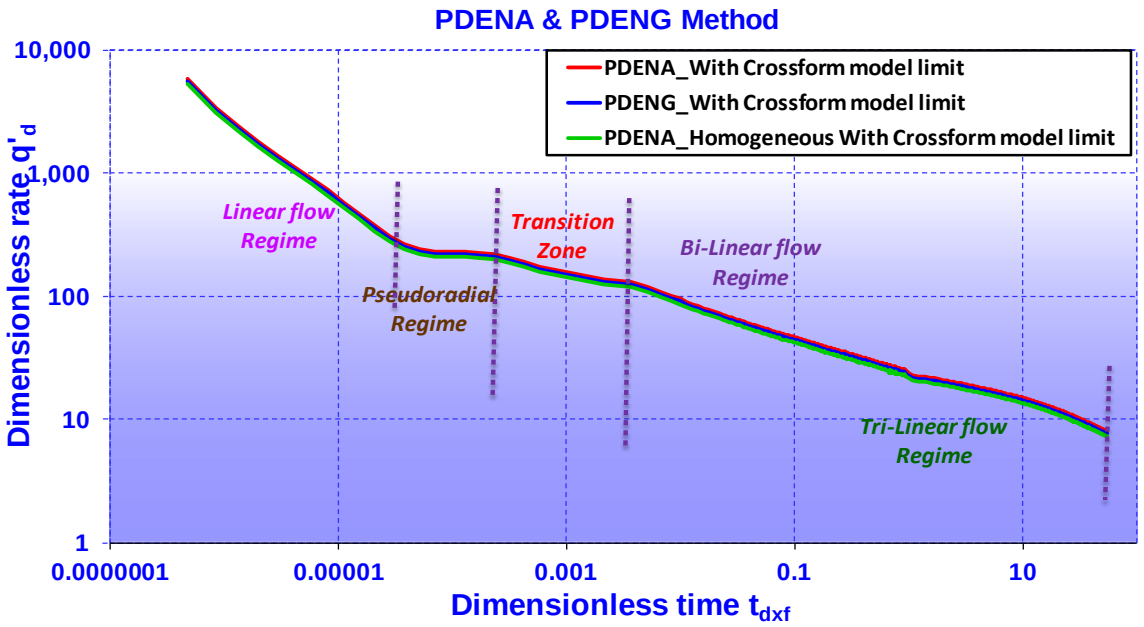

Figure 5.19; Crossform fracture model→derivative dimensionless rate behaviour for constant pressure solution with model limitation constraints

Result from Figure 5.19 supports the five flow regions identified with the new developed fracture flow models. Without the limitation using equations (5.35a), (5.38a) and (5.43a), only three flowing regions Linear-Transition-Linear are identified as shown in Figure 5.20

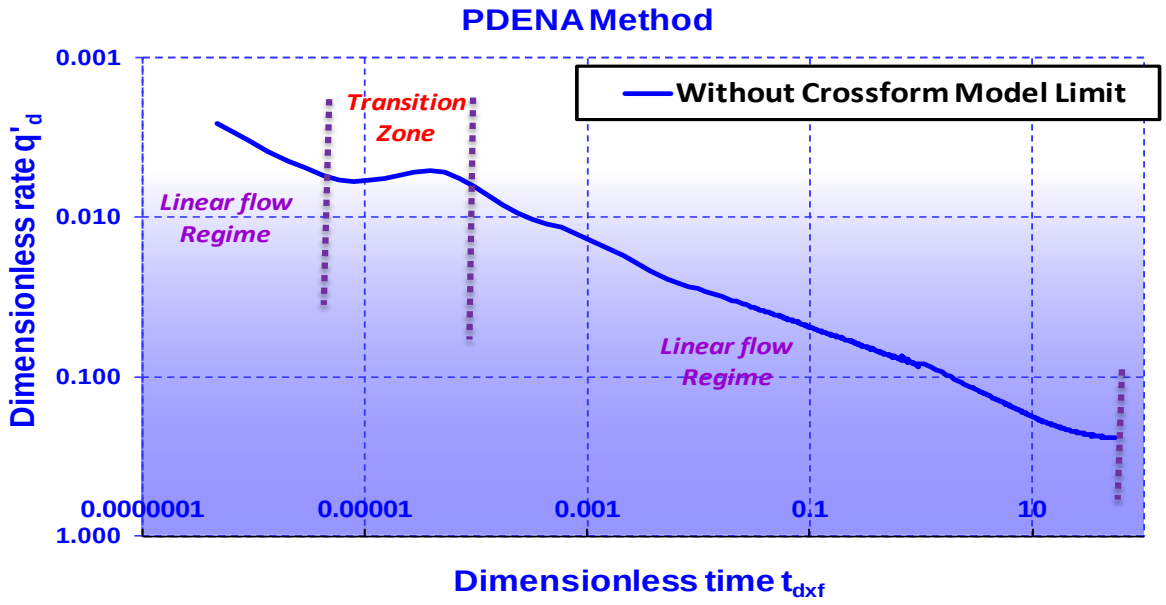

Figure 5.20; Crossform fracture model→derivative dimensionless rate behaviour for constant pressure solution without model limitation constraints

To test this approach changing the fracture conductivities, F_{CD} ranges from 1.0 to 1000 mD are simulated with possibly four flowing regions, Linear-Bilinear-Transition-Linear identifiable.

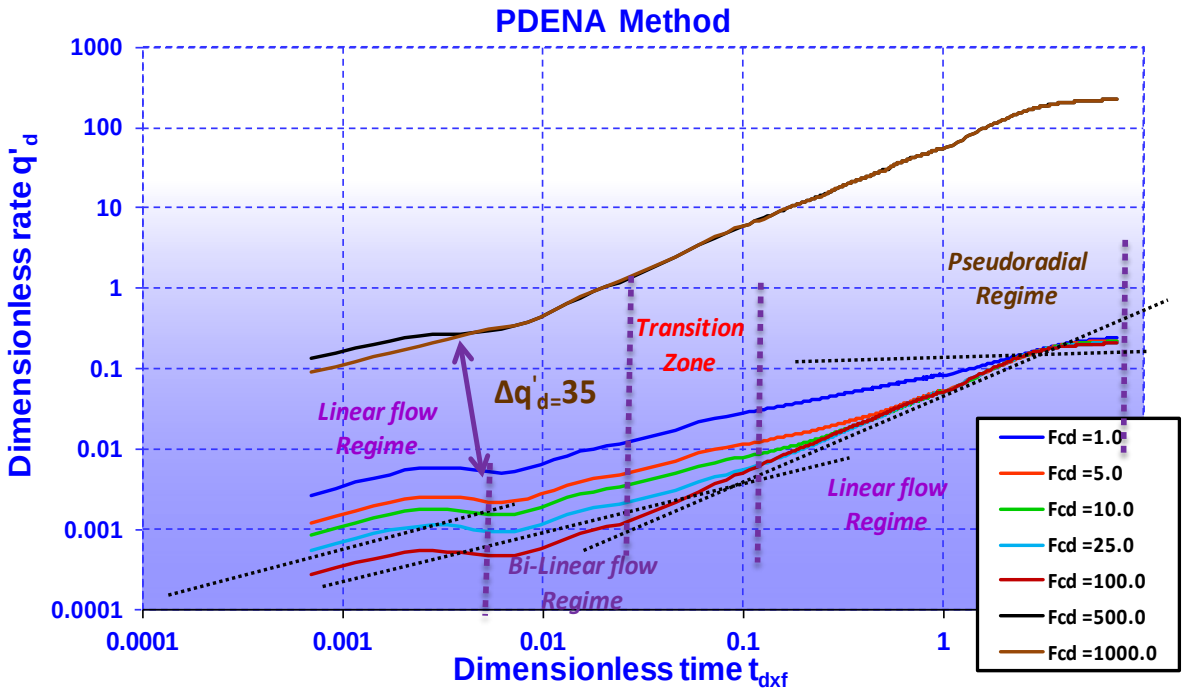

Figure 5.21; Crossform fracture model derivative dimensionless rate type curve for range of F_{CD} for constant pressure solution

Result in Figure 5.21 shows the numerical simulation of seven dimensionless fractures conductivities for dimensionless pressure and dimensionless time depicting the lower the fracture conductivities, the lower the number flowing regions that can be identified. This is consistent with the study by Cinco-Ley et al[18] which established that a relationship between pressure behaviour depends on the dimensionless fracture conductivity, $F_{CD.}$

5.5.3.2 Constant Pressure Sensitivity Analysis

5.5.3.2.1 Gas Production Rate

In the gas production rate sensitivities result shown in Figure 5.22, the log-log plot of gas rate versus time depicts three flow regions: Linear-Bilinear-Linear at $F_{CD} < 5$ and two flow regions: Linear-Linear at $F_{CD} > 25$.

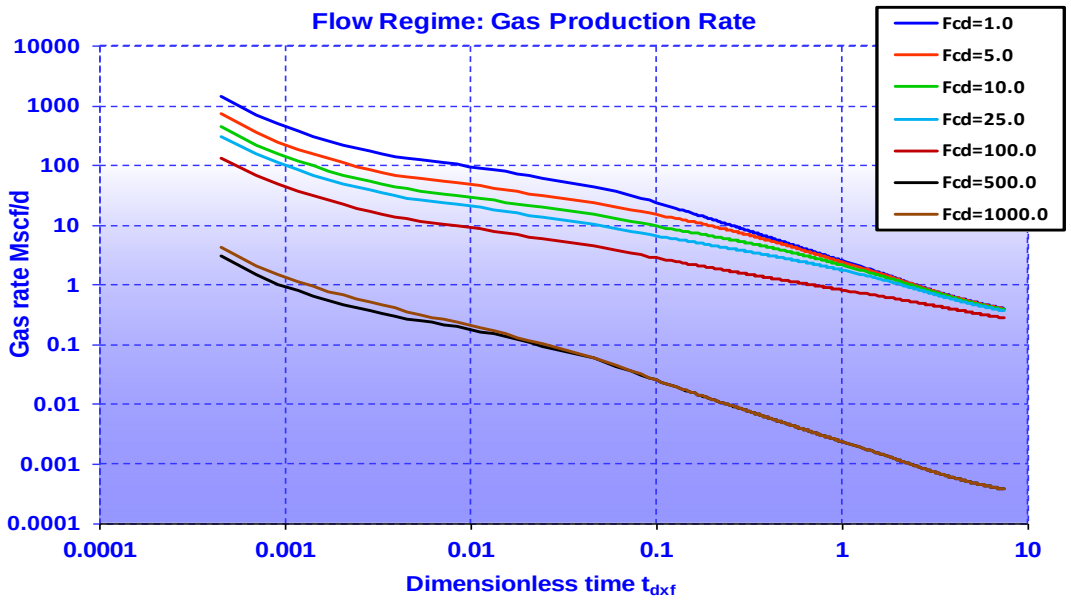

Figure.5.22; Crossform fracture model→Gas production rate type curve for range of F_{CD} for constant pressure solution

5.5.3.2.2 Fracture Aperture

The fracture aperture is increased from the equivalent fracture width w_e = 2ft to 16ft (incremental of 2ft). At w_e > 2ft, three flow regions: Linear-Transition-Linear are depicted as the sensitivities on production with constant bottom hole pressure as shown in Figure 5.23. It was discovered that for constant pressure solution, the smaller the fracture aperture, the lower the number of fracture regions to be seen.

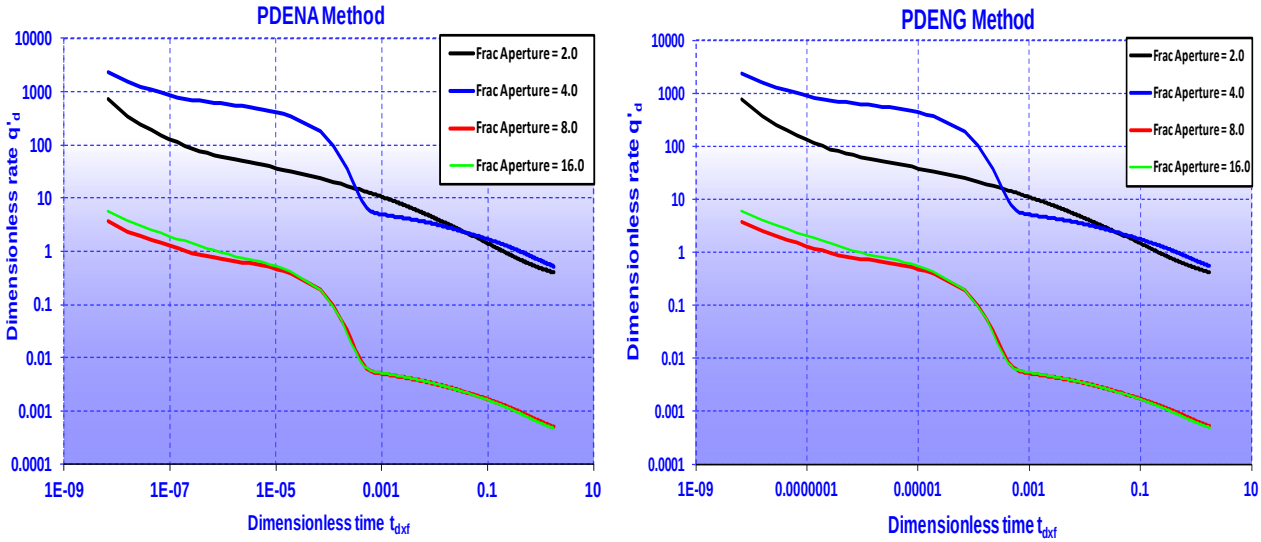

Figure 5.23; Constant pressure solution for Crossform fracture model→derivative dimensionless rate curves for range of fracture Aperture

5.5.3.2.3 Sensitivity on Distance from bottom perforated depth to WOC

If the distance of perforation ranges from 20 - 80 ft to the top of GWC, three flow regions: Linear- Transition-Linear are depicted in Figures 5.24 and 5.25 which is similar to the case of fracture aperture > 2ft. This fingerprint is also seen in all the densities derivative output: PDENG and PDENA.

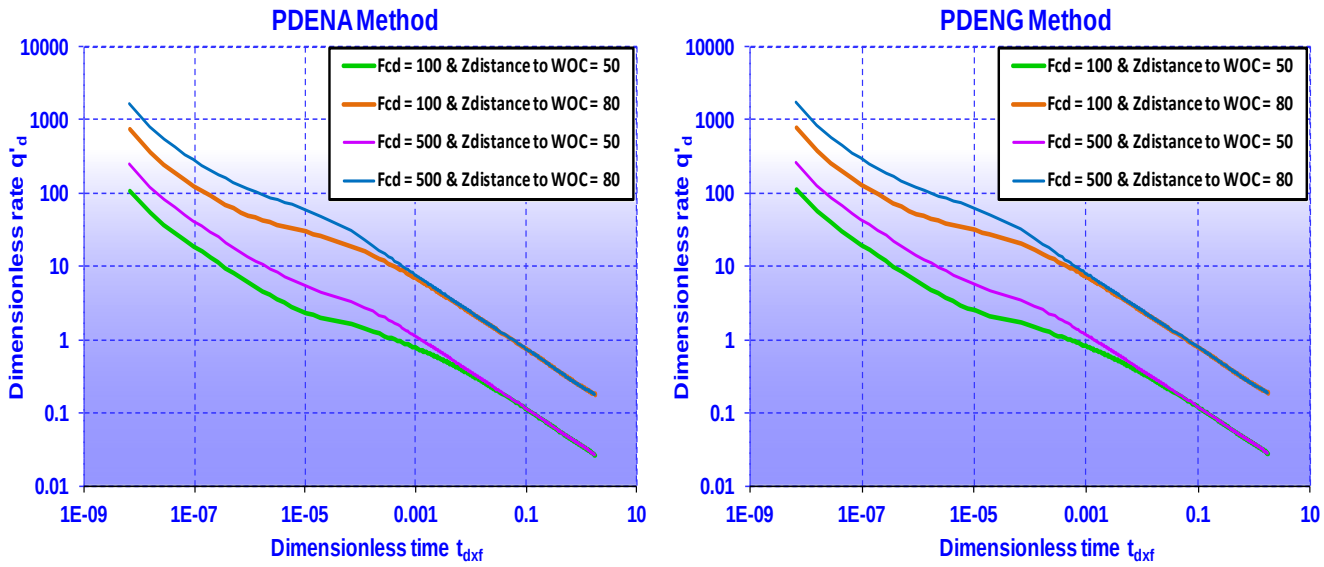

Figure 5.24; Constant pressure solution for Crossform fracture model→derivative dimensionless rate curves for range of Distance from bottom perforated depth to WOC

5.5.3.2.4 Skin Effect

The effect of change in skin is investigated assuming F_{CD} =100 to observe the effect on number flow regions that can be identified. From Figure 5.26, the dimensionless derivative signature indicates that, there is no skin effect on the derivative fingerprint for skin value ranging from 0 to 13.0. Also four flow regions: Linear-Transition-Bilinear-Linear are identifiable. This is similar to the number regions for $\mathbf{F_{CD} < 100}$ as seen in Figure 5.21. it is important to note that the developed type curves for different skin are not sensitive to the number of flowing regions.

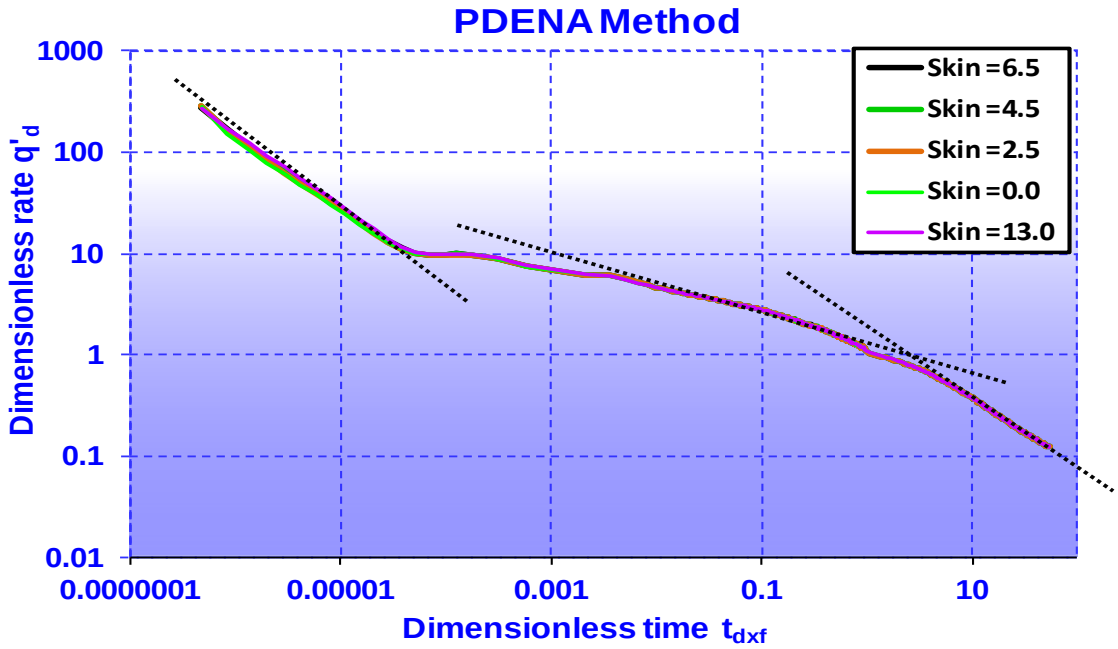

Figure 5.26; Constant pressure solution for Crossform fracture model→derivative dimensionless rate curves for range of skin

5.5.3.3 Constant Flow Rate Case

For constant flowing rate condition, the fracture conductivity, F_{CD} for each dimensionless pressure and time in Bennett type curves is dependent on the fracture porosity. The fracture porosity is calculated from equation 5.51 and also the real fracture porosity adjusted to 35% and its equivalent is calculated due to the change of the fracture width. Table 5.4 below shows the calculated data.

For calculating fracture permeabilities, input data that have been used are listed below:

Table 5.4: Data for calculated real and equivalent fracture permeabilities

Parameters	Symbol	Data for real fracture permeability	Data for equivalent fracture permeability Calculation	Units
Formation permeability	k	0.1	0.1	md
Fracture half length	w_f	2043	2043	ft
Fracture width	w_f	0.5	2	"

As stated earlier, the equivalent fracture width must be higher than the well bore radius, so it is necessary to adjust the fracture width to 2 ft because the dimension of the grid block with

well is 2ft. The calculated real and equivalent fracture permeability using equations (5.52) and (5.53) are given in Table 5.5.

Table 5.5: Calculated real and equivalent fractures permeability

Dimensionless Fracture Conductivity	Real Fracture Conductivity	Equivalent Fracture Permeability
F_{CD}	k_f (md)	k_{fe}(md)
1	409	102
5	2043	511
10	4086	1022
25	10215	2554
100	40860	10215
500	204300	51075
1000	408600	102150
10000	409	102

Seven numerical model data files are created for each fracture dimensionless conductivities, F_{CD} listed in Table 5.5 with only difference in equivalent fracture permeability (keyword: EQUALS) which is the function of the F_{CD}. See Appendix C for data sets.

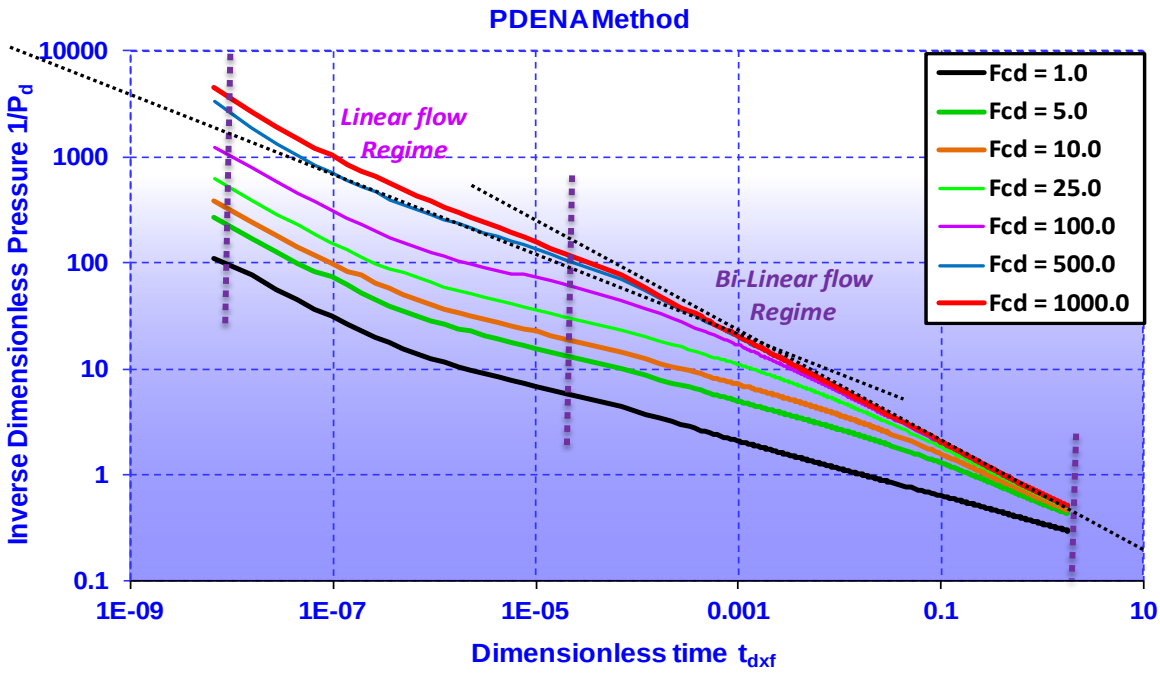

Figure 5.27; Crossform fracture model→inverse derivative dimensionless pressure type curve for range of F_{CD} for constant rate solution

First, the density change for each phase at the wellbore is obtained, then the fluid density equivalent pressures are calculated at bottom hole flowing conditions. Furthermore, the inverse derivative dimensionless pressure is calculated from the Pressure Equivalent of Density Weighted Average (PDENDWA→PDENA) as discussed and applicable in Chapter 4.

In this case, two fracture flowing regions seen in Figure 5.27 are identified as linear-bilinear. Region 1 which is linear is due to transient flow only in the fractures while Region 4 is bilinear flow and occurs when the matrix drainage begins simultaneously with the transient flow in the fractures

5.5.3.4 Constant Rate Sensitivity Analysis

5.5.3.4.1 Fracture Aperture

Fracture aperture is increased from the equivalent fracture width w_e = 2 – 16ft (incremental of 2ft). Figure 5.28 shows that for constant rate solution, the smaller the fracture aperture, the lower the number of fracture regions to be seen. At w_e > 2ft, three flow regions: Linear-Bilinear-Linear are depicted which differ slightly with the constant pressure solution.

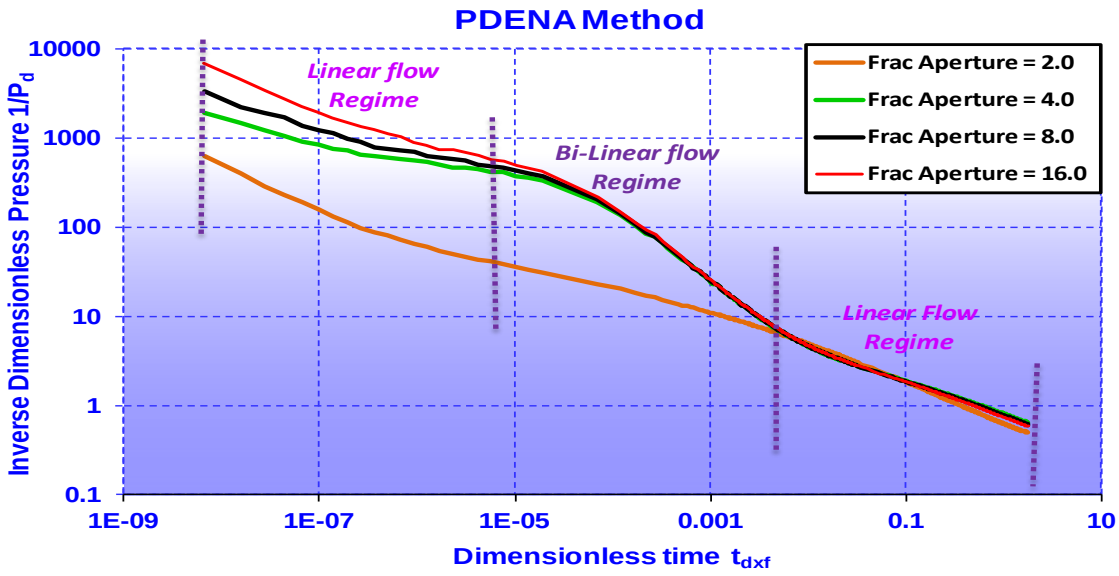

Figure 5.28; Constant rate solution for Crossform fracture model→inverse derivative dimensionless pressure curve for range of fracture aperture.

5.5.3.4.2 *Sensitivity on F_{CD} and Length to Distance LDR*

If the ratio of the fracture length to x distance of the reservoir range from 1.5 - 4.0 and F_{CD} = 25 and 500, three flow regions: Linear-Bilinear-Linear are identifiable are seen in Figure 5.29 which is similar to the case of fracture aperture > 2ft. This fingerprint is also seen in the densities derivative output PDENG and PDENA. At high $F_{CD,}$ the developed type curves for different F_{CD} are sensitive to the ratio of the fracture length to x distance of the reservoir. At higher F_{CD}, major impact is seen on the dimensionless derivative curve with separation after 0.001 hrs in Figure 5.29.

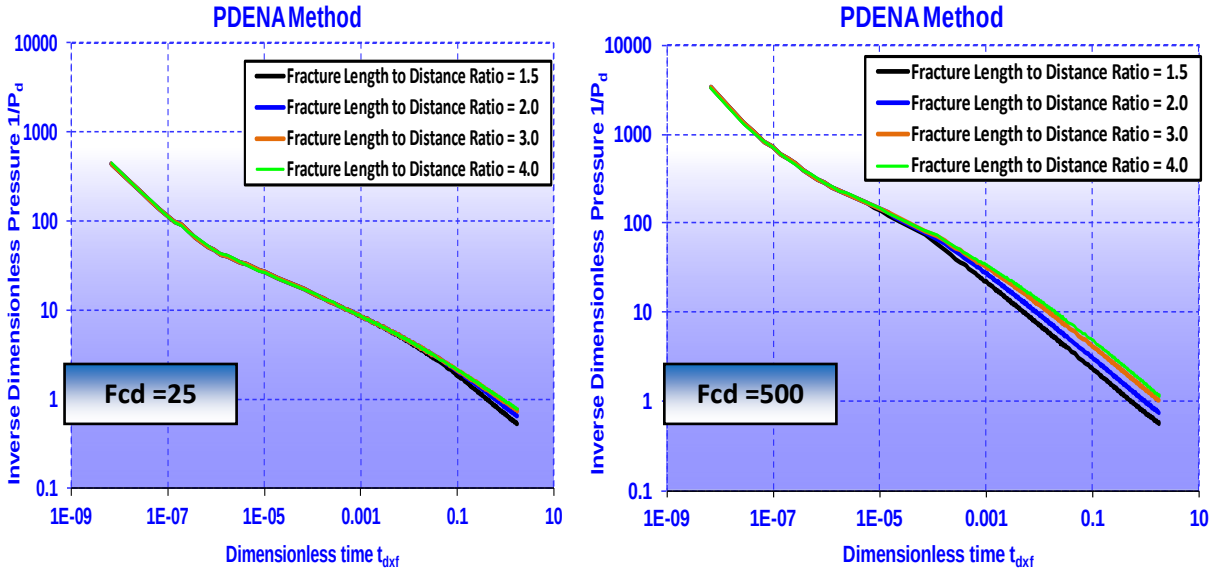

Figure 5.29; Constant rate solution for Crossform fracture model→inverse derivative dimensionless pressure curve for range of Fcd and Length to Distance LDR

5.5.3.5 *Summary of Result*

Numerical density transient analysis DTA using the pressure-density equivalent derivative is a robust approach that is applicable for identifying flowing regions in unconventional reservoir with fractured systems. The Pressure–density equivalent derivative can visualise the reservoir response, which in return provide clarity for possible flowing regions. Testing the numerical density derivative in unconventional reservoir with crossform fractures, several flowing regions including Linear-Bilinear-Trilinear regimes are identifiable considering the

limit of the fracture model developed. This observation is in accordance with the study by Cinco-Ley et al. [18] which established that a relationship between pressure behaviour depends on the dimensionless fracture conductivity, $F_{CD.}$ This demonstrated that DTA is suitable for low permeability reservoirs. Also, the results demonstrated that pressure responses and distinctive flow regions are influenced mostly by fracture's dimensions and reservoir's boundaries.

Chapter Six

Oil Field Data Review - Conventional Oil Reservoir

6.1 Example 1.0: Data Input

Table 6.1 presents a summary of the well and reservoir data of Field X in Offshore Niger Delta Nigeria used for the build-up well test interpretation with additional information given in Figure 6.1. It was required to generate the pressure-density equivalent and its derivative for each phase, compare their diagnostic signatures, then determine the phases permeability and average reservoir permeability.

Table 6.1: Reservoir and fluid data for example 1.0

Parameters	Design Value
Flowrate bopd	54
Oil formation volume factor B_o rb/stb	1.08
Oil viscosity μ_o cP	0.51
Thickness ft	30
Porosity %	30
Well diameter ft	0.45
water saturation Swi %	30
Total compressibility C_t	2.30E-04
Oil compressibility C_o	3.30E-04
Water compressibility C_w	1.00E-06
Initial Pressure, Pi, psia	3008.7
Formation Temperature, T, ^oF	200
Shut in Duration hrs	18

Field X located in the Niger delta

Well drilled and tested in 1989

Completed in a reservoir A.

- Good quality sand reservoir

Data available for the 1st DST conducted

- Oil API = 18.2 (slight heavy)
- Formation GOR = 299 rb/scf
- Average oil rate = 54 stb/d
- Reservoir initially under saturated with P = 3008psia
- Core k = 400 - 4500 mD (dependent on genetic unit description

Figure 6.1: Additional reservoir and fluid data for example 1.0

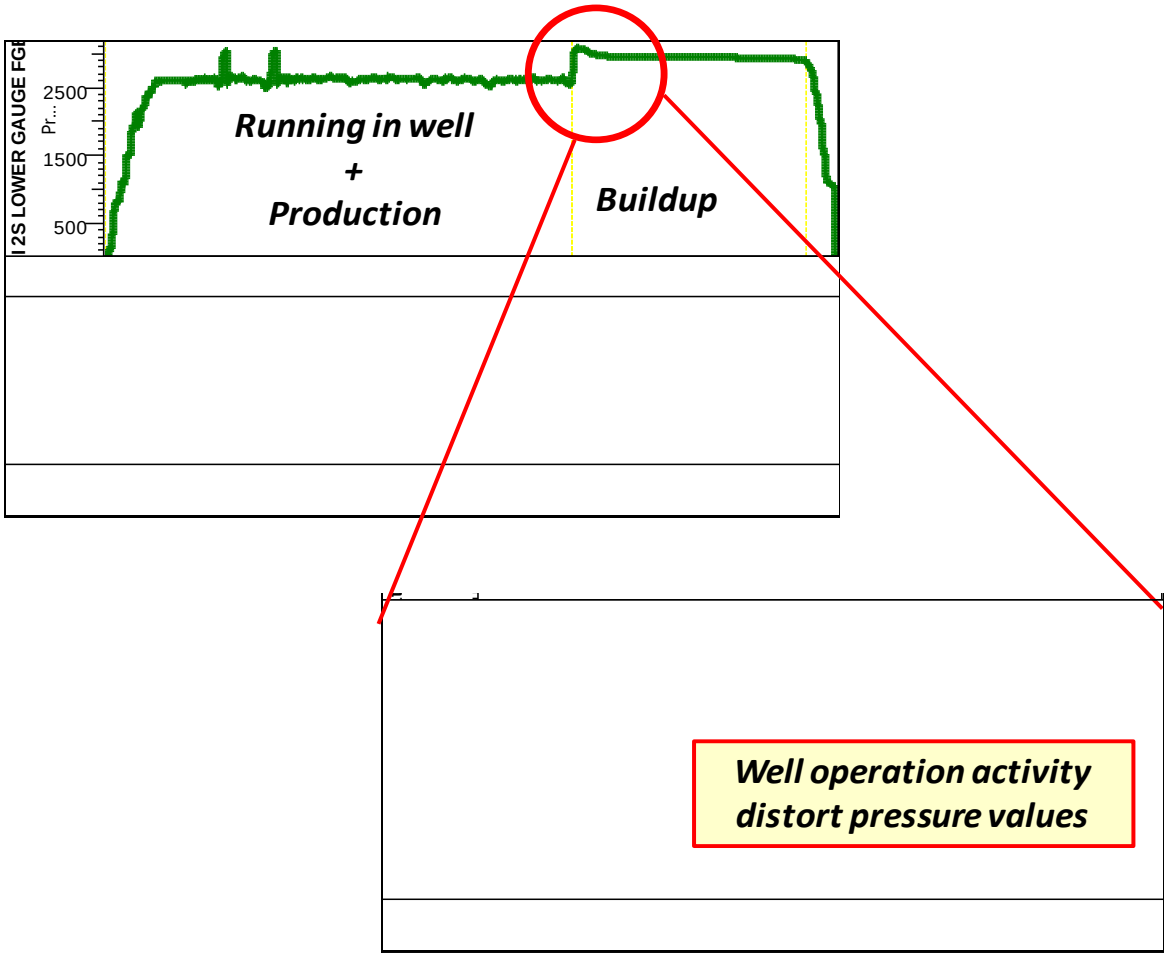

Figure 6.2: Production and shut-in data for example 1.0 showing pressure distortion due to well operational activity

6.1.1 Data Screening and Derivative Calculation

Figure 6.2 shows the production and shut-in rate and pressure with distortion in pressure after 2.0hrs of build-up due to surface operational activities. The derivative for more than 85000 pressure data points as seen in Figure 6.3 is plotted without smoothing in order to capture the real data behaviour. The interpretation from the existing report indicates 100 points per log circle was selected for the analysis. However, from the pressure derivative plot, it is difficult to identify the radial stabilisation as seen in Figure 6.4 since the derivative points are negative at the radial flowing period. The best option is to overlay the statistical and convention 'pressure' derivative using superposition time.

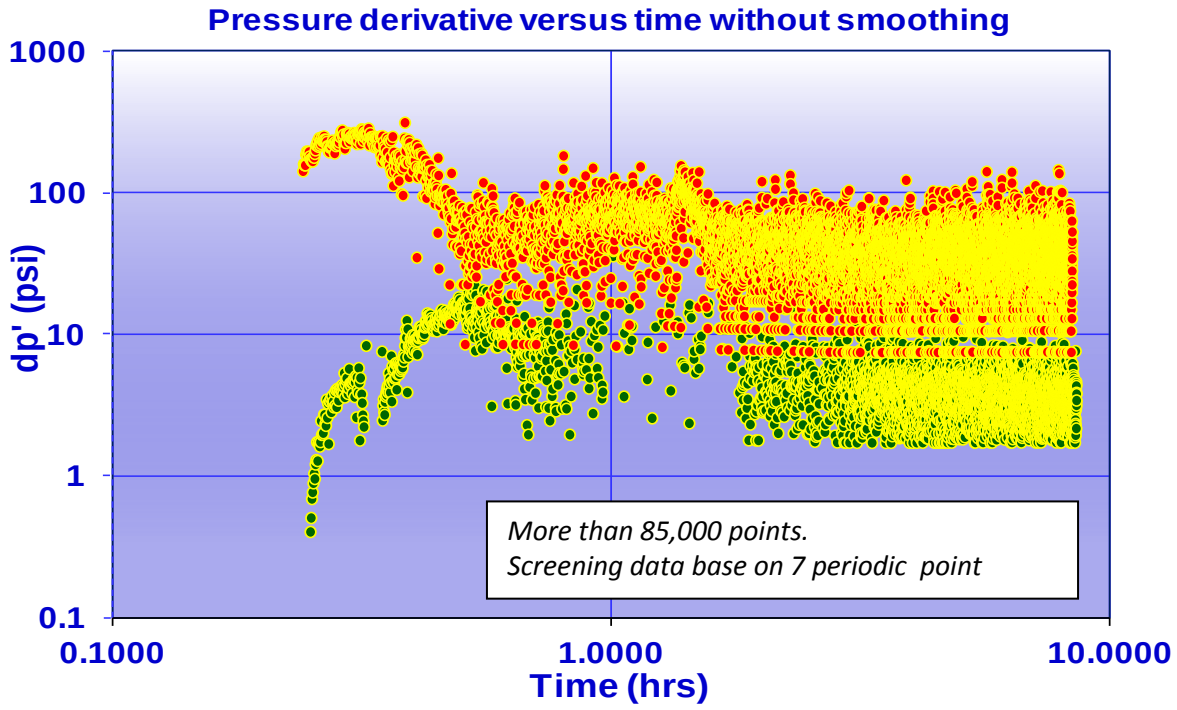

Figure 6.3: Pressure derivative versus time without smoothing with more than 85000 original data point. Difficult to visualise radial stabilisation and late time response.

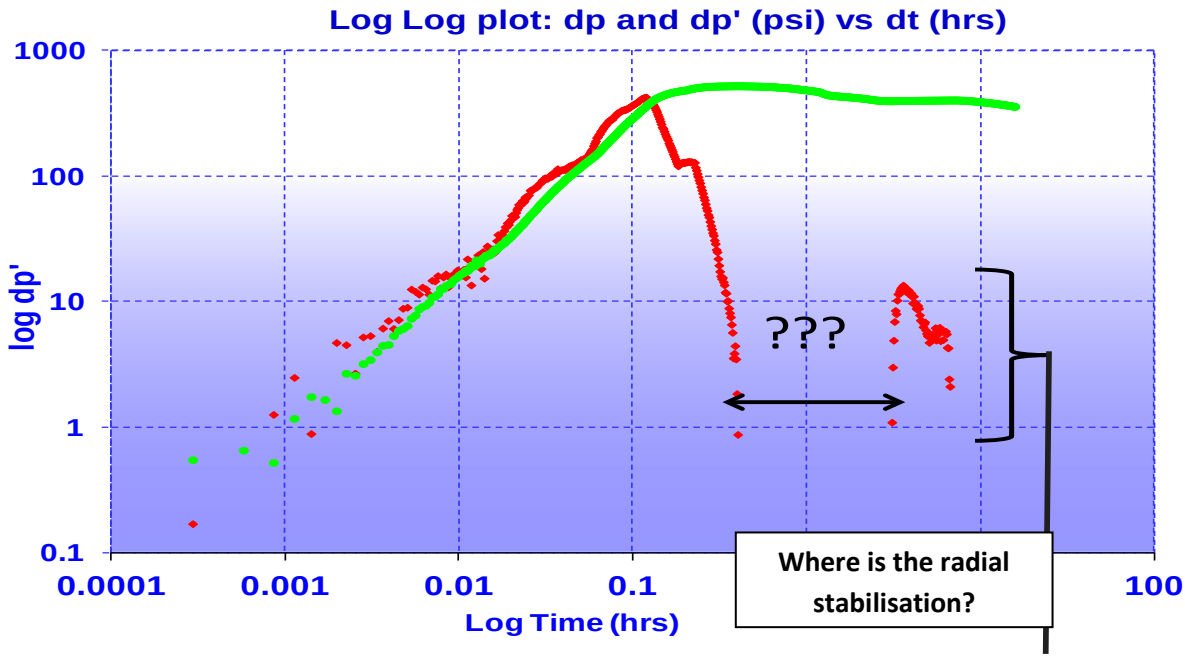

Figure 6.4: Pressure derivative versus time using 100 data points per log circle with smoothing factor. Missing pressure derivative points seen at radial stabilisation

6.1.2 Method Comparison and Permeability K Calculation

As shown in Figure 6.5, 100 pressure points per log circle are applied to the conventional and statistical 'pressure' derivative with and without superposition time. An exponential smoothing method with $\alpha = 0.04$ is used to smooth all three cases. The derivative without superposition time differs from that using the superposition time. The derivative based on superposition time represents the actual derivative interpretation from existing report with missing data at the radial stabilisation, so it is difficult to choose the radial stabilization and impossible to estimate the permeability. However, the derivative without superposition time completely differs and depicts decreasing mobility after a short unstable radial stabilisation. This feature cannot be geologically justified, therefore unreliable since there are no NFB close to the well.

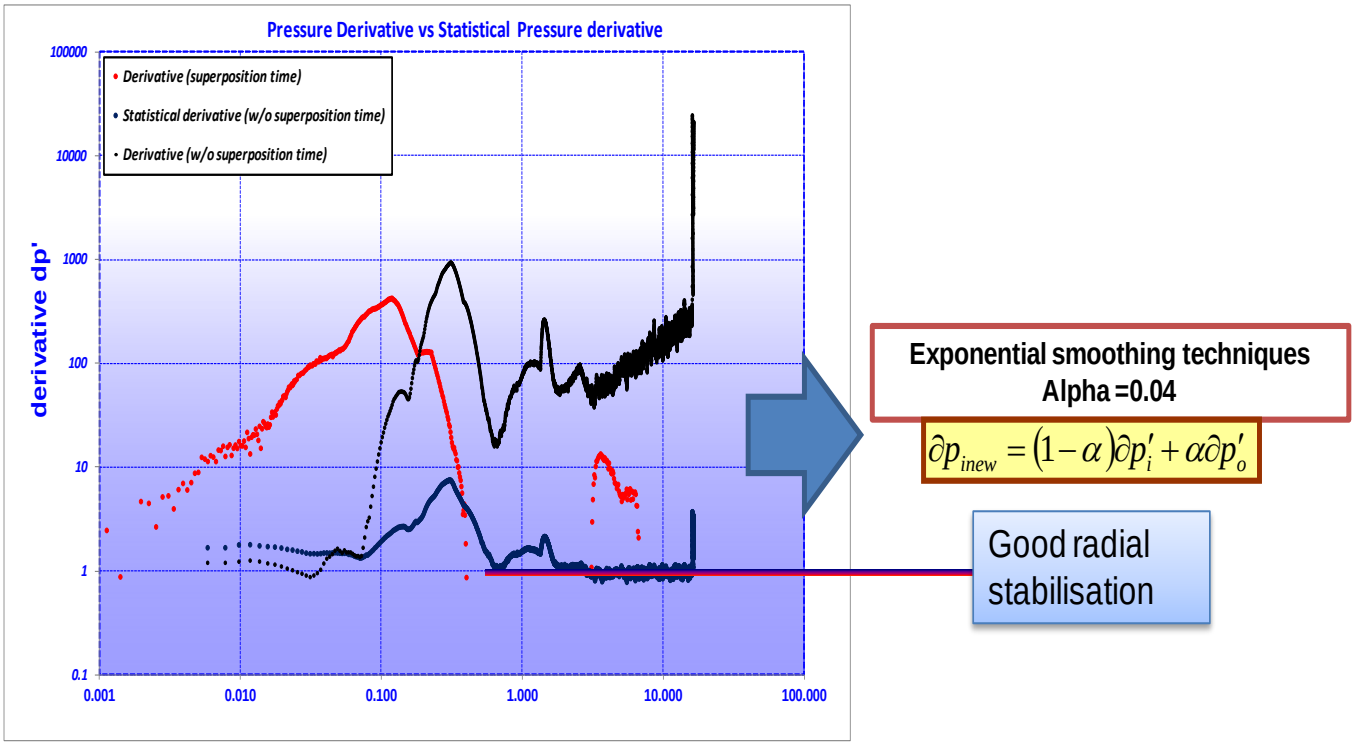

Figure 6.5: Comparison of Conventional & Statistical Derivatives with/without superposition time

The statistical 'pressure' derivative depict a clear radial stabilization fingerprint which is continuous and without noise. The k_{ave} estimated from equation $k = \frac{141.2qB\mu}{mh}$ is between

400-500 mD depending on the movement of the derivative flat line. This is within the range of uniform k from core sample collected in this level indicating a good estimation of permeability is justifiable at this point.

6.1.3 Numerical density approach (k Estimation)

The input data is used to generate numerical density derivatives for all three phase produced by the well (gas, oil and water) and compared with the conventional method as shown in Figures 6.6 and 6.7.

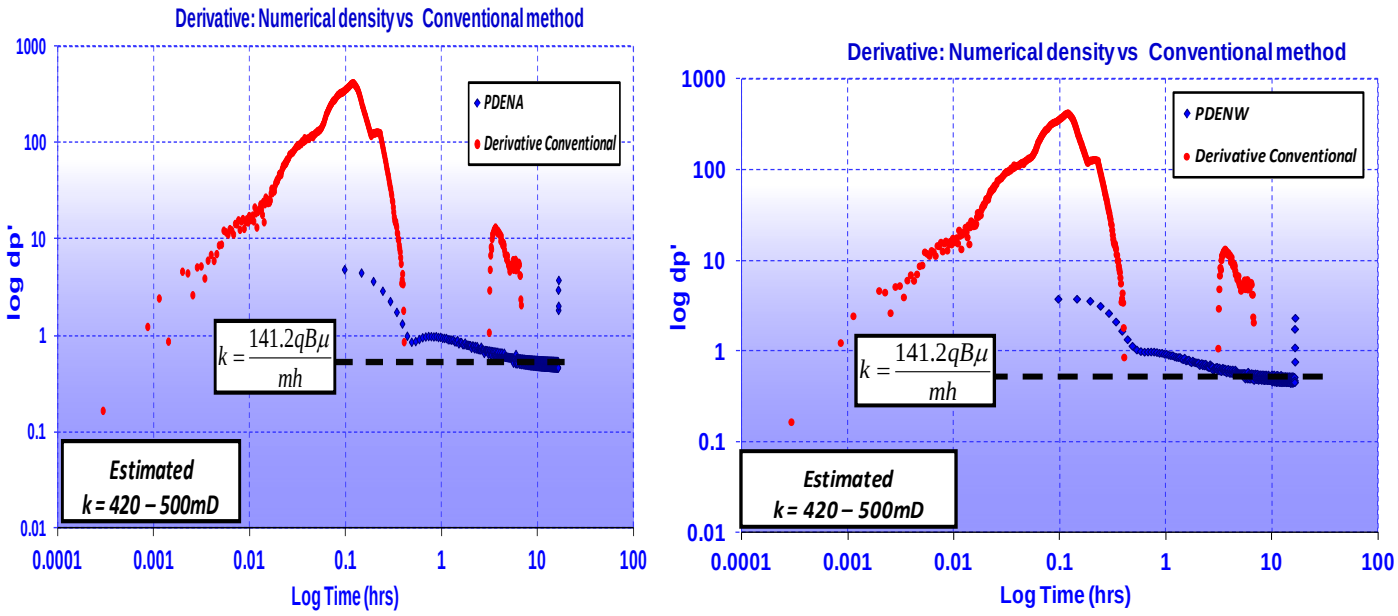

Figure 6.6: Comparison of Conventional & Numerical density Derivatives versus time

The derivative shows a good radial flow with no boundary response. Although the wellbore storage was not modelled because of little information on wellbore configuration. Also the k_{ave} estimated from equation $k = \frac{141.2qB\mu}{mh}$ for PDENW and PDENA is between 400-500 mD which is consistent with the statistical 'pressure' derivative result and uniform k from core data.

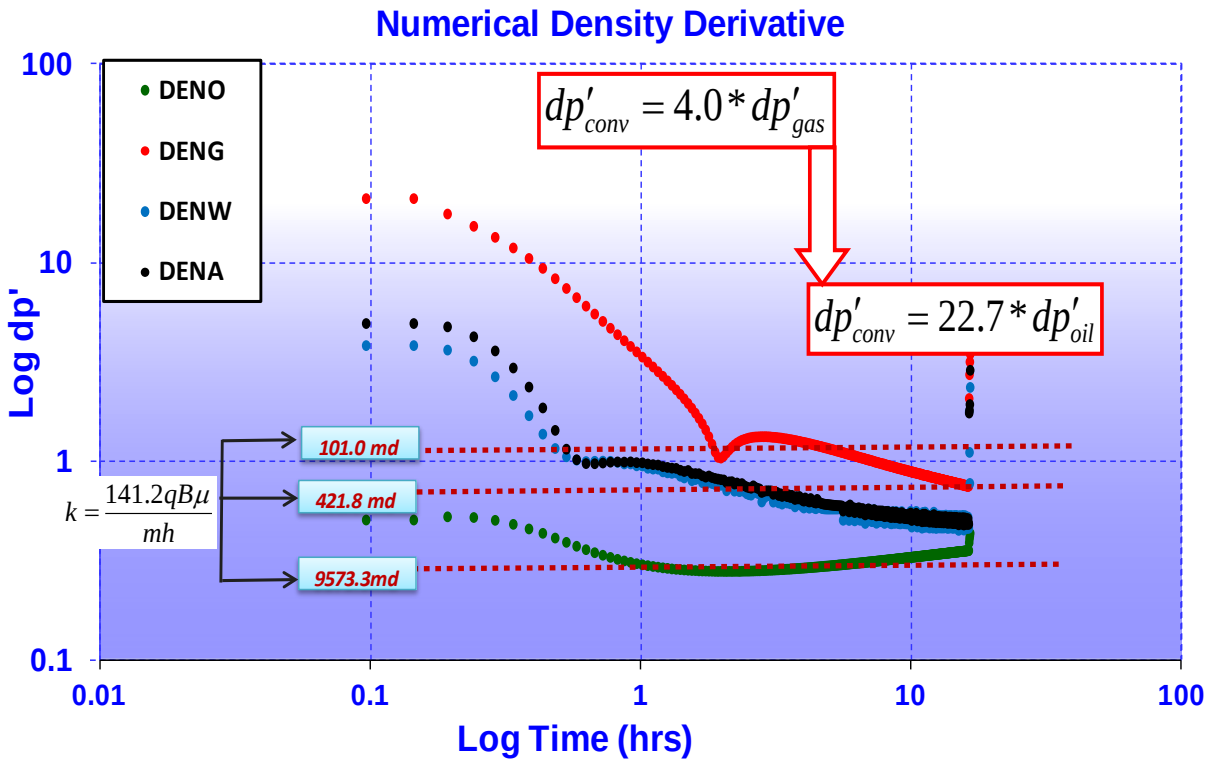

Figure 6.7: Derivative and K estimation for Numerical density Derivatives versus time

BPR gives a permeability value of 422 mD which is the same for PDENDWA and PDENWAT but differs from PDENGAS and PDENOIL that gives 101 and 9573 mD respectively. At h =30 ft, 95% of mobile fluid is oil thickness, followed by 4% water at the reservoir sand face. The estimated k_{ave} for fluid phase permeabilities using the geometrical equation 4.46 is given as:

$$k_{ave} = \sqrt[4]{k_o k_w k^2_g} = 450mD$$

This is consistent with the statistical 'pressure' derivative result and uniform k from core data. The estimated phase permeabilities provide a better understanding of % fluid contribution to flow at sand face condition.

6.2 Example 2.0: Data Input

Table 6.2 presents a summary of the well and reservoir data of Field Y in Offshore Niger Delta Nigeria used for the build-up interpretation with additional well log information given in Figure 6.8. In this example, only the statistical and convention 'pressure' derivative method will be analysed and used to estimate average reservoir permeability.

Table 6.2: Reservoir and fluid data for example 2.0

Parameters	**Design Value**
Flowrate bopd	2800
Pressure psia	
Fluid	
Oil formation volume factor B_o rb/stb	1.82
Oil viscosity μ_o cP	0.253
Saturation pressure P_b psia	3164.2
Oil compressibility C_o 1/psi	3.16E-05
Water compressibility C_w 1/psi	5.00E-06
Total compressibility C_t 1/psi	2.70E-05
Reservoir	
Thickness ft	19
Porosity %	29
water saturation Swi %	20
Rock Compressibility C_r 1/psi	1.00E-06
Well diameter ft	0.354

Other information includes:

- Appraisal well, penetrated several reservoir levels, located in conventional offshore Niger Delta
- Structural maps indicate hydrocarbons in crestal part of the block with some possible potential in the eastern part
- Reservoir facies associations and their lateral correlation, high sand to shale ratio, suggest very good reservoir potential.
- Amalgamated channel fill or delta front facies associations constituting continuous coalescing sandstone bodies in a rather constant stacking pattern.

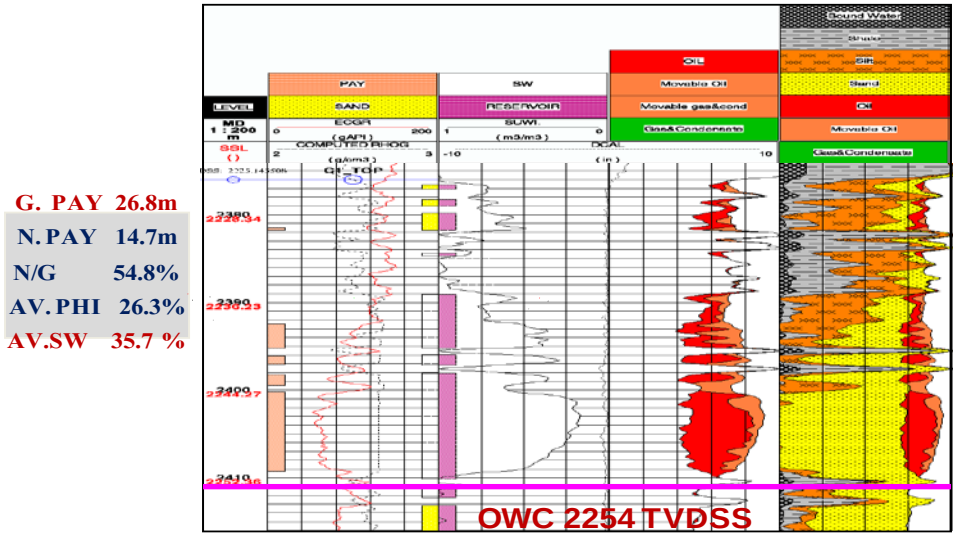

Figure 6.8: Well log and Petrophysical data for example 2.0

6.2.1 Data Screening and Derivative Calculation:

Figure 6.9 shows the flowing and shut-in pressure with distortion prior to the beginning of flow with the main section for interpretation unaffected. 600 pressure points per log circle are applied to the conventional and statistical 'pressure' derivative.

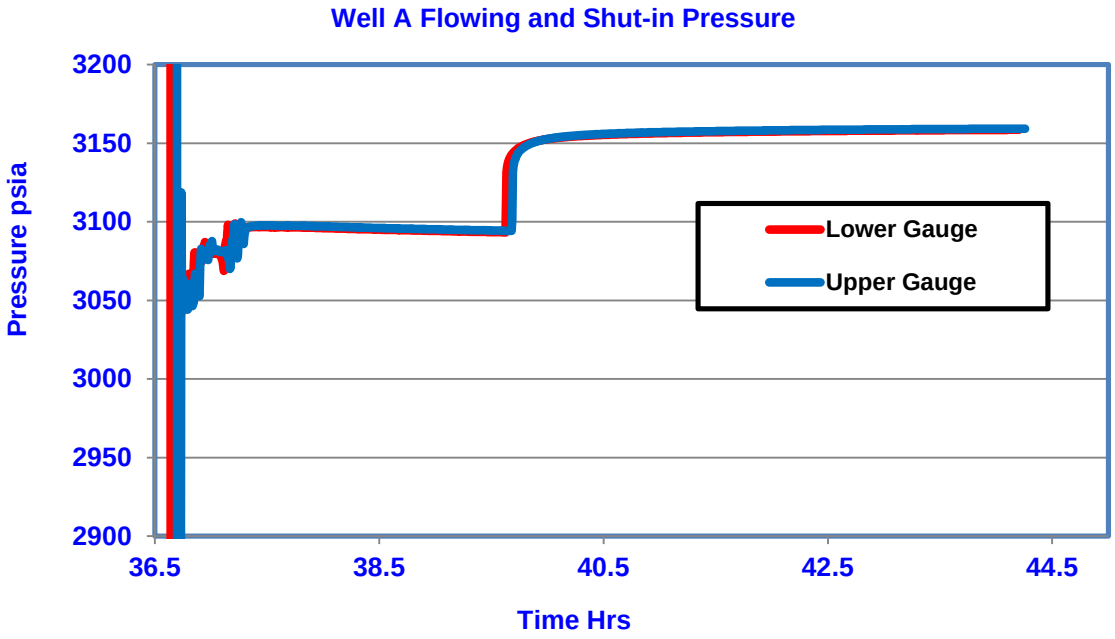

Figure 6.9: Production and Shut-in data for example 2.0

6.2.2 Method Comparison and Permeability K Calculation

An exponential smoothing method with $\alpha = 0.02$ was used to smooth all three cases. The statistical 'pressure' derivative shown in Figure 6.10 depicts a clear radial stabilization fingerprint without boundary effect. The response behaves like an infinite acting system which is continuous, without noise. Statdev depicts a continuous drop in derivative which could be increasing mobility features away from the well but there is little geological information on increasing thickness away from the well to justify this hypothesis.

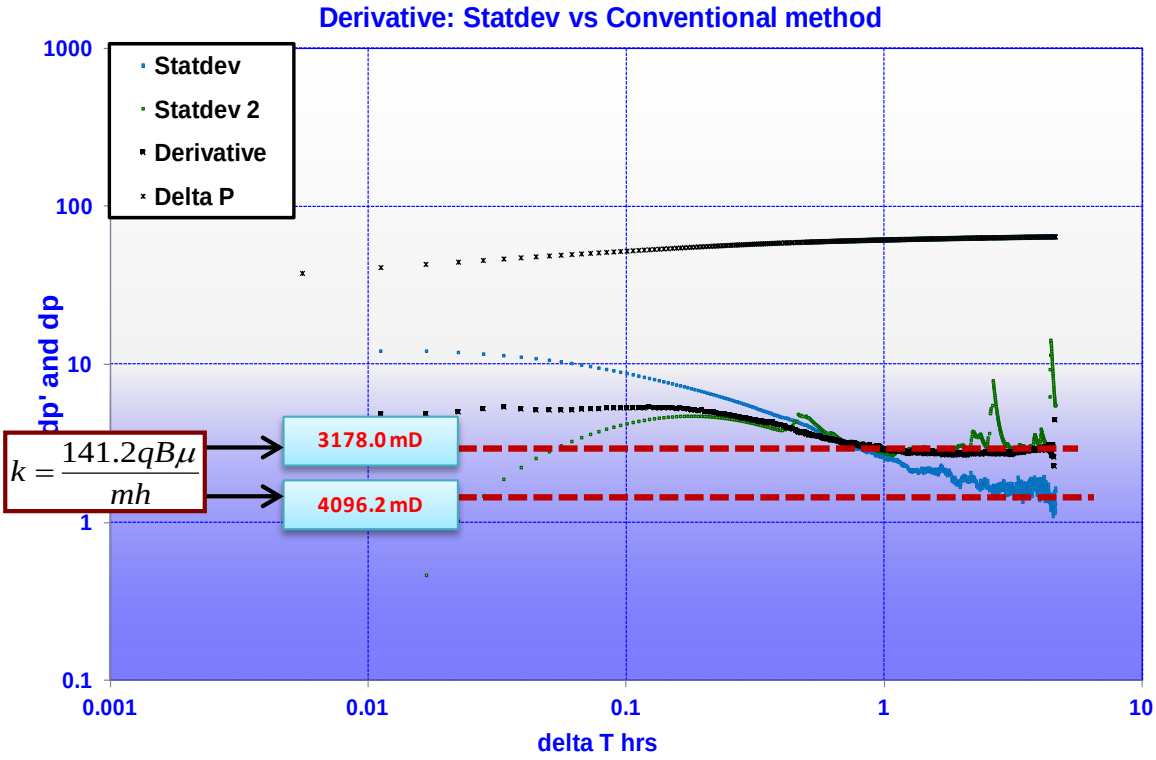

Figure 6.10: Comparison of Conventional & Statistical Derivatives versus time

The k_{ave} estimated from equation $k = \frac{141.2qB\mu}{mh}$ is between 3100 – 4100 mD depending on the movement of the derivative flat line. This is within the range of uniform k from core sample and existing well test interpretation for this reservoir; a good estimation of permeability is justifiable.

Generally, the field cases reviewed show the robustness of the statistical 'pressure' and numerical density derivatives applicable in pressure transient analysis. The results

demonstrated that clearer radial flow regimes can be visualised with increasing confidence on formation permeability estimation. Also, individual fluid phase permeability can be estimated in multiphase condition for better reservoir characterisation with improved understanding of the true contribution of each phase to flow at the sand face.

Chapter Seven

Conclusion and Further Work

7.1 Conclusion

This research introduces a new technique for analysing and interpreting reservoir pressure transient data as well as estimating reservoir properties. So far, two PTA diagnostic methods have been discussed and tested with synthetic and field data, these include:

1) Statistical 'pressure' derivative
2) Numerical density transient analysing DTA (numerical density derivative)

Five major research tasks were accomplished in the course of this research. These include developing:

1) A mathematical statistical derivative algorithm for PTA diagnostic and interpretation
2) A comprehensive workflow for easy application of the algorithms
3) Pressure-density equivalent PDE algorithm for generating its derivatives and easy application in PTA software.
4) Mathematical radial density diffusivity equation and analytical DTA solutions for PTA interpretation
5) Test the methods with synthetic data in conventional reservoirs (oil and gas-condensate), unconventional reservoirs (shale gas and cross form fractures) and field data.

We have described in detail how the models were developed and their application.

For constant pressure, constant rate and well with high water production conditions tested with synthetic data, the statistical 'pressure' derivative has demonstrated that the drawdown fingerprint can be replicated in the build-up pressure responses, hence a good match of the data. In addition, for high water production well, radial stabilization can be identified for permeability estimation without smoothing the data.

Numerical density transient analysis DTA solution is a robust approach for interpreting multiphase flow condition which is presently limited to only numerical well testing approach. The pressure–density equivalent and numerical density derivatives can derive individual phase permeability along with good visualisation of each phase derivative response which gives the true picture of the reservoir response. This ensures that the derived permeability is right from the formation radial flow. With synthetic and field data, the numerical density derivatives yield a clearer reservoir radial flow regime in comparison with the conventional pressure derivatives; therefore estimates formation permeability with higher level of confidence. In one of the field data tested, radial flow was unidentifiable with conventional pressure derivative diagnostic method, hence unable to estimate the reservoir permeability. In contrast, the fluid phase numerical density and pressure-density equivalent derivatives gave very clear radial flow stabilizations on the diagnostic plot, from which the reservoir permeability which is consistent with the scaled core permeability was estimated. In all synthetic cases investigated, the heavier fluid such as water and the weighted average pressure-density equivalent derivatives yield better k values which are often the same with conventional derivative results or within acceptable range of available core samples for field cases. Additionally, there was better estimation of individual fluid phase permeability, reflecting the contribution of each phase to flow at a given point, therefore the formation effective and phase permeabilities can be derived with confidence.

Testing the numerical density derivative in unconventional reservoir with crossform fractures, several flowing regions including Linear-Bilinear-Trilinear regimes were identified considering the limit of the fracture model developed. This is also consistent with the study by Cinco-Lee et al [18] which established that a relationship between pressure behaviour depends on the dimensionless fracture conductivity, F_{CD}, demonstrating the robustness of DTA in low permeability reservoirs.

7.2 Further Work

An empirical model integrating the fluid phase's permeabilities for a given system was formulated to determine the average reservoir permeability. This mathematical model can be redeveloped from the diffusivity equation integrating all fluid phase and compared with the empirical model which gives accurate result as the conventional BPR method.

A field density data obtained from bottom hole density gauges would be needed to further validate the simulation results on the synthetic data. This will trigger more discussion and provide a new approach on fluid phase permeability estimation and transient data interpretation in multiphase reservoir conditions.

References

[1] Aanonsen, S.I. (1985-a),” Nonlinear Effects During Transient Fluid Flowin Reservoirs as Encountered in Well Test Analysis”, Dissertation - Dr. Scient., Univ. of Bergen, Norway.

[2] Agarwal, R.G., AL-Hussainy, R., and Ramey, H.J.JR (1970). “An investigation of wellbore and skin effect in unsteady liquid flow I". Analytical; treatment. SPE J., Sept 279-290

[3] Agarwal, R.G., Carter, R.D., and Pollock, C.B.: “Evaluation and Performance Prediction of Low-Permeability Gas Wells Stimulated by Massive Hydraulic Fracturing,” J. Pet. Tech. (Mar. 1979), 362-372.

[4] AI-Khalifah, A.A., (1988) “Determination of absolute and relative permeability Using well test analysis”, PhD thesis, Stanford University, California, US

[5] Al-Khalifah, A.A. (1985), “Two Phase Pulse Testing”, Master thesis, Univ. of Petroleum and Minerals, Dhahran, Saudi Arabia

[6] AI-Khalifah, A.A., Aziz, K. and Home, R.N. (1987), "New Approach to Multiphase Well Test Analysis," Paper SPE 16743 presented at the 62nd Annual Technical Conference and Exhibition, Dallas, Texas, Sept. 27-30

[7] Alpheus O, Tiab D (2008) Pressure transient analysis in partially penetrating infinite conductivity hydraulic fractures in naturally fractured reservoirs. SPE 116733 presented at the SPE annual technical conference and exhibition, Denver, 21–24 Sept. doi: 10.2118/116733-MS

[8] Ayan, C. and Lee, W.J. (1986), "The Effects of Multiphase Flow on the Interpretation of Buildup Tests," paper SPE 15537 presented at the 61st Annual Technical Conference and Exhibition held in New Orleans, LA October 5-8.

[9] Ayestaran, L.C., Nurmi, R.D., Shehab, G.A.K., and Elsi W.S., (1989). "Well Test Design and Interpretation Improved by Integrated Well Testing and Geological Efforts". SPE 17945.

[10] Bennett, C.O., Camacho, R.G., Reynolds, A.C., Raghavan, R., – Approximate Solutions for Fractured Wells Producing Layered Reservoirs - SPE Journal – October 1985, 729-742

[11] Bennett, C.O., Reynolds, A.C., Raghavan,R., Jacques, L.E., – Performance of Finite Conductivity, Vertically Fractured Wells in Single-Layer Reservoirs – SPE Formation Evaluation – August 1986, 399-412

[12] Biu..V T. and Zheng, S.Y,: “A New Approach In Pressure Transient Analysis Part I: Improved Diagnosis Of Flow Regimes In Oil And Gas Wells” Proceedings of Third EAGE/AAPG Workshop on Tight Reservoirs in the Middle East Abu Dhabi, October 4-6, 2015

[13] Biu V.T., Biu E.O., and, Onyekonwu M.O. (2009) “Statistical Diagnosis (VEMST) of Flow Regime; Alternative to Pressure Derivative Approach in Pressure Transient Analysis” Presented at the 33rd Annual SPE International, Technical Conference and Exhibition in Abuja, Nigeria, August 3-5, 2009.

[14] Bourdet, D. et al. (1983)." A new set of type curves simplifies well test analysis". World Oil, 196(6), 95-106.

[15] BΦe, A., Skjaeveland, S.M. and Whitson, C.S. (1981), "Two-Phase Pressure Transient Test Analysis," Paper SPE 10224 presented at the 56th Annual Fall Technical Conference and Exhibition, San Antonio, Texas, Oct. 5-7.

[16] Chu, W.C., Reynolds, A.C., Jr. and Raghavan, R (1986), "Pressure Transient Analysis of Two-Phase Flow Problems," SPE Formation Evaluation, April.

[17] Cinco-Ley H (1974) Unsteady-state pressure distribution created by a slanted well or a well with an inclined fracture. Ph.D. Dissertation, Stanford University, California

[18] Cinco-Ley, H., Samaniego, V.F., Dominguez, N.,– Transient Pressure Behavior for a Well With Finite-Conductivity Fracture – SPE Journal, August 1978, 253-264, Trans. AIME 265

[19] Cinco-Ley, H., Samaniego, V.F., – Transient Pressure Analysis for Fractured Wells – SPE paper 7490, Journal of Petroleum Technology, September 1981, 1749-1766

[20] Darcy, H. (1856), Les Fontaines Publiques de la Vie de Dijon, Dalmount, Paris (reprinted in
Hubbert, 1969).

[21] Dave Touretzky and Kornel Laskowsk (2006) Lecture Notes Neural Networks for Time Series Prediction 15-486/782:Artificial Neural Networks Fall 2006

[22] David, P.C, (2006),"Analytical modeling of a fracture-injection/falloff sequence and the development of a refracture candidate diagnostic test", PhD Thesis submitted to Graduate School, Texas A & N University

[23] Dinh AV, Tiab D (2009a) Transient pressure analysis of a well with an inclined hydraulic fracture using Tiab’s direct synthesis technique. SPE 120545 presented at SPE production and operation symposium held in Oklahoma City, 4–8 Apr. doi:10.2118/120545-MS

[24] Dinh AV, Tiab D (2009b) Transient pressure analysis of a well with an inclined hydraulic fracture using type curve matching. SPE 120540 presented at SPE production and operation symposium held in Oklahoma City, 4–8 Apr. doi:10.2118/120540-MS

[25] Du, K.F. and Stewart, G., (1994). "Reservoir Description from Well Test Interpretation". North Sea Oil and Gas Reservoir - III, pp. 339-356, Norwegian Institute of Technology (NTH).

[26] Earlougher, R.C., Jr. (1977), “Advances in Well Test Analysis”, Monograph Series, Society of Petroleum Engineers of AIME, Dallas, "X, 5.

[27] Ehlig-Economides, C.A.; Hegeman, P.; Vik, S. (1994) "Guidelines simplify well test interpretation". Oil and Gas Journal, Jul. 1994.

[28] Eric A. Plummer (July, 2000) A thesis submitted to the Department of Computer Science, and The Graduate School of The University of Wyoming in partial fulfillment of the requirements for the degree of Master of Science Computer Science.

[29] Evinger, H.H. and Muskat, M. (1942),"Calculation of Theoretical productivity Factor ,'I Trans.,AIME 146, 126-139

[30] Fetkovich, M.J.(1973), “The Isochronal Testing of Oil Wells," Paper SPE 4529 presented at the 48th Annual Fall Meeting, Las Vegas, Nevada, Sept. 30 - October 3,. (SPE Reprint
Series No. 14, 265.)

[31] Fetkovich, M.J. and Vienot, M.E. (1980) ,"Rate Normalization of Buildup Pressure by Using Afterflow Data," J. Pet. Tech. Oct, 1813-1824.

[32] Freddy, H.E., Universidad Surcolombiana, Juan Miguel Navarrete, Hydrocarbon services Ltd., Hernan Dario Losada, Hydrocarbon Services Ltd., (2004). “Evaluation of Pressure Derivative Algorithms for Well-Test Analysis”, SPE 86936.

[33] Gringarten A.C, Bourdet D.P, Landel, P.A, and Kniazeff V.J, (1979)." A comparison between different skin and wellbore storage typecurve for early time transient analysis", SPE paper 8205, 54th Annual fall meeting Las Vegas Texas.

[34] Gringarten A.C., and Ramey H. J. (1974) “Unsteady-State Pressure Distributions Created By A Well With A Single Horizontal Fracture, Partial Penetration, Or Restricted Entry”, Society Of Petroleum Engineers Journal, Vol:14, Issn:0197-7520, Pages:413-426

[35] Gringarten A, and Ramey H. J, 1973, Use Of Source And Greens Functions In Solving Unsteady Flow Problems In Reservoirs, Society Of Petroleum Engineers

[36] Gringarten, A.C., Ramey, H.J. Jr. and Raghavan, R (1974): ‘Unsteady-State Pressure Distributions Created by a.Well With a Single Infinite-Conductivity Vertical Fracture,” SPEJ 347-360.

[37] Horne, R.N. (1995). Modern welltest analysis. Petroway Inc, Palo Alto, California.

[38] Horne, R.N. and Temeng, K.O., (1981). "The Recognition and location of Pinch - Out Boundaries by Pressure Transient Analysis". SPE 9905.

[39] Horner. D. R., (1951)." Pressure build-ups in wells". PROC.Third world Pet-congs E.L. Brill. Leiden II.503-521. Also reprint series, No 9 Pressure analysis methods, SPE of AIME. Dallas (1967) 25-43.

[40] Islam, R.M (2014), "Unconventional Gas Reservoirs: Evaluation, Appraisal, and Development" book published by Gulf professional Publishing, Elsevier. Pp 519-524

[41] Jackson, R.R., SPE, and Banerjee.R., SPE, Schlumberger, (2000). "Advances in multiplayer reservoir testing and analysis using numerical well testing and reservoir simulation", SPE 62917.

[42] Jalali, J., Mohaghegh, S.D. and Gaskari, R. (2006). "Identifying Infill Locations and Underperformer Wells in Mature Fields Using Monthly Production Rate Data, Carthage Field, Cotton Valley Formation, Texas," paper SPE 104550 presented at SPE Eastern Regional Meeting, 11-13 October 2006, Canton, Ohio, USA

[43] Jones, R and Raghavan, R. (1985) "Interpretation of Flowing Well Responses in Gas Condensate Wells," Paper SPE 14204 presented at the 60th Annual Technical Conference and Exhibition of the SPE of AIME, Las Vegas, Nevada, Sept. 22-25.

[44] Kamal, M.M., Pan.Y. and Landa, J.L., Chevron Corp., and Thomas, O.O., Stanford U. (2005). "Numerical well testing –A method to use transient testing results in reservoir simulation", SPE 95905.

[45] Kazemi, H. (1975), "A Reservoir Simulator for Studying Productivity Variation and Transient Behavior of a Well in a Reservoir Undergoing Gas Evolution," Trans. AIME 259, 1401-1412

[46] Kristopher,l.K,(2006)"Laplace transform analytic element method for transient groundwater flow simulation" A PhD dissertation submitted to the university of Arizona

[47] Landa, J.L., SPE, and Horne, R.N., SPE, Stanford U., Kamal, M.M., SPE and Jenkins, C.D., SPE, Arco Exploration and Production Technology, (2000) "Reservoir Characterization Constrained to Well-Test Data: A Field Example", SPE 65429.

[48] Lee, W. J. (1982)," Well Testing", Textbook Series, Society of Petroleum Engineers of AIME, Dallas, 1, 45-50

[49] Levine, J.S. and Prats, M. (1961), "The Calculated Performance of Solution Gas-Drive Reservoirs," Soc. Pet. Eng. J. (Sept) 222, 142-152.

[50] Martin, J.C (1959), "Simplified Equations of Flow in Gas Drive Reservoirs and the Theoretical Foundation of Multiphase Pressure Buildup Analysis," Trans. AIME, 216, 309-
311.

[51] Massonnat, G.J and Bandiziol D., (1991). "Interdependence Between Geology and Well Test Interpretation". SPE 22740.

[52] Matthews, C.S, Brons, F. and Hazebroek, P.,(1954)." A method for determination of average pressure in a bounded reservoir". TRANS AIME, 201, 182-1914. Also reprint series NoP- Pressure analysis method, SPE, 51-60.

[53] Matthews, C.S. and Russell, D.G. (1967), “Pressure Buildup and Flow Tests in Wells”, Monograph Series, Society of Petroleum Engineers of AIME, Richardson, TX, I , 130-133.

[54] Meunier, D., Wittmann, M.J., and Stewart, G., (1985) “Interpretation of Pressure Buildup Test Using In-Situ Measurement of Afterflow”, JPT (January), 143-152.

[55] Miller, C.C, Dyes, A.B., and Hutchinson, C.A.,(1950). "Estimation of k and reservoir pressure from bottomhole pressure buildup characteristics". TRANS AIME, 189, 91-104

[56] Moridis, G.J., Blasingame, T.A., and Freeman, C.M. (2010). “Analysis of Mechanisms of Flow in Fractured Tight-Gas and Shale-Gas Reservoirs”. Paper SPE 139250 presented at the SPE Latin American and Caribbean Petroleum Engineering Conference, Lima, Peru. doi: 10.2118/139250-MS.

[57] Muskat, M., (1934). "The flow of compressible fluid through porous media and some problems in heat conduction physics", march

[58] Neuman S. P. and Di Federico V. (2003).”Multifaceted nature of hydrologic scaling and its interpretation”, Reviews of Geophysics, 41(3):1014

[59] Nnadi.M., SPE, Laser Engineering and Resources Consultants Ltd., Port Harcourt; Onyekonwu.M., SPE, University of Port Harcourt., (2004.). “Numerical Welltest Analysis”, SPE 88876,

[60] Nygard, R. (1982),”Calculating Relative Permeabilities from Two-Phase Drawdown Tests”, thesis for the C and. Techn. Degree. Rogaland Regional College, Stavanger (In Norwegian).

[61] Olufemi, M.O,(2011),“ Numerical modelling of fractured shale-gas and tight-gas reservoirs using unstructured grids” a thesis submitted to the Texas A&M University

[62] Onyekonwu, M.O (1997). "General Principle of bottomhole pressure tests". Laser Engineering Consultant, Port Harcourt, pp56-58

[63] Perrine, R.L (1956), "Analysis of pressure Buildup Curves," Drill and Prod. Prac., API , 482-509.

[64] Priestley, M. B. (1981). Spectral Analysis and Time Series. Academic Press. ISBN 0-12-564922-3.

[65] Raghavan, R. (1976),"Well Test Analysis: Wells Producing by Solution Gas Drive Wells," SOC. Pet. Eng. J. Aug. 196-208.

[66] Raghavan, R. (1986), "Well Test Analysis for Multiphase Flow," paper SPE 14098 presented at the SPE 1986 International Meeting on Petroleum Engineering held in Beijing, China March 17-20

[67] Raghavan, R. (1986), "Well Test Analysis for Multiphase Flow," paper SPE 14098 presented at the SPE 1986 International Meeting on Petroleum Engineering held in Beijing, China March 17-20.

[68] Raghavan, R. S., Chen, C. and Agarwal, B. 1997. An Analysis of Horizontal Wells Intercepted by Multiple Fractures. SPEJ 2 (3): 235-245. SPE 27652-PA.

[69] Ramey, H.J. Jr. (1970)."Short-Time Well Test Data Interpretation in the Presence of Skin Effect and Wellbore Storage," JPT, 97- 101; Trans., AIME, 249.

[70] Ramey, H.J., Jr., And Kruger, P., Eds (1979),"Proceedings, Fifth Annual workshop On Geothermal Reservoir Engineering," Stanford, California, Dec

[71] Rapoport, L.A. and Leas, W.J. (1951), "Relative Permeability to Liquid in Liquid-Gas Systems," Trans. AME, 192, 83-98.

[72] Spivey, J.P., and Lee, W.J.: “”Estimating the Pressure-Transient Response for a Horizontal or a Hydraulically Fractured Well at an Arbitrary Orientation in an Anisotropic Reservoir,” SPE Reservoir Evaluation and Engineering (Oct. 1999), 462-469.

[73] Svjetlana L.2008,” Fracture face interference of finite conductivity fractured Wells using numerical simulation” a thesis submitted to the University of Oklahoma

[74] Theis, C.V., (1935). "The relation between the lowering of the piezonmetric surface and the rate and duration of discharges of well using ground-water storage" TRANS. AGU 519-524.

[75] Tiab, D. (1975), “ A New Approach To Detect and Locate Multiple Reservoir Boundaries By Transient Well Pressure Data , M.Sc Thesis , New Mexico Institute of Mining ad Technology, Socorro New Mexico

[76] Tiab, D. And Kumar, A. (1976), “ Application Of PD Function To Interference Analysis, Paper SPE 6053 presented at the 51st Annual fall meeting of the Society of Petroleum Engineers of AIME, New Orleans LA

[77] Tiab, D. And Kumar, A. (1976), “ Detection And Location Of Two Parallel Sealing Fault Around A Well”, SPE Paper SPE 6056 presented at the 51st Annual fall meeting of the Society of Petroleum Engineers of AIME, New Orleans LA

[78] Tiab, D – Analysis of Pressure Derivative Without Type-Curve Matching: Vertically Fractured Wells in Closed Systems – Journal of Petroleum Science and Engineering, 11 (1994), Paper SPE 26138

[79] Uraiet, A.A. and Raghavan, R. (1980), "Pressure Buildup Analysis for a Well produced at Constant Bottomhole Pressure," J. Per. Tech. (Oct.) 1813- 1824.

[80] Van Everdigen, A.F, and Hurst, W. (1949)."The application of Laplace transformation for flow problem inreservoirs". TRANS AIME.186, 305-324.

[81] Verbeek, C.M.J. (1982), "Analysis of Production Tests of Hydraulically Fractured Wells in a Tight Solution Gas-Drive Reservoir," Paper SPE 11084 presented at the SPE annual Technical Conference and Exhibition, New Orleans, Sept. 26-29.

[82] Warren, J.E. and Root, P.J. 1963. The Behavior of Naturally Fractured Reservoirs. SPE J. 3 (3): 245–255. SPE-426-PA

[83] Weiland, J., Shell Exploration & Production; Azari.M., SPE, Suparman, (2008). "Case History Review of the Applocation of Pressure Transient Testing and Production Logging in Monitoring the Performance of the Mars Deepwater Gulf of Mexico Field", SPE 115591.

[84] Weiss,N.A, (2012),"Elementary statistics, 5/E"
http://wps.aw.com/wps/media/objects/15/15512/formulas.pdf

[85] Weller, W.T. (1966), "Reservoir Performance during Two-Phase Flow," J. Per. Tech. Feb.
240-246.

[86] Windowstm Application Welltest Software (1995)." Test and Examples of welltest, Demo copy" Petroway Inc,Palo Alto, California.

[87] Winestock, A.G. and Colpitis, G.P. (1965),"Advances in Estimating Gas Well Deliverability," J. Cdn. Per. Tech. (July-Sept. 11 1-1 19.

[88] Whitson, C.S, (1983)." Topics on Phase Behavior and Flow of Petroleum Reservoir Fluid", Dissertation - Doctor of Technical Sciences, University of Trondheim, Norway, (Aug)

[89] Zakirov, S.N., Indrupskiy, I.M., Zakirov, E.S., SPE, Anikeev,D.P., Tarasov, A.I., and Bradulina, O.V., Inst. of the Russian Academy of Sciences, (2006). "New Approaches in well Testing", SPE 100136.

[90] Zerzar A, Bettam Y, Tiab D (2003) Interpretation of multiple hydraulically fractured horizontal wells in closed systems. SPE 84888 presented at SPE international improved oil recovery conference in Asia Pacific, Kuala Lumpur, 20–21 Oct.

[91] Zheng, S.Y.,(1997). "Well Testing and Characterisation of Meandering Fluvial Channel Reservoirs". Unpublished Ph.D thesis, Heriot-Watt University 226 pp.

[92] Zheng, S.-Y. (2006)."Fighting against non-unique solution problems in heterogeneous reservoirs through numerical well testing",SPE Asia Pacific Oil and Gas Conference and Exhibition, Adelaide, Sep. 2006, SPE 100951.

[93] Zheng, S.Y., Corbett, P.W.M. and Stewart, G., (1996). "The Impact of Variable Formation Thickness on Pressure Transient Behavior and Well Test Permeability in Fluvial Meander Loop Reservoirs". SPE 36552.

[94] Zheng, S.-Y. (2006)."Fighting against non-unique solution problems in heterogeneous reservoirs through numerical well testing",SPE Asia Pacific Oil and Gas Conference and Exhibition, Adelaide, Sep. 2006, SPE 100951.

[95] http://petrowiki.org/Fluid_flow_in_hydraulically_fractured_wells

[96] https://en.wikipedia.org/wiki/Standard_deviation

[97] http://www.itl.nist.gov/div898/handbook/pmc/section4/pmc442.htm

[98] http://www.petroway.com/amw.htm; Automate

[99] Warren, J. E., and Price, H. S., (1961), "Flow in heterogeneous porous media*": Society of Petroleum Eng. Journal. vol. 1,* p. 153–169. http://www.petroway.com/amw.htm; Automate

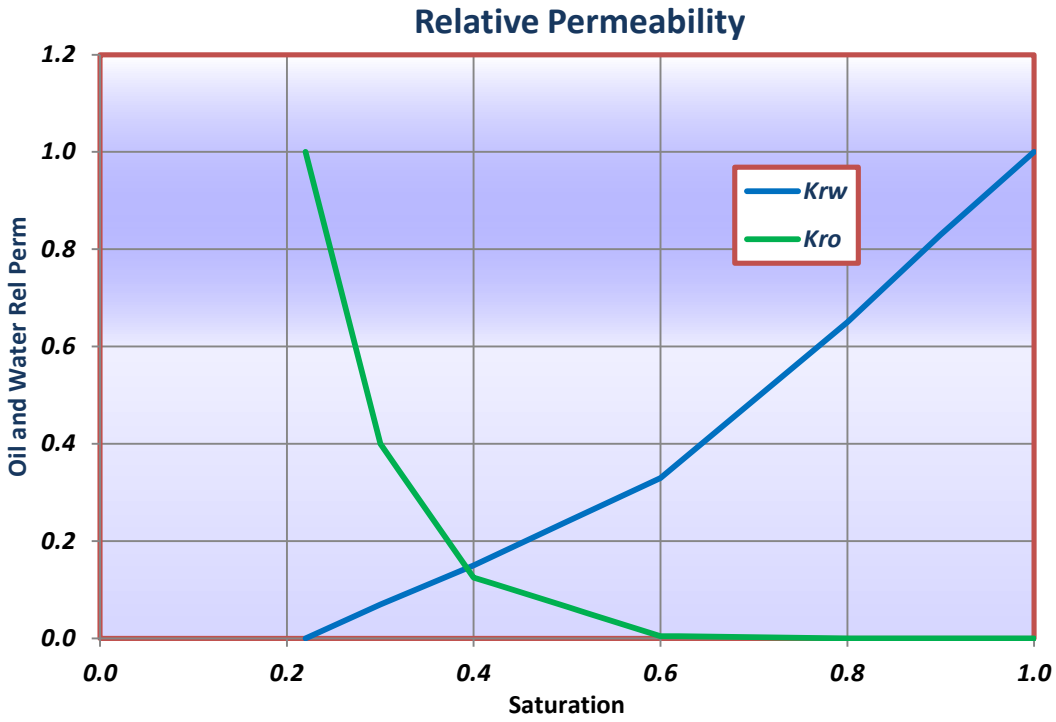

Figure 4.23: Simulation model for Gas cap + oil + water reservoir –Rel Perm vs sat

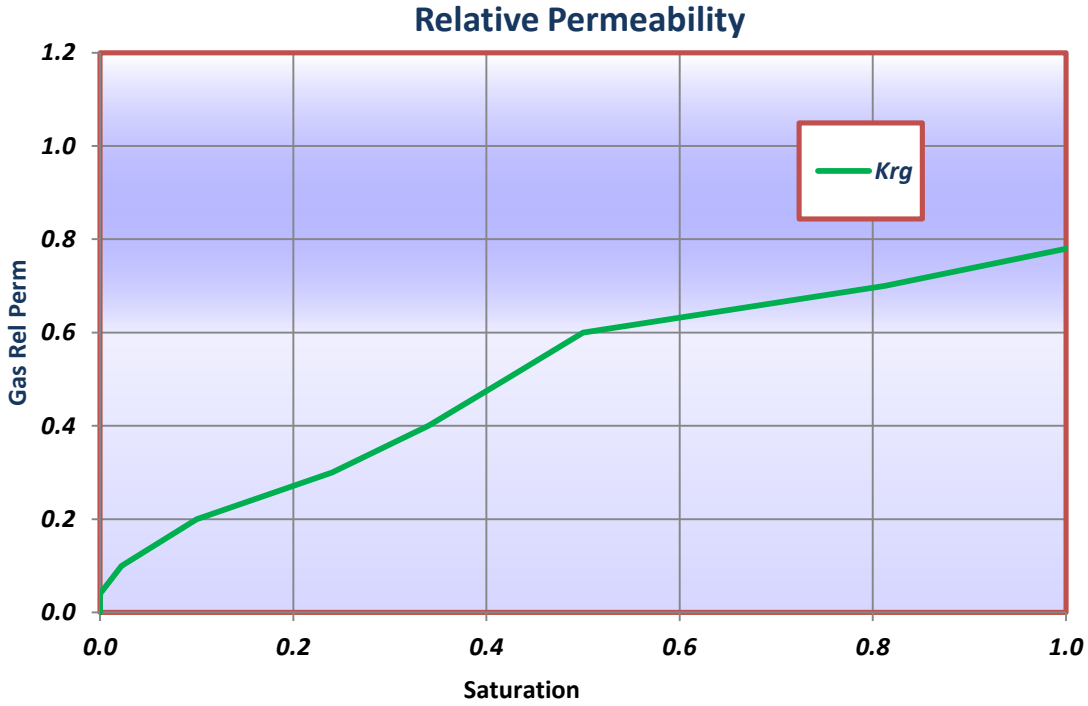

Figure4.24: Simulation model for Gas cap + oil + water reservoir –Rel Perm vs sat

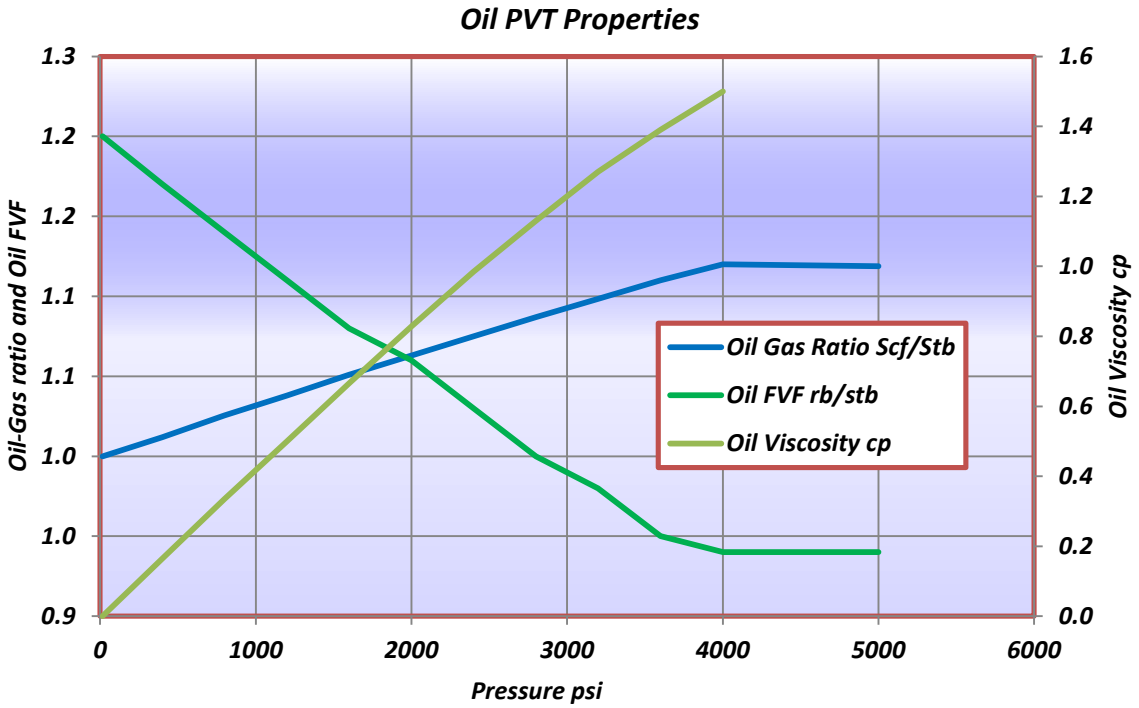

Figure 4.25: Simulation model for Gas cap + oil + water reservoir – Oil properties

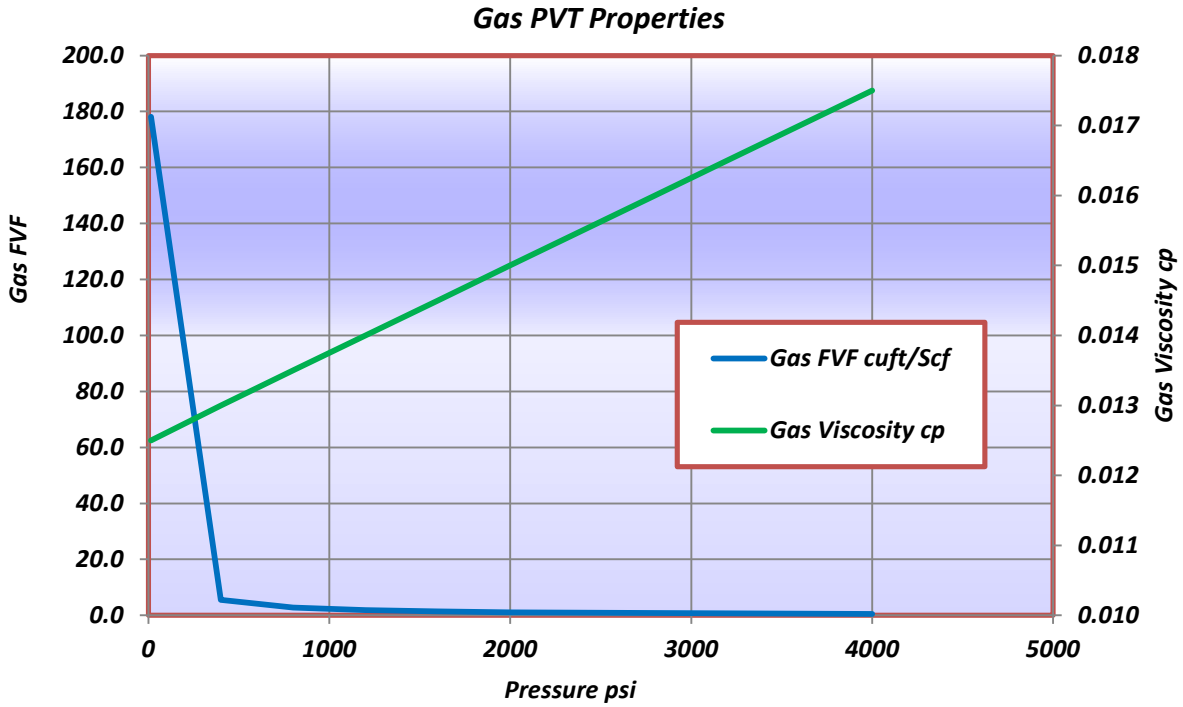

Figure 4.26: Simulation model for Gas cap + oil + water reservoir – Gas properties

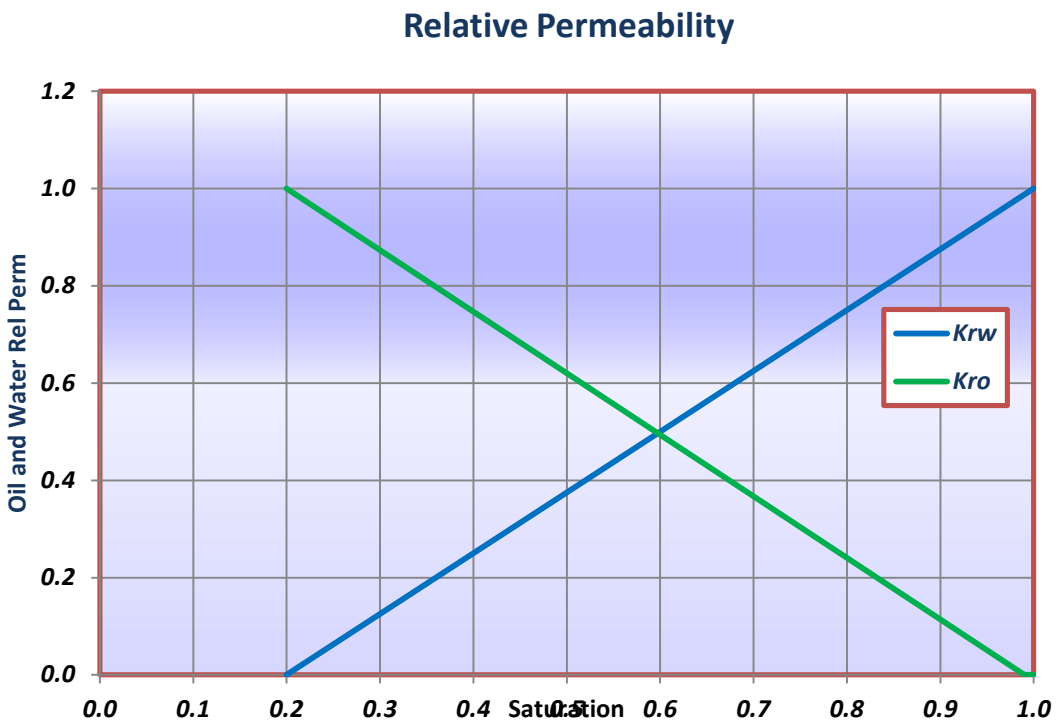

Figure 4.27: Simulation model for Gas condensate+ water – Rel Perm vs sat

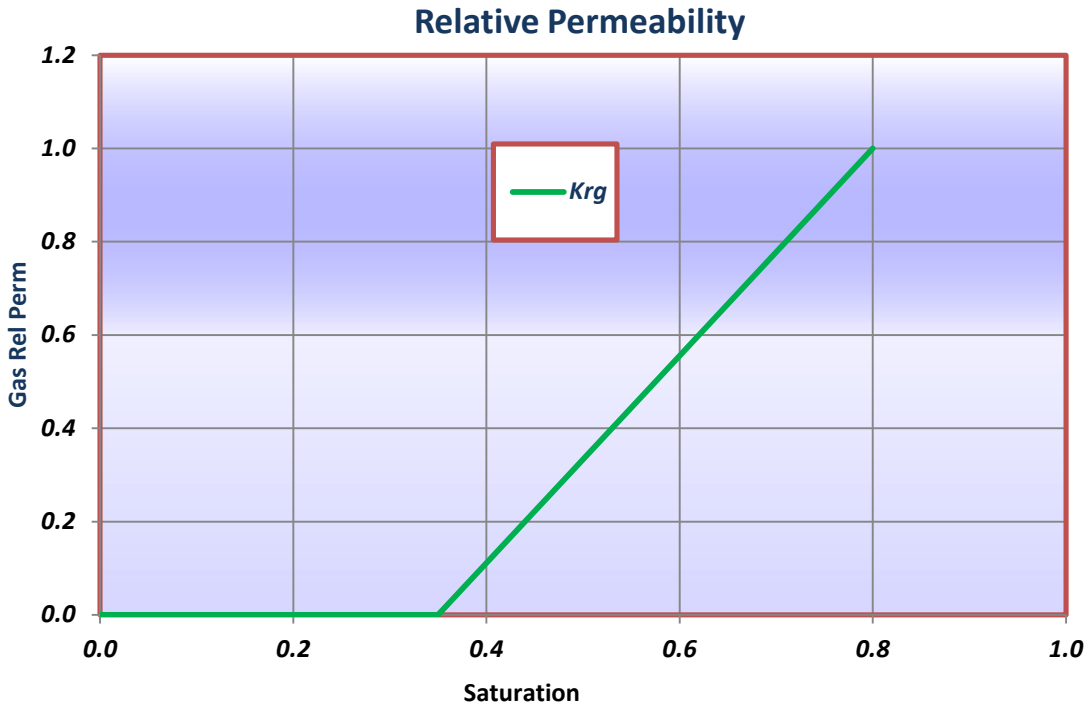

Figure 4.28: Simulation model for Gas condensate+ water –Rel Perm vs sat

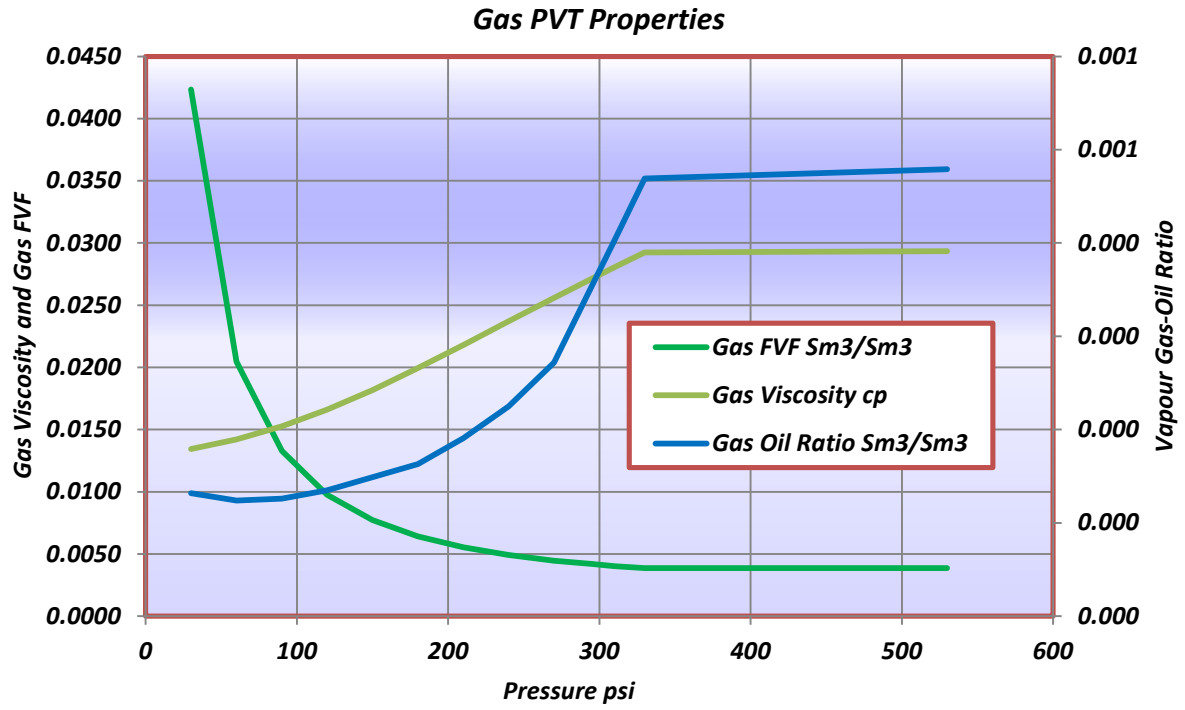

Figure 4.29: Simulation model Gas condensate+ water – Gas properties

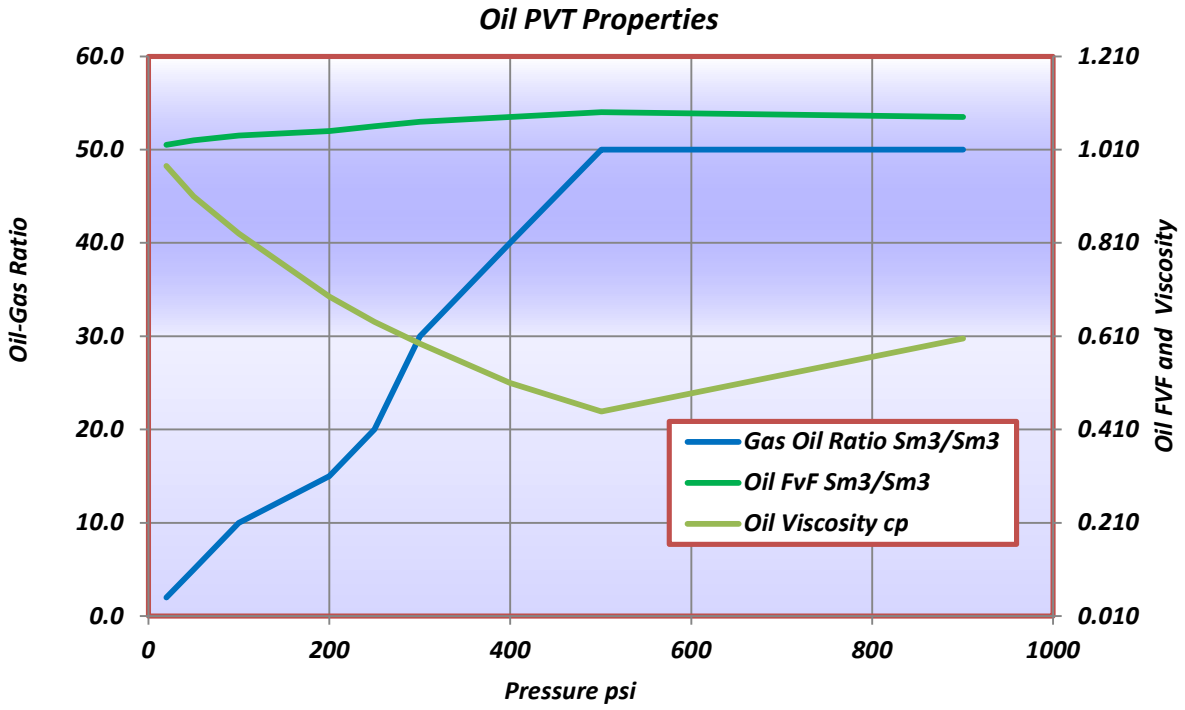

Figure 4.30: Simulation model for Gas condensate+ water condensate properties

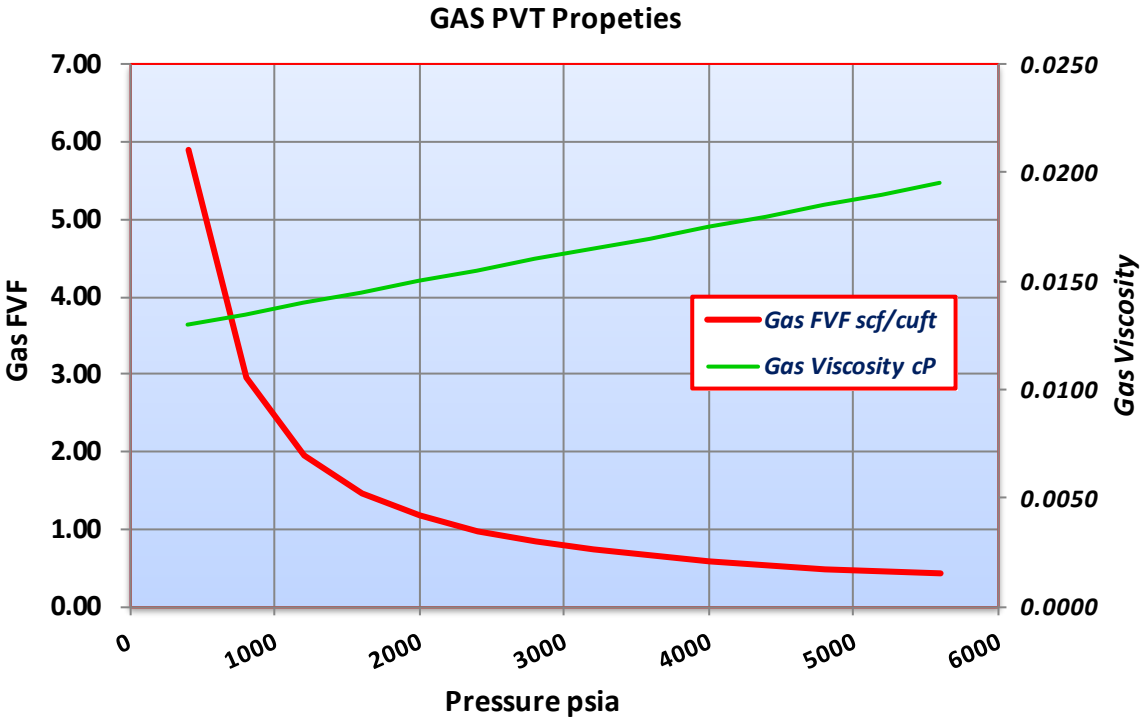

Figure 5.30: simulation model e model for shale gas + water – Gas propeties

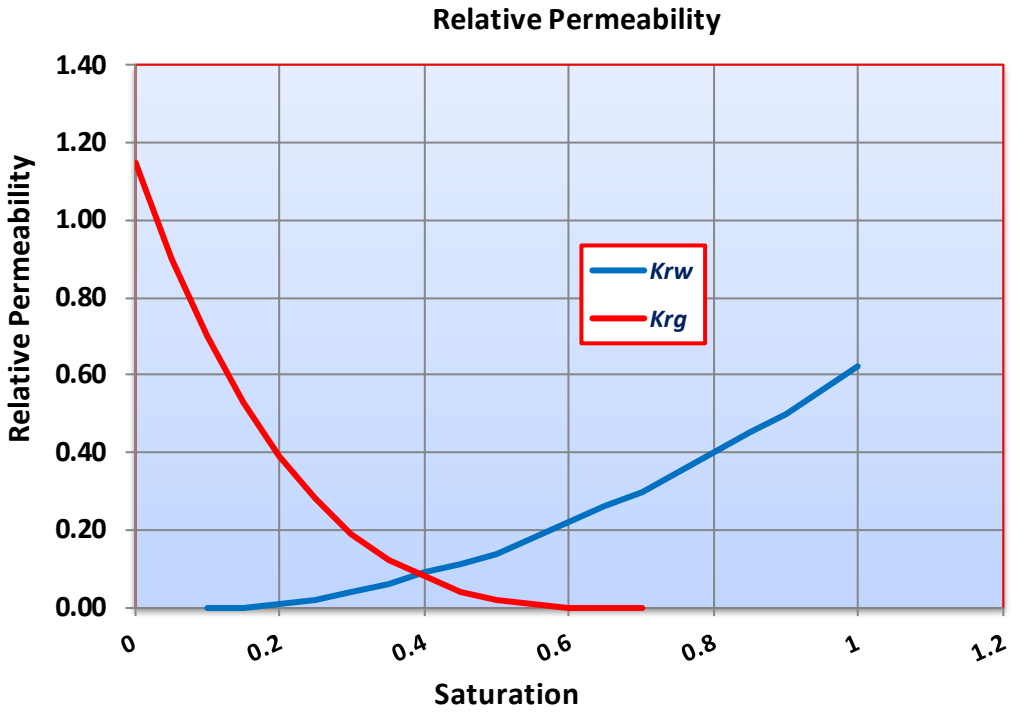

Figure 5.31: simulation model e model for shale gas + water –Rel Perm vs sat

a. Relative Permeability

The values are taken from experimental work on very tight sandstone by mass (2011). The relative permeability curves were constructed by applying the Corey function for a gas/water system

$$K_{rw} = K_{rw}\left(S_{g\min}\right)\left[\frac{S_w - S_{wcr}}{S_{w\max} - S_{wcr} - S_{g\min}}\right]^{C_w}$$

$$K_{rg} = K_{rg}\left(S_{w\min}\right)\left[\frac{S_{w\max} - S_w - S_{g\min}}{S_{w\max} - S_{wi} - S_{g\min}}\right]^{C_g}$$

The Van Genuchten relation was used to compute the capillary pressure curves.

$$P_c = P_{entry}\left(\left[\frac{S_w - S_{wcr}}{S_{w\max} - S_{wcr}}\right]^{-1/\lambda} - 1\right)^{1-\lambda}$$

APPENDIX B

Crossform fracture model derivation

The following dimensionless parameters are defined for the formulation.

Dimensionless Pressure:

$$P_{lfd} \Rightarrow P_{ld} \Rightarrow \frac{2\pi kh\Delta p}{q_t \mu B} \quad \text{i}$$

Dimension Time:

$$t_{lfd} \Rightarrow \frac{k_f t}{[[\phi c_t]_m + [\phi c_t]_t]\mu l_f{}^2} \quad \text{ii}$$

Dimensionless Length Coordinate (L)

Assuming Isotropic Properties

$$x_D = \frac{x}{L_c}\sqrt{\frac{k}{k_x}} \quad \text{iii}$$

$$y_D = \frac{y}{L_c}\sqrt{\frac{k}{k_y}} \quad \text{iv}$$

$$z_D = \frac{z}{l_{f1}/2} = \frac{z}{l_{f2}/2} \quad \text{v}$$

$$z_D = \frac{z}{L_c}$$

For isotropic system:

$$L_{fD} \Rightarrow \frac{l_f}{L_c} \quad \text{vi}$$

$$h_D \Rightarrow \frac{h}{L_c} \quad \text{vii}$$

$$L_{fD} \Rightarrow \frac{l_f}{L_c}\sqrt{\frac{k\cos^2\theta}{k_x} + \frac{k\sin^2\theta}{k_y}} \quad \text{viii}$$

The dimensionless fracture conductivity is defined as:

$$C_{fD} = \frac{k_f w_f}{k\lambda_{mf}} \qquad \text{ix}$$

Interporosity flow parameter:

$$\lambda_{mf} \Rightarrow \frac{12k_m}{l_f{}^2 k_f} A_{mf} \qquad \text{x}$$

as defined by Warren and Root, 1963

Dimensionless storativity: xa

$$\omega \Rightarrow \frac{[\phi c_t]_f}{[\phi c_t]_m + [\phi c_t]_f}$$

For fracture one (Primary fracture) the diffusivity equation is given as:

$$\frac{\partial^2 P_f}{\partial x^2} = \left[\frac{\varphi \mu c_t}{k}\right]_f \frac{\partial P_f}{\partial t} - \frac{k_m}{k_f \, l_{f1}/2} \frac{\partial P_m}{\partial z}\Big|_{z = l_{f1}/2} \qquad \text{xi}$$

For fracture two {Secondary fracture}

$$\frac{\partial^2 P_f}{\partial y^2} = \left[\frac{\varphi \mu c_t}{k}\right]_f \frac{\partial P_f}{\partial t} - \frac{k_m m}{k_f \, l_{f1}/2} \frac{\partial P_m}{\partial z}\Big|_{z = l_{f2}/2} \qquad \text{xii}$$

If the fractures are of same length, then

$$l_{f1} = l_{f2} = l_f$$

First the diffusivity equation for the matrix is given as:

$$\frac{\partial P_m}{\partial z^2} = \left[\frac{\varphi \mu c_t}{k}\right]_m \frac{\partial P_m}{\partial t} \qquad \text{xiii}$$

For the matrix and fracture interflowing period, the diffusivity equation is same for both fractures, therefore the following BC are applicable

Initial condition:

$$P_m(z,0) = P_i \qquad \text{xiii(a)}$$

Initial boundary:

$$\frac{\partial P_m}{\partial z}\Big|_{z=o} = O \qquad \text{xiii(b)}$$

Outer boundary

$$\left|P_m\right|_{z=l_f/2} = P_f \qquad \text{xiii(c)}$$

Resolving equation (xiii) into dimensionless form using equation (i), (ii) and (v)

$$\frac{\partial^2 P_{lmD}}{\partial z_D{}^2} \Rightarrow (1-\omega)\frac{l^2{}_f}{4}\frac{k_f}{k_m}\frac{1}{A_{mf}}\frac{\partial P_{lmD}}{\partial t_{AD}} \qquad \text{xiv}$$

Therefore

$$\frac{\partial^2 P_{lmD}}{\partial z_D{}^2} \Rightarrow \frac{3}{\lambda_{mf}}\left[1-\omega\right]\frac{\partial P_{lmD}}{\partial t_{AD}} \qquad \text{xv}$$

Where $\lambda_{mf} = \frac{12k_m}{l_f{}^2 k_f}A_{mf}$ [Warren and Root Interporosity flow parameter]

Introducing the boundary conditions xiii(a), xiii(b), xiii(c) into equation xv

$$\frac{\partial^2 P_{lmD}}{\partial z_D{}^2} \Rightarrow \frac{3\left[1-\omega\right]}{\lambda_{mf}}\left[sP_{lmD} - P_{lmD}\left[Z_D, O\right]\right] \qquad \text{vi}$$

Since dimensionally

$$P_{lmD}\left[Z_D, O\right] = 0$$

Therefore

$$\frac{\partial^2 P_{lmD}}{\partial z_D{}^2} - \frac{3(1-\omega)}{\lambda_{mf}}sP_{lmD} = 0 \qquad \text{xvii}$$

The characteristic equation for this differential equation is and its roots are:

$$v^2 - \frac{3(1-\omega)s}{\lambda_{mf}} = 0$$

$$v = \sqrt{\frac{3(1-\omega)s}{\lambda_{mf}}}i$$

The general solution to this differential equation is given as:

$$P_{lmD} \Rightarrow A\cosh\sqrt{\frac{3(1-\omega)s}{\lambda_{mf}}Z_D} + B\sinh\sqrt{\frac{3(1-\omega)s}{\lambda_{mf}}Z_D}$$

The constant A and B are obtained by the derivatives of equation xvii is given by

$$P_{lmD} \Rightarrow -A\sqrt{\frac{3(1-\omega)s}{\lambda_{mf}}}Sinh\sqrt{\frac{3(1-\omega)s}{\lambda_{mf}}Z_D} + B\sqrt{\frac{3(1-\omega)s}{\lambda_{mf}}}Cosh\sqrt{\frac{3(1-\omega)s}{\lambda_{mf}}Z_D}$$

Taking into consideration the inner boundary condition

$$\left|\frac{\partial P_{lmD}}{\partial Z_D}\right|_{Z_D=0} = 0$$

Substitute into equation xviii to obtain B

$$0 \Rightarrow 0 + B\sqrt{\frac{3(1-\omega)s}{\lambda_{mf}}}\cos(0)$$

Therefore B = 0

Substitute B into equation xvii to obtain A with outer boundary condition.

$$P_{lfD} = P_{lmD} = ACosh\sqrt{\frac{3(1-\omega)s}{\lambda_{mf}}}$$

Outer boundary condition

$$\left|P_{lmD}\right|_{Z_D=1} = P_{fD}$$

Therefore

$$A = P_{lfD} \Big/ \cosh\sqrt{\frac{3(1-\omega)s}{\lambda_{mf}}} \qquad \text{xi}$$

Therefore the general solution for the matrix flow solution is given as:

$$P_{lmD} = \frac{P_{lfD}\cosh\sqrt{\frac{3(1-\omega)s}{\lambda_{mf}}Z_D}}{\cosh\sqrt{\frac{3(1-\omega)s}{\lambda_{mf}}}}$$

The fracture solution for the crossform fracture model is formulated as follows:

The primary fracture

The diffusivity equation as stated in equation (xi) is given as:

$$\frac{\partial^2 P_f}{\partial x^2} = \left[\frac{\varphi\mu c_t}{k}\right]_f \frac{\partial P_f}{\partial t} - \frac{k_m}{k_f \, l_{f1}/2} \frac{\partial P_m}{\partial z}\Big|_{z = l_{f1}/2} \qquad \text{xxi}$$

Resolving the equation in dimensionless form using equation (i), (ii) and (v)

$$\frac{\partial^2 P_{lfD}}{\partial x_D^2} \Rightarrow R^2 \cos^2\theta \frac{k}{k_x}\left[\frac{\varphi\mu c_t}{k}\right]_f - \frac{k_f}{\left[(\varphi c_t)_m + (\varphi c_t)_f\right]\mu l_{f1}^2} \frac{\partial P_{lfD}}{\partial t_{AD}} - \frac{4k_m}{k_f} \frac{R^2\cos^2\theta}{l_{f1}^2} \cdot \frac{\partial P_{lmD}}{\partial z_D}$$ Substitute for $l_{f1} = 4R^2\cos^2\theta$ along x axis, we have:

$$\frac{\partial^2 P_{lfD}}{\partial x_D^{\,2}} \Rightarrow \frac{R^2\cos^2\theta}{l^2{}_{f1}} \frac{k}{k_x} \omega \frac{\partial P_{lfD}}{\partial t_{AD}} - \frac{4k_m}{k_f} \frac{\partial P_{lmD}}{\partial z_D} \qquad \text{xxii}$$

For secondary fracture resolve in y axis from equation xxii

$$\frac{\partial^2 P_f}{\partial y^2} = \left[\frac{\varphi\mu c_t}{k}\right]_f \frac{\partial P_f}{\partial t} - \frac{k_m}{k_f \, l_{f2}/2} \frac{\partial P_m}{\partial z}\Big|_{z = L_{f2}/2}$$

Converting the equation dimensionless form using equation (i), (ii) and (v)

$$\frac{\partial^2 P_{lfD}}{\partial y_D^2} \Rightarrow R^2 \sin^2\theta \frac{k}{k_y}\left[\frac{\varphi\mu c_t}{k}\right]_f - \frac{k_f}{\left[(\varphi c_t)_m + (\varphi c_t)_f\right]\mu l_{f2}^2} \frac{\partial P_{lfD}}{\partial t_{AD}} - \frac{4k_m}{k_f} \frac{R^2\sin^2\theta}{l_{f2}^2} \cdot \frac{\partial P_{lmD}}{\partial z_D}$$

Substituting for $l_{f2} = 4R^2\sin^2\theta$ along y axis

$$\frac{\partial^2 P_{lfD}}{\partial y_D^2} \Rightarrow \frac{R^2\sin^2\theta}{l_{f2}^2} \frac{k}{k_y} \omega \frac{\partial P_{lfD}}{\partial t_{AD}} - \frac{4k_m}{k_f} \frac{\partial P_{lmD}}{\partial z_D} \qquad \text{xxiii}$$

Assuming the flux is uniform along the fracture and the pressure at the wellbore is a summation of pressure along the fractures segment, hence P_{fD} x axis $= P_{fD}$ y axis

Combining equation (xxii) and (xxiii)

$$\frac{\partial^2 P_{lfD}}{\partial x_D^2} + \frac{\partial^2 P_{lfD}}{\partial y_D^2} \Rightarrow \left[\frac{k\cos^2\theta}{k_x l_{f1}^{\,2}} + \frac{k\sin^2\theta}{k_y l_{f2}^{\,2}}\right]\omega R^2 \frac{\partial P_{lfD}}{\partial t_{AD}} - \frac{8k_m}{k_f} \frac{\partial P_{lmD}}{\partial z_D}$$

Resolving in x axis

$$\frac{\partial^2 P_{lfD}}{\partial x_D^2} \Rightarrow \left[\frac{k\cos^2\theta}{k_x l_{f1}^{\,2}} + \frac{k\sin^2\theta}{k_y l_{f2}^{\,2}}\right] \frac{\omega R^2}{2} \frac{\partial P_{lfD}}{\partial t_{AD}} - \frac{8k_m}{k_f} \frac{\partial P_{lmD}}{\partial z_D}$$

$$\frac{\partial^2 P_{lfD}}{\partial x_D^2} \Rightarrow \left[\frac{k\cos^2\theta}{k_x} + \frac{K\sin^2\theta}{k_y}\right] \frac{\omega R^2}{2 l_f^{\,2}} \frac{\partial P_{lfD}}{\partial t_{AD}} - \frac{8k_m}{k_f} \frac{\partial P_{lmD}}{\partial z_D}$$

(Spivey and Lee, 1999) provide a solution for multiple arbitrarily oriented Infinite fracture system with K anisotropy in an infinite slab reservoir.

The dimensionless variable rescaling the anisotropy system to an equivalent isotropic system is given as;

$$L_{fD} = \frac{l_f}{L_C}\sqrt{\frac{k\cos^2\theta}{k_x} + \frac{k\sin^2\theta}{k_y}}$$

Where $\frac{k\cos^2\theta}{k_x} + \frac{k\sin^2\theta}{k_y} \Rightarrow \frac{L_{fD}{}^2 L_c{}^2}{l_f{}^2}$

Substitute into the above equation

$$\frac{\partial^2 P_{lfD}}{\partial x_D{}^2} \Rightarrow \frac{L_{fD}{}^2 L_c{}^2}{l_f{}^2}\frac{\omega R^2}{2l_f{}^2}\frac{\partial P_{lfD}}{\partial t_{AD}} - \frac{8k_m}{k_f}\frac{\partial P_{lmD}}{\partial z_D}$$

From Warren and Root interporosity flow parameter

$$\lambda_{mf} = \frac{12}{l_f{}^2}\frac{k_m}{k_f}A_{mf}$$

and $\frac{8k_m}{k_f} \Rightarrow \frac{\lambda_{mf} l_f{}^2}{1.5A_{mf}}$

Therefore

$$\frac{\partial^2 P_{lfD}}{\partial x_D{}^2} \Rightarrow \frac{L_{fD}{}^2 L_c{}^2}{l_f{}^2}\frac{\omega R^2}{2l_f{}^2}\frac{\partial P_{lfD}}{\partial t_{AD}} - \frac{\lambda_{mf} l_f{}^2}{1.5A_{mf}}\frac{\partial P_{lmD}}{\partial z_D}$$

Since the flow region modelling is within the fracture tips, therefore from equation vi:

$$\lim_{L_{fD}\to 1}\frac{l_f}{L_c} = 1$$

From dimensionless length coordinate (vi) and (vii)

$$\frac{\partial^2 P_{lfD}}{\partial x_D{}^2} \Rightarrow \frac{\omega R^2}{2l_f{}^2}\frac{\partial P_{lfD}}{\partial t_{AD}} - \frac{\lambda_{mf} L_C{}^2}{1.5A_{mf}}\frac{\partial P_{lmD}}{\partial z_D} \quad \text{xxiv}$$

Mathematically

$l_{f1} = R\cos\theta$ ----------Fracture (i) (Primary)

$l_{f2} = R\sin\theta$ ---------- Fracture (ii) (Secondary)

Invariably

$$2l_f^2 \Rightarrow R^2\left[\cos^2\theta + \sin^2\theta\right]$$

$$R^2 = 2l_f{}^2$$

Substitute into equation (xxiv)

$$\frac{\partial^2 P_{lfD}}{\partial x_D{}^2} = \omega\frac{\partial P_{lfD}}{\partial t_{AD}} - \frac{\lambda_{mf} l_f{}^2}{1.5A_{mf}}\frac{\partial P_{lmD}}{\partial z_D}$$

$$\frac{\partial^2 P_{lfD}}{\partial x_D{}^2} = \omega\frac{\partial P_{lfD}}{\partial t_{AD}} - \frac{\lambda_{mf} l_f{}^2}{1.5A_{mf}}\frac{\partial P_{lmD}}{\partial z_D}$$

Case a

If the cross-sectional area of the wall face is far away the fracture face,

$$A_{mf} = 2\pi L_c h$$

$$\frac{\partial^2 P_{lfD}}{\partial x_D{}^2} \Rightarrow \omega\frac{\partial P_{lfD}}{\partial t_{AD}} - \frac{\lambda_{mf} l_f{}^2}{1.5A_{mf}}\frac{\partial P_{lmD}}{\partial z_D}$$

$$\frac{\partial^2 P_{lfD}}{\partial x_D{}^2} \Rightarrow \omega\frac{\partial P_{lfD}}{\partial t_{AD}} - \frac{\lambda_{mf} l_f}{3\pi L_{fD} h}\frac{\partial P_{lmD}}{\partial z_D} \qquad \text{xxv}$$

Case b

Assuming the cross-sectional area of the fracture wall face

$$A_{mf} = 2\pi l_f h$$

Substitute into equation. Also apply equation (vi) and (vii)

$$\frac{\partial^2 P_{lfD}}{\partial x_D{}^2} \Rightarrow \omega\frac{\partial P_{lfD}}{\partial t_{AD}} - \frac{\lambda_{mf} l_f}{3\pi h}\frac{\partial P_{lmD}}{\partial z_D} \qquad \text{xxvi}$$

For case a

Resolving this equation in Laplace form,

The cross-sectional area of the wall face

$$\frac{\partial^2 P_{lfD}}{\partial x_D{}^2} = \omega \frac{\partial P_{lfD}}{\partial t_{AD}} - \frac{\lambda_{mf} l_f}{3\pi L_{fD} h} \frac{\partial P_{lmD}}{\partial z_D}$$

Taking into account the boundary conditions

Initial BC

$$P_{lfD}\left[x_D, 0\right] = 0 \qquad \text{xxvii}$$

Inner BC

(Craig 2006) formulate inner boundary condition describing transient flow in a finite conductivity fracture oriented along x axis.

The dimensionless Laplace domain is given as r.

$$\frac{\partial^2 P_{lfD}}{\partial^2 x_D} + \frac{2}{C_{fD}} \frac{\partial P_{lfD}}{\partial y_D}\bigg|_{y_{D=}{}^{w_D}\!/_2} = 0 \qquad \text{xxviii}$$

For $-1 \le x_D \le 1$

It is also written as

$$\frac{\partial^2 P_{lfD}}{\partial^2 x_D} - \frac{\pi}{C_{fD}} \bar{q}_D(x_D) = 0$$

Where the dimensionless variables are defined as

$$\bar{q}_D(x_D) = \frac{2L_f \bar{q}(x,5)}{q_w} \Rightarrow \frac{-2}{\pi} \frac{P_{lfD}}{\partial x_D}\bigg|_{x_{D=}{}^{w_D}\!/_2}$$

$w_D = {}^{w_f}\!/_{L_f}$ and $C_{fD} = \dfrac{k_f w_f}{k L_f}$

$\bar{q}$(x,5) = Laplace domain flow rate per unit length into fracture

q_w = Total well flow rate.

K_f = fracture permeability

Therefore for constant rate, the inner BC for fracture face is given as:

$$\frac{\partial P_{lfD}}{\partial x_D}\Big|_{X_D=0} \Rightarrow \frac{-\pi}{sC_{fD}} \qquad \text{xxix}$$

and the outer BC for no flow through the fracture hp in Laplace form is given as:

$$\frac{\partial P_{lfD}}{\partial x_D}\left[\frac{x}{L_c}, s\right]_{X_D=0} \Rightarrow 0 \qquad \text{xxx}$$

Substitute the initial BC into equation (xxv)

$$\frac{\partial P_{lfD}}{\partial x_D^2} \Rightarrow \omega\left[sP_{lfD} - P_{lfD}[x_D,0]\right] - \frac{\lambda l_f}{3\pi h L_{fD}}\frac{\partial P_{lmD}}{\partial^2 z_D}$$

$$\frac{\partial^2 P_{lfD}}{\partial x_D^2} \Rightarrow \omega\left|sP_{lfD} - \frac{\lambda_{mf} l_f}{3\pi h L_{fD}}\frac{\partial P_{lmD}}{\partial^2 z_D}\right. \qquad \text{xxxi}$$

Recall equation (xx)

$$P_{lmD} = \frac{P_{lfD}\cosh\sqrt{\frac{3(1-\omega)s}{\lambda_{mf}}}z_D}{\cosh\sqrt{\frac{3(1-\omega)s}{\lambda_{mf}}}}$$

Differentiate w.r.t Z_D

$$\frac{\partial P_{lmD}}{\partial^2 x_D} \Rightarrow P_{lfD}\sqrt{\frac{3(1-\omega)s}{\lambda_{mf}}}z_D \tanh\sqrt{\frac{3(1-\omega)s}{\lambda_{mf}}}$$

Substitute into equation (xxxi)

$$\frac{\partial^2 P_{lmD}}{\partial x_D^{\ 2}} \Rightarrow \omega\left|sP_{lfD} - \frac{\lambda_{mf} l_f}{3\pi h L_{fD}}\left[P_{lfD}\sqrt{\frac{3(1-\omega)s}{\lambda_{mf}}}\tanh\sqrt{\frac{3(1-\omega)s}{\lambda_{mf}}}\right]\right.$$

$$\frac{\partial^2 P_{lmD}}{\partial x_D^{\ 2}} \Rightarrow \omega\left|SP_{lfD} - \frac{\lambda_{mf} l_f}{\pi h L_{fD}}\left[\sqrt{\frac{\lambda_{mf}}{3s}(1-\omega)}\tanh\sqrt{\frac{3(1-\omega)s}{\lambda_{mf}}}\right]\right.$$

$$\frac{\partial^2 P_{lmD}}{\partial x_D^{\ 2}} \Rightarrow -sP_{lfD}\left[\omega + \frac{l_f}{\pi L_{fD} h}\sqrt{\frac{\lambda_{mf}(1-\omega)}{3s}}\tanh\sqrt{\frac{3(1-\omega)s}{\lambda_{mf}}}\right]$$

Where $m = \omega + \frac{l_f}{\pi h L_{fD}}\left[\sqrt{\frac{\lambda_{mf}}{3s}(1-\omega)}\tanh\sqrt{\frac{3(1-\omega)s}{\lambda_{mf}}}\right]$

$$\frac{\partial^2 P_{lmD}}{\partial x_D{}^2} - msP_{lfD} = o \qquad \text{xxxii}$$

The characteristic equation for this differentiate equation and its roots are

$$V^2 - ms = 0$$

$$V = \sqrt{msi}$$

The General solution for this differential equation is given as:

$$P_{lfD} \Rightarrow A\cosh(\sqrt{ms}x_D) + B\sinh\left(\sqrt{msx_D}\right) \qquad \text{xxxiii}$$

Differentiate w.s.t. X_D

$$P'_{lfD} \Rightarrow -A\sqrt{ms}\sinh\sqrt{ms}x_D + B\sqrt{ms}\cosh\sqrt{ms}x_D \qquad \text{xxxiv}$$

Applying the inner BC,

$$\frac{\partial P_{lfD}}{\partial x_D}\Big|_{X_D=0} \Rightarrow \frac{-\pi}{sC_{fD}} \quad \text{Where} \quad C_{fD} = \frac{k_f w_f}{kh_f}$$

Substitute into equation above;

$$\frac{-\pi}{sC_{fD}} \Rightarrow B\sqrt{ms}\cos(0)$$

$$B = \frac{-\pi}{sC_{fD}\sqrt{ms}}$$

Apply outer BC;

$$\frac{\partial P_{lfD}}{\partial x_D}\left[\frac{x}{h}, s\right]_{x_D = x/L_C} = 0$$

Introduce into equation xxxiv

$$0 = -A\sqrt{ms}\sinh\sqrt{ms}\,{}^{x}\!/_{L_C} + \left[\frac{-\pi}{sC_{fD}\sqrt{ms}}\cosh\sqrt{ms}\right]{}^{x}\!/_{L_C}$$

$$A \Rightarrow \frac{-\pi}{sC_{fD}\sqrt{ms}}\frac{\cosh\left(\sqrt{ms}\,{}^{x}\!/_{L_c}\right)}{\sinh\left(\sqrt{ms}\,{}^{x}\!/_{L_c}\right)}$$

Substitute A and B into equation xxxiii

$$P_{lmD} = \frac{-\pi}{sC_{fD}\sqrt{ms}} \frac{\cosh\left(\sqrt{ms}\ {}^{x}/_{L_c}\right)}{\sinh\left(\sqrt{ms}\ {}^{x}/_{L_c}\right)} \cosh\left(\sqrt{ms}x_D\right) - \frac{\pi}{sC_f\sqrt{ms}} \sinh\left(\sqrt{ms}x_D\right)$$

All the Wellbore condition $X_D = 0$

$$P_{lmD} = \frac{-\pi}{sC_{fD}\sqrt{ms}} \frac{\cosh\left(\sqrt{ms}\ {}^{x}/_{L_c}\right)}{\sinh\left(\sqrt{ms}\ {}^{x}/_{L_c}\right)}$$

$$P_{lmD} = \frac{-\pi}{sC_{fD}\sqrt{ms}} \frac{1}{\tanh\left(\sqrt{ms}\ {}^{x}/_{L_c}\right)}$$

$$P_{lmD} = \frac{-\pi}{sC_{fD}\sqrt{ms}} \coth\left(\sqrt{ms}\ {}^{x}/_{L_c}\right)$$

Also in Laplace domain, the constant pressure case at the Wellbore can be obtained from the solution of the constant rate using the equation.

Therefore

$$\frac{1}{P_{lwD}} \Rightarrow \frac{-\pi s}{C_{fD}\sqrt{ms}} \coth\left(\sqrt{ms}\ {}^{x}/_{L_c}\right)$$

Where $x_D = {}^{x}/_{L_c}$

$$\frac{1}{P_{lwD}} = \frac{-\pi s}{C_{fD}\sqrt{ms}} \coth\left(\sqrt{ms}x_D\right) \qquad \text{xxxv}$$

This is general solution for 2w fracture connecting at the Wellbore. This equation can be inverted to obtain time dependant solution using Laplace inversion such as Stehfest's inversion algorithm.

$$\frac{1}{q_{lwD}} = \frac{-\pi s}{C_{fD}\sqrt{ms}} \coth\left(\sqrt{ms}x_D\right)$$

At $x > 4.5 \qquad \coth(x) = 1$

Hence

$$\coth\left(\sqrt{ms}x_D\right) = 1 \quad \text{if} \quad \sqrt{ms}x_D > 4.5$$

Therefore

$$\frac{1}{q_{lwD}} \Rightarrow \frac{-\pi s}{C_{fD}\sqrt{ms}}$$

Where

$$m = \omega + \frac{l_f}{\pi L_{fD} h}\left[\sqrt{\frac{\lambda_{mf}(1-\omega)}{3s}}\tanh\sqrt{\frac{3(1-\omega)s}{\lambda_{mf}}}\right]$$

case i

If $\omega = 0$

$$m = \frac{l_f}{\pi L_{fD} h}\sqrt{\frac{\lambda_{mf}}{3s}}\tan\sqrt{\frac{3s}{\lambda_{mf}}}$$

$\sqrt{\frac{3s}{\lambda_{mf}}} \geq 4.5$ If $\tanh\left[\sqrt{\frac{3s}{\lambda_{mf}}}\right] = 1.0$

Therefore

$\sqrt{ms}x_D \geq 4.5$ If $Cosh\left(\sqrt{ms}x_D\right) \Rightarrow 1.0$

$$\frac{1}{q_{lwD}} \Rightarrow \frac{-\pi s}{C_{fD}\sqrt{ms}}$$

And $\sqrt{\frac{3s}{\lambda_{mf}}} \geq 4.5$ $\tanh\left[\sqrt{\frac{3s}{\lambda_{mf}}}\right] = 1.0$

Hence

$$m = \frac{l_f}{\pi L_{fD} h}\sqrt{\frac{\lambda_{mf}}{3s}}$$

Therefore

$$\frac{1}{q_{lwD}} \Rightarrow -\frac{\pi s}{C_{fD}\sqrt{\frac{l_f}{\pi L_{fD} h}\sqrt{\frac{\lambda_{mf}}{3s}} * s}}$$

$$\frac{1}{q_{lwD}} \Rightarrow -\frac{\pi s}{C_{fD}\left[\frac{l_f}{\pi L_{fD} h}\right]^{1/2}\left[\lambda_{mf}/3\right]^{1/4}\left[\frac{s^{1/2}}{s^{1/4}}\right]}$$

$$\frac{1}{q_{lwD}} \Rightarrow -\frac{\pi s^{3/4}}{C_{fD}\left[\frac{l_f}{\pi L_{fD} h}\right]^{1/2}\left[\lambda_{mf}/3\right]^{1/4}}$$

Converting to time dependent function using Laplace inverse

$$q_{lwD} \Rightarrow \frac{C_{fD}\sqrt{\frac{l_f}{\pi L_{fD} h}}\, t_{AD}^{-0.25}\left[1/3\right]^{1/4}}{\pi * \Gamma 0.75}$$

Where Γ = Gamma Function

$\Gamma 0.75 = 1.225$

$$q_{lwD} \Rightarrow \frac{C_{fD}\sqrt{l_f/\pi L_{fD} h}\left[\lambda_{mf}/3\right]^{1/4} t_{AD}^{-0.25}}{\pi * 1.25}$$

$$q_{lwD} \Rightarrow \frac{C_{fD}}{6.82}\sqrt{\frac{l_f}{L_{fD} h}}\left[\lambda_{mf}/3\right]^{1/4} t_{AD}^{-0.25}$$

$$q_{lwD} \Rightarrow \frac{C_{fD}}{6.84 t_{AD}^{1/4}}\sqrt{\frac{l_f}{L_{fD} h}}\left[\lambda_{mf}/3\right]^{1/4} \qquad \text{xxxvii}$$

This equation is due to bilinear flow period.

However considering the assumptions, the flow regime is limited by;

$$\sqrt{\frac{3s}{\lambda_{mf}}} \geq 4.5$$

$$\frac{3s}{\lambda_{mf}} \geq 20.3$$

$$\frac{3s}{s\lambda_{mf}} \geq \frac{20.3}{s^2}$$

Converting by Laplace inverse function

$$\frac{3}{\lambda_{mf}} \geq 20.3 t_{AD}, \quad \frac{3}{20.3\lambda_{mf}} \geq t_{AD}$$

Therefore

$$t_{AD} < \frac{3}{16\lambda_{mf}}$$ Condition (1)

Also

$$\sqrt{ms}x_D \geq 4.5,\ msx_D{}^2 \geq 20.3$$

$$\frac{mx_D{}^2}{s} \geq \frac{20.3}{s^2} \qquad mx_D{}^2 \geq t_{AD}20.3$$

$$\frac{mx_D{}^2}{16} \geq t_{AD}$$

Therefore equation (xxxvi) is applicable if

$$t_{AD} \leq \frac{3}{20.3\lambda_{mf}} \text{ and } t_{AD} \leq \frac{mx_D{}^2}{20.3\lambda_{mf}}$$

Case (ii)

$$\omega = 1$$

$$m = \omega + \frac{l_f}{\pi L_{fD} h}\left[\sqrt{\frac{\lambda_{mf}(1-\omega)}{3s}}\tanh\sqrt{\frac{3(1-\omega)s}{\lambda_{mf}}}\right]$$

$$m \Rightarrow 1+0$$

$$m \Rightarrow 1$$

Therefore

$$\frac{1}{q_{lwD}} \Rightarrow -\frac{\lambda_{mf}s}{C_{fD}\sqrt{ms}}\coth\left[\sqrt{ms}x_D\right]$$

Where

$$\coth\left[\sqrt{ms}x_D\right] \Rightarrow 1.0 \text{ if } \sqrt{ms}x_D \geq 4.5$$

$$\frac{1}{q_{lwD}} \Rightarrow -\frac{\pi s}{C_{fD}\sqrt{ms}} \Rightarrow -\frac{\pi s^{1/2}}{C_{fD}}$$

$$q_{lwD} \Rightarrow \frac{C_{fD}}{\pi s^{1/2}} \Rightarrow \frac{C_{fD}}{\pi\sqrt{\pi t_{AD}}}$$

$$q_{lwD} \Rightarrow \frac{C_{fD}}{5.57 t_{AD}^{1/2}} \qquad \text{xxxviii}$$

This equation is due to the linear flow period with assumption limiting to t.

$$\sqrt{ms}x_D \geq 4.5,\ msx_D{}^2 \geq 20.3$$

$$\frac{mx_D{}^2}{s} \geq \frac{20.3}{s^2}$$

$$mx_D{}^2 \geq 20.3 t_{AD},\ t_{AD} \leq \frac{mx_D{}^2}{20.3}$$

Equation (xxxviii) is limited to the region $t_{AD} \leq \frac{mx_D{}^2}{20.3}$

Case (iii)

$f(s) \Rightarrow 1.0$, This is for homogenous case.

Recall that for matrix slab

$$f(s) = \omega + \sqrt{\frac{\lambda_{mf}(1-\omega)}{3s}} \tanh \sqrt{\frac{3(1-\omega)s}{\lambda_{mf}}}$$

$$\sqrt{\frac{\lambda_{mf}(1-\omega)}{3s}} \tanh \sqrt{\frac{3(1-\omega)s}{\lambda_{mf}}} \Rightarrow 1-\omega$$

Therefore

$$m = \omega + \frac{l_f}{\pi L_{fD} h} \sqrt{\frac{\lambda_{mf}(1-\omega)}{3s}} \tanh \sqrt{\frac{3(1-\omega)s}{\lambda_{mf}}}$$

$$m = \omega + \frac{l_f(1-\omega)}{\pi L_{fD} h}$$

Substitute into equation (xxxv)

$$\frac{1}{q_{lwD}} \Rightarrow -\frac{\pi s}{C_{fD}\sqrt{ms}} \coth\left[\sqrt{ms}x_D\right]$$

$$\Rightarrow -\frac{\pi s}{C_{fD}\sqrt{\left(\omega + \frac{l_f(1-\omega)}{\pi L_{fD} h}\right)s}} Coth\left[\sqrt{ms}x_D\right]$$

If

$$Coth\left[\sqrt{ms}x_D\right] \Rightarrow 1.0\,,\ \sqrt{ms}\,x_D \geq 4.5$$

$$\frac{1}{q_{lwD}} \Rightarrow -\frac{\pi s^{1/2}}{C_{fD}\sqrt{\omega + \frac{l_f(1-\omega)}{\pi L_{fD} h}}}$$

$$q_{lwD} \Rightarrow -\frac{C_{fD}\sqrt{\omega + \frac{l_f(1-\omega)}{\pi L_{fD} h}}}{\pi s^{1/2}}$$

Converting to time dependent function using Laplace inverse function.

$$q_{lwD} \Rightarrow -\frac{C_{fD}\sqrt{\omega + \frac{l_f(1-\omega)}{\pi L_{fD} h}}}{\pi\sqrt{\pi t_{AD}}}$$

$$q_{lwD} \Rightarrow -\frac{C_{fD}\sqrt{\omega + \frac{l_f(1-\omega)}{\pi L_{fD} h}}}{5.57 t_{AD}^{1/2}} \qquad \text{xxxix}$$

This equation represents the homogenous phase.

Also this equation is limited by

$$Coth\left[\sqrt{ms}x_D\right] \Rightarrow 1.0 \quad \text{if} \quad \sqrt{ms}\,x_D \geq 4.5$$

$$\frac{mx_D^{\,2}}{s} \geq \frac{20.3}{s^2},\ t_{AD} \leq \frac{mx_D^{\,2}}{20.3}$$

Case (iv)

If $f(s) \Rightarrow 0$ and ω is a function of the Laplace parameter as defined below:

$$\left.\begin{array}{l} \frac{1}{s^{3/4}} \\ \frac{1}{\omega\sqrt{s^3}} \\ \frac{1}{s^{3/2}} \end{array}\right\} \text{ Asymptons}$$

Recall that for matrix slab

$$f(s) = \omega + \sqrt{\frac{\lambda_{mf}(1-\omega)}{3s}} \tanh \sqrt{\frac{3(1-\omega)s}{\lambda_{mf}}}$$

$$\sqrt{\frac{\lambda_{mf}(1-\omega)}{3s}} \tanh \sqrt{\frac{3(1-\omega)s}{\lambda_{mf}}} \Rightarrow -w$$

If

$$\tanh\left[\sqrt{\frac{3s}{\lambda_{mf}}}\right] = 1.0$$

$$\sqrt{\frac{\lambda_{mf}(1-\omega)}{3s}} \Rightarrow -\omega$$

Therefore

$$1-\omega = \frac{-\omega^2 3s}{\lambda_{mf}} \qquad \text{xxxx}$$

Recall

$$m = \omega + \frac{l_f}{\pi L_{fD} h} \sqrt{\frac{\lambda_{mf}(1-\omega)}{3s}} \tanh \sqrt{\frac{3(1-\omega)s}{\lambda_{mf}}}$$

Substitute equation 35 and the asympton

into above equation

$$m = \frac{1}{s^{3/4}} - \frac{l_f}{\pi L_{fD} h s^{3/2}} \qquad \text{xxxxi}$$

Substitute into equation

$$\frac{1}{q_{lwD}} \Rightarrow -\frac{\pi s}{C_{fD}\sqrt{ms}} \coth\left[\sqrt{ms}\, x_D\right]$$

$$\Rightarrow -\frac{\pi s}{C_{fD}\sqrt{\left(s^{-3/4} - \frac{l_f}{\pi L_{fD} h s^{3/2}}\right)s}} Coth\left[\sqrt{ms}\, x_D\right] \qquad \text{xxxxii}$$

$$\Rightarrow -\frac{\pi s}{C_{fD}\sqrt{\left(s^{1/4} - \frac{l_f}{\pi L_{fD} h s^{1/2}}\right)}} Coth\left[\sqrt{ms}\, x_D\right]$$

$$\Rightarrow -\frac{\pi s}{C_{fD}\left(s^{1/8}-\frac{l_f}{\pi L_{fD} h s^{1/4}}\right)} Coth\left[\sqrt{ms}\,x_D\right]$$

If

$$Coth\left[\sqrt{ms}\,x_D\right] \Rightarrow 1.0\,,\ \sqrt{ms}\,x_D \geq 4.5$$

$$q_{lwD} \Rightarrow -\frac{C_{fD}}{\pi s^{7/8}} - \frac{C_{fD} l_f}{\pi^2 s^{5/4} L_{fD} h}$$

Converting to time dependent function using Laplace inverse

$$q_{lwD} \Rightarrow -\frac{C_{fD} t_{AD}^{-0.125}}{\pi \Gamma 0.875} - \frac{C_{fD} l_f t^{-0.25}}{\pi^2 \Gamma 0.75 L_{fD} h}$$

Where Γ = Gamma Function

$\Gamma 0.875 = 1.456$

$\Gamma 0.75 = 1.225$

Therefore

$$q_{lwD} \Rightarrow -C_{fD}\left(\frac{0.22}{t^{1/8}} - \frac{0.083 l_f}{t^{1/4} L_{fD} h}\right) \qquad \text{xxxxiii}$$

This equation is due to trilinear flow period. Also this equation is limited by

$$t_{AD} \leq \frac{m x_D^{\,2}}{20.3}$$

For case b

Assuming the cross-sectional area of the wall face

$$A_{mf} = 2\pi l_f h$$

And from equation xxvi

$$\frac{\partial^2 P_{lfD}}{\partial x_D^{\,2}} \Rightarrow \omega \frac{\partial P_{lfD}}{\partial t_{AD}} - \frac{\lambda_{mf} l_f}{3\pi h} \frac{\partial P_{lmD}}{\partial z_D}$$

Taking into account the boundary conditions as in case a

and applying the same steps from equation xxvi to xxxvii, the resolve equation is given as :

$$\frac{\partial^2 P_{lmD}}{\partial x_D^{\ 2}} \Rightarrow -sP_{lfD}\left[\omega + \frac{l_f}{\pi h}\sqrt{\frac{\lambda_{mf}(1-\omega)}{3s}}\tanh\sqrt{\frac{3(1-\omega)s}{\lambda_{mf}}}\right]$$

Where $m = \omega + \frac{l_f}{\pi h}\left[\sqrt{\frac{\lambda_{mf}}{3s}(1-\omega)}\tanh\sqrt{\frac{3(1-\omega)s}{\lambda_{mf}}}\right]$

$$\frac{\partial^2 P_{lmD}}{\partial x_D^{\ 2}} - msP_{lfD} = 0$$

The general solution for this differential equation is given as:

$$P_{lfD} \Rightarrow A\cosh(\sqrt{ms}x_D) + B\sinh\left(\sqrt{msx_D}\right)$$

Differentiate w.s.t. X_D

$$P'_{lfD} \Rightarrow -A\sqrt{ms}\sinh\sqrt{ms}x_D + B\sqrt{ms}\cosh\sqrt{ms}x_D$$

Applying the inner and outer BC, the Laplace solution is given as:

$$\frac{1}{q_{lwD}} = \frac{-\pi s}{C_{fD}\sqrt{ms}}\coth\left(\sqrt{ms}x_D\right)$$

This is general solution for 2w fracture connecting at the Wellbore. This equation can be inverted to obtain time dependant solution using Laplace inversion such as Stehfest's inversion algorithm.

At $x > 4.5$ $\coth(x) = 1$

Hence

$$\coth\left(\sqrt{ms}x_D\right) = 1 \quad \text{if} \quad \sqrt{ms}x_D > 4.5$$

Therefore

$$\frac{1}{q_{lwD}} \Rightarrow \frac{-\pi s}{C_{fD}\sqrt{ms}}$$

Where

$$m = \omega + \frac{l_f}{\pi h}\left[\sqrt{\frac{\lambda_{mf}(1-\omega)}{3s}}\tanh\sqrt{\frac{3(1-\omega)s}{\lambda_{mf}}}\right]$$

Case i

If ω = 0

$$\sqrt{\frac{3s}{\lambda_{mf}}} \geq 4.5 \quad \text{If } \tanh\left[\sqrt{\frac{3s}{\lambda_{mf}}}\right] = 1.0$$

Therefore

$$\sqrt{ms}\,x_D \geq 4.5 \quad \text{If } Coth\left(\sqrt{ms}\,x_D\right) \Rightarrow 1.0$$

$$\frac{1}{q_{lwD}} \Rightarrow \frac{-\pi s}{C_{fD}\sqrt{ms}}$$

Therefore

$$\frac{1}{q_{lwD}} \Rightarrow -\frac{\pi s}{C_{fD}\sqrt{\frac{l_f}{\pi h}}\sqrt{\frac{\lambda_{mf}}{3s}} * s}$$

Converting to time dependent function using Laplace inverse

$$q_{lwD} \Rightarrow \frac{C_{fD}}{6.84 t_{AD}^{1/4}}\sqrt{\frac{l_f}{h}}\left[\lambda_{mf}/3\right]^{1/4} \qquad \text{xxxxiv}$$

This equation is due to bilinear flow period. The flow regime is limited by;

$$t_{AD} \leq \frac{3}{20.3\lambda_{mf}} \text{ and } t_{AD} \leq \frac{m x_D^{\,2}}{20.3\lambda_{mf}}$$

Case (ii)

ω = 1

$$m = \omega + \frac{l_f}{\pi h}\left[\sqrt{\frac{\lambda_{mf}(1-\omega)}{3s}}\tanh\sqrt{\frac{3(1-\omega)s}{\lambda_{mf}}}\right]$$

$$m \Rightarrow 1$$

Therefore

$$\frac{1}{q_{lwD}} \Rightarrow -\frac{\lambda_{mf} s}{C_{fD}\sqrt{ms}}\coth\left[\sqrt{ms}\,x_D\right]$$

Where

$$\coth\left[\sqrt{ms}x_D\right] \Rightarrow 1.0 \quad \text{if} \quad \sqrt{ms}x_D \geq 4.5$$

$$\frac{1}{q_{lwD}} \Rightarrow -\frac{\pi s}{C_{fD}\sqrt{ms}} \Rightarrow -\frac{\pi s^{1/2}}{C_{fD}}$$

$$q_{lwD} \Rightarrow \frac{C_{fD}}{5.57 t_{AD}^{1/2}} \qquad \text{xxxxv}$$

Equation (xxxxv) is limited to the region $t_{AD} \leq \frac{mx_D^2}{20.3}$

Case (iii)

$f(s) \Rightarrow 1.0$, This is for homogenous case.

Recall that for matrix slab

$$f(s) = \omega + \sqrt{\frac{\lambda_{mf}(1-\omega)}{3s}} \tanh \sqrt{\frac{3(1-\omega)s}{\lambda_{mf}}}$$

Therefore

$$m = \omega + \frac{l_f(1-\omega)}{\pi h}$$

Substitute into equation (xxxv)

$$\frac{1}{q_{lwD}} \Rightarrow -\frac{\pi s}{C_{fD}\sqrt{ms}} \coth\left[\sqrt{ms}x_D\right]$$

If $Coth\left[\sqrt{ms}x_D\right] \Rightarrow 1.0$, $\sqrt{ms}x_D \geq 4.5$

$$q_{lwD} \Rightarrow -\frac{C_{fD}\sqrt{\omega + \frac{l_f(1-\omega)}{\pi h}}}{\pi s^{1/2}}$$

Converting to time dependent function using Laplace inverse function.

$$q_{lwD} \Rightarrow -\frac{C_{fD}\sqrt{\omega + \frac{l_f(1-\omega)}{\pi h}}}{5.57 t_{AD}^{1/2}} \qquad \text{xxxxvi}$$

This equation represents the homogenous phase.

Also this equation is limited by

$$\frac{mx_D^{\ 2}}{s} \geq \frac{20.3}{s^2},\ t_{AD} \leq \frac{mx_D^{\ 2}}{20.3}$$

Case (iv)

If $f(s) \Rightarrow 0$ and w is a function of the Laplace parameter as defined below:

$$\left.\begin{array}{l} \frac{1}{s^{3/4}} \\ \frac{1}{s^{2}} \\ \frac{1}{s^{3/2}} \end{array}\right\} \text{ Asymptons}$$

Recall that for matrix slab

$$\sqrt{\frac{\lambda_{mf}(1-\omega)}{3s}} \tanh \sqrt{\frac{3(1-\omega)s}{\lambda_{mf}}} \Rightarrow -\omega$$

If $\tanh\left[\sqrt{\frac{3s}{\lambda_{mf}}}\right] = 1.0$, then $\sqrt{\frac{\lambda_{mf}(1-\omega)}{3s}} \Rightarrow -\omega$

Recall

$$m = \omega + \frac{l_f}{\pi h}\sqrt{\frac{\lambda_{mf}(1-\omega)}{3s}}) \tanh \sqrt{\frac{3(1-\omega)s}{\lambda_{mf}}}$$

$$q_{lwD} \Rightarrow -\frac{C_{fD}}{\pi s^{7/8}} - \frac{C_{fD} l_f}{\pi^2 s^{5/4} h}$$

Converting to time dependent function using Laplace inverse

$$q_{lwD} \Rightarrow -C_{fD}\left(\frac{0.22}{t^{1/8}} - \frac{0.083 l_f}{t^{1/4} h}\right) \qquad \text{xxxxvii}$$

This equation is due to trilinear flow period. Also this equation is limited by

$$t_{AD} \leq \frac{mx_D^{\ 2}}{20.3}$$

```
NOECHO
--memory
--600 /

RUNSPEC
============================================================

TITLE
Statistical and Numerical density simulation
--  5 layers model

DIMENS
  10   5   5  /

NONNC

OIL

WATER

GAS

DISGAS

FIELD

TABDIMS
   1    1   30   20    1   20  /

WELLDIMS
  30   10    2   30 /

--LGR
--MaxLGRs MaxCellsLGR  MaxAmalCoarseCells MaxAmal MaxAmalLGR
--   2     500000              0          0    0  1* INTERP    /

NUPCOL
   4 /
VFPPDIMS
   7    3    4    2    0    1 /

VFPIDIMS
   6    3    1 /


START
```

```
  1 'JAN' 1990  /

NSTACK
  24 /

GRID
============================================================

--INIT
EQUALS
    'DX'     400     /
    'DY'     400     /
    'DZ'     50     /
    'PERMX'  50     /
    'PERMY'  50     /
    'PERMZ'  50      /
    'PORO'   0.2     /
    'TOPS'   8800      1  10  1  5  1  5   /
/

COPY
 'PERMX' 'PERMY'  1 10 1 5 1 5 /
 'PERMX' 'PERMZ'  1 10 1 5 1 5 /
/
MULTIPLY
 'PERMZ' 0.025 1 10 1 5 1 5 /
/
CARFIN
-- NAME -- I1 I2  J1 J2 K1 K2  NX   NY   NZ  NWMAXZ--
 'CARF1'   7  10   2  5  1  5  120  120  25    5 /

ENDFIN

PSEUDOS


PROPS
============================================================
=====
SWFN

  0.22  0     7
  0.3   0.07  4
  0.4   0.15  3
  0.5   0.24  2.5
  0.6   0.33  2
  0.8   0.65  1
  0.9   0.83  0.5
  1     1     0      /
```

SGFN

```
 0     0       0
 0.04  0       0.2
 0.1   0.022   0.5
 0.2   0.1     1
 0.3   0.24    1.5
 0.4   0.34    2
 0.5   0.42    2.5
 0.6   0.5     3
 0.7   0.8125  3.5
 0.78  1       3.9    /
```

SOF3

```
0       0        0
0.2     0        0
0.38    0.00432  0
0.4     0.0048   0.004
0.48    0.05288  0.02
0.5     0.0649   0.036
0.58    0.11298  0.1
0.6     0.125    0.146
0.68    0.345    0.33
0.7     0.4      0.42
0.74    0.7      0.6
0.78    1        1        /
```

PVTO

```
--     Rs       Pbub       Bo        Vo
      .0        14.7     1.0000     1.20  /
      .165       400.    1.0120     1.17  /
      .335       800.    1.0255     1.14  /
      .500       1200.   1.0380     1.11  /
      .665       1600.   1.0510     1.08  /
      .828       2000.   1.0630     1.06  /
      .985       2400.   1.0750     1.03  /
     1.130       2800.    1.0870     1.00  /
     1.270       3200.    1.0985      .98  /
     1.390       3600.    1.1100      .95  /
     1.500       4000.    1.1200      .94
                 5000.    1.1189      .94  /
/
```

PVDG

```
--    Pg       Bg       Vg
      14.7    178.08    .0125
       400.    5.4777   .0130
       800.    2.7392   .0135
```

```
     1200.    1.8198  .0140
     1600.    1.3648  .0145
     2000.    1.0957  .0150
     2400.    0.9099  .0155
     2800.    0.7799  .0160
     3200.    0.6871  .0165
     3600.    0.6035  .0170
     4000.    0.5432  .0175  /

PVTW
--Depth  Bw      Comp   Vw    Cv
  3600. 1.0034  1.0E-6  0.96  0.0 /

ROCK
--Ref   Comp
--Pres
  3600.  1.0E-6 /

DENSITY
-- Oil   Water   Gas
 44.98  63.01  0.0702  /


--RPTPROPS
-- SWFN SGFN SOF2 SOF3 /

SOLUTION
================================================================
===

EQUIL
--Datum    Press     WOC   Pcwoc  GOC   Pcgoc
  8910.    3600.    9000.  0.0    8820.  0.0   1  /

PBVD
--Pb     Depth
  5000.  3600.
  9000.  3600. /


-- OUTPUT CONTROLS (SWITCH ON OUTPUT OF INITIAL GRID BLOCK
PRESSURES)

RPTSOL

  1  0  1  1  0  1  0  1  1  0  1  0  0  0  0  0  0
  0  0  0  0  0  0  0  0  0  0  0  0  0  0  0  0  0
  0  0  0  0  0  0  0  0  0  0  0  0  0  0  0  0  /
```

```
SUMMARY
================================================================================

RUNSUM
'FIPRESV'  /
WGPR
'PROD1' /

WWPR
'PROD1' /

WOPR
'PROD1' /

-- WELL BOTTOM-HOLE PRESSURE
LBDENO
'CARF1' 60  60  8 /
/
LBDENG
'CARF1' 60  60  8 /
/
LBDENW
'CARF1' 60  60  8 /
/
WBHP
PROD1  /

LBPR
'CARF1' 60  60  8 /
 /

FOPR
FGPR
FWPR

FWGR

EXCEL

SCHEDULE
================================================================================

-- CONTROLS ON OUTPUT AT EACH REPORT TIME
--REQUIRED FOR FAST RESTART. USE AS REQUIRED
--SKIPREST
--DEFINE COMPUTATIONAL CONTROLS
TUNING
```

```
----TSINIT  TSMAXZ  TSMINZ  TSMCHP  TSFMAX  TSFMIN  TSFCNV  TFDIFF
THRUPT
   1*      4/
----TRGTTE  TRGCNV  TRGMBE  TRGLCV  XXXTTE  XXXCNV  XXXMBE
XXXLCV  XXXWFL  TRGFIP  TRGSFT
/  DEFAULTS
---- NEWTMX  NEWTMN  LITMAX  LITMIN  MXWSIT  MXWPIT  DDPLIM  DDSLIM
TRGDPR  XXXDPR
    2*            200      1*     20          /

RPTRST
'BASIC=4' 'FREQ=1'   'FLOWS'   'FIP'  /

RPTSCHED
'RESTART=2' 'NEWTON=2' 'RECOV' 'FIP=2' 'WELSPECS' 'WELLS=2' 'CPU' /

IMPES
 1.0 1.0 10000.0 /

-- CONTROLS ON OUTPUT AT EACH REPORT TIME

-- LOCAL WELL SPECIFICATION DATA
--
--    WELL   GROUP GRID     LOCATION  BHP   PI
--    NAME   NAME  NAME      I  J   DEPTH DEFN
WELSPECL
   'PROD1' 'G' 'CARF1'     60  60  8910.0 'OIL'  /
      /

-- LOCAL COMPLEION SPECIFICATION DATA
--
--    WELL     -LOCATION- OPEN/ SAT CONN  WELL
--    NAME     I  J  K1 K2 SHUT  TAB FACT  DIAM
COMPDATL
   'PROD1'     60  60  8 12 'OPEN' 2* 0.65 1* -1.5 /
    /

-- PRODUCTION WELL CONTROLS
--
--     WELL    OPEN/  CNTL   OIL  WATER   GAS  LIQU   RES   BHP
--     NAME    SHUT   MODE  RATE   RATE  RATE  RATE  RATE
WCONPROD
    'PROD1    ' 'OPEN' 'ORAT'  100 4*  1000  /
    /

SEPVALS
-- separator name Bob Rsi
SEP1 1.251 0.510  /
/
```

```
GSEPCOND
G SEP1  /
/

 -- Simulation for 76.8 hrs
TSTEP

1.32E-05    1.78E-05    2.40E-05    3.24E-05    4.38E-05    5.91E-05
7.98E-05    0.00010775  0.00014547  0.0001964   0.00026511  0.0003579
0.00048317  0.00065228  0.00088058  0.0011888   0.00160485  0.00216655
0.00292485  0.00394854  0.00533053  0.0071962   0.0097149   100*0.01
          /
-- PRODUCTION WELL CONTROLS
--
--     WELL    OPEN/  CNTL   OIL  WATER   GAS  LIQU   RES   BHP
--     NAME    SHUT   MODE  RATE   RATE  RATE  RATE  RATE
WCONPROD
    'PROD1'   'STOP' 'ORAT'  0 4*   0.0  /
      /
SEPVALS
-- separator name Bob Rsi
SEP1 1.251 0.510  /
/

GSEPCOND
G SEP1  /
/

 -- Simulation for 76.8 hrs
TSTEP

1.32E-05    1.78E-05    2.40E-05    3.24E-05    4.38E-05    5.91E-05
7.98E-05    0.00010775  0.00014547  0.0001964   0.00026511  0.0003579
0.00048317  0.00065228  0.00088058  0.0011888   0.00160485  0.00216655
0.00292485  0.00394854  0.00533053  0.0071962   0.0097149   100*0.01
          /
-- PRODUCTION WELL CONTROLS
--
--     WELL    OPEN/  CNTL   OIL  WATER   GAS  LIQU   RES   BHP
--     NAME    SHUT   MODE  RATE   RATE  RATE  RATE  RATE
WCONPROD
    'PROD1    ' 'OPEN' 'ORAT'  100 4*  1000  /
    /

SEPVALS
-- separator name Bob Rsi
SEP1 1.251 0.510  /
/

GSEPCOND
```

```
G SEP1  /
/

 -- Simulation for 76.8 hrs
TSTEP

1.32E-05    1.78E-05    2.40E-05    3.24E-05    4.38E-05    5.91E-05
7.98E-05    0.00010775  0.00014547  0.0001964   0.00026511  0.0003579
0.00048317  0.00065228  0.00088058  0.0011888   0.00160485  0.00216655
0.00292485  0.00394854  0.00533053  0.0071962   0.0097149   100*0.01
          /
-- PRODUCTION WELL CONTROLS
--
--     WELL    OPEN/ CNTL   OIL  WATER   GAS  LIQU   RES   BHP
--     NAME    SHUT  MODE  RATE   RATE  RATE  RATE  RATE
WCONPROD
    'PROD1'   'STOP' 'ORAT'  0 4*   0.0  /
      /
SEPVALS
-- separator name Bob Rsi
SEP1 1.251 0.510  /
/

GSEPCOND
G SEP1  /
/

 -- Simulation for 76.8 hrs
TSTEP

1.32E-05    1.78E-05    2.40E-05    3.24E-05    4.38E-05    5.91E-05
7.98E-05    0.00010775  0.00014547  0.0001964   0.00026511  0.0003579
0.00048317  0.00065228  0.00088058  0.0011888   0.00160485  0.00216655
0.00292485  0.00394854  0.00533053  0.0071962   0.0097149   200*0.01
          /


END
```

APPENDIX D

```
--
--THIS IS A RUN DEMONSTATING THE GAS CONDENSATE AND SOLUTION
--OPTIONS IN ECLIPSE. THE RUN IS THREE PHASE AND THREE
--DIMENSIONAL, STARTING WITH GAS ABOVE THE DEW POINT.
--A SINGLE GAS PRODUCER LOWERS THE PRESSURE, AND OIL DROPOUT
--OCCURS. THE RESERVOIR IS DOME SHAPED, WITH A GAS WATER CONTACT
--AT THE EDGES
--
RUNSPEC
TITLE
                GAS CONDENSATE TEST

DIMENS
   9   9   3 /

NONNC

OIL

WATER

GAS

DISGAS

VAPOIL

METRIC

TABDIMS
   1   1  20  20   1  15 /

WELLDIMS
  18   5   2  10 /
--LGR
--MaxLGRs MaxCellsLGR  MaxAmalCoarseCells MaxAmal MaxAmalLGR
--   20     200000              0          0    0  1* INTERP    /

NUPCOL
   4 /

VFPPDIMS
   7   3   4   2   0   1 /

VFPIDIMS
```

```
   6   3   1 /

START
  1 'JAN' 1983  /

NSTACK
   4 /

GRID       ================================================

EQUALS
    'DX'     400     /
    'DY'     300     /
    'DZ'     15      /
    'PERMX'  400     /
    'PERMY'  300     /
    'PERMZ'  300     /
    'PORO'   0.3     /
/
TOPS
243*2070.0  /

COPY
 'PERMX' 'PERMY'  1 9 1 9 1 2 /
 'PERMX' 'PERMZ'  1 9 1 9 1 2 /
/
MULTIPLY
 'PERMZ' 0.02  1 9 1 9 1 2 /
/

RPTGRID
  13*0 1 /

CARFIN
-- NAME -- I1 I2  J1 J2 K1 K2 NX   NY   NZ  NWMAXZ--
 'CARF1'   6  9   6  9  1  3  160  120  15    5 /

ENDFIN

PROPS
============================================================

SWFN
0.2  0   0
0.6  0.5 0
1.0  1.0 0 /

SGFN
0      0   0
0.35   0   0
```

```
0.575 0.5  0
0.8   1.0  0  /

SOF3

0     0    0
0.01  0.0  0.0
0.8   1.0  1.0 /

PVTW
306.1  1.03 0.000041    0.3  0  / ( BAR RM3/SM3 1/BAR CP )

ROCK
306.1     0.000053    /       ( BAR 1/BAR )

DENSITY
  800   1022  0.9907    /     ( KG/M3 )

--THE GAS PVT DATA----------------------------------------------

--FOR EACH GAS PRESSURE SPECIFIED IN THE FIRST COLUMN ( 30,60,..)
--AT LEAST ONE OIL/GAS RATIO (RV) VALUE IS SPECIFIED (0.000132,0.0..)
--FOR WHICH VAPOUR FORMATION VALUES AND VISCOSITIES ARE GIVEN

--THE FIRST RV VALUE FOR A GIVEN PRESSURE IS ASSUMED TO BE THE
--SATURATED VALUE ( IE AT THE DEW POINT )

--ANY SUBSEQUENT RV VALUES ARE FOR UNDERSATURATED STATES

PVTG                        ( BAR SM3/SM3 RM3/SM3 CP )

   30  0.000132  0.04234     0.01344
      0         0.04231     0.01389   /
   60  0.000124  0.02046     0.01420
      0         0.02043     0.01450   /
   90  0.000126  0.01328     0.01526
      0         0.01325     0.01532   /
  120  0.000135  0.00977     0.01660
      0         0.00973     0.01634   /
  150  0.000149  0.00773     0.01818
      0         0.00769     0.01752   /
  180  0.000163  0.006426    0.01994
      0         0.006405    0.01883   /
  210  0.000191  0.005541    0.02181
      0         0.005553    0.02021   /
  240  0.000225  0.004919    0.02370
      0         0.004952    0.02163   /
  270  0.000272  0.004471    0.02559
      0         0.004511    0.02305   /
  295  0.000354  0.004194    0.02714
```

```
      0        0.004225    0.02423   /
  310  0.000403  0.004031    0.02806
      0.000354  0.004059    0.02768
      0        0.004081    0.02492   /
  330  0.000469  0.003878    0.02925
      0.000354  0.003910    0.02832
      0        0.003913    0.02583   /
  530  0.000479  0.003868    0.02935
      0.000354  0.003900    0.02842
      0        0.003903    0.02593   /
    /

--THE OIL PVT DATA----------------------------------------------

--FOR EACH GAS/OIL RATIO (RS) VALUE (2,5...), AT LEAST ONE
--OIL PRESSURE VALUE MUST BE SPECIFIED (20.0,50.0...)
--FOR WHICH SOLUTION FORMATION VALUES AND VISCOSITIES ARE GIVEN

--THE FIRST PRESSURE VALUE IS ASSUMED TO BE THE SATURATED (BUBBLE
--POINT) PRESSURE FOR THAT RS VALUE.

--ANY SUBSEQUENT PRESSURES ARE FOR UNDERSATURATED STATES

PVTO
      2    20.0 1.02   0.975   /
      5    50.0 1.03   0.91    /
     10    100.0 1.04   0.83    /
     15    200.0 1.05   0.695   /
     20    250.0 1.06   0.641   /
     30    300.0 1.07   0.594   /
     40    400.0 1.08   0.51
           500.0 1.07   0.549
           900.0 1.06   0.74    /
     50    500.7 1.09   0.449
           900.7 1.08   0.605   /
/
RPTPROPS
0  0  0  0  0  0  0  0  /

SOLUTION
============================================================

-- INITIAL CONDITIONS - 310 BARS AT 2070 METERS, GWC AT 2100 METERS
-- TILTED BLOCK EQUILIBRATION
--
EQUIL      1 TABLES    2 NODES IN EACH          METRIC  11:29 14 OCT 83
--Datum    Press     WOC   Pcwoc  GOC   Pcgoc
  2070.0  310.0  2100.0  .0 2100  .0    1      1      10 /
-- OIL INITIALLY SET SATURATED, ALTHOUGH NO LIQUID OIL IN INITIAL
STATE
```

```
RSVD      1 TABLES    2 NODES IN EACH          METRIC  11:31 14 OCT 83
  2000.0   100
  2500.0   100
/

-- VAPOUR INITIALLY UNDER-SATURATED WITH RV = 0.00035

RVVD      1 TABLES    2 NODES IN EACH          METRIC  11:31 14 OCT 83
  2000.0   .00035
  2500.0   .00035
/
--
-- INITIAL SOLUTION REPORTS
--
RPTSOL                                 METRIC  12:45 14 OCT 83
  1  0  1  1  0  1  0  1  1  0  1  0  0  0  0  0  0
  0  0  0  0  0  0  0  0  0  0  0  0  0  0  0  0  0
  0  0  0  0  0  0  0  0  0  0  0  0  0  0  0  0  /
--
SUMMARY
=============================================================
RUNSUM
'FIPRESV'  /
WOPR
'PROD1' /

WGPR
'PROD1' /

WWPR
'PROD1' /

-- WELL BOTTOM-HOLE PRESSURE
LBDENO
'CARF1' 80 60 8 /
/
LBDENG
'CARF1' 80 60 8 /
/
LBDENW
'CARF1' 80 60 8 /
/
WBHP
PROD1  /

LBPR
'CARF1' 80 60 8 /
 /
```

```
FOPR

FWPR

FWGR

EXCEL

SCHEDULE
============================================================
--
-- REPORT SWITCHES
--
RPTSCHED                                  METRIC  12:44 14 OCT 83
  1   1   1   0   0   1   2   1   2   1   2   2   0   1   2   0   0
  0   0   0   0   0   0   0   0   0   0   0   0   0   0   0   0   0
  0   0   0   0   0   0   0   0   0   0   0   0   0   0   0   0   /
IMPES
 1.0 1.0 10000.0 /


-- LOCAL WELL SPECIFICATION DATA
--
--    WELL   GROUP GRID     LOCATION  BHP   PI
--    NAME   NAME  NAME     I  J   DEPTH DEFN
WELSPECL
   'PROD1' 'G' 'CARF1'     80 60    2100.0 'GAS'  /
      /

-- LOCAL COMPLEION SPECIFICATION DATA
--
--    WELL     -LOCATION- OPEN/ SAT CONN  WELL
--    NAME     I  J K1 K2 SHUT  TAB FACT  DIAM
COMPDATL
   'PROD1'  80  60  8 12 'OPEN' 0 -1  0.65  1* 0.2 /
    /
-- PRODUCTION WELL CONTROLS
--
--     WELL    OPEN/  CNTL   OIL  WATER   GAS  LIQU   RES   BHP
--     NAME    SHUT   MODE  RATE   RATE  RATE  RATE  RATE
WCONPROD
    'PROD1    ' 'OPEN' 'GRAT'  2* 0.5E6    /
    /
-- Simulation for 76.8 hrs
TSTEP

1.32E-05      1.78E-05      2.40E-05      3.24E-05      4.38E-05      5.91E-05
7.98E-05      0.00010775    0.00014547    0.0001964     0.00026511    0.0003579
0.00048317    0.00065228    0.00088058    0.0011888     0.00160485    0.00216655
0.00292485    0.00394854    0.00533053    0.0071962     0.0097149     100*0.02
```

```
        /
-- PRODUCTION WELL CONTROLS
--
--    WELL    OPEN/ CNTL   OIL  WATER   GAS  LIQU   RES   BHP
--    NAME    SHUT  MODE RATE   RATE  RATE  RATE  RATE
WCONPROD
   'PROD1    ' 'STOP' 'GRAT'  2*   0.0  /
     /
 -- Simulation for 76.8 hrs
TSTEP

1.32E-05      1.78E-05      2.40E-05      3.24E-05      4.38E-05      5.91E-05
7.98E-05      0.00010775    0.00014547    0.0001964     0.00026511    0.0003579
0.00048317    0.00065228    0.00088058    0.0011888     0.00160485    0.00216655
0.00292485    0.00394854    0.00533053    0.0071962     0.0097149     100*0.02
        /
-- PRODUCTION WELL CONTROLS
--
--    WELL    OPEN/ CNTL   OIL  WATER   GAS  LIQU   RES   BHP
--    NAME    SHUT  MODE RATE   RATE  RATE  RATE  RATE
WCONPROD
   'PROD1    ' 'OPEN' 'GRAT'  2* 0.8E6    /
   /

-- Simulation for 76.8 hrs
TSTEP

1.32E-05      1.78E-05      2.40E-05      3.24E-05      4.38E-05      5.91E-05
7.98E-05      0.00010775    0.00014547    0.0001964     0.00026511    0.0003579
0.00048317    0.00065228    0.00088058    0.0011888     0.00160485    0.00216655
0.00292485    0.00394854    0.00533053    0.0071962     0.0097149     100*0.02
        /
-- PRODUCTION WELL CONTROLS
--
--    WELL    OPEN/ CNTL   OIL  WATER   GAS  LIQU   RES   BHP
--    NAME    SHUT  MODE RATE   RATE  RATE  RATE  RATE
WCONPROD
   'PROD1    ' 'STOP' 'GRAT'  2*   0.0  /
     /
 -- Simulation for 76.8 hrs
TSTEP

1.32E-05      1.78E-05      2.40E-05      3.24E-05      4.38E-05      5.91E-05
7.98E-05      0.00010775    0.00014547    0.0001964     0.00026511    0.0003579
0.00048317    0.00065228    0.00088058    0.0011888     0.00160485    0.00216655
0.00292485    0.00394854    0.00533053    0.0071962     0.0097149     100*0.01
        /

END
```

APPENDIX E

```
- Constant Flow Rate Case q = 100 [STB/DAY]
-- Vertical fracture FCD=100
--NOECHO
RUNSPEC
=========================================================================
=======
TITLE
Vertical fracture model, (Wf)r=0.5 in ==> (Wf)e=2 ft
DIMENS
---- dx dy dz
100 100 3 /
-- Fluid phases present

WATER

GAS
-- Units
FIELD
--length of stack used by linear solver
NSTACK
50 /
------------ #wells, # connections, #groups, #wells per group
TABDIMS
   1    1   20   20    2    5 /
WELLDIMS
   2   13    1    2 /
-- Start simulation date
START
1 JAN 1997 /
 -- run to be restarted from unified restart file
UNIFIN
-- Restart and summary files written are to be unified
UNIFOUT

=========================================================================
======
GRID
TOPS
10000*4000 /
DX
340     340     340     340     340     340     340     340     340     340 xxxxxxxxxxxxxxxxx
/

DZ
10000*30 10000*40 10000*30 /
```

```
EQUALS
PERMX 0.1 1 100 1 100 1 3 / -- reservoir X permeability
PERMY 0.1 1 100 1 100 1 3 / -- reservoir X permeability
PORO 0.1 1 100 1 100 1 3 / -- reservoir Porosity
PERMX 2554 31 69 50 50 2 2 / -- equivalent fracture X permeability
PORO 0.0873 31 69 50 50 2 2 / -- equivalent fracture porosity/
PERMY 2554 50 50 31 69 2 2 / -- equivalent fracture X permeability
PORO 0.0873 50 50 31 69 2 2 / -- equivalent fracture porosity
/
COPY
PERMX PERMZ 1 100 1 100 1 3 /
/
INIT
GRIDFILE
0 1 /
RPTGRID
TRANX TRANY /
 ====================================================
PROPS

-- Connate gas saturation
--
SWFN
0.10    0.00    0
0.15    0.00    0
0.20    0.01    0
0.25    0.02    0
0.30    0.04    0
0.35    0.06    0
0.40    0.09    0
0.45    0.11    0
0.50    0.14    0
0.55    0.18    0
0.60    0.22    0
0.65    0.26    0
0.70    0.30    0
0.75    0.35    0
0.80    0.40    0
0.85    0.45    0
0.90    0.50    0
0.95    0.56    0
1.00    0.62    0
/

SGFN
0.30    0.00    0
0.35    0.00    0
0.40    0.00    0
0.45    0.01    0
0.50    0.02    0
```

```
0.55     0.04     0
0.60     0.08     0
0.65     0.12     0
0.70     0.19     0
0.75     0.28     0
0.80     0.39     0
0.85     0.53     0
0.90     0.70     0
0.95     0.90     0
1.00     1.15     0
/
PVTW       1 TABLES       FIELD  12:00 1 JAN 1997
  .0000000   1.00000    3.03E-06    .50000    0.00E-01 /

--   PGAS   BGAS   VISGAS
PVDG
     400    5.9   0.013
     800    2.95  0.0135
    1200    1.96  0.014
    1600    1.47  0.0145
    2000    1.18  0.015
    2400    0.98  0.0155
    2800    0.84  0.016
    3200    0.74  0.0165
    3600    0.65  0.017
    4000    0.59  0.0175
    4400    0.54  0.018
    4800    0.49  0.0185
    5200    0.45  0.019
    5600    0.42  0.0195 /
ROCK
 4000.00        .30E-05 /

DENSITY
 52.0000  64.0000   .04400 /

RPTPROPS
/

================================================================
=======
SOLUTION
-- DATUM DATUM OWC OWC GOC GOC RSVD RVVD SOLN
-- DEPTH PRESS DEPTH PCOW DEPTH PCOG TABLE TABLE METH
EQUIL
4015 4000 4100 1* 4100 0 /

RPTSOL
-- Fluid Create init
-- in place Restart file
```

```
FIP=1 RESTART=2 /
RPTRST
BASIC=2 /
RPTSOL                                  FIELD  12:00 1 JAN 1997
  1   0   1   1   0   1   0   1   1   0   1   0   0   0   0   0   0
  0   0   0   0   0   0   0   0   0   0   0   0   0   0   0   0   0
  0   0   0   0   0   0   0   0   0   0   0   0   0   0   0   0   /
--


================================================================
========
SUMMARY
-- Well quantities
-- Well BHP
-- Well Gas production rate
WGPR
/
-- Well Water production rate
WWPR
/
-- Well Oil production rate
WOPR
/
BDENG
50 50 2 /
/
BVGAS
50 50 2 /
/
BDENW
50 50 2 /
/
BVWAT
50 50 2 /
/
BPR
50 50 2 /
/
BTCNFHEA
50 50 2 /Block Temperature
/
-- WELL BOTTOM-HOLE PRESSURE
BDENO
50 50 2 /
/
BVOIL
50 50 2 /
/
```

```
RUNSUM
EXCEL

================================================================
========
SCHEDULE
RPTRST
BASIC=2 /
RPTSCHED
WELSPECS /
WELSPECS
-- WELL GROUP -LOCATION- BHP PHASE DRAINAGE FLAG FLAG FLAG PRESS
FLAG
-- NAME NAME I J DEPTH RADIUS GAS SHUT CROSS TABLE DENS
W1 G 50 50 4000 GAS /
/
COMPDAT
-- WELL --LOCATION-- OPEN/ SAT CONN WELL EFF SKIN D PENETRATION
-- NAME I J K1 K2 SHUT TAB FACT DIAM KH FACTOR FACTOR DIRECTION
W1 50 50 2 2 OPEN 1* 1* 0.6 1* 0 0 Z /
/
WCONPROD
-- WELL OPEN/ CNTL OIL WATER GAS LIQU RES BHP THP VFP ALQ
-- NAME SHUT MODE RATE RATE RATE RATE RATE TABLE
W1 OPEN GRAT 2* 500 1* 1* 1* 1* 1* 1* 1* /
/
TSTEP
1.32E-05    1.78E-05    2.40E-05    3.24E-05    4.38E-05    5.91E-05
7.98E-05    0.00010775  0.00014547  0.0001964   0.00026511  0.0003579
0.00048317  0.00065228  0.00088058  0.0011888   0.00160485  0.00216655
0.00292485  0.00394854  0.00533053  0.0071962   0.0097149   600*0.1
        350*10.0
        /
```

APPENDIX F

Example 1.0a: Production Test
Flowing + Build-up Sequence:
Well perforated hp = 30ft between oil and water layer.
Net sand thickness h = 250ft

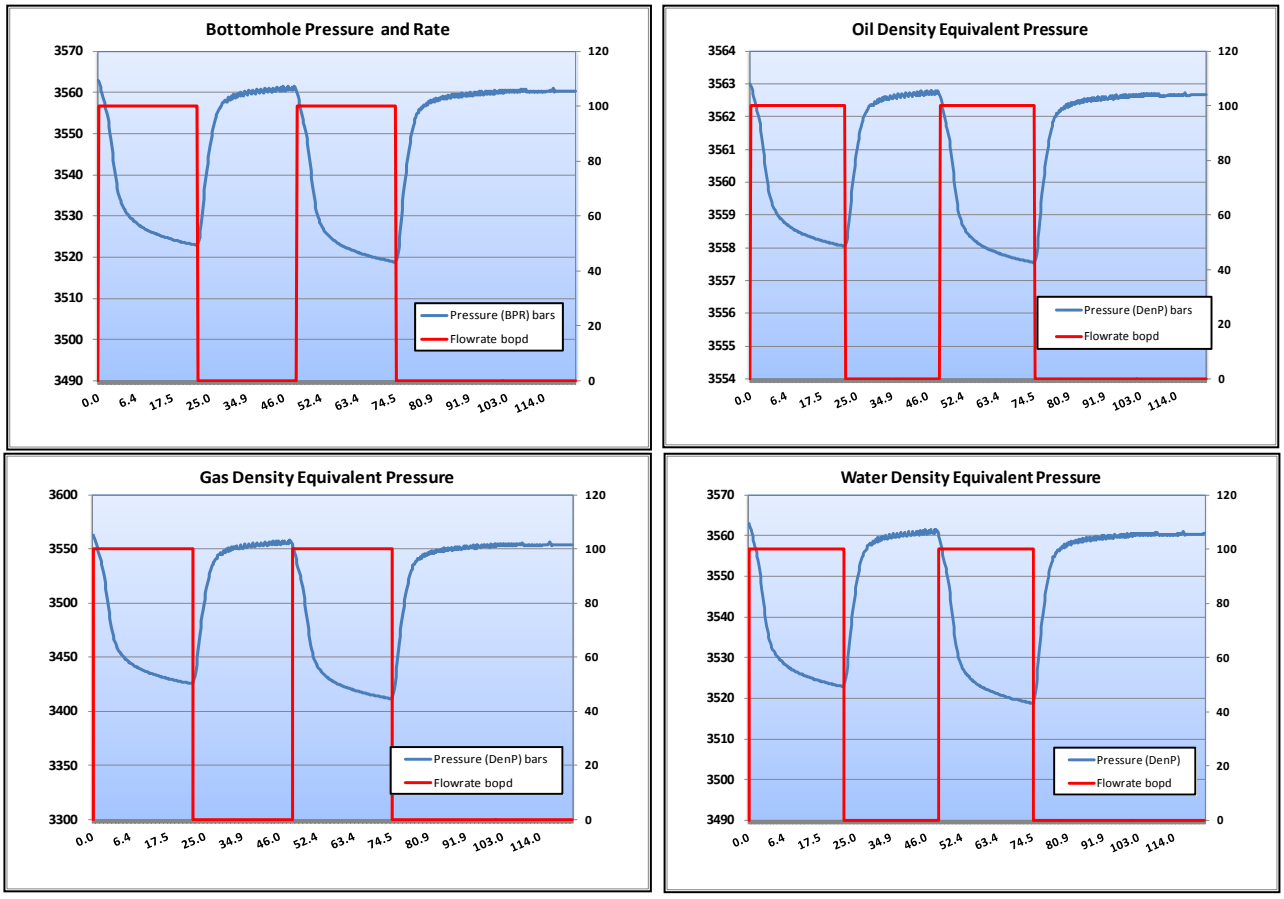

Figure I: ***Test Sequence:*** *Bottom-hole Pressure and Pressure equivalent from bottom-hole gas, oil and water density*

Example 1.0b: Production Test
Flowing + Build-up Sequence:
Well perforated hp = 30ft inside the oil layer.
Net sand thickness h = 250ft

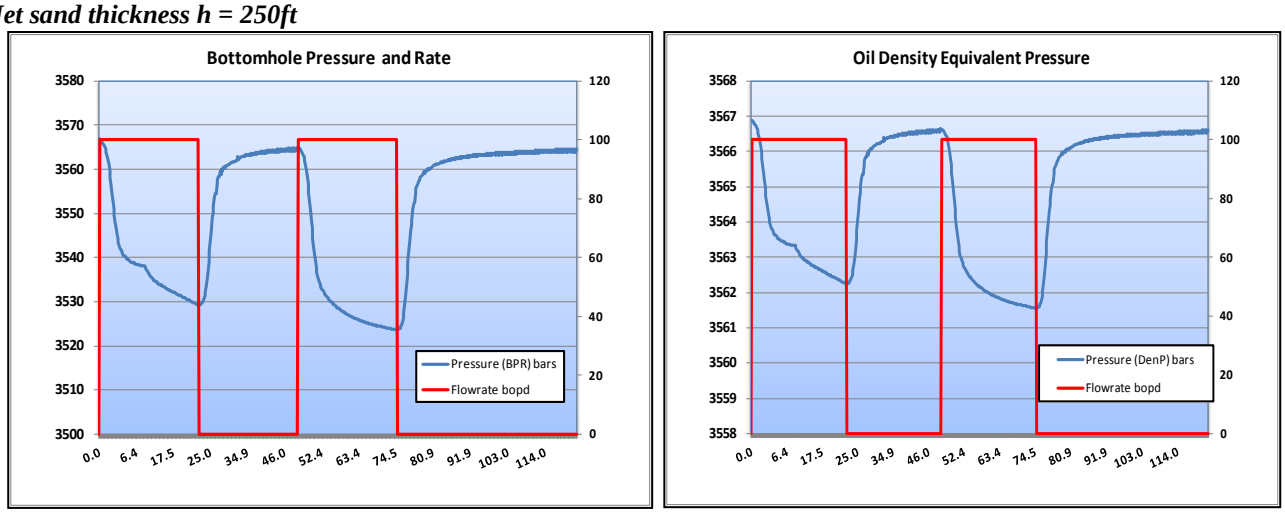

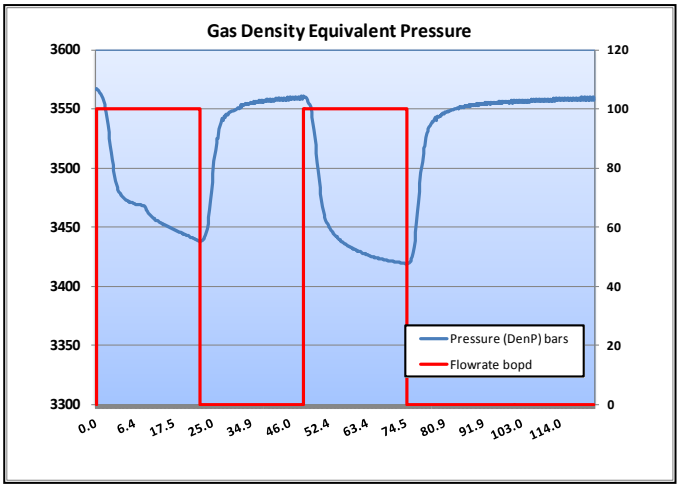

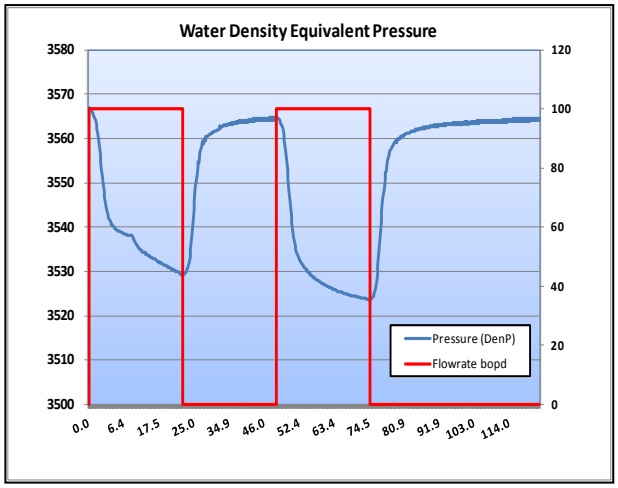

Figure II: ***Test Sequence:*** *Bottom-hole Pressure and Pressure equivalent from bottom-hole gas, oil and water density*

Example 1.0c: Production Test
Flowing + Build-up Sequence.
Well perforated hp = 30ft between gas and oil layer.
Net sand thickness h = 250ft

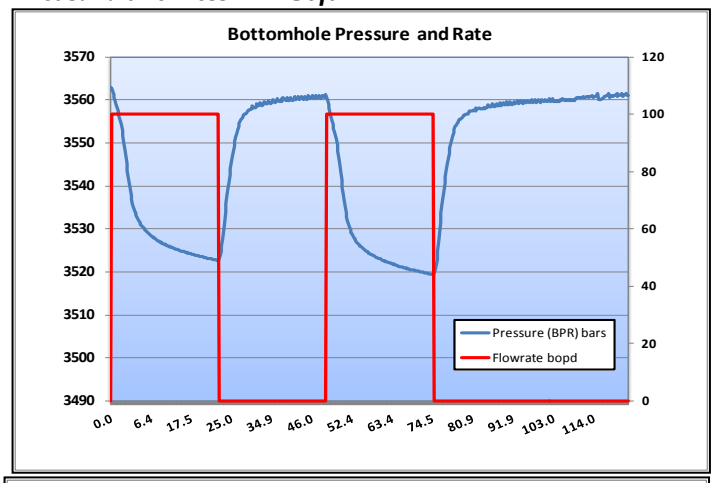

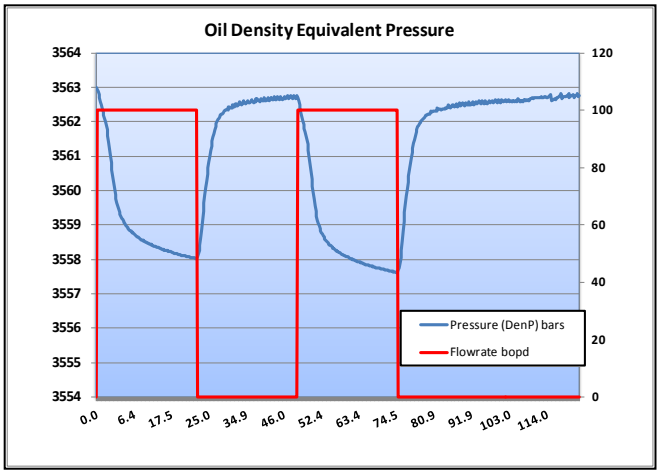

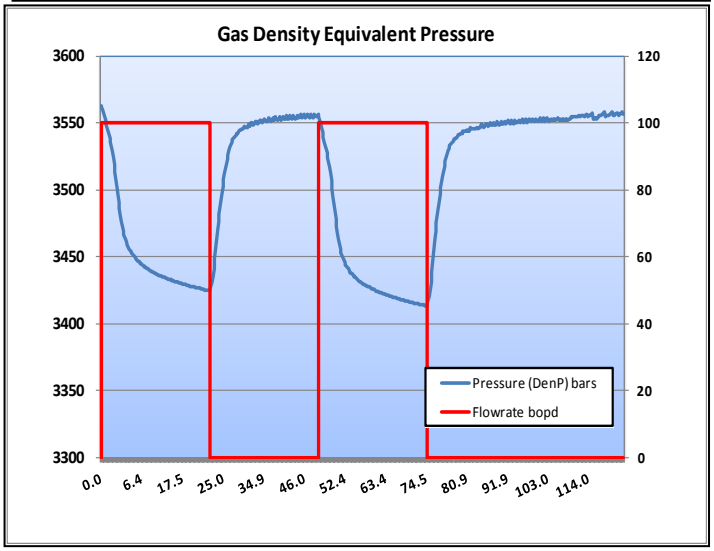

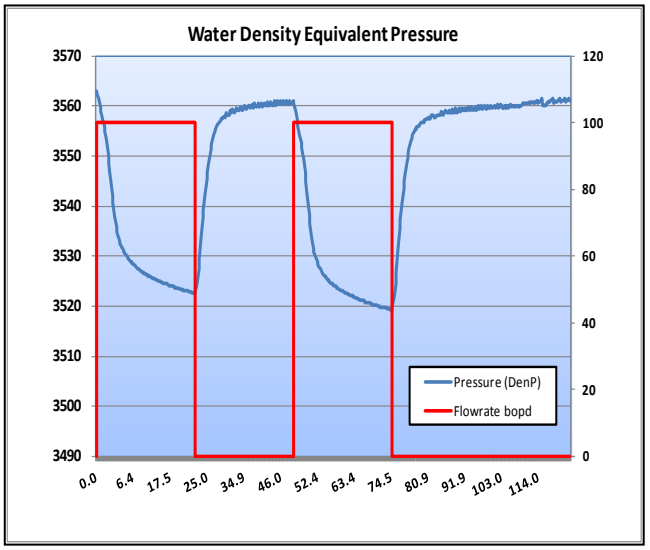

Figure III: ***Test Sequence:*** *Bottom-hole Pressure and Pressure equivalent from bottom-hole gas, oil and water density*

Example 1.0d: Falloff Test
Flowing + Build-up Sequence
Well perforated hp = 30ft between oil and water layer.
Net sand thickness h = 250ft

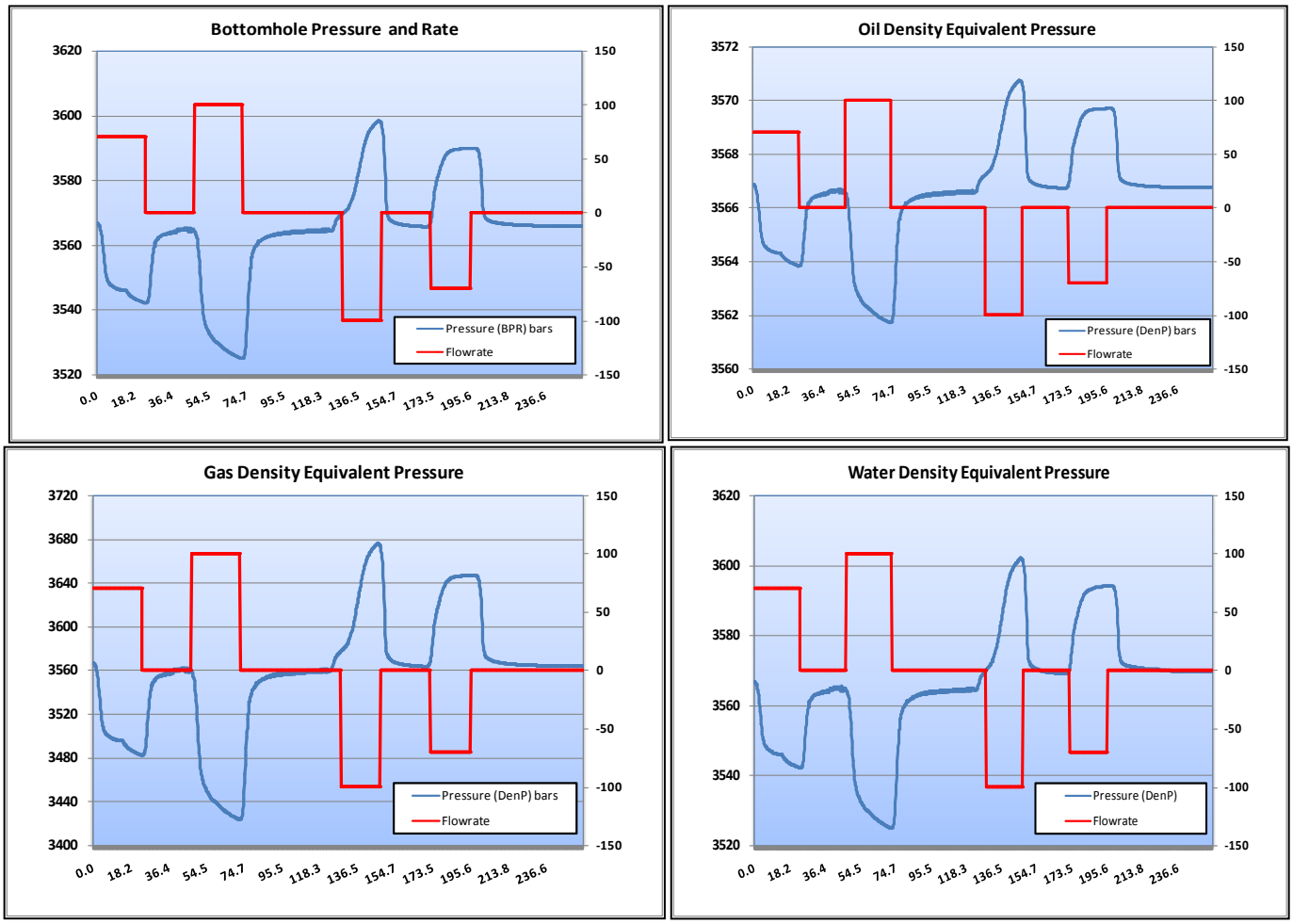

Figure IV: ***Test Sequence:*** *Bottom-hole Pressure and Pressure equivalent from bottom-hole gas, oil and water density*

Example 2.0a: Production Test
Flowing + Build-up Sequence
Well perforated hp = 30ft between gas condensate and water layer.
Net sand thickness h = 148ft

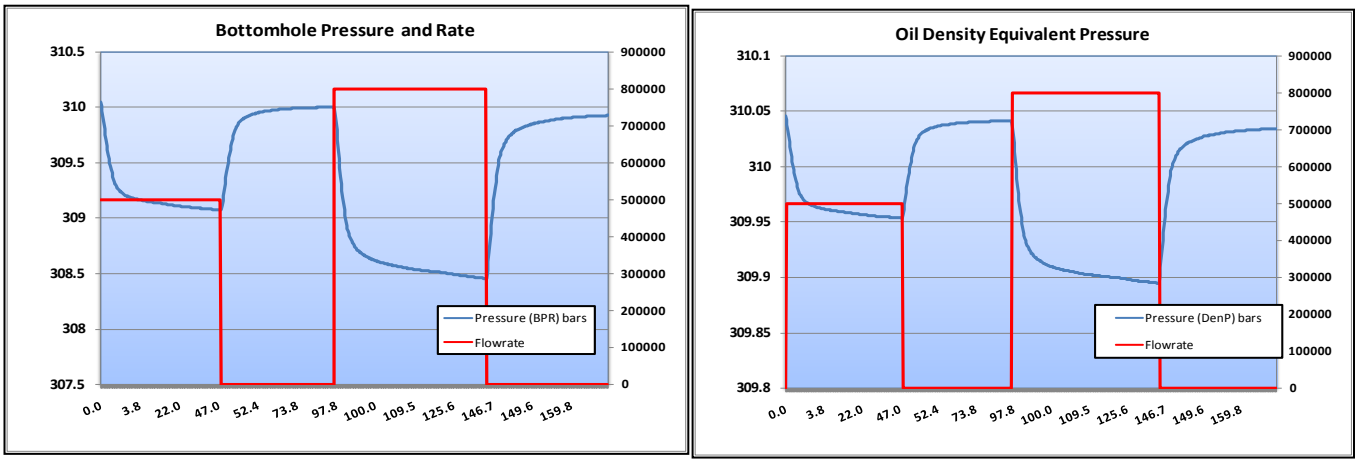

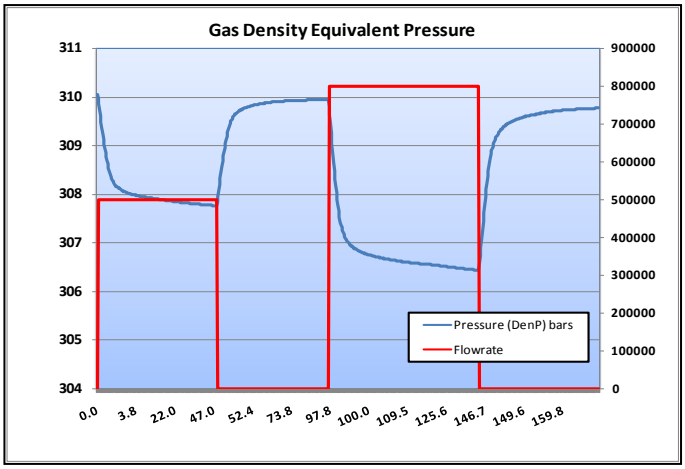

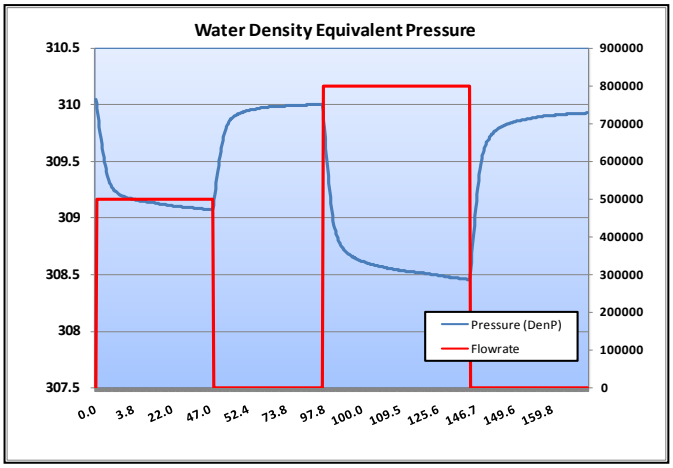

Figure V: ***Test Sequence:*** *Bottom-hole Pressure and Pressure equivalent from bottom-hole gas, oil and water density*

Example 2.0b: Production Test
Flowing + Build-up Sequence
Well perforated hp = 30ft inside the gas condensate layer.
Net sand thickness h = 148ft

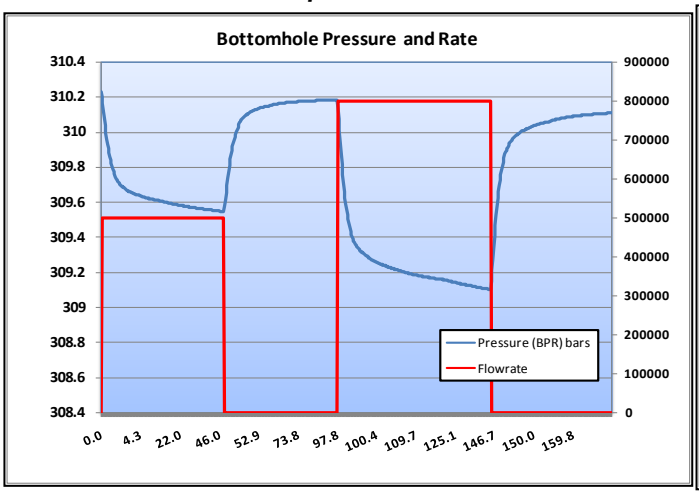

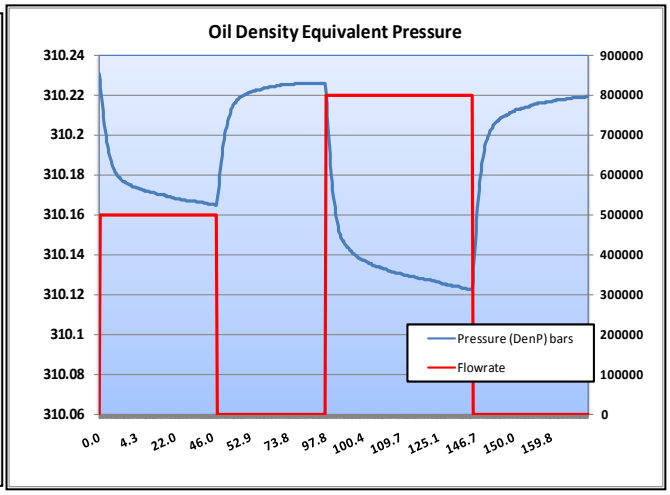

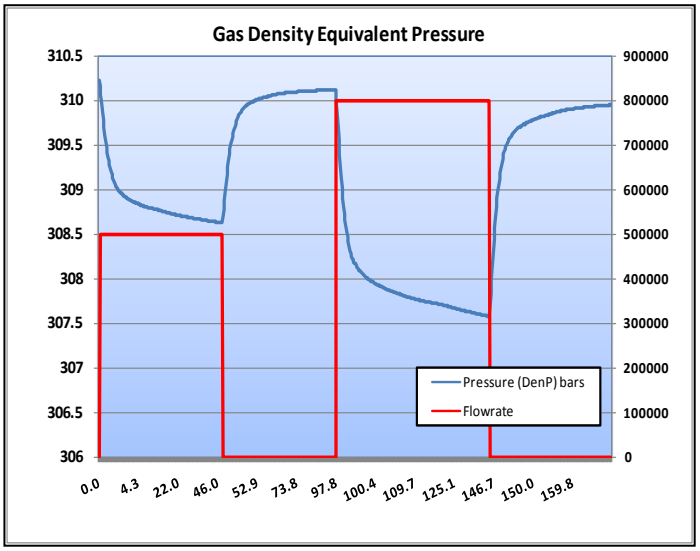

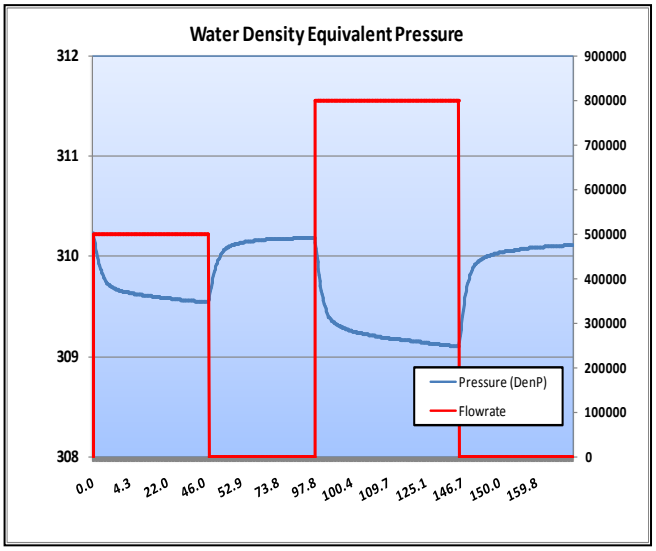

Figure VI: ***Test Sequence:*** *Bottom-hole Pressure and Pressure equivalent from bottom-hole gas, oil and water density*